Novel functions of the pyrenoid and the large subunit of ribulose-1, 5-bisphosphate carboxylase/oxygenase in *Chlamydomonas reinhardtii*

Yu Zhan

A Thesis

In

The Department

of

Biology

Presented in Partial Fulfillment of the Requirements

For the Degree of Doctor of Philosophy at

Concordia University

Montreal, Quebec, Canada

Sep 2015

CONCORDIA UNIVERSITY

SCHOOL OF GRADUATE STUDIES

This is to certify that the thesis prepared

By: Yu Zhan

Entitled: Novel functions of the pyrenoid and the large subunit of ribulose-1, 5-bisphosphate carboxylase/oxygenase in *Chlamydomonas reinhardtii.*

and submitted in partial fulfillment of the requirements for the degree of Ph.D

complies with the regulations of the University and meets the accepted standards with respect to originality and quality.

Signed by the final examining committee:

Dr. Gilles Peslherbe Chair

Dr. Peter Moffett External Examiner

Dr. Ann English External to Program

Dr. Alisa Piekny Examiner

Dr. Luc Varin Examiner

Dr. William Zerges Thesis Supervisor

Approved by

Dr. Patrick Gulik

Chair of Department or Graduate Program

2015. 09. 09 Dr. André G Roy

Director Dean of Faculty

Abstract

Novel functions of the pyrenoid and the large subunit of ribulose-1, 5-bisphosphate carboxylase/oxygenase in *Chlamydomonas reinhardtii*

Yu Zhan, Ph.D.

Concordia University, 2015

This thesis describes my research in the cell and molecular biology of the chloroplast of the green alga *Chlamydomonas reinhardtii.* Following a general introduction to all relevant topics in Chapter 1, Chapters 2 to 4 present different projects, each with the organization of a publication.

Chapter 2 describes my investigation of the management of oxidized RNA in the chloroplast a semi-autonomous, bacterial-type cell organelle. I show that the large subunit of Rubisco, RBCL, has a "moonlighting" function in controlling the level of oxidized RNA in the chloroplast. I also show in this chapter that a complex of RBCL, correlates with the RBCL moonlighting function, with results of native polyacrylamide gel electrophoresis and size-exclusion chromatography. The identification of this RBCL complex and aggregated form is a step towards understanding how RBCL mitigates RNA oxidation.

Results of immunofluorescence microscopy reveal that oxidized RNA localized in the pyrenoid, a chloroplast micro-compartment where CO_2 is assimilated by the Calvin cycle enzyme Rubisco. This finding, together with previous research of chloroplast stress granules, provoked my interest in the potential functions of pyrenoid in RNA metabolism and led me to undertake a

proteomic characterization of this microcompartment. Chapter 3 reports a partial pyrenoid proteome. I optimized the subcellular fractionation methods to obtain pyrenoid-enriched fractions and devised a means of identifying contaminant proteins, by preparing equivalent fractions from mutants that lack a pyrenoid. Results of bioinformatic analyses of this pyrenoid proteome further substantiate its role in RNA metabolism, and also confirm its long-suspected role in starch metabolism. The results also suggest additional unexpected possible functions in translation, lipid metabolism, chlorophyll biosynthesis and stress responses.

Chapter 4 describes results that further support the role of the pyrenoid in chlorophyll synthesis and reveal other new and unexpected findings. The localization of chlorophyll synthesis could closely relate to the assembly of photosystem or light harvesting complex proteins. These results also give hints regarding the location(s) of thylakoid biogenesis. My work reveals a novel function of the photosynthesis protein RBCL in the control of oxidized RNA and the important potential functions of the pyrenoid, in RNA metabolism and chlorophyll biosynthesis.

Acknowledgements

I thank my colleague, James Dhaliwal who worked together with me on the project of the RNA oxidant function of RBCL and Dr. James Uniacke who initiated this project. I also thank Dr. Rachid Mazroui and Ms. Pauline Adjibade for their contribution of research work with mammalian cells in this project.

I thank Dr. Stephan Lemaire, Dr. Christophe Marchand and Ms. Adeline Mauries for their collaboration in the mass spectrometry analysis of the pyrenoid proteome. I also thank Simon Arragain who participated in optimizing the experimental conditions for this project.

I thank Marc Champange in Centre for Structural and Functional Genomics for their help and technical advice

I thank all the members of Dr. Zerges lab, past and present, Yi Sun, Melissa Valente, Mehrnaz Jamaat, Marco Schottkowski and Matthew Peters.

I thank Dr. Alisa Piekny and Dr. Luc Varin for their helpful comments and advice as my committee members. I specially thank my supervisor Dr. William Zerges for his guidance and help throughout my entire Ph.D. studies.

Table of Contents

List of Figures

List of Tables

List of Abbreviations

2-PG	2-phosphoglycolate
3-PGA	3- Phosphoglyceric acid
8-oxoG	8-oxoguanine
Auf1	AU-rich element RNA binding protein 1
CA	Carbonic anhydrase
CCM	Carbon concentrating mechanism
CCP	Chloroplast carrier protein
CIA5	Inorganic accumulation factor 5
cpSGs	Chloroplast stress granules
CTM	Chloroplast translation membrane
DV-Pchlide	divinyl-protochlorophyllide
DVR	Divinyl (proto) chlorophyllide 8-vinyl reductase
FISH	Fluorescent *in situ* hybridization
HCO_3^-	Bicarbonate ions
HLA3	High light induced gene 3
HSM	High salt minimal medium
IF	Immunofluorescence
LCI	Low-CO_2 induced
LCIR1	Low-CO_2 response regulator 1
LHC	Light-harvesting complex
LD-POR	Light-dependent protochlorophyllide oxidoreductase

LID-POR	Light-independent protochlorophyllide oxidoreductase
MS	Mass spectrometry
Pchlide	Protochlorophylide
RBCL	Large subunit of Rubisco
RBCS	Small subunit of Rubisco
RISC	RNA-induced silencing complex
RNP	Ribonucleoproteins
ROS	Reactive oxygen species
Rubisco	Ribulose-1,5-bisphosphate carboxylase/oxygenase
RuBP	Ribulose-1,5-bisphosphate
SG	Stress granule
PB	Processing body
PABP	Poly (A)-binding protein
PPMT	Mg-Protoporphyrin IX methyltransferase
TAP medium	Tris-acetate phosphate medium
YB-1	Y box-binding protein I

Chapter 1: General Introduction

1. 1 *Chlamydomonas reinhardtii* as a model organism.

1.1.1 *C. reinhardtii* is a model organism in molecular and cellular biology

C. reinhardtii is a unicellular eukaryotic green alga that is widely used as a model organism in research of many cell biological processes; chloroplast biogenesis, photosynthesis, flagella-based motility, flagella biogenesis, organelle genetics and non-Mendelian inheritance [1]. *C. reinhardtii* was described in 1888 by Dangeard and has been used as model organism for studies of chloroplast biology since the 1950s when Ruth Sager discovered the non-Mendalian or "cytoplasmic" inheritance of traits that were later shown to be transmitted with the chloroplast genome [2, 3].

C. reinhardtii cells have a highly stereotypical intracellular organization of their nucleus and organelles. Each cell contains a central region with the nucleus, cytoplasm, endoplasmic reticulum and the Golgi apparatus. Two flagella are organized by basal bodies at the apical cell pole. Each cell normally has one to more contractile vacuoles for osmoregulation [4, 5]. The single chloroplast has a large globular region in the basal (posterior) region of the cell, from which lobes emerge to surround the central nuclear-cytosolic region. These lobes can be interconnected, making the chloroplast resemble a basket. Mitochondria are present throughout the cytosol and also at its periphery, between the chloroplast and plasma membrane [6]. The cell is enclosed by a cell wall, which is constituted by hydroxyproline-rich glycoproteins [7].

1.1.2 Chloroplasts

Chloroplasts are the organelles which carry out photosynthesis, synthesis of amino acids,

lipids and pigments, and the assimilation of sulfur, nitrogen and phosphorus [8]. The chloroplast is surrounded by an envelope, which is composed of outer and inner membranes. Within the chloroplast, a network of membranous vesicles, called thylakoids, carry out the light-dependent reactions of photosynthesis and ATP synthesis. The aqueous-proteinaceous stroma contains many enzymes involved in diverse biochemical pathways. The chloroplasts of most algae and the hornworts (a group of aquatic plant) have a large spherical pyrenoid which carries out the assimilation of CO_2 in the Calvin cycle and, therefore, contains most of the pool of Ribulose-1, 5-bisphosphate carboxylase/oxygenase (Rubisco) [9].

The light-driven reactions of photosynthesis are carried out by photosystem I and photosystem II (PSI and PSII) with their associated light-harvesting antenna complexes, chlorophyll *a* and *b* and carotenoids. PSI and PSII are in an electron transport chain with an intermediary complex, cytochromes b_6/f. This photosynthetic electron transport chain oxidizes water to provide electrons for the reduction of NADP, and the generation of an electrochemical proton gradient, which is used for the synthesis of ATP. The LHCI (light harvesting complex I) associated with PSI and LHCII complex with PSII collect light for photosynthesis and determine how much light energy is transferred to photosystems [10].

C. reinhardtii has three distinct genetic systems: in the nucleus, chloroplast, and the mitochondria. The nuclear genome contains 17,737 protein-coding genes and is GC rich (64%) [11]. Introns are present in most genes [11, 12]. The genome has been sequenced and fully annotated providing an invaluable resource [11].

The chloroplast contains a bacterial-type genetic system because this organelle has been evolved from an endosymbiotic cyanobacterium [13]. Chloroplasts also have retained the

bacterial-type transcription and translation machinery of this endosymbiont [14-16]. The chloroplast genome is 203,828 bp and encodes 99 genes (64 protein-coding genes, 29 tRNA genes and 6 rRNA genes. It has a particularly low GC content (35%) [17]. The chloroplast DNA is present in 80-100 copies per chloroplast and it is packaged in irregular shape bodies called nucleoids, which can be seen by fluorescence microscopy [18]. There are about 10 nucleoids in each *C. reinhardtii* chloroplast [19].

Most of chloroplast proteins are encoded by the nuclear genome, synthesized by 80S cytoplasmic ribosomes, and then imported into the chloroplast [20]. A smaller subset of chloroplast proteins are encoded by the chloroplast genome and synthesized within the organelle by the 70S bacterial-like ribosomes [21]. Moreover, some products of nuclear genes can control the expression of chloroplast genes [22].

1.1.3 The pyrenoid

The pyrenoid is a non-membrane bound spherical body within the chloroplasts of most algae and aquatic plants, the hornworts [23, 24]. It is surrounded by starch under low [CO_2] growth conditions [25]. There is only one pyrenoid per chloroplast in most *Chlamydomonas* species [26]. The pyrenoid is the major reservoir of Rubisco. The pyrenoid is believed to provide a low [O_2]/[CO_2] ratio to favor the carboxylase activity of Rubisco in the Calvin cycle over its non-productive oxygenase activity. A carbon concentrating mechanism (CCM) involving the pyrenoid is reviewed below [27]. In addition, the sequestration of Rubisco in pyrenoid protects Rubisco from the O_2 generated by PSII in thylakoid membranes throughout the chloroplast [28]. Rubisco activase has also been shown to be localized within the pyrenoid [29]. There are also some enzymes that appear to be associated with the periphery of the pyrenoid, like nitrate

reductase, ferredoxin-$NADP^+$ reductase and phosphoribulokinase [29, 30]. The integrity of pyrenoid is essential for the CCM while some mutant strains lacking Rubisco and CCM enzymes also lack a pyrenoid [31, 32].

The formation of pyrenoid in *C. reinhardtii* requires the Rubisco small subunit (RBCS) and specifically two solvent-exposed alpha-helices thereof [33]. Since the amino acid composition of algae RBCS is more hydrophobic compared to the higher plant RBCS, packaging Rubisco in pyrenoid may be a spontaneous aggregation of Rubisco by hydrophobic interactions [33].

Although there is no membrane surrounding the pyrenoid, a three-dimensional reconstruction shows thylakoid tubules extending through windows between starch plates and into the pyrenoid matrix where they interconnect to form a network [34]. Recently, mini-tubules inside these thylakoid tubules were identified. These mini-tubules contain stroma and have opposite openings outside and inside the pyrenoid. Therefore, they provide a pathway for molecules to diffuse in and out directly between pyrenoid and stroma [35].

Whether or not pyrenoids have other functions is unknown. There are indications of possible roles of pyrenoids in the metabolism of DNA and RNA. Several studies have shown that the pyrenoid stains for DAPI in certain green algae, but not in *C. reinhardtii.* However, chloroplast nucleoids had been shown localized adjacent to the pyrenoid in *C. reinhardtii* [18, 36]. A DNA endonuclease UVI31+ which was related to DNA repair was found to localize to the pyrenoid, and to leave the pyrenoid under stress induced by UV light exposure [37]. These findings suggest that the pyrenoid may have a role in the maintenance, inheritance, replication or expression of the chloroplast genome.

A role of the pyrenoid in RNA metabolism is suggested by the finding of stress granules at

the vicinity of the pyrenoid in *C. reinhardtii* [38].

The pyrenoid has been proposed to be a location of thylakoid membrane biogenesis [39]. The pulse-labeling with [^{3}H] acetate of membrane lipids revealed significant labeling of the pyrenoid thylakoid tubules, supporting membrane synthesis in these locations [39]. Acyltransferase activity, which is involved in membrane lipid synthesis, was also detected in the pyrenoid by histochemical staining and electron microscopy [40]. These results suggest that the thylakoid tubules in pyrenoid are generated inside pyrenoid and then connected with the outside thylakoid membrane.

1.1.4 Rubisco and RBCL

Rubisco is a key enzyme in carbon assimilation; it takes gaseous CO_2 and RuBP as substrates and generates two molecules of 3-phosphoglyceric acid (3-PGA) or one molecule of 3-PGA and one molecule of 2-phosphoglycolate (2-PG) in the oxygenation reaction [41, 42]. The competition between the carboxylase activity of Rubisco and its oxygenase activity lead to inefficient CO_2 fixation. This inefficiency is thought to be the reason of the high abundance of this enzyme (about 50%) in plants and algae [43]. The Rubisco holoenzyme contains eight copies each of RBCL and RBCS. RBCL is encoded by the chloroplast *rbcL* gene, while RBCS is encoded by two nuclear genes; *RBCS1* and *RBCS2* [17, 44]. *C. reinhardtii* is widely used for studies of Rubisco function and biogenesis because, in addition to the above-mentioned advantages as a model organism, its *rbcL* gene can be modified by chloroplast transformation and there are mutants strains that lack both *RBCS* genes, which are adjacent in a single genetic locus [9, 26, 29, 45-49].

The promoter of the *rbcL* gene contains typical -35/-10 bacterial-like elements with an enhancer to maintain high expression [50]. There is an RNA-stabilizing stem-loop structure in

the *rbcL* 5’ untranslated region (UTR) and fusion of this region to the GFP coding region can drive high levels of expression in chloroplast transformants [51]. The two step-loop structures in the 3’ UTR stabilize the transcript against exonucleolytic decay [52]. Moreover, the accumulation of the chloroplast *rbcL* transcript is regulated by a nuclear factor, maturation of *rbcL* (MRL1), which stabilizes the *rbcL* mRNA via its 5' UTR [53]. Under reducing conditions, the 5’ UTR region of *rbcL* can specifically bind proteins of 81, 62, 51, and 47 kDa in UV-cross-linking experiments. However, under oxidizing condition, the binding of these proteins is interrupted because RBCL binds with *rbcL* mRNA by its non-specific RNA binding activity. The amino terminus of RBCL shares a common βαββαβ structure, which is known as “ferredoxin-like” domain found in a number of RNA-binding proteins [54].

Although the ratio of RBCL to RBCS in Rubisco holoenzyme is 1:1, both transcript and protein ratios of these two components are 5:1, which indicates that RBCS is the limiting factor for the assembly of the holoenzyme [55]. Thus there is a substantial pool of RBCL which is not in the holoenzyme and, therefore, may have a function other than Rubisco.

1.2 Carbon Concentrating Mechanism (CCM)

CO_2 concentration is a major factor contributing to plant growth rate, photosynthesis rate and expression of genes [56]. A CCM helps aquatic photosynthetic algae to increase the CO_2 concentration around the carbon fixation enzyme, Rubisco. The CCM is induced by the ambient (0.03-0.05%) or lower CO_2 concentration and it is important for the aquatic organisms due to their lower availability of CO_2 resulting from the low diffusion rates in water than in air. Moreover, most CO_2 in water near pH 7, the range found in natural water, is converted to the bicarbonate ion (HCO_3^-). Unlike CO_2, the bicarbonate ion cannot cross membranes and enter

cells and organelles by simple diffusion [57]. The CCM involves a set of transport proteins and enzymes to help the efficient uptake of inorganic carbon (Ci), like CO_2 and HCO_3^- into cells to the site of Rubisco for fixation.

1.2.1 Cell surface and plasma membrane:

As was mentioned above, unlike CO_2, HCO_3^- cannot directly cross plasma membrane by simple diffusion. There are several transporters in the plasma membrane to transport HCO_3^- into the cytosol. Low- CO_2 inducer1 (LCI1), the first identified membrane protein which is up-regulated by limiting CO_2, is localized in plasma membrane [58]. An ATP-binding cassette transporter HLA3, which is encoded by *high light induced gene 3* (*HLA3*) is another plasma membrane transporter for HCO_3^- [59]. Both CO_2 and HCO_3^- in the environment can be taken in as the Ci source. There is a pH-dependent equilibrium between these two Ci species. The low CO_2 induced periplasmic carbonic anhydrase 1 (CAH1) can maintain the equilibrium between these two Ci species for uptake of either HCO_3^- via transporters or CO_2 via simple diffusion [60].

1.2.2 Cytosol and chloroplast envelope:

No carbonic anhydrase (CA) was found in the cytoplasm and this may serve to maintain a high HCO_3^- concentration in this compartment. Leakage of CO_2 could be minimized since there is no CA to dehydrate accumulated Ci as HCO_3^- [61]. There are two CAs, CAH4 and CAH5, in the mitochondria [62]. Although, the function of these two enzymes may not directly relate to CCM, CAH4 is induced under low CO_2 conditions [62]. The protein low CO_2 induced A (LCIA) has been identified as a HCO_3^- transporter in the inner chloroplast envelope membrane [31, 63]. The other putative Ci transporters for chloroplast envelope are chloroplast carrier protein 1 and 2 (CCP1/CCP2). They are strongly up-regulated in low CO_2 conditions and they are members of the

mitochondria carrier family, although they function in the chloroplast envelope [64]. The other protein that is required for Ci transport into the chloroplast is CemA, a protein of the chloroplast envelope which is encoded by the chloroplast gene *ycf10* [65]. Instead of acting as a Ci transporter, it mainly plays a role in electrical and pH homeostasis to affect Ci transport [66].

1.2.3 Chloroplast stroma:

Another group of low-CO_2-induced genes include *LCIB* and three related genes; *LCIC, LCID, LCIE,* which encode proteins implicated in CO_2 uptake in the stroma [67]. LCIB functions under both low CO_2 and very low CO_2 (<0.02%) conditions for CO_2 acclimation and it is proposed to catalyze unidirectional hydration of CO_2 to HCO_3^- for CO_2 accumulation [67]. LCIB localizes at the vicinity of the pyrenoid when CCM is active and moves to the stroma after cells are shifted to high CO_2 conditions [68]. This localization may let LCIB capture the leaking CO_2 from the pyrenoid and hydrates it back to the HCO_3^- pool in the stromal. Another stromal CA, CAH6, can covert CO_2 to HCO_3^- in alkaline stroma to maintain high Ci concentration [69].

1.2.4 Pyrenoid:

As mentioned above, the pyrenoid is the major site of localization for Rubisco and almost 90% of total pool of this enzyme complex is therein when CCM is induced [70]. Rubisco catalyzes the first step of Calvin Cycle and it incorporates CO_2 into organic carbon by combining it with RuBP [71].

One of the carbonic anhydrases (CAs) in the pyrenoid, CAH3, catalyzes the conversion of HCO_3^- to CO_2 near Rubisco [72]. Originally, it was considered to localize to the lumen of thylakoid tubules when phosphorylated [73]. Some recent research revealed that phosphorylated CAH3 might localized in stroma either in mini-tubules or very close to the

opening of the mini-tubules [35]. The mini-tubules could provide a direct route for diffusion of stromal HCO_3^- into the pyrenoid, eliminating the need for a CA in the thylakoid lumen, the previously proposed route. In addition, the only "missing" transporter, which was proposed to transport HCO_3^- into the lumen of thylakoid tubules to meet CAH3, is not needed anymore.

1.2.5 CCM model:

The results of cryo-electron tomography of *C. reinhardtii* architecture, reviewed in the previous subsection (1.2.4), support an updated CCM model [35, 66, 74]. The CO_2 in the environment can diffuse into the pyrenoid to meet Rubisco. This CO_2 can be generated from HCO_3^- by CAH1 (dehydrates HCO_3^- to CO_2) in the periplasm. In addition, cells can also take up bicarbonate by the transporters. LCI1 and HLA3 would transport HCO_3^- into cytoplasm and LCIA would take it across the chloroplast envelope to the stroma. Instead of finding a way to reach the thylakoid lumen in pyrenoid, HCO_3^- could be dehydrated to CO_2 by phosphorylated CAH3 localized in or very close to the openings of the mini-tubules at the surface of the pyrenoid. Then the stromal HCO_3^- and the Rubisco substrate ribulose-1, 5-bisphosphate (RuBP) can be directly delivered to the pyrenoid matrix via the mini-tubules. The product of carbon fixation, like 3-PGA, can also be transported from pyrenoid to stroma directly via these mini-tubules (Fig 1.1).

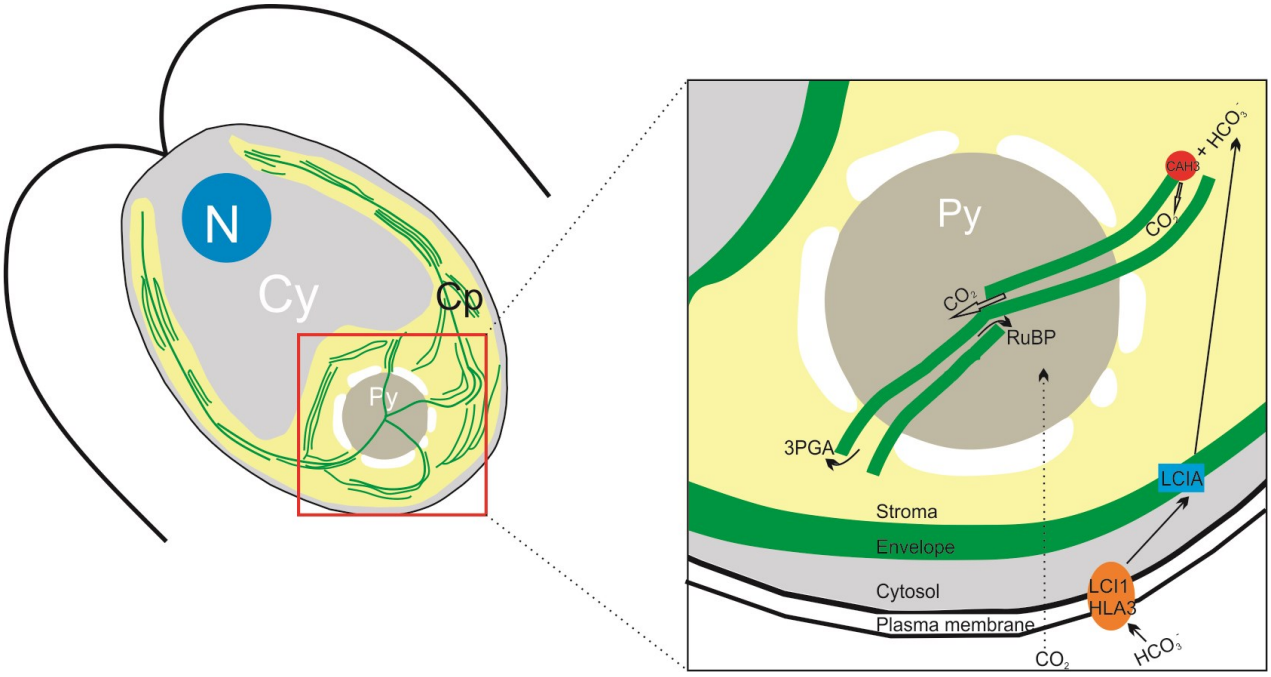

Figure 1.1 The CCM model involving pyrenoid of *C. reinhardtii*.

New CCM model modified from previous paper. Those mini-tubules in the thylakoid tubules provide a direct content exchange between the stroma and the pyrenoid, as Rubisco substrate, RuBP and carbon assimilation product, 3-PGA. Bicarbonate is transported from outside to chloroplast stroma by plasma transporter HLA3 and LCI1 (orange), and envelope transporter LCIA (blue). CAH3 (red) could locate close to or within the mini-tubules to hydrate bicarbonate to CO_2 and CO_2 could be delivered to Rubisco in the mini-tubules without transporters.

1.2.6 Regulation of CCM

The expression of protein components of the CCM is regulated by two transcription factors: Ci accumulation 5 (CIA5 or CCM1) and low-CO_2 response regulator 1 (LCR1) [75]. CIA5 regulates most Ci transporters and some carbonic anhydrases like LCIA, LCI1, HLA3 and CCP1/2. Although CIA5 is called the master regulator of CCM, its transcript levels are independent of CO_2 concentration [76]. That means the posttranscriptional activation of CIA5 in limiting CO_2 is required for its regulation. LCR1 regulates at least three low CO_2 induced genes: *CAH1*, *LCI1* and *LCI6* [77].

1.2.7 What else happens under low CO_2 conditions?

Some photorespiratory enzyme activities also increase during low CO_2 conditions, including phosphoglycolate phosphatase, glycolate dehydrogenase and glutamine synthetase [78, 79].

The subcellular organization can also be changed during the limiting CO_2 acclimation. The starch sheath surrounding the pyrenoid is developed and possibly acts as a diffusion barrier to minimize loss of CO_2 from Rubisco-rich- pyrenoid when CCM is induced and disassembled when CCM is repressed [80, 81]. The distribution of mitochondria also changes from a central position inside the “cup” of the chloroplast to the periphery between the chloroplast and the plasma membrane [82]. This relocalization of mitochondria may relate to the scavenging of the photorespiratory product glycolate when CO_2 is limiting [83].

1.3 Chlorophyll biosynthesis

C. reinhardtii synthesizes several pigments including chlorophyll a and b. Chlorophyll absorbs light energy in the light-harvesting antenna complexes and transfers this energy to the reaction centers of PSI and PSII [84]. The chlorophylls are composed of two parts: the tetrapyrrole ring

and the isoprenoid phytol “tail” [85]. Most of the genes related to chlorophyll biosynthesis are nuclear and is tightly regulated [86]. Although most chlorophyll biosynthesis-related genes have been identified in *C. reinhardtii*, the precise localization of this pathway within chloroplasts is still not clear.

The whole chlorophyll synthesis pathway can be described by the formation of tetrapyrrole ring and the addition of isoprenoid phytol tail. First, the universal tetrapyrrole precursor 5-aminolevulinic acid (ALA) is formed from glutamate in the chloroplast [87]. After the macrocyclic tetrapyrrole forms, the pathway has two branches: the “oxidative pathway” to form protoporphyrin IX; the “reducing pathway” to generate siroheme as another important product in the tetrapyrrole synthesis [88]. Protoporphyrin IX can either form protoheme as another side product, with the insertion of Fe^{2+} by protoporphyrin IX ferrochelatase (FeC) [89] or continue chlorophyll synthesis by the insertion of Mg^{2+} [90] (Fig 1.2) .

Here, I pay more attention to the steps following protoporphyrin IX synthesis and Mg^{2+} insertion, which are specific to chlorophyll biosynthesis.

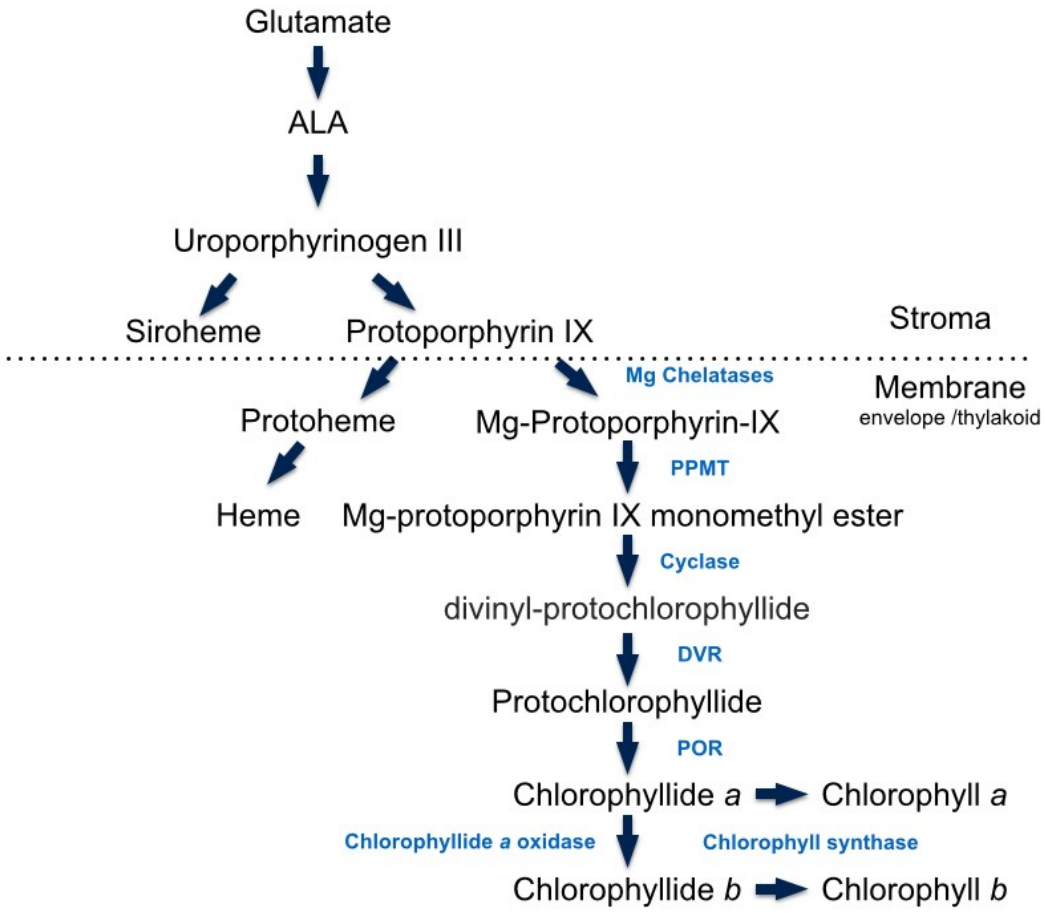

Figure 1.2 Chlorophyll biosynthesis.

The process of chlorophyll synthesis happens in chloroplast. Stroma is the major location to generate protoporphyrin IX and the latter steps to generate chlorophyll take place on the membrane system. PPMT; Mg-Protoporphyrin IX methyltransferase, DVR; Divinyl (proto) chlorophyllide 8-vinyl reductase, POR; protochlorophylilde oxidoreductase.

1.3.1 Chelation of Mg^{2+}

Mg^{2+} is inserted into protoporphyrin IX by the chloroplast ATP-dependent Mg-chelatase [91]. There are two steps for Mg insertion: activation of Mg-chlelatase and Mg chelation. Both steps are ATP dependent [92]. The enzyme has a Mg^{2+}-dependent membrane association [93]. Mg-chelatase is synthesized in the cytoplasm and imported through the envelope to the stroma [90]. The enzyme was originally thought to be associated with envelope membranes [90]. However, others consider the thylakoid membrane as the major location of Mg-chelatase, although no evidence was provided to support this hypothesis [92]. There are three subunits of the Mg-chelatase complex: CHLD, CHLI, CHLH. These are encoded by nuclear genes and targeted to the chloroplast in *C. reinhardtii* [94]. The above-mentioned three proteins are sufficient for Mg chelation, however, there is another cofactor protein that can greatly increase the Mg chelation rate; GUN4 [95].

1.3.2 Methylation of the 13^3–propionate carboxyl group of Mg-protoporphyrin IX

Mg-Protoporphyrin IX methyltransferase (PPMT) catalyzed the methylation of 13^3–propionate carboxyl group of Mg-protoporphyrin IX. This enzyme activity was found in fractions containing either envelope or thylakoid membranes [92]. PPMT has important interactions with Mg-chelatase [96]. They may act together to regulate the intermediate Mg-protoporphyrin IX. There is one candidate gene in *C. reinhardtii* encoding PPMT, however, there are no reports of the activity of this protein in *C. reinhardtii* [88].

1.3.3 Formation of the isocyclic ring

The Mg-protoporphyrin IX monomethyl ester oxidative cyclase is the most common enzyme that forms the isocyclic ring from 13-methylpropionate. The Mg-protoporphyrin IX

monomethyl ester is converted to divinyl-protochlorophyllide. The *C. reinhardtii* cyclase activity is associated with membranes, inhibited by EDTA and other metal chelators, but recovered by adding Fe^{2+} [97]. There is an indication that the cyclase is localized to the inner envelope membrane [90]. There are two cyclases in *Chlamydomonas*: *CHL27A* (*CRD1*) and *CH27B* (*CTH1*). CRD1 (Copper response defect 1) is the cyclase that accumulates under conditions of either copper-deficiency and oxygen-deficiency while CTH1 is expressed under copper-sufficient and oxygenated conditions [98].

1.3.4 Reduction of the 8-vinyl group

Divinyl (proto) chlorophyllide 8-vinyl reductase (DVR) catalyzes the reduction of the 8-vinyl group of the tetrapyrrole to form an ethyl group. The activity of DVR is detected on the plastid membrane, but not the stroma, and it requires NADPH as reductant [99] [100]. The *C. reinhardtii* genome contains a gene that is predicted to encode DVR, although this has not been confirmed experimentally [101].

1.3.5 Reduction of pyrrole ring D of protochlorophylide

This step coverts the porphyrin molecule protochlorophyllide *a* into the chlorin chlorophyllide *a*. In most green algae and gymnosperms, two different protochlorophylilde oxidoreductase (PORs) are involved depending on light; one is light-dependent and the other light-independent. Angiosperms have only the light-dependent POR.

1) light-dependent POR

Light-dependent POR (LD-POR) is a peripheral membrane-associated protein and is encoded by a signal nuclear gene in the *C. reinhardtii* [102]. LD-POR is found mainly associated with thylakoid membranes during the greening process. “Greening” refers to the development

of the chloroplast from a proplastid or, in angiosperm seedlings, the etioplast [103]. However, in the mature chloroplast, the amount of POR drops and the distribution shifts to the envelope membrane [104]. There are some other evidence to show that LD-POR localized at the outer leaflet of the outer envelope membrane [105]. The enzyme forms a three-component complex with NADPH and protochlorophyllide *a* [106]. This complex can convert protochloropyllide to chlorophyllide in a reaction requiring a photon.

2) light-independent POR

Three chloroplast genes- *chlB, chlL and chlN* encode subunits of the light-independent POR; which catalyzes the reduction of ring D in the protochlorophyllide [107]. ChlL is not essential for the protochlorophyllide reduction and can be replaced by another protein in a limited level since a ChlL-deficient mutant of *Synechocystis* (a cyanobacteria) can synthesize a small amount of chlorophyll [108].

ChlB and ChlN exist in cells cultured in the light, while ChlL is only present in cells cultured in the dark or under low light, although the transcript level of these proteins are almost the same in both light and dark [109]. In the light-cultured cells, it is proposed that the translation of ChlL is blocked by the energy state and redox poise in the chloroplast. Additionally, CHlL is destabilized by the production of O_2 in cyanobacterium Leptolyngbya boryana [110]. Some LD-POR mutants cannot grow under high light intensity unless at very low O_2 concentration [110]. However, a *C. reinhardtii* LD-POR-deficient mutant accumulates about half as much chlorophyll as wild type in the light, which means the light-independent system is more resistant to O_2 [111].

In addition to the plastid encoded ChlB, ChlN and ChlL, the light-independent pathway

requires nucleus-encoded components in *Chlamydomonas*. At least 7 nuclear loci, *y1, y5-y10* are required for the light-independent system. Mutations at these loci cause the accumulation of protochlorophyllide in the dark [112]. *Y* mutants accumulate ChlB and ChlN, and lack ChlL except *y7* mutant [109]. The *y* gene products are required for translation of the ChlL or for the synthesis of some metal clusters which are present in the ChlB-ChlN complex and ChlL [113].

Why is light-dependent protochlorophyllide reduction needed in organisms that can form chlorophyll without light? First, LD-POR is more efficient than the light independent enzyme [114]. Secondly, LD-POR has a signaling function with the light induction. The activation of LD-POR by light may generate a signal within cells and let them initiate the other reactions in order to adapt to light [114].

1.3.6 Phytylation

Esterification of the 17-propionic acid with the C_{20} polyisoprene alcohol phytol is the last step of chlorophyll *a* formation. After the esterification, the pigment-bound geranylgeranyl is reduced at the three positions with NADPH and ATP [115, 116]. A single thylakoid-localized esterifying enzyme, chlorophyll synthase (CHS) is required for this step [117].

1.3.7. Biosynthesis of chlorophyll *b*

O_2 is required to form chl *b* from chl *a*. This is consistent with the finding that all chl *b*-containing organisms are aerobic [118, 119]. Chl *b* accounts for 15-20% of the total chlorophyll content in plants and green algae. It absorbs the light in the spectrum of 425 nm to 475 nm to supplement chl *a*, but it is not essential for photosynthesis. The *CAO* gene (chlorophyllide *a* oxidase) is necessary for chl *b* accumulation and its 51 kDa product, CAO, prefers chlorophyllide *a* over chlorophyll *a* as substrate [120, 121].

1.4 Tools and techniques available for *C. reinhardtii* research

Many research tools have been developed for *C. reinhardtii* using the approaches of cell and molecular biology, biochemistry, genetics, and biophysics [122, 123]. *C. reinhardtii* is ideal for genetic analyses of photosynthesis because photosynthesis-deficient mutants are fully viable when provided with a reduced carbon source for energy (typically acetate). Sexual reproduction by *C. reinhardtii* was first found in 1875 and has allowed genetic analyses [1]. The sexual cycle can be induced by nitrogen deprivation which induces haploid vegetative cells to differentiate into gametes. Gametes of opposite mating-type fuse to form the diploid zygotes, which then undergo meiosis to form four haploid progeny. These begin as spores within an ascus. Therefore, tetrad analysis is possible. Vegetative progeny develops from the spores and then divide by mitosis. While traits encoded by nuclear genes show Mendelian inheritance, chloroplast genes are inherited uniparentally; *i.e.* only from the mating-type *plus* parent [124]. Many mutant strains are available which can be used to identify gene functions. For example, genes in nitrogen assimilation were identified first through mutants with altered responses to nitrogen availability [125].

Many excellent protocols for biochemical analyses and cellular subfractionation are available [10]. The ability to obtain large amounts of cells from liquid cultures makes it easy to generate material for these approaches. Standard techniques are available for the isolation of chloroplasts and other compartments; however, chloroplast isolation is especially prone to contamination by other organelles. One can also transform the genomes of the nucleus and the chloroplast, and this can be used to disrupt chloroplast genes by homologous recombination [126, 127]

1.5 *C. reinhardtii* as a model organism for studying stress responses

C. reinhardtii is also an excellent model system to research stress responses. *C. reinhardtii* cells adapt quickly to changing environments and have an extensive repertoire of enzymes and metabolic pathways that are conserved through evolution. Therefore, research with *C. reinhardtii* can reveal conserved fundamental principles of stress physiology. Global gene expression responses to stress induced by high intensity light, ROS, and deficiency for metals, phosphate and sulfur have been characterized by microarray analyses and recently RNA-seq [3, 128]. *C. reinhardtii* is also emerging as a popular model system for studies of metal toxicity and tolerance to toxic trace metals, particularly cadmium [129-133].

1.6 Reactive oxygen species (ROS), RNA oxidation and RNPs

1.6.1 ROS and RNA oxidation

Oxidative stress can occur in any organism when a biotic or abiotic condition causes the production of reactive oxygen species (ROS) in excess of the capacity of antioxidant systems to detoxify them. ROS are special forms of oxygen (O_2), including hydrogen peroxide (H_2O_2), superoxide (O_2^-), hydroxyl radical ($^{\cdot}HO$), and singlet oxygen (O_2*) [134]. In chloroplasts electrons can be directed from PSI in an alternative electron transport pathway which shunts electrons to O_2 to form water, in order to relieve over-reduction of intermediates in the photosynthetic electron transport system [53]. O_2^- is formed as the primary product of oxygen reduction which is converted to H_2O_2 by superoxide dismutase. The H_2O_2 is then converted to water by ascorbate peroxidase (APX). Some of the O_2^- can be converted to the highly toxic $^{\cdot}HO$. The point here is that ROS are intermediates in an alternate electron transport pathway and can potentially cause oxidative damage to cellular components. ROS are also produced during

various stress conditions, e.g. exposure to high intensity or ultraviolet light, high temperature stress (heat shock), hyperosmotic stress, nutrient deprivation and heavy metal [135]. Excessive ROS are toxic because they induce oxidative damage of diverse molecules; thereby affecting physiology at all levels, from molecules to organ systems. Indeed, ROS damage has been proposed to be an underlying cause of aging and many diseases, including cancer and neurodegenerative diseases [136].

In addition to their adverse and toxic effects, the steady-state level of ROS can be used to monitor the stress levels experienced by plants. Since the over-accumulation of ROS can result in cell death, their levels must be kept under tight control, a process called ROS homeostasis [134]. Cells have antioxidant systems that scavenge and detoxify intercellular ROS. In chloroplasts, these include the enzymes superoxide dismutase (SOD), ascorbate peroxidase (APX) and glutathione peroxidase (GPX) [137]. The enhanced production of ROS can also act as signals to activate stress responses and defense to oxidative stress [138]. One such response is programmed cell death (PCD) by either apoptosis or necrosis [139]. Due to the importance of oxidative stress to health and disease of humans, livestock and agricultural plants, intensive research is addressing questions at each of these levels.

The major ROS targets have been considered to be proteins, DNA and lipids. However, RNA has recently been added to this list as a ROS-induced damage target. For example, RNA oxidative damage may be an early event in the development of Alzheimer's disease and other neurodegenerative diseases [140]. RNA is damaged more readily than DNA due to its single-stranded structure, abundance, close localization to mitochondria and less protection by bound proteins in the cells. ROS induces the formation of 8-hydroxyguanine and 8-hydroxyguanosine

(8-oxoG) in DNA and RNA, respectively [141, 142]. Compared to the other types of oxidized purines and pyrimidines, 8-oxoG is the most abundant base due to the high reactivity of guanine [143]. The amount of 8-oxoG in both RNA and DNA can be detected by HPLC-ECD and HPLC-MS/MS in the isolated RNA and DNA as well as some cell lines [144]. Moreover, 8-oxoG can also be recognized by a commercial antibody and therefore subjected by quantification by immunodetection, ELISA, or immunoprecipitation [143]. Thus, 8-oxoG is used as a common marker to show the level of RNA oxidation. It should be noted that RNA oxidation could be in many forms other than 8-oxoG, such that the actual level of RNA oxidation can be higher than the detected 8-oxoG level. The oxidized bases in mRNA can slow the translation process and so decrease protein expression due to ribosome stalling [145]. Oxidized RNA can also produce non-functional proteins or short peptides that risk to aggregate or disrupt the functions of their partner proteins [140].

RNA oxidation also has a regulatory function in the cells. For example, oxidation of specific RNAs activates seed germination [146].

Organisms have systems for RNA surveillance and quality control. The mechanisms by which cells handle oxidized RNA still remain largely unknown. Cells could protect intact RNA from oxidation or degrade/ repair oxidized RNA as required.

Damaged RNA can be removed from the functional pool through degradation by ribonucleases, although little is known about this process because the selective degradation activity for oxidized RNA has not been identified [136]. However, the rapid degradation of oxidized RNA suggests the presence of a specific degradation mechanism. The oxidized RNA amount dropped to the normal level within one generation time in *E. coli* after removal of

oxidant [147]. The authors proposed that a selective degradation mechanism of oxidized RNA must happen in the cells for such a quick reduction to occur.

The multifunctional protein polynucleotide phosphorylase (PNPase) also plays an important role in mitigating RNA oxidation in various organisms. It has a higher affinity to the oxidized RNA than non-oxidized one [148]. PNPase deficiency leads to a hypersensitive phenotype to UV and H_2O_2 [149]. The PNPase mutant in *E. coli* showed higher 8-oxoG level in RNA under oxidative stress and this could be corrected by transformation of plasmid containing PNPase [148]. The human PNPase (hPNPase) is localized to the intermembrane space of mitochondria [150]. In Hela cells, the level of 8-oxoG RNA was elevated when PNPase was knocked down while the effect was opposite when PNPase was over-expressed [151]. How PNPase controls RNA oxidation is still unclear. It could selectively degrade the oxidized RNA or help to maintain stability of mitochondria under oxidative stress [143].

Several other RNA-binding proteins may also function in the oxidized RNA quality control. They all have an oxidized RNA-binding activity, such as mammalian Y box-binding protein I (YB-1), AU-rich element RNA binding protein 1 (Auf 1) and Ro autoantigen [152-154]. Lacking these proteins in the cells could cause hypersensitivity to the oxidant [155].

The repair of oxidized RNA is not as well understood as it is for oxidized DNA. The 8oxo-dG/C base pair in DNA can be repaired in the base excision repair pathway involved in a DNA glycosylase (OGG1), AP endonuclease APE1, DNA polymerase (Pol) β, and DNA ligase I [156]. This mechanism is not known to occur in the repair of oxidized RNA. However, the alkylation damage in RNA is repaired in the same way as DNA by hydroxylation of the methyl group [156]. Moreover, APE in DNA repair is also involved in rRNA quality control by acting as

apurinic/apyrimidinic endonuclease [157]. MutT protein in *E. coli* is known to hydrolyze some ribonucleotide analogs as well as 8oxo-dGTP [158]. This offers a possibility that MutT protein can hydrolyze 8-oxo-GTP to 8-oxo-GMP to control the RNA quality at the transcriptional level when using nucleotides to form RNA [159].

Two types of RNA granules, stress granules (SGs) and processing bodies (P-bodies), are proposed to be cytoplasmic locations of oxidized RNA quality control (Mentioned below). SGs are large non-membrane cytoplasmic ribonucleoproeins (RNP) complexes which response to multiple stress stimuli [160]. SGs recruit oxidized RNA binding protein like YB-1 and Auf 1 when they form under oxidative stress conditions [152, 161]. P-bodies are associated with RNA turn over and increase in size and number during the oxidative stress and contain the RNA degradation machinery [162]. Both of these two RNA granules are involved in RNA metabolism under physiological and stress condition [155].

1.6.2 Cytoplasmic mRNPs

The life event of mRNA, such as processing, localization, translation and degradation is controlled by mRNPs [163]. In addition to non-translated mRNAs, the mRNP contain RNA-binding proteins and non-coding RNA as major components. The mRNPs assemble and grow into a visible size in the eukaryotic cytoplasm, like P-bodies and SGs, the two most well known RNA granules.

Although, different mRNPs contain some cellular contents that are specific to them, the RNP granules have some common features. They all need non-translated mRNA and share some RNA-binding proteins and mRNA species [164-166]. Some mRNP granules interact with each other by docking and fusing [167]. Several types of mRNP granules have common mechanisms

of assembly, for example, they all require non-translating RNA, self-interaction domains in the granule proteins, cytoskeleton with motor proteins and protein modifications like phosphorylation, acetylation and ubiquitination [168]. The principles of mRNP granules disassembly are associated to the re-entry of the mRNA from the RNA granule to translated pool on polysomes [169]. In addition, mRNA decay could also disassemble the mRNP [163]. Any modification to impair the protein interaction and granule scaffolds can cause granules disassembly [170, 171]. Two recent studies also show that mRNP granules can also be cleared by autophagy [172, 173].

1.6.3 Stress granules and processing bodies

SGs contain translation initiation factors, translationally stalled RNA, small not large subunit of ribosomes. Their formation needs the phosphorylation of the eukaryotic translation initiator 2 (eIF2) [174]. The SGs are remarkable with their dynamic nature: they can assemble very quickly in response to stress and disassemble quickly when stresses are removed [169]. Additionally, stabilizing mRNA on the polysomes or disassembling polysomes with antibiotic indicates that the SGs are in a dynamic equilibrium with polysomes. There is an mRNA shuttle between SGs and polysomes when the stress conditions change [166].

Despite the intensive research on SGs, their functions have not been demonstrated. There are several hypothesizes based on a partial inventory of SG components and the fact that they form during stress. First, The assembly of the SGs offers a docking place with high local concentrations of protein factors and substrate mRNAs to favor forward reactions in repair processes [168]. For example, SGs are enriched with mRNA and translation initiation factors, possibly to favor translational initiation reactions and re-entry of these mRNAs to the translating

pool. Secondly, keeping the mRNA and protein in the SGs may separate biochemical reactions that could affect each other [175, 176]. Third, since the primary components of granules are mRNPs, which participate in every step of mRNA life cycle, the hypothesized functions of SGs could relate to mRNAs metabolism and quality control [163]. For example, mRNA could be stabilized in SGs by recruiting stabilizing proteins, such as HuR and Pab1. Moreover, the deadenylation is also inhibited in SGs [177, 178]. As mentioned above, the recruitment of oxidized RNA binding protein Auf1 and YB1 to the SG suggests that SG is also involved in control of RNA oxidation under stress condition [152, 153].

P-bodies are another kind of RNA granule in the cytoplasm. These RNA-granules increase in size and number during stress, but are also present under physiological conditions [162]. Like stress granules, P-bodies contain translationally repressed mRNA. In addition, they contain proteins related to mRNA decapping and the mRNA decay machinery: Dcp1p/2p [179-181] and the 5’ to 3’ exonuclease, Xrn1p [182]. The function of P-bodies is, therefore, presumed to relate to translational repression, mRNA decapping and degradation. P-bodies and stress granules have some common components, like the cap-binding factor eIF4E, CPEB and the tristetraprolin proteins (TTP) suggesting they may have some common functions related to translational control and mRNA stability [167, 183]. The formation of SGs is dependent on P-bodies while the formation of PBs is independent of SGs. Some protein like TTP can promote the docking between PBs and SGs to let the RNP move from one to the other.

1.6.4 Chloroplast stress granules (cpSGs)

Stress granules can also form in the chloroplast of *C. reinhardtii*. cpSGs can form under various stresses, such as hydrogen peroxide, UV, nutrient starvation and DCMU treatment, but

not following heat shock or osmotic stress. cpSGs have similar components as cytoplasmic SGs; untranslated mRNAs, translation initiation factors, the small (but not the large) ribosomal subunit, and mRNA binding proteins as assembly factors [38]. Moreover, cpSGs also contain the large subunit of ribulose bisphosphate carboxylase-oxygenase (Rubisco). RBCL in cpSGs is probably not enzymatically active, because cpSGs are not enriched for the small subunit of Rubisco (RBCS), which is required for Rubisco activity [184].

As mentioned above, RBCL in cpSGs may have a role as an assembly factor because this protein was shown to have a cryptic RNA-binding activity that is activated under oxidizing conditions in *C. reinhardtii* and vascular plants [54, 185-187]. RBCL also can form complexes as large as polysomes under stress conditions [186]. During oxidative stress, the Rubisco holoenzyme disassembles into RBCL and RBCS, whereupon most RBCS is degraded and RBCL becomes competent to bind RNA with little or no sequence specificity. Thus, the excess of RBCL is potentially for cpSG formation. These properties of RBCL would be expected for a cpSG assembly factor. In this model, RBCL concurrently binds to mRNAs, or one mRNA and another RBCL, thereby forming mRNP assemblies of indefinite size. Other proteins may bind by virtue of their association with these mRNAs or other proteins bound to them.

Chapter 2: RBCL mitigates RNA oxidation in *C. reinhardtii*.

Note: many of the results in this chapter are described in a manuscript authored by myself, my colleagues and Dr. William Zerges (Appendix II).

2.1 Introduction

Reactive oxygen species (ROS) can cause oxidative damage to diverse biological molecules [134]. Most studies have focused on the mechanisms and consequences of oxidation of DNA, proteins and lipids. Recently, RNA has been recognized as another important target of oxidation [155]. For example, RNA oxidation is an early event in neurodegenerative diseases, such as Alzheimer's disease [188]. In addition, the oxidation of RNA can be regulatory or involved in a signalling pathway [146, 189]. RNA oxidation level can be detected by the level of a modified base induced by ROS; 8-oxoguanine (8-oxoG). 8-oxoG is the most common oxidized base and, therefore, it is widely a used marker of oxidative damage to both RNA and DNA [190].

Compared to the many known antioxidant systems dedicated to DNA, proteins and lipids, systems that manage RNA oxidation are still poorly understood. It has been proposed that RNA oxidation may be managed in the cytoplasmic RNA granules, such as SGs and P-bodies (see Chapter 1) [191]. The recruitment of oxidized RNA-binding protein, such as Auf 1 and YB-1, to SGs under oxidative stress suggests that SGs are a location of quality control of oxidized RNA [152, 153]. "Quality control" refers to the specific recognition of aberrant molecule and its repair or selective degradation. P-bodies increase in number and size during oxidative stress and they are known to contain RNA decay machinery [192]. The normal RNA decay mechanism could also apply to the oxidized RNA degradation, although this has not been demonstrated to

my knowledge. While our understanding of the quality control of oxidized RNA is advancing, the precise mechanisms are still unknown.

In the chloroplasts of green algae and plant, antioxidant systems and molecular quality control are particularly important because photosynthesis generates ROS [134]. While chloroplasts are known to have quality control systems for oxidized DNA, proteins, and lipids [193], nothing is known about how they manage oxidized RNAs. A former student in our laboratory, James Uniacke, found a SG-like structure in the chloroplast of *C. reinhardtii,* which are identified as cpSGs [38]. Like SGs, the cpSGs could play a role in handling oxidized RNA. Analyses of the composition of cpSGs revealed a factor which could be related to cpSG function in controlling RNA oxidation; the large subunit of Rubisco holoenzyme (RBCL).

RBCL has an RNA-binding activity under oxidizing condition and this may be required for its recruitment to the cpSGs [38, 54]. RBCL in the cpSGs is not paired with RBCS. RBCL in cpSGs should have another independent “moonlighting” function in addition to its known function in photosynthesis [38] [54]. We hypothesized that RBCL can mitigate RNA oxidation by protecting RNA from oxidation, or repairing oxidized RNA with RBCL-associated proteins, or selectively degrading them. The proposed function that RBCL mitigates the oxidation of RNA, agrees with the definition of antioxidant as a molecule that inhibits or delays the oxidation of other molecules [194]. Hereafter, I refer to this “moonlighting” function of RBCL as “an antioxidant function”.

In this chapter, my results show that RBCL has a Rubisco independent function, which is required for cell survival and viability during oxidative stress and to control the level of oxidized RNA in the chloroplast. The 8-oxoG containing RNA was found to localize within the pyrenoid,

the main intracellular reservoir of Rubisco [195]. A complex about 100 KDa which contains RBCL is also identified by the non-denaturing gel and size-exclusion chromatography as the possible form to confer the "moonlighting" function of RBCL.

2.2 Materials and Methods

The strains I used in this Chapter are listed below:

Strain Name	*rbcL*	*RBCS*	Rubisco/ photosynthetic	Parental strain	Mutation
4A+ (CC-4051) (wild-type)	+	+	+	/	/
ΔrbcL-MX3312	-	+	-	CC-3269 mt+	Replacement of *rbcL* gene by *aadA* [10]
ΔRBCS-dim1	+	-	-	*4A+* (CC-4051)	Deletion of the 2 *RBCS* genes (*RBCS1* and *RBCS2*) [196][9]
ΔrbcL; ΔRBCS (double mutant)	-	-	-	*ΔrbcL-MX3312 & ΔRBCS*	Progeny from crossing two parental strains
ΔRBCS-RBCS2 (rescue mutant)	+	+	+	*ΔRBCS-dim1*	*RBCS2* gene on pSS2 plasmid was transformed back to *ΔRBCS-dim1*

Table 2.1 Strains used in the phenotypic analyses.

Survival and viability tests.

Because Rubisco mutants are highly light-sensitive [137, 197], all cultures were grown and tested in the dark on Tris-acetate phosphate (TAP) medium and at 24^{o}C with orbital shaking [198]. Growth curves were obtained using cultures inoculated with 5 x 10^5 cells/ml in TAP medium, whereupon cell density was measured at OD_{720} and verified by cell counts obtained with a haemocytometer. It was critical to test cultures in mid-exponential growth phase with cell densities in the range of 2-4 X 10^6 cells/ml. Cell survival and viability were assayed following addition of H_2O_2 to 4.0 mM. Cell survival was determined by counting the proportion of live cells with the Trypan blue exclusion assay (Sigma-Aldrich). Viability was determined as colony forming units on agar-solidified non-selective TAP medium by plating 10^3 cells at each test hour.

Analysis of oxidized RNA and DNA

Oxidized RNA and DNA were quantified using aliquots of the same cultures. Where indicated, cells were pre-incubated with 100 µg/ mL chloramphenicol or 100 µg/ mL lincomycin for 15 min. Cells were treated with 2 mM H_2O_2 for 15 min prior to the collection where indicated. Total RNA was extracted using the TRI-reagent (Sigma-Aldrich) according to the manufacturer's protocol. Total DNA was extracted using hexadecyltrimethylammonium bromide, as described previously [199]. RNA and DNA concentrations were quantified with a 2100 Bioanalyzer (Agilent) and from OD_{260} values obtained with a UV spectrophotometer, respectively. Total RNA (5 µg) and DNA (1 µg) samples were transferred to a 0.45 µm pore size nitrocellulose membrane (Bio-rad) with a Minifold-II slot blot system (Schleicher & Schuell). Filters were blocked with 5% (w/v) non-fat dried milk in 1XPBST (NaCl 137 mM, KCl 2.7 mM, Na_2HPO_4 10 mM, KH_2PO_4 1.8 mM, Tween 20 0.1%) at room temperature for 1 h and reacted with a commercial antibody against 8-oxoG with 1:500 dilution (QED Bioscience Inc., clone 15A3) overnight, at 4 ^{o}C [200]. A goat anti-mouse secondary antibody (KPL) was used and ECL detection was performed with a commercial kit (Millipore). Quantification and statistical analyses of the signals were carried out as describe in the previous paper [201]. This quantification was complicated by the fact that each replicate gave only relative signal ECL strengths for RNA (or DNA) from each of the strains and conditions. Therefore, because the signal strength from the *ΔrbcL* RNA was consistently high, it was designated as 100% and the ECL signals from the other samples were expressed as a percentage value. One sample t-tests were used to ask whether the average ECL signal differed from 100%.

***C. reinhardtii* microscopy and IF-staining.**

The protocols for cell fixation, permeabilization, and IF staining in *C. reinhardtii* were reported

previously [202]. Where indicated, slides were treated for 1h at 37^{o}C with 10 µg/ml RNase or 50 µg/ml DNase, following cell fixation and permeabilization. 8-oxoG was immunodetected with a monoclonal mouse antibody (QED Bioscience Inc., clone 15A3). For the antibody block experiment, 1 µg of antibody against 8-oxoG was pre-incubated with 10 µg 8-OHdG (Sigma-Aldrich) for 3 h before probing. *psbA* mRNA probe conjugated with Alexa Fluor 488 (Invitrogen Inc.) was used in the FISH experiment. Rabbit antibodies were used to immunodetect RBCL (Agrisera AS03037), the 30S subunit chloroplast ribosomal-protein (S-20) and a stromal protein; HSP70 [203]. Secondary antibodies were: Alexa Fluor 488 goat anti-mouse IgG and Alexa Fluor 568 goat anti-rabbit IgG (Invitrogen Inc.). Images were acquired by epifluorescence microscopy using a Leica DMI 6000 microscope (Leica Microsystems) with a 63X/ 1.4 oil objective, a Hamamatsu OrcaR2 camera and Volocity acquisition software (Perkin-Elmer). Z-stacks were taken by series capture at a thickness of 0.2 µm per section. Stacks were deconvoluted with AutoQuant X3 (Media Cybernetics Inc.) [204]. Co-localization pattern was determined by the co-localization finder plugin of ImageJ.

Sucrose Density Gradient Ultracentrifugation

Cultures with a cell density of 2-4 X 10^6 cells/ mL and in exponential growth were collected by centrifugation at 5000 rpm for 5 min and immediately frozen in liquid nitrogen. The frozen pellet was ground to a power with a mortar and pestle on dry ice. The resulting frozen cell "grindate" was transferred to a pre-chilled tube and 5 volumes of extraction buffer (0.2 M Tris-Cl [pH 9.0], 0.2 M KCl, 35 mM $MgCl_2$, 25 mM EGTA, 0.2M sucrose, 1% Triton x-100 [v/v], 0.5 mg/ml heparin, 0.7% β-mercaptoethanol [v/v], 0.03 mg/ml PMSF) were added. The samples were resuspended and then maintained on ice for 10-15 min. Sodium deoxycholate was added to a

final concentration of 0.5% (wt/v). Samples were incubated on ice for 5 min. After centrifugation at 14,000 rpm at 4^{O}C for 20 min, the supernatant was loaded onto a 15%-55% continuous sucrose gradient (40 mM Tris-Cl [pH8], 20 mM KCl, 10 mM $MgCl_{2,}$ 0.5 mg/ml Heparin). The gradient was dispensed using an Econo pump (Bio-Rad). The gradients were centrifuged at 35, 000 rpm for 65 min, at 4 ^{O}C (Beckmen Optima XL-100K Ultracentrifuge, SW T41 rotor). Fractions of 1 ml were collected through a needle which pierced the bottom of the centrifuge tube. Fractions in microfuge tubes were frozen and maintained at -80 ^{O}C.

Polyacrylamide gel electrophoresis under non-denaturing conditions

Non-denaturing polyacrylamide gel (5% [wt/v] acrylamide containing 0.2% [wt/v] *N,N'*-methylene-bisacrylamide) electrophoresis was carried out as described previously [205]. Samples of fractions collected from the polysome-containing fractions of a sucrose gradient were loaded on the gel and electrophoresis was carried out at 10 mA for 16 h at 4 ^{O}C. High molecular weight native markers were used to identify the size of bands (GE).

Immunoblot of the non-denaturing gel

All procedures followed standard protocols [206]. Proteins on non-denaturing gels were electro-transferred to PVDF membrane at 300 mA for 2.5 h in transfer buffer (25 mM Tris, 190 mM glycine, 0.1% SDS [w/v] and 20% methanol [v/v]). RBCL was detected using a commercial polyclonal rabbit antibody from Agrisera (AS03037) at a 1:2000 dilution. A chemiluminescent HRP substrate (ECL) (Milipore) was used and the chemiluminescent signal was collected by film (Hyblot) and developed in a Kodak developer.

Size-exclusion chromatography

To identify the protein complex in the *ΔRBCS*, cells in a 300 ml culture of *ΔRBCS* cells were

pelleted by centrifugation (4,000 x g, 5 min), frozen in liquid nitrogen and then ground with a mortar and pestle to a fine power in lysis buffer (0.2 M Tris-Cl [pH 9.0], 0.2 M KCl, 35 mM $MgCl_2$, 25 mM EGTA, 0.2 M Sucrose, 1% Triton X-100 [v/v], 0.5 mg/ml Heparin, 0.03 mg/ml PMSF). Thawing this material gave cell lysates, which were concentrated using 10 kDa Amicon Ultra centrifugal filter units (Fisher). Protein concentration was determined by standard BCA assay (Thermo scientific). 5 mg samples were loaded either onto a HiLoad 16/600 Superdex 200 pg column or a Superose 12, 10/300 GL column (GE Healthcare). The Amersham Pharmacia AKTA Explorer 10 chromatography system was used to separate the proteins according to their sizes and collect the fractions (1 mL each). The first 6 mL of an elute was discarded. Elution was performed with gel filtration buffer (10 mm EDTA, 10 mm Tricine/KOH pH 7.5, and 5.0 mM KCl) at 1 mL/ min flow rate. Fractions were analyzed by SDS-PAGE and immunoblotting, as described above for the non-denaturing gels.

Detection of the mRNA levels of the ROS induced genes

Levels of marker transcripts of oxidative stress were measured with the Quantigene2 assay (Panomics Inc.) following the standard protocol. The marker genes are glutathione peroxidase 5 (*GPX5*) (XM_001698523), which is induced by singlet oxygen and glutathione S- transferase 2 (*GSTS2)* (XM_001699214), which are induced by various oxidative stresses [207]. Transcript levels were normalized to the level of the transcript of *RPS26* (XP_001691901). Then the normalized transcript levels in the mutant strains were compared with that in wild-type strain (100%) to generate a bar graph.

2.3 Results

2.3.1 RBCL is required for tolerance to H_2O_2.

I used a genetic approach to determine whether an oxidative stress condition that is associated with cpSG assembly necessitates an unknown novel function of RBCL. Cultures of an *rbcL* null mutant, *ΔrbcL-MX3312* (hereafter "*ΔrbcL*") and a wild-type strain were exposed to a toxic concentration of H_2O_2 (4.0 mM) and the percentage of live cells in each culture was monitored at each hour over an 8 h time course experiment (Fig. 2. 1 A). Prior to the addition of H_2O_2, cultures of *ΔrbcL* and the wild-type strain grew at similar rates and showed no evidence of oxidative stress (Sup Fig 2.1). Following the addition of H_2O_2, I found that *ΔrbcL* cells died significantly faster than did the wild-type cells (Fig. 2.1 A). These results revealed that RBCL is required for H_2O_2 tolerance, consistent with a putative oxidative stress tolerant function of this protein.

Rubisco-deficient mutants lack photosynthesis, photorespiration, and a pyrenoid [208, 209]. To determine whether one or more of these defects impairs H_2O_2 tolerance in *ΔrbcL*, we tested another Rubisco-deficient mutant, *ΔRBCS-dim1* (hereafter *"ΔRBCS"*), which carries a deletion of the two nuclear genes but is wild-type for the *rbcL* gene [196]. If one or more Rubisco-dependent traits are involved in H_2O_2 tolerance, then both Rubisco-deficient mutants should show similarly impaired H_2O_2 tolerance. Alternatively, if a Rubisco-independent function of RBCL is involved, *ΔRBCS* should be more H_2O_2 tolerant than *ΔrbcL*. In this case, we expected a marginal difference because *ΔRBCS* accumulates RBCL to 1-10% of the wild-type level (Zhan et al. submitted, Fig 4, Appendix II). Surprisingly, *ΔRBCS* showed even higher H_2O_2 tolerance than that of the wild-type strain (Fig. 2.1 A). The H_2O_2 hypertolerance of *ΔRBCS* was also observed in

a more stringent viability assay measured as the percentage of the initial CFU (Fig. 2.1 B). The finding that *ΔrbcL,* but not *ΔRBCS*, is impaired in H_2O_2 tolerance supports our hypothesis that RBCL has a Rubisco-independent function and that this function affects tolerance to a ROS. The unexpected H_2O_2 hypertolerance of *ΔRBCS* suggests that the RBCL in this mutant has *enhanced* antioxidant activity relative to the RBCL in the wild-type strain. This could reflect greater availability of RBCL for the moonlighting function in the control of oxidized RNA when it cannot be assembled into the Rubisco holoenzyme complex.

Substantiation of our hypothesis that RBCL has a Rubisco-independent function required the following control experiments to rule out alternative hypotheses. For example, if the H_2O_2 hypertolerance of *ΔRBCS* is due to genetic background or epigenetic effects, then it would not serve as a control for effects of the Rubisco-deficiency of *ΔrbcL*. This is not the case; transformation of *ΔRBCS* with *RBCS2* reduced its H_2O_2 tolerance to the wild-type level (Fig. 2.1 C and D). The H_2O_2 hypertolerance of *ΔRBCS* is not due to deficiency for some unknown function of RBCS; a double mutant lacking both RBCL and RBCS showed impaired H_2O_2 tolerance similar to that of *ΔrbcL* (Fig. 2.1 E and F). In other words, the hypertolerance of *ΔRBCS* is RBCL-dependent and not due to RBCS deficiency *per se*. Finally, the differences in H_2O_2 tolerance between the strains do not reflect inherent differences in oxidative stress, viability (Sup Fig. 2.1). Therefore, we propose that RBCL has a Rubisco-independent function.

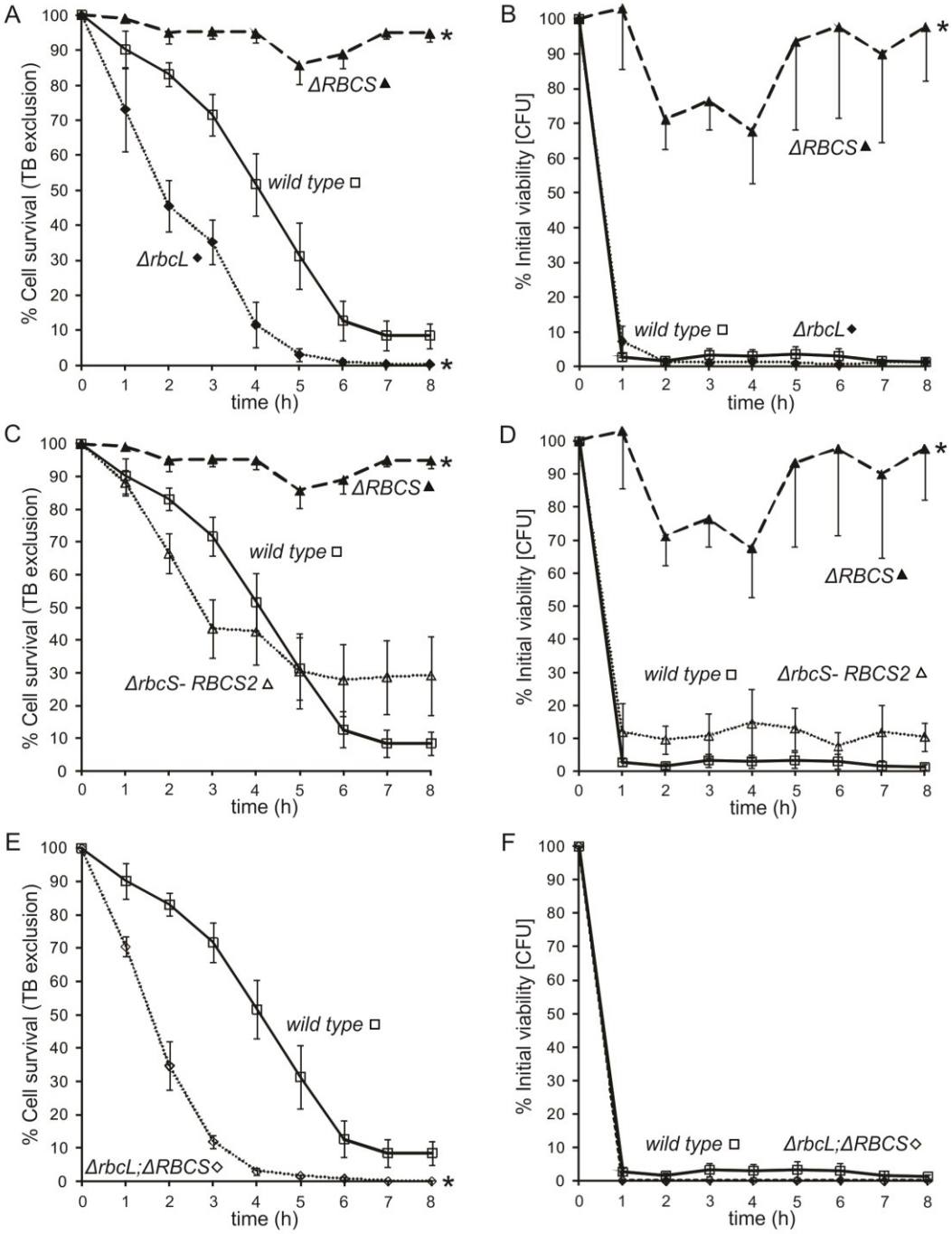

Figure 2.1 RBCL functions in H_2O_2 tolerance. Following addition of H_2O_2, cell survival (*A*, *C*, *E*) and viability (*B*, *D*, *F*) were monitored as Trypan blue exclusion and CFU concentration (1000 cells plated), respectively, and graphed as the mean percentages of the initial values (i.e. immediately prior to H_2O_2 exposure). The strains analyzed are indicated in each panel. Asterisks indicate a significant difference from the *wild-type* strain, as determined by mixed analysis of variance (ANOVA) ($p \leq 0.05$).

2.3.2 RBCL is an RNA antioxidant.

We examined whether RBCL functions in the control of oxidized RNA as an RNA antioxidant. As stated above, RNA bound by RBCL might be protected from oxidation or, once oxidized, be repaired or degraded by RBCL-associated proteins. In any of these cases, the level of such an RBCL function would determine the level of oxidized RNA that accumulates in the chloroplast. To determine whether RBCL functions as an RNA antioxidant, we measured the relative levels of oxidized RNA in the mutant and wild-type strains (described above) by comparing their levels of 8-oxoguanine (8-oxoG) (Chapter 1.4.1) [191] (Fig. 2.2 A). The results of immuno-slot-blot analyses using a commercial antibody against 8-oxoG revealed a significantly higher mean level of oxidized RNA in *ΔrbcL* than in either the wild-type strain or *ΔRBCS*. The high mean 8-oxoG RNA level in *ΔrbcL* is not due to Rubisco-deficiency because *ΔRBCS* showed an even lower mean level of 8-oxoG RNA than that of the wild-type strain (Fig. 2.2 A). The low mean 8-oxoG RNA level in *ΔRBCS* is not due to genetic background effects because transformation of this mutant with a wild-type copy of *RBCS2* restored the 8-oxoG RNA level to nearly that of the wild-type strain (Fig. 2.2 A). Finally, the low 8-oxoG RNA level from *ΔRBCS* is not due to its deficiency for some unknown RBCS function because a double mutant lacking both RBCL and RBCS showed high mean 8-oxoG RNA levels, similar to that of *ΔrbcL* (Fig. 2.2 A). Therefore, we propose that RBCL controls the level of oxidized RNA independently of Rubisco, consistent with the proposed function in the control of oxidized RNA.

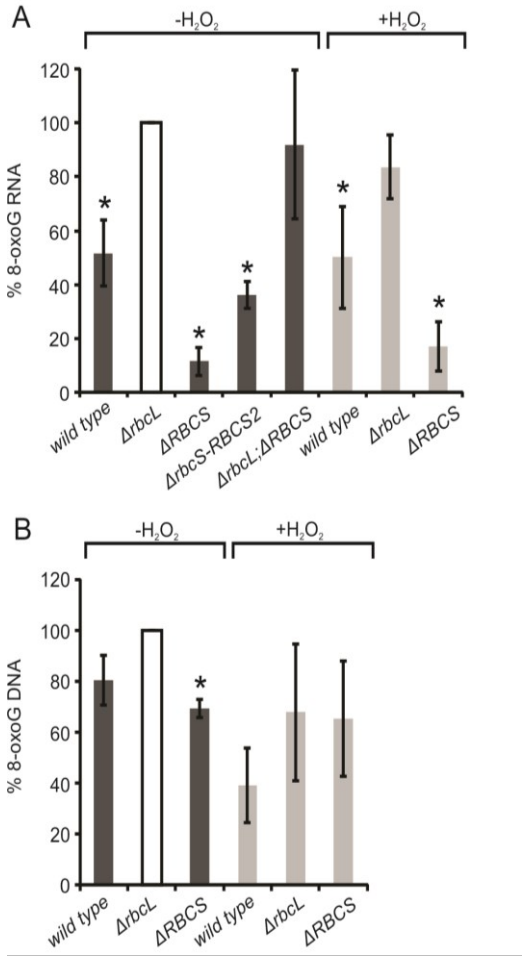

Figure 2.2 RBCL controls the level of oxidized RNA, but not the levels of oxidized DNA. A) Levels of 8-oxoG in RNA from the wild-type strain, *ΔrbcL*, *ΔRBCS*, the rescued-*ΔRBCS*, and the double mutant are shown (dark bars). Levels of 8-oxoG in RNA from cells exposed to 2.0 mM H_2O_2 were analyzed from the wild-type strain, *ΔrbcL*, *ΔRBCS* (grey bars). Bar height represents the percentage of 8-oxoG enhanced chemo-luminescent signal of *ΔrbcL* strain before stress (white bar; 100%). *B*) The relative levels of 8-oxoG in DNA from the wild-type strain, *ΔrbcL*, and *ΔRBCS* are presented as described for RNA in panel A. Results were analyzed and are presented as described in Materials and Methods. Error bars indicate the standard error of the mean. Asterisks indicate a significant difference from *ΔrbcL*, as determined by one-sample t-tests ($p \leq 0.05$).

Exposure of the cells to H_2O_2 did not significantly change the mean level of 8-oxoG RNA in the wild-type strain, *ΔrbcL*, or *ΔRBCS* (Fig. 2.2 A). These results suggest that the Rubisco-independent function of RBCL in the control of oxidized RNA is constitutive, i.e. that it acts under both non-stress and stress conditions.

RBCL deficiency in *ΔrbcL* was not associated with an elevated mean level of 8-oxoG in total DNA, relative to the wild-type strain (Fig. 2.2 B). The level of 8-oxoG in DNA was higher in *ΔrbcL* than in *ΔRBCS*. We did not consider the latter as supportive of a role of RBCL in controlling the level of oxidized DNA because this difference was 1.4 fold versus 10 fold for the same comparison of 8-oxoG in RNA and because there was no significant difference in the level of 8-oxoG in DNA between *ΔrbcL* and the wild-type strain (Fig. 2.2 B). Treating cultures with H_2O_2 increased the variability between biological replicate experiments but did not increase the mean levels relative to DNA from the non-treated cultures (Fig. 2.2 B). The detection of level of carbonylated amino acid as a marker of protein oxidation also did not show significant difference among all three strains (Zhan et al. submitted, Figure 4, Appendix II). Therefore, RBCL is not involved in controlling the oxidation levels of DNA or protein.

2.3.3 RBCL mitigates RNA oxidation under various stresses other than H_2O_2-induced oxidative stress

In addition to H_2O_2, could RBCL mitigate RNA oxidation under other stresses that are known to induce RNA oxidation? Various stress inducers were chosen to treat cells, like ultraviolet light and high light stress. The RNA oxidation already appeared in *ΔrbcL* before treatment with all stresses and was higher than that in *wild-type* strain (Fig 2.3). Similar to the results from the H_2O_2 treatment, no increase of 8-oxoG RNA levels was found in *ΔrbcL* under

any of these stress conditions (Fig 2.3). Levels of 8-oxoG RNA signal increased in the wild-type strain after stress treatment in this experimental trial, however, indeed the levels of 8-oxoG varied in *wild-type* strain. In RNA from *ΔRBCS*, 8-oxoG RNA was not detected before stress and it increased with the UV, Cu^{2+} treatment and two stress inducers; Rose Bengal and Methyl viologen, photosensitizers of the production of singlet oxygen and super oxide radical, respectively (Fig 2.3) [210]. However, *ΔRBCS* still showed less RNA oxidation compared to *ΔrbcL* and *wild-type* strain. Different stresses treatment did not revealed an obvious different result from H_2O_2 treatment. These results indicate that RBCL might mitigate RNA under other oxidative or non-oxidative stress conditions other than H_2O_2.

Since H_2O_2, UV and high light all induce the formation of cpSGs and RBCL is an important component of cpSGs, we were wondering if this moonlighting function of RBCL is related to cpSGs formation.

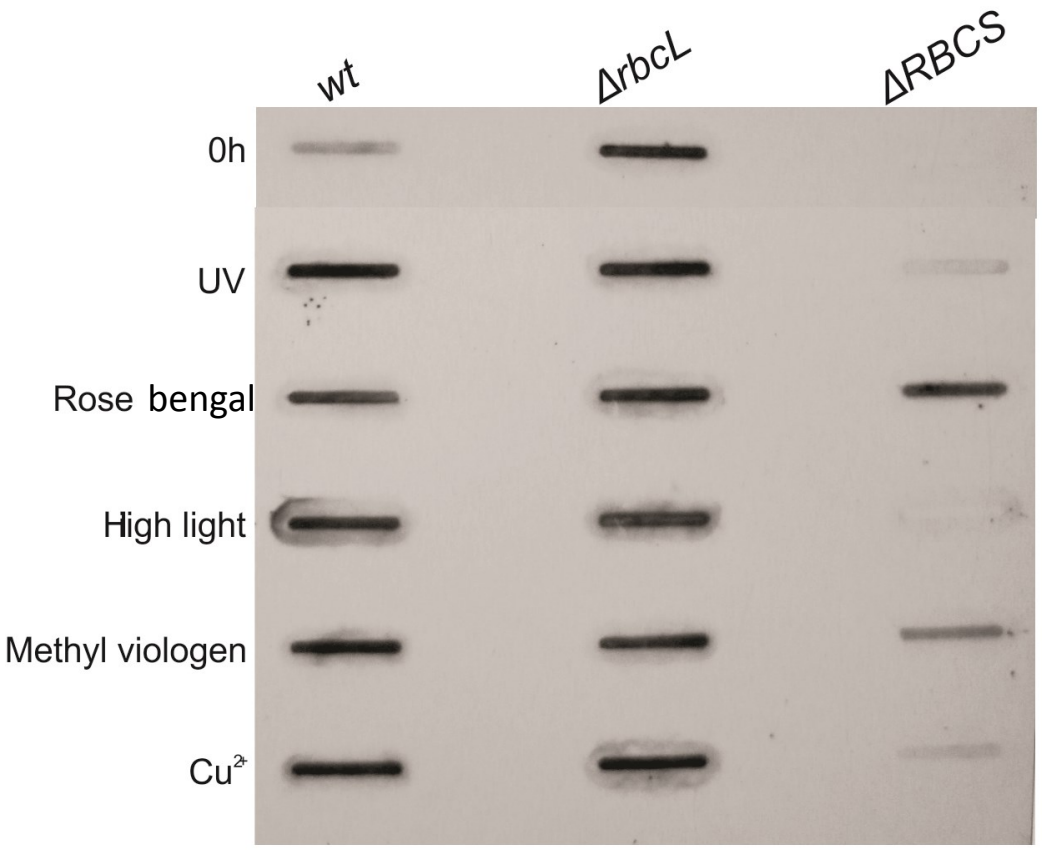

Figure 2.3 8-oxoG RNA was detected under various stresses conditions.

UV, rose bengal, high light, methyl viologen and copper were used to induce stress. Total RNA was extracted from the different stresses treated cells of the same culture of different strains and loaded on the slot blot. Levels of 8-oxoG in RNA from the wild-type strain, *ΔrbcL*, *ΔRBCS* were detected in immuno-slot blot with the commercial antibody against 8-oxoG.

2.3.4 Formation of cpSGs is related to the level of RNA oxidation.

Cytoplasmic SGs have been proposed to function in the quality control of oxidized RNA [191]. This hypothesis is based on the fact that SGs assemble under oxidative stress conditions, when RNA oxidation is presumed to be elevated. In addition, SGs recruit oxidized RNA-binding proteins [152, 161].

In order to test the hypothesis that cpSGs are involved in the control of oxidized RNA in the chloroplast, I asked whether the RNA oxidation level changes when cpSGs are stabilized or eliminated using inhibitors of different steps of translation [38]. If cpSGs are involved in controlling the level of oxidized RNA, the level of oxidized RNA should decrease when cpSGs are stabilized and increase when cpSGs are eliminated. A previous study in our lab reported that a translation inhibitor that disassembles polysomes, lincomycin, preserves cpSGs for hours [38]. By contrast, an inhibitor that stabilizes polysomes, chloramphenicol, prevents the formation of cpSGs [38]. Wild-type cells were treated with either lincomycin or chloramphenicol for 15 min prior to exposure to H_2O_2. The RNA samples from these treatments were examined by immuno-slot blot to determine the level of 8-oxoG RNA. Treatment with H_2O_2 elevated the level of 8-oxoG in RNA from the wild-type strain. When wild-type cells were treated with lincomycin, the level of 8-oxoG in RNA did not increase in response to H_2O_2 (Fig 2.4). By contrast, treatment of cells with chloramphenicol did not affect the increased 8-oxoG signal in RNA (Fig 2.4). Therefore, the prediction of the hypothesis is met; lincomycin could preserves cpSGs and lowers oxidized RNA level and chloramphenicol prevents the formation of cpSGs thus it does not reduce the level of 8oxoG compared to the samples with H_2O_2 treatment. However, it is also possible that the differences in 8-oxoG RNA reflect the assembly state of chloroplast polysomes.

For example, if mRNA or rRNA on polysomes is especially sensitive to oxidation, then this could also explain the lower level of 8-oxoG RNA in the lincomycin-treated cells (which lack chloroplast polysomes) and the elevated level of 8-oxoG of chloramphenicol treatment (which stabilizes chloroplast polysomes).

I also treated the cultures of the mutants *ΔrbcL* and *ΔRBCS* with lincomycin or chloramphenicol prior to exposing them H_2O_2 and assayed their RNA for 8-oxoG, as I did for the wild-type strain (described in the previous paragraph). In both mutants, the level of 8-oxoG RNA signal did not show much difference with or without pre-treatment of lincomycin or chloramphenicol (Fig 2.4). *ΔrbcL* showed higher RNA oxidation level while *ΔRBCS* showed lower level of oxidized RNA as showed before in Fig 2.1. According to the previous research in our lab, cpSGs were not detected in those two mutants. However, RBCL-RNP could exist in *ΔRBCS* and function consistently under physiological or stress condition.

We can take the formation of cpSGs in wild-type stain as a marker to represent the increase amount of RBCL which functions in control RNA oxidation. Thus, the formation of cpSGs was related to the RNA oxidation level in this strain. I speculate that the unchanged level of 8-oxoG RNA in *ΔrbcL* is due to its high RNA oxidation level at the physiological conditions almost arrives to the limit cells can handle. Trace amount of ROS could lead the death of this strain. The RNA oxidation level does not change because of rapid death. All the RBCL in *ΔRBCS* could form RBCL-RNPs and consistently undertake the moonlighting function before and after stress. These RNPs could let *ΔRBCS* be more resistant to treatment of 2 mM H2O2 for 15 mins. However, the level of RNA oxidation could be induced by other types of stress in *ΔRBCS* (Fig 2.3).

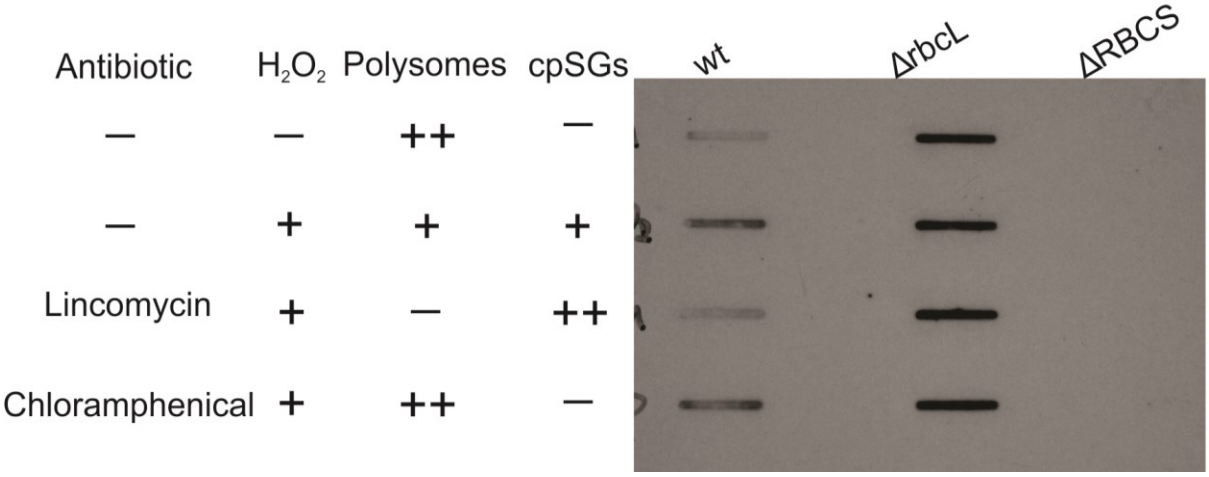

Figure 2.4 The assembly and disassembly of cpSGs effected the 8-oxoG RNA level.

Total RNA (5 μg) of *wild-type* strain, *ΔrbcL* and *ΔRBCS* was isolated and loaded to slot blot. Levels of 8-oxoG in RNA were detected in immuno-slot blot by antibody against 8-oxoG. H_2O_2 was added to induce the formation of cpSGs and cause polysomes disassembly. Lincomycin or chloramphenicol pre-treatment was used to stabilize or prevent the assembly of cpSGs respectively. The "+", "++"and "-" indicates the presence and the approximate amount of different components.

2.3.5 During sucrose density gradient ultracentrifugation, oxidized RNA co-migrated with RBCL and ribosomes/monosomes, but not with polysomes.

How RBCL controls oxidized RNA is unknown and the localization of 8-oxoG RNA is relevant to understand how RBCL carries out this function. As mentioned above, when the cells were treated with lincomycin (to stabilize cpSGs), RNA oxidation did not increase in response to H_2O_2 exposure (Fig. 2.4). On the other hand, when polysomes was stabilized with chloramphenicol, the level of RNA oxidation increased with H_2O_2 treatment. One possible explanation is that RNAs maintained trapped on polysomes get oxidized more easily. In this case, polysomes would be expected to have 8-oxoG RNA. Alternatively, if oxidized bases in mRNA stall translating ribosomes or cause the mRNA to be recruited to RNP particles (such as cpSGs), then 8-oxoG RNA would be expected to be in a complex smaller than polysomes, possibly the size of ribosomes or monosomes. To determine the size(s) of complexes with oxidized RNA, I resolved ribosomes/monosomes and polysomes from the wild-type strain by sucrose gradient ultracentrifugation and 12 fractions were collected from the bottom to top. Total RNA was isolated from each fraction. According to the OD_{260} values measured of the fractions, the top fractions 1 to 4 should be ribosome subunits and monosomes and the bottom part of the gradient (fraction 7 to 12) should contain the polysomes (Fig 2.5 A). This was confirmed by the detection of mRNA *psbC* signal in bottom fractions of gradient (by the results of Northern blot analysis) (fractions 7 to 12, Fig 2.5 B). The RNA samples were examined for RNA oxidation by immunoslotblot analyses with the antibody against 8-oxoG. The 8-oxoG signal was detected on the top part of the sucrose gradient in the RNA from fractions 1-4 (Fig 2.5 C). There was no 8-oxoG RNA detected in the polysome fractions (Fraction 7-12) (Fig 2.5 C). The fact that oxidized

RNAs did not co-migrate with polysomes suggests that polysome associated RNA is not a preferential target of oxidation. 8-oxoG RNA may not be trapped on polysomes. The oxidized RNA could be on ribosomes, monosomes, in the rRNA of the ribosome subunits, or more than one of these possibilities. Alternatively, it could be in RNP particles that have the size of monosomes, but have other components. While a firm conclusion cannot be based on these results, they do provide valuable information for understanding and exploring the metabolism of oxidized RNA.

I also asked how RBCL is distributed on this polysome profile. RBCL was mostly detected in the top fractions (1-4) of the polysome gradient in by immunoblot analysis (Fig 2.5 D). There was no co-migration between RBCL and polysomes. This result showed that RBCL co-sedimented with the 8-oxoG RNA. The co-migration of RBCL and 8-oxoG RNA did not offer an evidence for their physical association, however it is consistent with the proposed function of RBCL in the control of the level of 8-oxoG RNA.

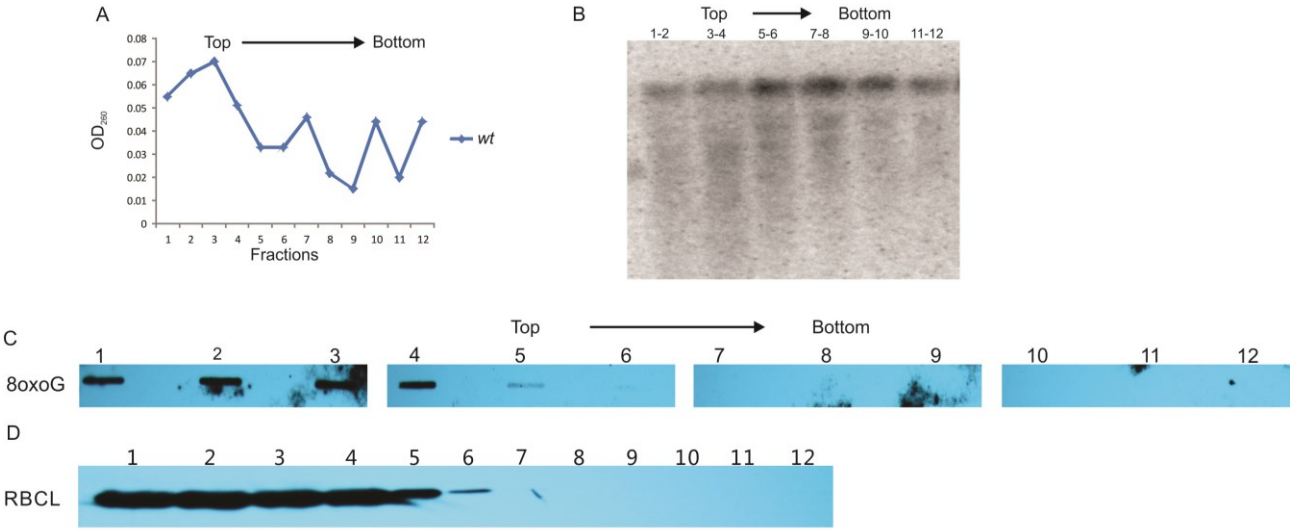

Figure 2.5 8-oxoG RNA and RBCL did not co-sediment with polysomes on the sucrose gradient.

Twelve fractions were collected from polysome isolation sucrose gradient from top to bottom. A) OD_{260} was measured by spectrophotometer of all twelve fractions. B) The distribution of *psbC* mRNA was detected by northern blot analysis. Two fractions were put together as one sample. The presence of *psbC* in the fraction 7-12 indicated the successful isolation of polysomes. C) The 8-oxoG RNA were found in the 1-4 fraction by immumo-slot blot analysis. D) Immuno-blot showed that RBCL co-sediment with 8-oxoG RNA in the top fractions 1-6.

2.3.6 Oxidized RNA localizes to the pyrenoid; the major intracellular location of RBCL.

In order to determine whether oxidized RNA accumulates in cpSGs, I characterized the distribution of 8-oxoG in *C. reinhardtii* by IF microscopy using a commercial antibody against 8-oxoG. The IF signal (Fig. 2.6 A) was specific to 8-oxoG because it was eliminated when the antibody was incubated with 8-oxoG prior to staining (Fig. 2.6 B).

Inspection of cell images in Fig. 2.6 A revealed higher 8-oxoG IF signal in the chloroplast than in the central region with the nucleus and most cytosolic compartments. The 8-oxoG IF signal was in two distinct patterns; throughout the pyrenoid and in punctate foci located either in or near the chloroplast. In order to determine whether these patterns represent 8-oxoG in DNA or RNA, we used two approaches. First, I co-stained cells with DAPI, to visualize the nucleus and the chloroplast nucleoids (the latter contain the multicopy chloroplast genome). These DNA-containing structures only weakly IF-stained for 8-oxoG (Fig. 2.6 A) and both were clearly distinct from the 8-oxoG IF-staining of the pyrenoid and foci. Therefore, most 8-oxoG is not in the genomic DNA of either the nucleus or chloroplast. Second, I asked whether RNase or DNase treatment altered the 8-oxoG IF-staining of the pyrenoid, the foci, or both. The 8-oxoG IF signal in the pyrenoid was eliminated by treatment with RNase, but not DNase, suggesting that it represents oxidized RNA (Fig. 2.6 C). By contrast the 8-oxoG IF signal in most punctate foci was eliminated by treatment with DNase, but not with RNase, suggesting it is in DNA (Fig. 2.6 D). These foci could be the DNA of mitochondria, which are often between the chloroplast and the plasma membrane [211]. These foci were not explored further here.

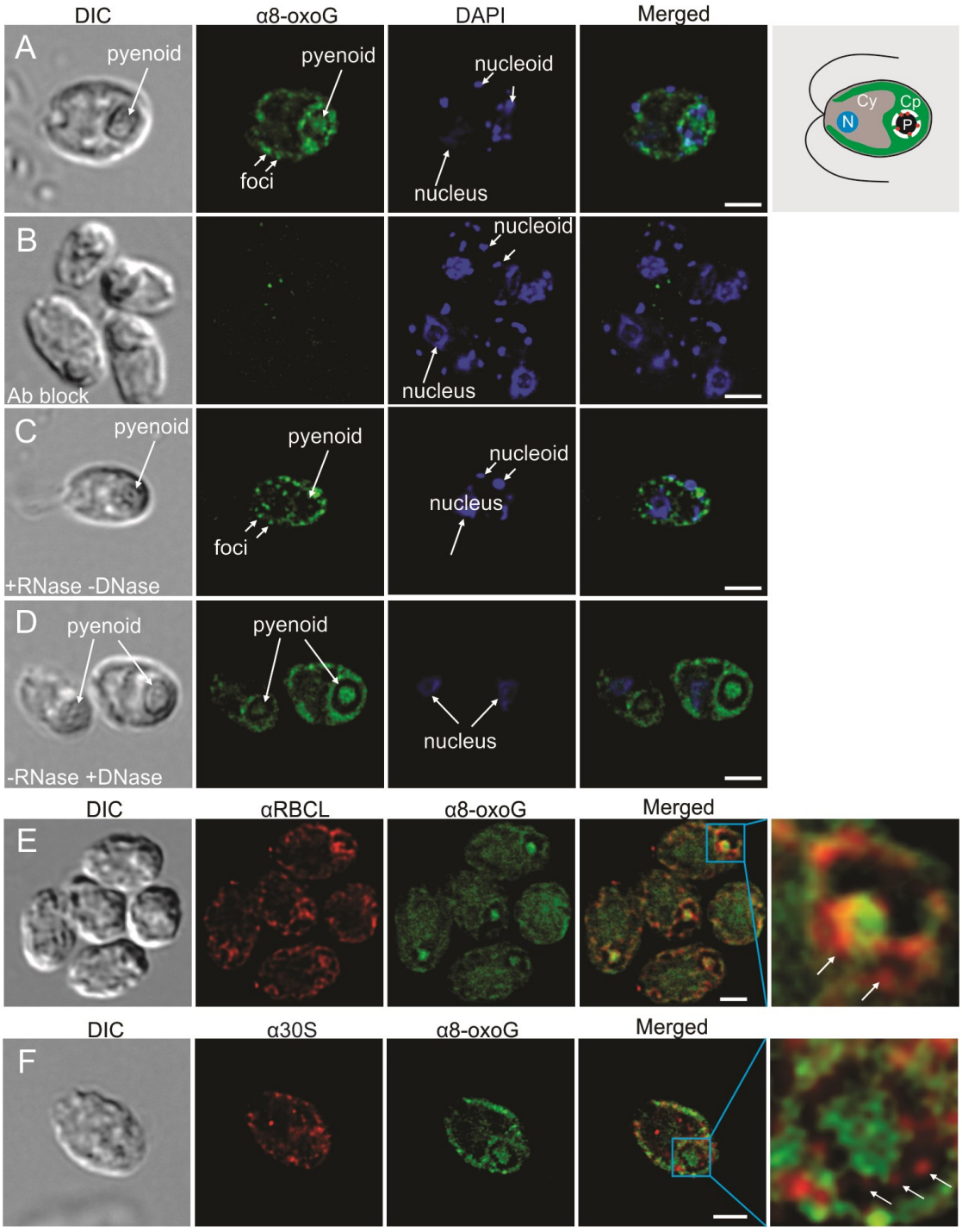
DIC
α8-oxoG
DAPI
Merged
A
pyenoid
pyenoid
foci
nucleoid
nucleus
Cy
Cp
N
P
B
Ab block
nucleoid
nucleus
C
pyenoid
+RNase -DNase
pyenoid
foci
nucleoid
nucleus
D
pyenoid
-RNase +DNase
pyenoid
nucleus
DIC
αRBCL
α8-oxoG
Merged
E
DIC
α30S
α8-oxoG
Merged
F

Figure 2.6 The *in situ* distribution of 8-oxoG RNA in Chlamydomonas. A) Wild-type cells were IF-stained for 8-oxoG (green) and co-stained with DAPI to visualize DNA. The pyrenoid is seen in differential interference contrast (DIC) images. A cell illustration (right-hand most image in A) shows the locations of the nucleus (N), cytosol (Cy), and chloroplast (Cp), wherein the pyrenoid (P) is surrounded by a starch sheath (white) and contains cpSGs (red). B) The IF signal from 8-oxoG was eliminated by pre-incubating the primary antibody with 8-oxoG. C) The 8-oxoG IF signal in the pyrenoid is sensitive to RNase (10 μg/ml) treatment. D) DNase (50 μg/ml) treatment did not reduce the 8-oxoG signal in the pyrenoid but did in the punctate foci. E and F) In cells that had been treated with 2.0 mM H_2O_2 to induce cpSG formation, the 8-oxoG IF signal (green) was seen throughout the pyrenoid and not in cpSGs (white arrows), which were IF-stained (red) for either RBCL (E) or the protein of the 30S chloroplast ribosomal subunit (F). Size bars = 5.0 μm.

I focused on the 8-oxoG IF-staining of the pyrenoid because it represents oxidized RNA and was atypical; except for the bona fide pyrenoid proteins RBCL and RBCS, we have not seen the presence in pyrenoid for any of the four chloroplast mRNAs or nine chloroplast proteins analyzed previously in the lab [38, 201, 212-214]. Therefore, 8-oxoG IF-staining of the pyrenoid represents the specific localization of oxidized RNA and is not due, for example, to nonspecific entry into the pyrenoid of chloroplast stroma, which contains RNA. Considering that the pyrenoid is the major location of RBCL, these results provide circumstantial evidence in support of the moonlighting function of RBCL.

When cells were exposed to H_2O_2, a ROS used to induce oxidative stress, the percentage of cells in which the pyrenoid IF-stained for 8-oxoG increased from 44% (n=215) to 64% (n=189). This result suggests that oxidized RNA may localize to the pyrenoid for quality control.

I then asked whether cpSGs are enriched in oxidized RNA. cpSGs were visualized by IF-staining cells for one of two cpSG marker proteins; RBCL or a protein of the 30S subunit of the chloroplast ribosome (Fig 2.6 E and F). As expected, the IF signals from these marker proteins were seen in cpSGs at the perimeter of the pyrenoid [38]. However, the IF signal from 8-oxoG remained throughout the pyrenoid and did not localize specifically in cpSGs (Fig. 2.6 E and F). Our finding that no cpSG was specifically enriched in 8-oxoG IF signal strongly suggests that cpSGs do not accumulate oxidized RNA. However, the assembly of cpSGs are related to the RNA oxidation level (Fig 2.4). Thus, instead of recruiting oxidized RNA, cpSGs may have other mechanisms to control RNA oxidation, i.e. protecting the intact RNA from oxidation.

2.3.7 cpSGs were not detected in *ΔRBCS*

ΔRBCS showed a lower mean level of RNA oxidation and higher tolerance to H_2O_2, relative to wild-type strain (Fig 2.1 and 2.2). The RNA oxidation of *ΔRBCS* is at the background level in IF (data not shown). I also found the formation of cpSGs was associated with lower level of RNA oxidation (Fig 2.4). Thus, I asked if there were constitutive or more cpSGs formed in *ΔRBCS*. If so, these cpSGs might explain the higher tolerance to H_2O_2 and low level of RNA oxidation. However, the previous study in our lab did not show the cpSGs in *ΔRBCS* (Jim Uniacke's unpublished data). cpSGs were detected at the perimeter of pyrenoids and pyrenoids offered a low background for fluorescent signal detection, but *ΔRBCS* lack a pyrenoid as a cpSGs localization indicator because the formation of pyrenoid needs two alpha helices in RBCS protein. Thus, *ΔRBCS* may still have the cpSGs, but which are more difficult to identify. For example, there may be a lot of small foci with cpSGs components dispersing throughout *ΔRBCS* which are difficult to distinguish. Therefore, I tried to localize an chloroplast mRNA and several cpSGs marker proteins by FISH and IF in *ΔRBCS* again, to determine whether I could detect cpSGs.

I found that the *psbA* message co-localized with RBCL in several foci throughout the cells (Fig 2.7 A). Moreover, the other cpSG marker proteins; RBCL and 30S ribosomal protein also showed a similar co-localized distribution (Fig 2.7 B). It was encouraging to find the co-localization pattern of the cpSGs markers in *ΔRBCS*. However, when I looked at localization of a non-cpSGs, stroma heat shock protein, HSP70 [215], I found that it also co-localized with RBCL in foci (Fig 2.7 C). Therefore, these foci with co-localization of cpSGs markers could just be pockets of stroma, instead of cpSGs.

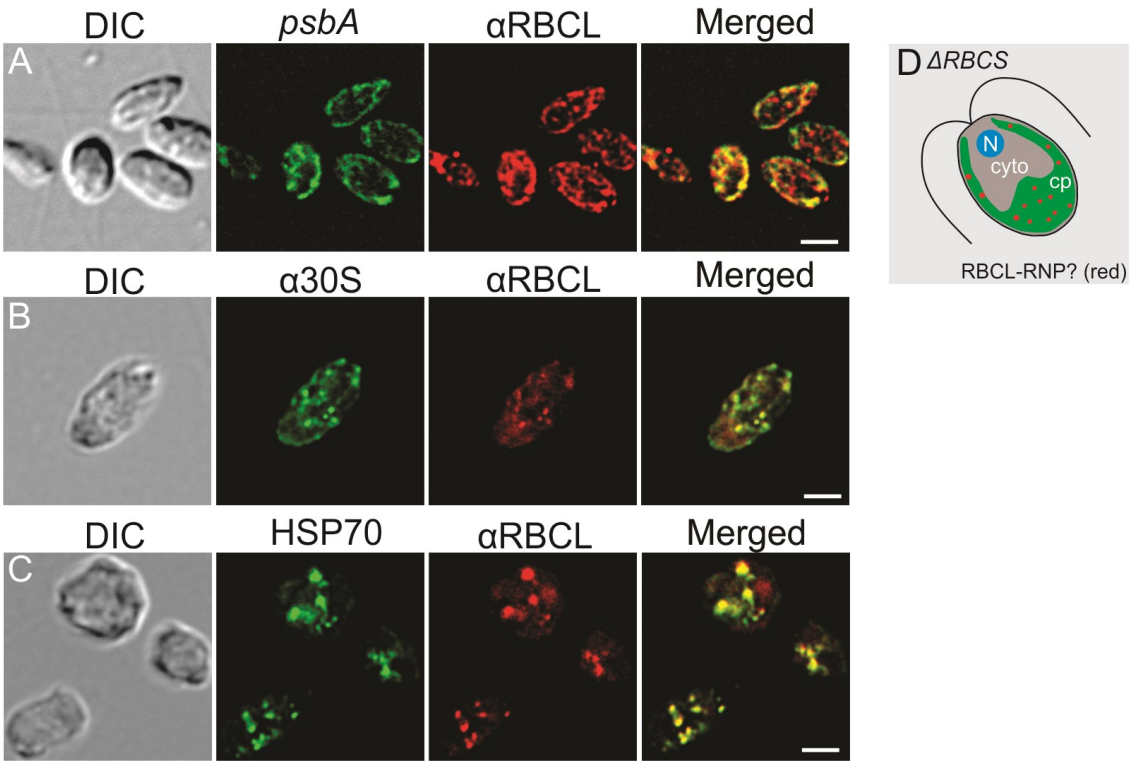

Figure 2.7 Detection of cpSGs in *ΔRBCS.* *ΔRBCS* cells were IF-stained with one cpSGs marker protein; RBCL (red). A) *PsbA* mRNA was detected with FISH (green). B) Another cpSGs marker protein; 30S ribosome (green) was co-stained with RBCL. C) The stroma was labeled by heat shock protein HSP70 (green). D) A cell illustration shows the locations of the nucleus (N), cytosol (Cy), and chloroplast (Cp), possible location for cpSGs or RBCL-RNPs (red). Size bar indicate 5 μm.

Since no obvious cpSGs were detected in *ΔRBCS*, the higher tolerance to H_2O_2 and lower mean level of RNA oxidation in this strain should be conferred by an unknown RBCL-RNP instead of the whole cpSGs. The results suggest that formation of cpSGs may be related to, but not required for, the moonlighting function of RBCL.

2.3.8 An RBCL complex might carry out the moonlighting function of RBCL in the wild-type strain and *ΔRBCS*.

Results presented earlier in this chapter suggest that RBCL has a "moonlighting" function in controlling the level of oxidized RNA in the chloroplast even under the physiological condition (Fig. 2.2). We want to understand how RBCL confers this function. A minor RBCL pool, which could be responsible for this Rubisco-independent function was identified by my colleague, James Dhaliwal (Fig 4, Appendix II). This RBCL pool was shown to pellet during centrifugation with membranes but unlike the membranes, it remains insoluble in the presence of Triton X-100. These results suggest that RBCL is in a non-membrane, very high molecular mass complex (Fig 4, Appendix II). The presence of this RBCL pool correlates with the Rubisco-independent moonlighting function. It was detected in fractionation experiments using both wild-type and *ΔRBCS* stains.

I address the assembly state of the RBCL that carries out the Rubisco-independent moonlighting function. Because the wild-type strain has a tremendous amount of RBCL in the Rubisco holoenzyme complex (constituting 30-50% of total protein) [216], identification of a minor RBCL pool would be hampered. *ΔRBCS*, however, lacks the Rubisco holoenzyme but has lower RNA oxidation than wild-type strain and all the RBCL in this strain is in a Triton X-100-insoluble pool (Fig 4, Appendix II). I hypothesize that this RBCL form is also present in wild type,

where it constitutes a minor pool along with the major RBCL pool in the Rubisco holoenzyme. Therefore, I characterized the RBCL complex in this mutant with non-denaturing polyacrylamide gel electrophoresis and immunoblotting as well as size-exclusion chromatography with the premise that it is the RBCL that carries out the moonlighting function involving oxidized RNA.

1) RBCL was detected in a complex in *ΔRBCS* and wild-type strain by non-denaturing gel.

I initially intended to use non-denaturing gel to identify an RBCL-containing complex in *ΔRBCS.* However, because the amount of RBCL in *ΔRBCS* is low, it was very difficult to detect in the crude cell lysates (data not shown). I found that the RBCL in *ΔRBCS* was enriched in the top fractions 1 to 4 of sucrose density gradients that resolved ribosomes and polysomes (Fig 2.8 A). Thus, I decided to use these fractions to identify protein complexes of RBCL in *ΔRBCS*. Most of the detectable RBCL was in these fractions and, therefore, I presume that this analysis is of the majority of RBCL in this mutant. Each of the fractions from the sucrose gradient was resolved on the non-denaturing polyacrylamide gel and RBCL was detected in immunoblot analysis. As expected for *ΔRBCS*, there was no band detectable with the size of the Rubisco holoenzyme (c.a. 560 kDa). The monomer of RBCL (56 kDa) was not detected on the gel, probably because it ran off. There was a band between 66 KDa and 140 KDa found in fraction 1-3 (Fig 2.8 B). This band showed that there might be a complex with RBCL present in *ΔRBCS*. Some RBCL did not enter the gel, because it is in a very high molecular weight form, probably an insoluble aggregate (Fig 2.8 B). I also detected this 100 KDa RBCL band in similar analyses using a *wild-type* strain; i.e. in top fractions of a polysome profile, although most intensive signal of RBCL was found in the Rubisco holoenzyme (Supplemental Fig 2.2 A). This band was absent in the *ΔrbcL* crude lysate, which means that it was not due to non-specific cross-reactivity of the

antibody (Supplemental Fig 2.2 A). In addition, there were other complexes with RBCL signal at different sizes detected in *ΔRBCS* in only one trial (Supplemental Fig 2.2). This might mean *ΔRBCS* could have RBCL complexes that are responsible for the moonlighting function in the control of oxidized RNA. However, these complexes could be very dynamic and hard to detect *in vitro*, explaining the poor reproducibility. The components of these RBCL complexes were very intriguing and they might reveal how RBCL carries out it moonlighting function in controlling the level of oxidized RNA.

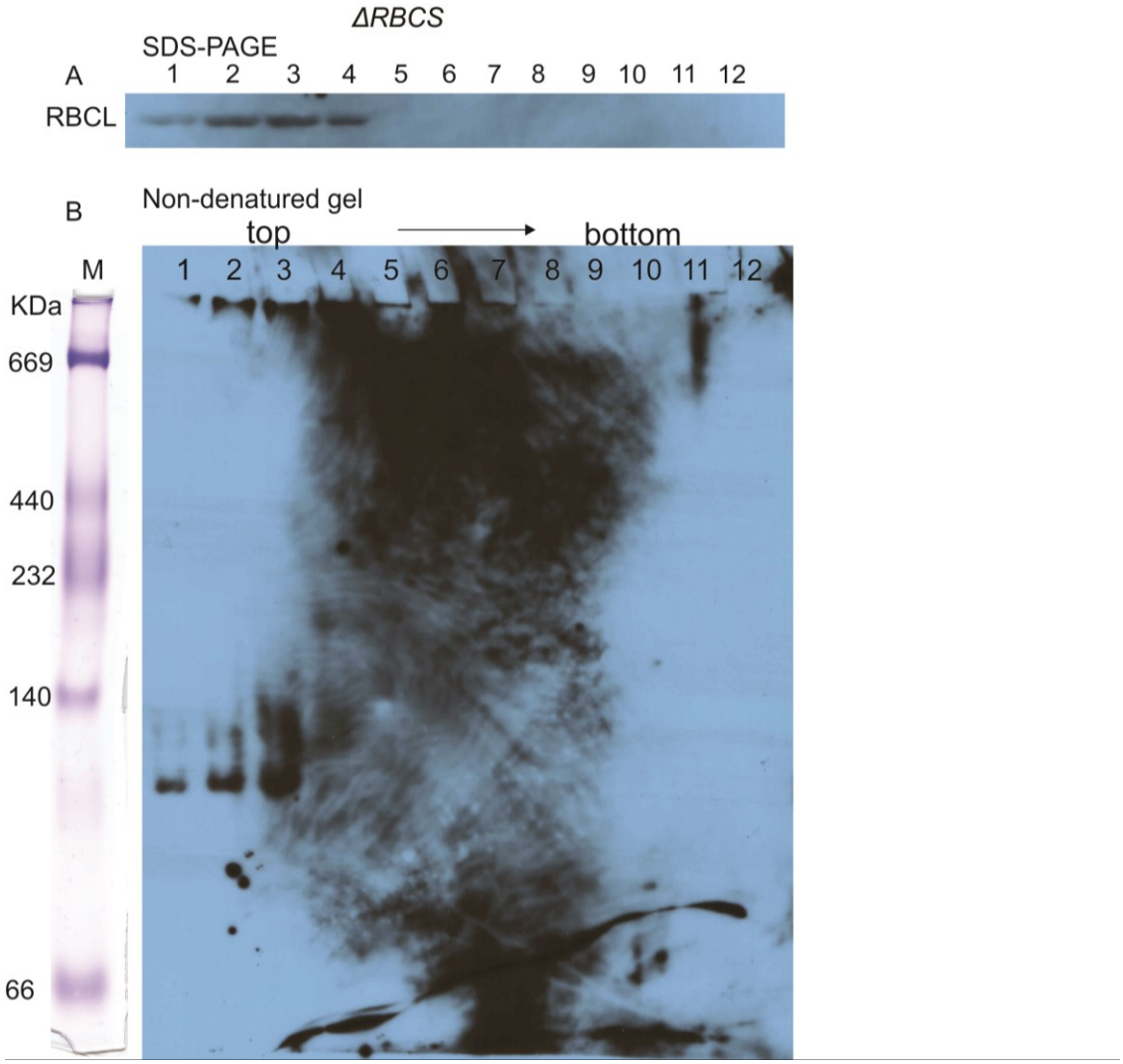

Figure 2.8 RBCL complex was detected in *ΔRBCS* on non-denatured gel.

Sucrose gradient fractions resolving ribosomes and polysomes of *ΔRBCS* were analyzed by A) SDS-PAGE and B) native PAGE, in which RBCL was detected by immunoblotting. A) All twelve samples were examined by SDS-PAGE and immunoblot analysis to show the location of RBCL. B) Immunoblot of non-denatured gel of all the polysome fractions from *ΔRBCS* showed there was an RBCL complex around 100 KDa in 1-3 fractions of polysome isolation. In addition, RBCL was detected at the very top of lanes 1-7, suggesting the presence of an aggregated form. High molecular weight marker was used to calculate approximate size of the complex.

2) Size-exclusion chromatography also revealed this RBCL complex in *ΔRBCS.*

Size-exclusion chromatography is another method to resolve and characterize complexes according to their approximate size [217]. First, I used a Superdex 200 column to separate the RBCL complexes in the *ΔRBCS* lysate as described for polysome isolation. All the membranes were solubilized with deoxycholate. As a negative control for cross-reactivity of the antibody, lysate of *ΔrbcL* was analyzed in parallel (data not shown). I collected 17 fractions and assayed them for RBCL using immunoblot analyses. RBCL was detected in Fractions 6 and 7 of the *ΔRBCS* lysate and it was not detected in any of the fractions from *ΔrbcL* (Fig 2.9 A). Fractions 6 and 7 correspond to the molecular mass range of 35-440 KDa (Fig 2.9 A). The monomer RBCL is 55 KDa and, therefore, it should have been in Fraction 7. The band detected in Fraction 6 is between 67 KDa to 440 KDa could contain RBCL complexes. Since 67 KDa to 440 KDa is a very wide range, the size of this complex is difficult to determine based on these results. Nevertheless, the results are consistent with the complex detected by native gel electrophoresis (Fig 2.8 B).

I used Superose 12 column because it provides better resolution in the size range of the RBCL complex described in the last paragraph, i.e. near 100 KDa (Fig 2.9 B). The fractions were separated and collected as described above. RBCL was assayed by immunoblot in *ΔRBCS* and negative control used lysate from *ΔrbcL.* I found RBCL only in fraction 6 of *ΔRBCS* and, again, it was undetectable in all the fractions from *ΔrbcL.* Fraction 6 corresponds to a molecular weight range of 67 to 150 KDa. This result suggested that RBCL is in a complex of this size in *ΔRBCS*, which is not Rubisco holoenzyme or monomer in the *ΔRBCS.* The size of the complex also correlates with the size of the band detected on non-denaturing gel (Fig 2.8). It was not

surprising to see that all the RBCL was in this complex form and no monomer RBCL (56 KDa) was found, since differential centrifugation result of *ΔRBCS* showed that all RBCL in *ΔRBCS* was in a triton insoluble pellet (Figure 4, Appendix II). To understand more about this RBCL complex, a proteomic research should be taken to characterize its components.

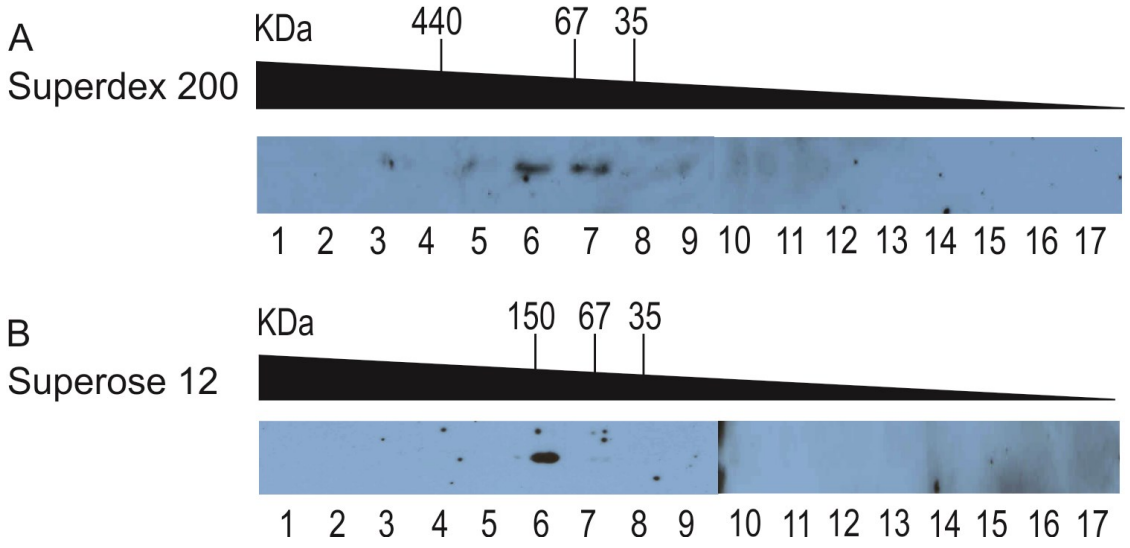

Figure 2.9 RBCL was identified in a complex in *ΔRBCS* by chromatography.

Total cell lysate from *ΔRBCS* (~5 mg) was fractionated by gel-filtration. Two different columns were used; Superdex 200 (A) and Superose 12 (B). Fractions 1-17 were subjected to immunoblot analysis to detect the location of the RBCL complex. The size or marker proteins is shown on the top together with the fraction numbers at the bottom.

2.4 Discussion

2.4.1 RBCL has a "moonlighting" function which controls the level of oxidized RNA in the chloroplast.

My results show that RBCL controls the level of oxidized RNA in the chloroplast and maintains viability during exposure to H_2O_2. These functions are independent of Rubisco and, therefore, could explain the evolutionary retention of RBCL in plant and algal lineages that have lost photosynthesis [218]. The unexpected *ΔRBCS* phenotypes; H_2O_2 hypertolerance and low 8-oxoG RNA level, relative to wild type, probably reflect an RBCL gain-of-function because they are RBCL-dependent. These phenotypes could result from enhanced availability of RBCL for its RNA moonlighting function when it is not sequestered by RBCS for assembly of the Rubisco holoenzyme. RBCL appears to be a particularly critical factor in the control of oxidized RNA in the chloroplast and in H_2O_2 tolerance because, if any other factor were more important than RBCL, then the RBCL in *ΔRBCS* would not be able to surpass the wild-type phenotypes for these traits.

RBCL is in a growing class of metabolic proteins that have dual functions as RNA-binding proteins [54]. These proteins have been proposed to coordinate metabolism and gene expression and to enhance the functional diversity of proteomes [219]. Only a few of these dual functional proteins have been demonstrated *in vivo*, as we have done here for RBCL with results of genetic and *in situ* analyses. RBCL is atypical among these metabolic proteins because its dual function involves the control of oxidized RNA.

2.4.2 The "moonlighting" function of RBCL is present in the absence of stress.

The RNA "moonlighting" function of RBCL is clearly active under physiological

conditions. RNA oxidation is believed to be detrimental because the translation of oxidized mRNAs results in the synthesis of aberrant proteins [220, 221]. However, under a certain level, oxidized RNA in cells might not affect cell viability [155]. This could explain our finding that *ΔrbcL* has an elevated level of oxidized RNA and yet a wild-type growth rate (Fig 2.2 A, Sup Fig 2.1 A). Perhaps the level of oxidized RNA in *ΔrbcL* is only marginally detrimental and does not affect growth under the optimal conditions, or the oxidized RNA is not related to cell survival, for example, the RNA which encodes photosynthesis protein. Alternatively, oxidized RNA in the chloroplast might only be detrimental in the presence of H_2O_2, for example under the conditions of the cell survival experiments in Fig 2.1 or when this ROS is produced by photosynthesis under physiological conditions. To explain how oxidized RNA could be detrimental only in the presence of H_2O_2, I can propose the following hypothesis. First of all, oxidized bases in certain chloroplast mRNAs could result in the synthesis of aberrant iron-binding proteins with Fenton activity; i.e. the metal-catalyzed conversion of H_2O_2 to the highly toxic hydroxyl radical, thereby potentiating H_2O_2 toxicity [137].

In a second hypothesis, RBCL and RNA oxidation could have a regulatory function. For example, the targeted oxidation of a specific RNA might be a signal in a process that regulates a biological response, such as cell survival or programmed cell death during oxidative stress. This is consistent with our finding that the *ΔrbcL* and *ΔRBCS* phenotypes for H_2O_2 tolerance and 8-oxoG RNA level are at opposite extremes of wild-type, i.e. they could reflect the alternate states of a regulatory decision involving RBCL and RNA oxidation.

2.4.3 The compartmentalization of 8-oxoG in the pyrenoid may open new avenues to RNA quality control.

I show that oxidized RNA is compartmentalized in the pyrenoid of the chloroplast. Our collaborators also showed that the oxidized RNA localized in Hela cells (Zhan et al. submitted, Fig 2, Appendix II with manuscript). These compartments in Hela cells are neither stress granules nor processing bodies, although they might be analogous to UV-induced RNA granules in yeast [222]. The compartmentalization of oxidized RNA in the phylogenetically distant systems studied here, an algal chloroplast and mammalian cells, suggests it has fundamental significance. Indeed, compartmentalization of DNA and protein quality control is occurring and it has been proposed recently for RNA [223-225]. The sequestration of damaged molecules prevents them from interfering with the processes in which they normally function. Compartmentalization of defective molecules could also prevent the degradation or attempted repair of undamaged substrates. In addition, compartmentalization might enhance local concentrations of damaged molecules and quality control factors to establish thermodynamic parameters that favor RNA repair or degradation. My results open avenues to study a new type of RNA granule, a potential role of the pyrenoid in RNA metabolism, and the factors and mechanisms involved in the handling of oxidized RNA in chloroplasts.

My findings also have potential relevance to cytoplasmic stress granules and processing bodies. These RNA granules have been implicated in fundamental cell biological processes but their functions and physiochemical properties are only partially understood. Our results strongly suggest that RBCL carries out its RNA moonlighting function 1) independently of chloroplast stress granules and 2) constitutively (i.e. under both non-stress and stress conditions), thereby raising the question of whether or not cytoplasmic stress granules and processing bodies function as submicroscopic RNP assemblies under non-stress conditions.

2.4.4 How RBCL mitigates RNA oxidation remains to be determined.

We have shown that RBCL mitigates RNA oxidation and 8-oxoG RNA is localized in the pyrenoid, the major reservoir of RBCL in wild-type strain. However, we do not know the mechanism by which RBCL carries out this function. I have three hypotheses for how RBCL mitigates RNA oxidation. The first one is that RBCL protects RNA from oxidation. RBCL can bind with non-specific RNA to form cpSGs [38] and I showed previously that preservation of cpSGs could reduce the RNA oxidation level (Fig 2.4). In addition, IF result also showed that 8-oxoG RNA did not localize in the cpSGs (Fig 2.6). That reveals that the mRNA in the cpSGs may not be oxidized and has the potential to go back to the translational pool as those in cytoplasmic SGs [226]. Thus, RBCL in the cpSGs may protect the non-oxidized RNA from oxidative damage to reduce the RNA oxidation level.

The second hypothesis is that RBCL degrades oxidized RNA to mitigate RNA oxidation. To verify this hypothesis, I need to know if there is an RNA degradation machinery associated with RBCL in Chlamydomonas. The characterization of RBCL-8oxoG RNA complex might give a better idea. In mammalian cells, PBs are main place for RNA degradation, but our collaborator Dr. Rachid Mazouri and his group did not detect the co-localization of 8-oxoG RNA and markers for PBs in Hela cells (Pouline Adjibade's unpublished data). Thus, 8-oxoG containing RNAs may have a different degradation mechanism in Hela cells.

In the absence of degradation, the oxidized RNA may also be repaired by RBCL-RNP and re-enter the translation pool. This repair mechanism is my third hypothesis. We do not know much about RNA repair mechanisms and the detection of other components binding with RBCL and 8-oxoG RNA in the chloroplasts may reveal a new mechanism of RNA repair mechanism.

2.4.5. What are the possible components of the RBCL complex in *ΔRBCS*?

RBCL was detected in two forms in the lysate of *ΔRBCS*, as a complex in the size range between 66 KDa and 150 KDa and as very high molecular weight form which did not enter the native gel (Fig 2.8 B). The larger form was not detected in the fractions of size-exclusion chromatography, probably because it is above the molecular mass that can enter these columns. The smaller complex could be the dimer of RBCL. It is known that RBCL forms a dimer when it assembles with RBCS to from the octameric Rubisco holoenzyme [227]. The size of the RBCL dimer is about 110 KDa, which is in the range of 67 KDa to 150 KDa. RBCL cannot form Rubisco in *ΔRBCS* due to the lack of its partner protein, RBCS. However, RBCL may keep the ability to form the dimer.

Alternatively, this 67-150 KDa complex with RBCL might not be a dimer, but rather be a complex with one or more other proteins. As mentioned in Chapter 2, *ΔRBCS* cells have a RBCL dependent higher survival rate with H_2O_2 treatment. It has low RNA oxidation, which is also possibly mitigated by RBCL (Fig 2.2). Additionally, I showed that there is no visible cpSGs in *ΔRBCS* (Fig 2.7). These results suggest that there may be RBCL-RNPs in *ΔRBCS* which perform the Rubisco-independent moonlighting function. These RBCL-RNPs may contain RNA and similar protein components as cpSGs. They could be primary cpSGs with a smaller size and less content. If the components of these complexes share similarity with cpSGs or have a known biochemical function, such a finding would suggest how RBCL mitigates RNA oxidation and the potential function of cpSGs.

Thirdly, the 67-150 KDa RBCL complex may contain some components related to oxidized RNA quality control. Although I mainly focused on identifying RBCL complex in *ΔRBCS*, this

complex was also detected in wild type (Sup Fig 5.1). RBCL is co-localized with 8-oxoG RNA in pyrenoid in wild type (Chapter 2). Thus, the RBCL complex could contain some protein components related to oxidized RNA quality control. The antioxidant function of RBCL could be performed by repairing or degrading 8-oxoG RNA in this RBCL complex.

Future characterization of the components of one or both of the forms of RBCL, the 67-150 KDa complex and the very high molecular weight form, could reveal the molecular mechanisms of the moonlighting function, for example whether RBCL controls oxidized RNA by protecting intact RNA or by repairing or degrading oxidized RNA.

Chapter 3: A partial characterization of the pyrenoid proteome suggests new functions of this microcompartment of the chloroplast.

3.1 Introduction

Pyrenoids are non-membrane micro-compartment in the chloroplasts of many algae and an aquatic plant; the hornworts [228, 229]. The single pyrenoid in each chloroplast is the major location for CO_2 fixation by Rubisco in the Calvin cycle. A review of pyrenoids structure and functions can be found in Chapter 1 of this thesis. A starch sheath surrounding the pyrenoid increases in thickness under low CO_2 conditions, when the CCM is activated [230]. The role of the pyrenoid in *C. reinhardtii* is similar to that of carboxysomes in cyanobacteria [231]; it provides a low O_2/CO_2 environment for Rubisco to favor its productive carboxylase (CO_2-fixing) activity in the Calvin cycle over its wasteful oxygenase activity [75]. How does the pyrenoid concentrate CO_2 and maintain low O_2 concentration? Firstly, the pyrenoid has the CCM, which concentrates CO_2 around Rubisco (Section 1.2). Secondly, the pyrenoid sequesters Rubisco away from photosystem II, the complex that produces O_2 as a byproduct of photosynthetic electron transport [33, 75, 232].

Although the pyrenoid is not bound by a membrane, it does contain a network of membranous tubules, which are connected to thylakoid membranous vesicles outside the pyrenoid [233]. Recently, an elaborate ultrastructure of pyrenoid has been revealed by cryo-electron tomography [35]. This study revealed mini-tubules inside the pyrenoid tubules. Each of these mini-tubules is open, on one end, to the stroma surrounding the pyrenoid. The other end has an opening within the pyrenoid matrix. Therefore, these mini-tubules are presumed to facilitate the direct exchange of metabolites and other molecules between the stroma and

pyrenoid matrix. The fact that the pyrenoid has a direct channel to connect with the stroma raises the possibility that the pyrenoid might contribute to other biosynthesis processes.

Some evidence suggests that processes involving the chloroplast genome occur in the pyrenoid. For example, DNA was detected in the pyrenoid of some green algae, but not in *C. reinhardtii*. However chloroplast nucleoids, the structures that contain the multiple-copy chloroplast genome, have been shown to be localized adjacent to pyrenoid in *C. reinhardtii* [18, 36]. Moreover, a protein with DNA endonuclease activity, UVI31+, was recently found to localize to the pyrenoid and then to leave it under UV stress [37]. All of these results suggest that the pyrenoids play some unknown role(s) in the maintenance, inheritance, replication or expression of the chloroplast genome.

Pyrenoid could have a role in RNA metabolism. Stress granules were found to form at the perimeter of pyrenoid during oxidative stress and other stress conditions in the chloroplast of *C. reinhardtii* [38]. These cpSGs recruit mRNAs, RNA binding proteins, and the small but not the large subunit of the chloroplast ribosome. Results in Chapter 2 report that pyrenoids contained oxidized RNA and reveal an alternate function of the major pyrenoid protein RBCL in controlling the level of oxidized RNA in the chloroplast of *C. reinhardtii*. The localization of cpSGs and oxidized RNA in the pyrenoid suggests that pyrenoids may have a role in RNA metabolism. Together, the detection of DNA and RNA in, or close to, pyrenoid suggests that the pyrenoid is a privileged location for some processes in nucleic acid metabolism involving both the chloroplast genome and RNAs encoded by it.

Nevertheless, except for CCM and Rubisco, little is known about the other biochemical and cell biological functions of the pyrenoid. Indeed, the pyrenoid is one of the final remaining

intracellular compartments yet to be characterized by proteomics. Therefore, a pyrenoid proteome could reveal more about the pathways and processes that occur therein.

Proteomics has been used to characterize the protein composites of specific intracellular compartments. This approach involves the isolation of the intracellular compartment of interest whereupon the proteins are identified by mass spectrometry and bioinformatics database searches [234]. Efficient purification methods are important because any contaminating proteins will be assigned erroneously to in the compartment under study. I modified previously reported procedures for pyrenoid isolation, to optimize the enrichment and minimize the exposure of pyrenoids to chemicals that might affect the results. For example, I did not use $HgCl_2$, which was used in previous methods as a fixative to preserve pyrenoid integrity. I also reduced the time between cell lysis and pyrenoid isolation, to minimize the time of exposure of pyrenoids to Triton X-100 and, therefore, prevent the potential solubilization of pyrenoid tubules.

Even with optimized methods, contamination by proteins from other compartments is always problematic in the purification of subcellular structures. To minimize this problem, I used a few approaches to increase the purity of pyrenoid preparations. First, pyrenoids were isolated from chloroplasts instead of whole cells. This helps to remove the contaminants from mitochondria and other cytoplasmic compartments before generating the pyrenoid-enriched fractions. Secondly, control samples from pyrenoid-deficient mutants were prepared and analyzed to subtract protein contaminants that co-fractionate with pyrenoids of wild-type strain. These two steps drastically improved the purity of pyrenoid-enriched samples and the stringency of pyrenoid protein identification. For example, many abundant non-chloroplast

proteins that were identified in initial trials of pyrenoid-enriched fractions obtained from whole cells were not detected in the fractions obtained from isolated chloroplasts. Analysis of fractions from pyrenoid-deficient mutants revealed many contaminant proteins, which could be subtracted from the pyrenoid proteome.

This was a collaborative project. My contributions involved the following: 1) The development of the pyrenoid isolation protocol, based on previously reported protocols (Jim Uniacke, unpublished data). 2) Preparation of the samples and contributed substantially to the analyses and interpretations of the proteomic results. Dr. Stéphane Lemaire with Dr. Christophe Marchand and Ms. Adeline Mauries (Institut de Biologie Physico-Chimique Paris, France) processed the samples and obtained all the spectrometry data, filtered the results, mapped the peptides to the annotated genome, and did the KEGG analyses.

The preliminary proteomic results of the pyrenoid (Sup Fig 3.4) supported the localization of CCM in pyrenoid by identifying six low CO_2-induced (LCI) proteins including CAH3, the carbonic anhydrase of pyrenoid tubules [35]. Proteins involved in starch metabolism; both synthesis and degradation, were identified. This provides the first evidence for a long-standing, controversial hypothesis that the pyrenoid makes and degrades the starch that surrounds it. Proteins in other pathways of carbon metabolism were also identified in this proteome. The subunits of RNA polymerase and twenty-two chloroplast ribosomal proteins were also identified, which suggest that the pyrenoid is a site of transcription and translation. RNA degradation enzymes identified in pyrenoid proteome supported the hypothesis that the pyrenoid is a location of RNA metabolism, supporting the results in Chapter 2 revealing that oxidized RNA localization to the pyrenoid and the function of the major pyrenoid protein RBCL in controlling the level of oxidized

RNA. In addition, many predicted proteins were identified, possibly implicating them in pyrenoid functions. This research provides the first proteomic analyses of a pyrenoid and opens new avenues to the function research of this chloroplast micro-compartment.

3.2 Materials and Methods

Chloroplasts Isolation

Cells were harvested from cultures (1-4 x10^6 cells/ml) by centrifugation (3000 g, 10 min, 4 ^oC). Pellet was washed by resuspension in 100 ml of 50 mM HEPES-KOH [pH 7.5] followed by centrifugation at 3000 g for 5 min at 4 ^oC. The cell pellet was resuspended to the density of 10^8 cells/ml in Isolation Buffer (IB) (300 mM sorbitol, 50 mM HEPES-KOH [pH7.5], 2 mM Na-EDTA, 1mM $MgCl_2$ and 1 % [w/v] BSA). Since IB is hypertonic to the cells, all the cells in it looked shrunken and irregular in shape. Then 10% saponin (w/v) (Sigma-Aldrich) was added to make a final concentration of 0.5% (w/v) and incubated for 15 -20 min. The time of the incubation was decided by the observation of cell shape under the light microscope. When about 80% of the cells swell to the round shape from the shrunken irregular shape, it was assumed that the saponin had solubilized the plasma membrane (Supplemental Fig. 3.1). IB is isotonic to the chloroplasts, thus the swell condition showed the sufficient solubilization of plasma membrane. The cells were pelleted and resuspended again in IB to 0.3 mg/ml chlorophyll. All of the following steps were carried at 4 ^oC. The cells were rapidly drawn into a 10 ml syringe, then a 27-guage needle was attached, and the cells were expulsed through the needle at a flow rate 0.5 ml/ second. This syringe passage step was repeated five times. From the eluted material, whole cells and chloroplasts were collected by centrifugation (700 g, 2 min, 4 ^oC). The pellet was gently resuspended in 2 ml of isolation buffer (0.1% BSA [w/v]) using a fine paintbrush to avoid

breakage of the chloroplasts. The suspension was overlaid on a discontinuous Percoll gradient (with steps of 20%, 45% and 65% [v/v]) and centrifuged for 20 min at 3,200 x g (Beckman Coulter, Allegra 6R, GH3.8A rotor). Intact chloroplasts form a band at the 45-65% interface. The desired bands were collected using a Pasteur pipet (using the wide bore end for collection and a rubber pipet bulb attached to the broken narrow end). Fractions were diluted with 10 ml isolation buffer (0.1% BSA [w/v]) and centrifuged (670 x g, 2 min, 4 ^{o}C) to collect the organelles and remove the Percoll. The chloroplastic pellet was resuspended in the buffer with 300 mM sorbitol, 50 mM HEPES (pH 7.5) and 5 mM $MgCl_2$.

Pyrenoid isolation

Name	Genotype	Pyrenoid	CCM	Rubisco	RBCL	RBCS
KA6 (pyrenoid wild-type)	*y-7/cw15*	+	+	+	+	+
MX3312/cw15 (pyrenoid deficient)	*ΔrbcL; cw15*	-	-	-	-	+
SS-AT (pyrenoid deficient)	*RBCS-Arabidopsis thaliana*	-	+ (reduced)	+	+	+

Table 3.1 Strains used in the pyrenoid isolation

Wild-type or pyrenoid-deficient cells of a density of 1-4 x10^6 cells/ ml were pelleted at 3,000 x g at 4 ^{o}C. The pellet was resuspended in Breaking Buffer (BB) (300 mM sorbitol, 10 mM Tricine pH 7.8 and 5 mM EDTA) to the density of 4 x 10^7 cells/ml. 200 µl of 5X BB was mixed with 800 µl Percoll (GE health) in a 1.5 ml microfuge tube. A 250 µl freshly made 2% (v/v) Triton 100-X (Sigma-Aldrich) was overlaid on the Percoll mix and then 250 µl of the cells in BB was added to the upper phase and the tube was immediately centrifuged at 10,000 x g in the bench top refrigerated centrifuge at 4 ^{o}C (Fig 3.1). After centrifugation, the 500 µl supernatant was kept for analysis, called “top”. The remaining liquid was discarded and the pellet was rinsed by BB once. The top and pellet fractions were frozen in the -80 ^{o}C freezer.

For the pyrenoid isolation from chloroplasts, the chloroplasts were first isolated as described above. The chlorophyll concentration of the chloroplast suspension was determined by spectrophotometer at the 652 nm and 665 nm [235]. The isolated chloroplasts which contain the amount of chlorophyll equal to that of the 1x 10^7 cells were pelleted by centrifugation and resuspended in 250 µl BB. The chloroplasts were solubilized with 0.5 % Triton X-100 and pelleted through an 80% Percoll gradient. The remaining steps are the same as described above for whole cells.

Protein extraction

Proteins were extracted from the "top" fraction by the methanol/chloroform method [236]. 200 µl of the "top" fraction was aliquoted to several 1.5 ml microfuge tubes. To each sample, 600 µl methanol, 150 µl chloroform and 450 µl H_2O were added followed by vortexing. The mixture was centrifuged at 15, 000 x g in a bench-top refrigerated centrifuge for 1-2 min at 4 ^oC (MBI lab equipment). The upper phase was removed after centrifugation and 450 µl methanol was added to the tube. After vortexing, the mixture was centrifuged again at 15,000 g for 5 min at 4 ^oC using the same centrifuge. The supernatant was removed and the pellet was dissolved in 50 µl SDS loading buffer (50 mM Tris-Cl [pH 6.8], 4% glycerol, 1.6% SDS and 4% (v/v) β-mercaptoethanol) for SDS-PAGE.

Figure 3.1

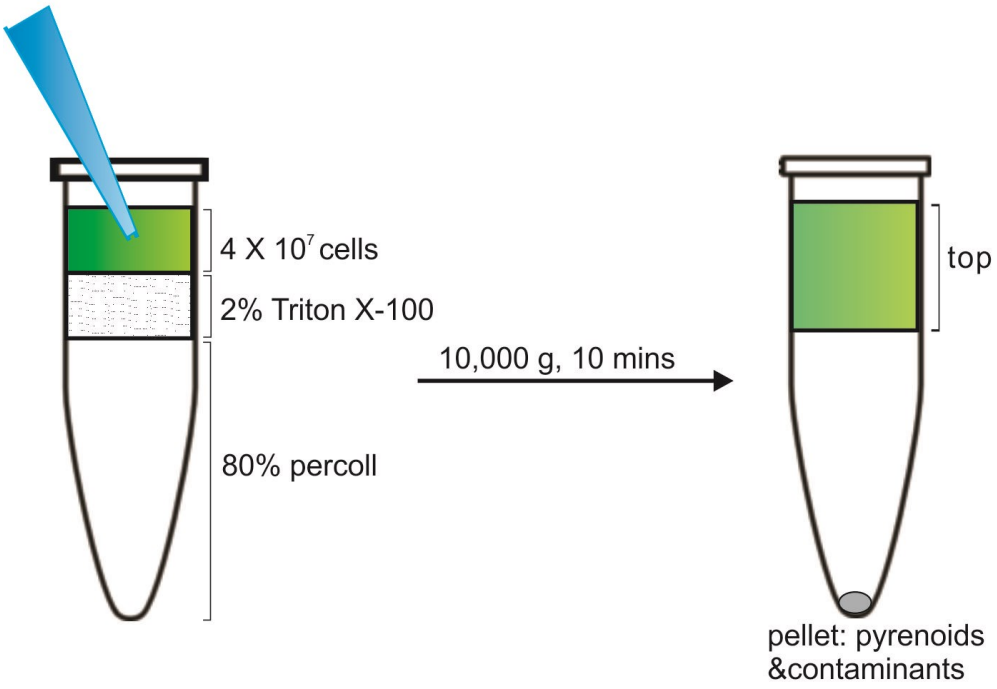

Figure 3.1 Flow chart to show how pyrenoid pellet was acquired.

$4X10^7$ cells were solubilized with 1% Triton-X100 and centrifuged through 80% Percoll. Crude pyrenoid fraction in the pellet and the top fraction containing left cell components were kept for further analysis.

Silver staining

A gel of 12% acrylamide-bis acrylamide (29:1) was made according to a standard protocol [206]. The samples were denatured with SDS loading buffer at 100 ^{o}C for 5 min. 6 µl of pre-stained protein ladder (Fermentas, SM0671) was used as marker to indicate the size of the protein. The gel was run overnight at 6 mA in Tris-glycine buffer (25 mM Tris-Cl 250 mM glycine, 0.1% SDS [w/v]) and sliver stained using commercial kit (Sigma-Aldrich), according to the manufacture' s protocol.

Immunoblot

Protein samples were prepared and resolved by electrophoresis as described above. The proteins on the gel were elec-transferred to a PVDF membrane (BioRad) with 30 V current overnight at 4 ^{o}C following the standard procedure [206]. The membrane was blocked using 5% (w/v) dried non-fat milk (Provigo Supermarket) in PBS with 0.1% (v/v) Tween-20 (Fisher) and probed with different primary antibodies for 2 h at room temperature. The primary antibodies and the dilutions used are list here:

Antibody	Distribution	Dilution	Protein detected
AOX1	Mitochondria	1:20000	Alternative oxidase 1 (Agrisera)
BIP	Endoplasmic Reticulum (ER)	1:200	Binding immunoglobulin protein (Agrisera)
Cyl4	Cytoplasm	1:10000	Cytoplasmic ribosome
L30	Chloroplast	1:6000	Large subunit of chloroplast ribosome
RBCL		1:4000	Large subunit of Rubisco
RBCS		1:4000	Small subunit of Rubisco

Table 3.2: The primary antibodies used in the immunoblot detection.

After washing the membrane three times for 10 min each with PBST (NaCl 137 mM, KCl 2.7 mM, Na_2HPO_4 10 mM, KH_2PO_4 1.8 mM, Tween-20 0.1% [v/v]), it was probed with the anti-rabbit horseradish peroxidase conjugated (HRP) secondary antibody (1:10000) for 1 h at room

temperature. Enhanced chemiluminescent (ECL) substrate (Pierce) was used to detect the HRP enzyme activity. The film (HyBlot CL) that was exposed to the ECL signal was developed with a developer (Kodak).

Immunofluorescent staining of pyrenoid

Freshly isolated pyrenoids from cells or chloroplasts were fixed in 100 µl BB with 4% (w/v) formaldehyde (BioShop) for 10 min. The fixed pyrenoids were collected by centrifugation at 10,000 x g for 2 min. Pellets were washed with BB twice, and the material was resuspended in 100 µl BB and then probed with antibodies against RBCL (1:1000) or RBCS (1:1000) for 75 min at room temperature. The conjugates were washed with BB twice, pelleted by centrifugation, and then resuspended in 100 µl BB. Alexa Fluor 488 goat anti-rabbit secondary antibody (1:200, Invitrogen) was incubated with the pyrenoid suspension for 45 min at room temperature. The pyrenoid-antibody conjugates were washed again in BB and resuspended in 50 µl BB. The liquid suspension was spread on the poly-lysine coated coverslip and air-dried for about 5 min. 13 µl prolong antifade solution (Invitrogen) was spotted on the coverslip, which was then affixed to a microscope slides using nail polish, which also sealed the edges. Specimens were observed with a Leica DMI 6000 microscope (Leica Microsystems) with a 63X/1.4 objective, a Hamamatsu OrcaR2 camera, and Volocity acquisition software (Perkin-Elmer) in DIC and GFP channel.

Mass spectrometry analysis

Our collaborator Dr. Stephan Lemaire (Curie Institute, Paris) and two members of his group carried out all the mass spectrometry (MS) analyses from the pyrenoid samples.

1) Chemicals and enzymes

Proteomics grade endoproteinases (Lys-C and Trypsin Gold) and ProteaseMax surfactant

were purchased from Promega (Charbonnières, France). Reversed phase C18 spin columns, precolumns and analytical columns were all obtained from Thermo Scientific (Les Ulis, France). Solvents and ion-pairing agents were certified LC-MS grade and all other chemicals were purchased from Sigma-Aldrich (Saint-Quentin Fallavier, France) with the highest purity available.

2) Digestion

Pyrenoid pellets were washed with prechilled acetone and maintained at -20°C for at least 2 hours. After centrifugation (21,500 *g*, 10 min, 4°C), pellets were dissolved in 60 µL of 50 mM ammonium bicarbonate (AMBIC) containing 6.5 M urea, 5 mM dithiothreitol (DTT) and 0.05% ProteaseMAX surfactant at 30°C for 30 min. Free cysteines were alkylated by adding 15 mM iodoacetamide (IAM) for 1 hour at 25°C in the dark. The excess of IAM was quenched by 2.5 mM DTT. Protein concentration was determined by BCA assay using bovine serum albumin as standard. Proteins were digested at 37°C for 3 hours with Lys-C endoproteinase in a 1:100 (w/w) enzyme:substrate ratio. Then, 450µL of 50 mM AMBIC were added to dilute urea. Samples were further incubated overnight at 37°C in the presence of modified porcin trypsine Gold in a 1:50 (w/w) enzyme:substrate ratio. The digestion was stopped by addition of 0.1% formic acid (FA) and peptide mixtures were centrifuged for 30 min at maximum speed (21,500 *g*) at 4°C. Tryptic peptides present in supernatants were thus subjected to desalting using reversed phase C18 spin columns as recommended by the supplier.

3) Tandem mass spectrometry

Peptide mixtures were prepared in 20 µL of 3% acetonitrile (ACN) containing 0.1% FA (solvent A) and analyzed on a Q-Exactive Plus (Thermo Fisher Scientific, San José, CA, USA) coupled to a

Proxeon Easy nLC 1000 reversed phase chromatography system (Thermo Fisher Scientific, San José, CA, USA) using a binary solvent system consisting of solvent A and solvent B (0.1% FA in ACN). 500 ng of tryptic digests were loaded on an Acclaim Pepmap C18 precolumn (2 cm x 75 µm i.d., 2 µm, 100 Å) equilibrated in solvent A and peptides were separated on an Acclaim Pepmap C18 analytical column (25 cm x 75 µm i.d., 2 µm, 100 Å) at a constant flow rate of 300 nL/min by two successive linear gradients of solvent B from 0% to 20% in 68 min, from 20% to 32% in 22 min and then up to 85% in 5 min followed by an isocratic step at 85% for 10 min. The instrument was operated in positive and data-dependent acquisition modes with survey scans acquired at a resolution of 70,000 (at m/z 200 Da) with a mass range of m/z 400-1,800. After each full-scan MS, up to 10 of the most intense precursor ions (except +1 or unassigned charge state ions) were fragmented in the HCD cell (normalized collision energy fixed at 27) and then dynamically excluded for 60 s. AGC target was fixed to $3x10^6$ ions in MS and 10^5 ions in MS/MS with a maximum ion accumulation time set to 100 ms for MS and MS/MS acquisitions. All other parameters were set as follows: capillary temperature, 250°C; S-lens RF level, 60; isolation window, 2 Th. Acquisitions were performed with Excalibur software (Thermo Fisher Scientific, San José, CA, USA) and to improve mass accuracy of full-scan MS spectra, a permanent recalibration of the instrument was allowed using polycyclodimethylsiloxane ($(C_2H_6SiO)_6$, m/z 445.12003 Th) as lock mass.

4) Data analysis and database searches

Raw Orbitrap data were processed with Proteome Discoverer 1.4 software (Thermo Fisher Scientific, San José, CA, USA) and searched against the NCBI database restricted to the *C. reinhardtii* taxonomy (31,910 entries on 2014.09.04) using an in-house Mascot search server

(Matrix Science, London, UK; version 2.4). Mass tolerance was set to 10 ppm for the parent ion mass and 20 mmu for fragments and up to two missed cleavages per peptide were allowed. Methionine oxidation, N-terminal acetylation of peptides and deamidation of asparagine and glutamine were taken into account as variable modifications and cysteine carbamidomethylation as fixed modification. Peptide False Discovery Rates (FDRs) were determined by searching against a reversed decoy database and peptide identifications were filtered at 1% FDR. Proteins were validated if they were identified with at least two different peptides passing the peptide FDR filter. For each extract (MX-CW15; SS-AT; WTcell, WTcp) two biological replicates and two analytical replicates were analyzed.

In addition to the steps described above, I contributed substantially to the analyses and interpretation of the results. The detailed protocol of the MS analyses is provided in the Appendix section. The functional analysis was carried out by KEGG (http://www.kegg.jp), BLAST (http://blast.ncbi.nlm.nih.gov/Blast.cgi), Algal Functional Annotation Tool (http://pathways.mcdb.ucla.edu/algal/pathways.html) and PredAlgo (https://giavap-genomes.ibpc.fr/cgi-bin/predalgodb.perl?page=main).

3.3 Results

3.3.1. Pyrenoids from the *wild-type* cells had RBCL and RBCS as two major proteins.

The pellets acquired from a wild-type strain (ambient CO_2 or 5% CO_2) and two pyrenoid-deficient stains were analyzed by silver staining (Fig 3.2). Two major bands at the size around 55 kDa and 15 kDa were seen in pyrenoid pellet isolated from wild-type cells cultured with ambient air or 5% CO_2 (Fig 3.2). These molecular mass values were consistent with those of RBCL and RBCS, the two protein subunits of the Rubisco holoenzyme [237]. The pyrenoid is known as the

major location for Rubisco [45]. The enrichment of RBCL and RBCS in the pellet indicated the possible successful isolation of pyrenoids. Although this did not reveal the purity of the pyrenoid, it showed that we obtained a pellet, which was highly enriched with Rubisco compared to the "top" fraction which was extremely complex in its protein composition (Fig. 3.2). "Top" fraction here indicated that the protein fraction from the 500 µl supernatant above the Percoll gradient after centrifugation.

Moreover, in *C. reinhardtii,* the pyrenoid is known to have the CCM and over 90% Rubisco is in the pyrenoid when CCM is induced [70]. Cells cultured under high CO_2 (5%) conditions have small or even rudimentary pyrenoids [70]. The pyrenoid isolated from high CO_2 cultured wild-type strain showed much lower levels of RBCL and RBCS compared with the ambient CO_2 grown culture (Fig 3.2) [70]. Equal numbers of cells grown in different CO_2 level were loaded on Percoll gradient for pyrenoid isolation. The difference in the amounts of RBCL and RBCS in the pellet fraction from cells cultured under high CO_2 conditions suggests that fewer pyrenoids were collected due to their smaller size, or there is less Rubisco in these pyrenoids because they lack CCM, or both. In any case, this result further supports the presence of pyrenoids in the pellet fraction of cells from the ambient CO_2 conditions.

Pellet fractions were also obtained from two pyrenoid-deficient strains. I used the same method to obtain pellet fraction from cells of the wild-type (pyrenoid-containing) strain and the pyrenoid-less mutants. The *SS-AT* mutant contains Rubisco holoenzyme but it does not have pyrenoids, while *MX3312/cw15* contains neither Rubisco nor a pyrenoid. If the RBCL and RBCS that I detected in wild-type strain (Fig. 3.2) represented Rubisco holoenzyme, I should also detect them in *SS-AT*. Compared to wild-type strain, only trace amount of RBCL without RBCS

was found in the pellet from *SS-AT*. Both RBCL and RBCS bands were absent in the pellet of *MX3312/cw15* (Fig. 3.2). Thus, RBCL and RBCS I got in wild-type cells could be from isolated pyrenoid.

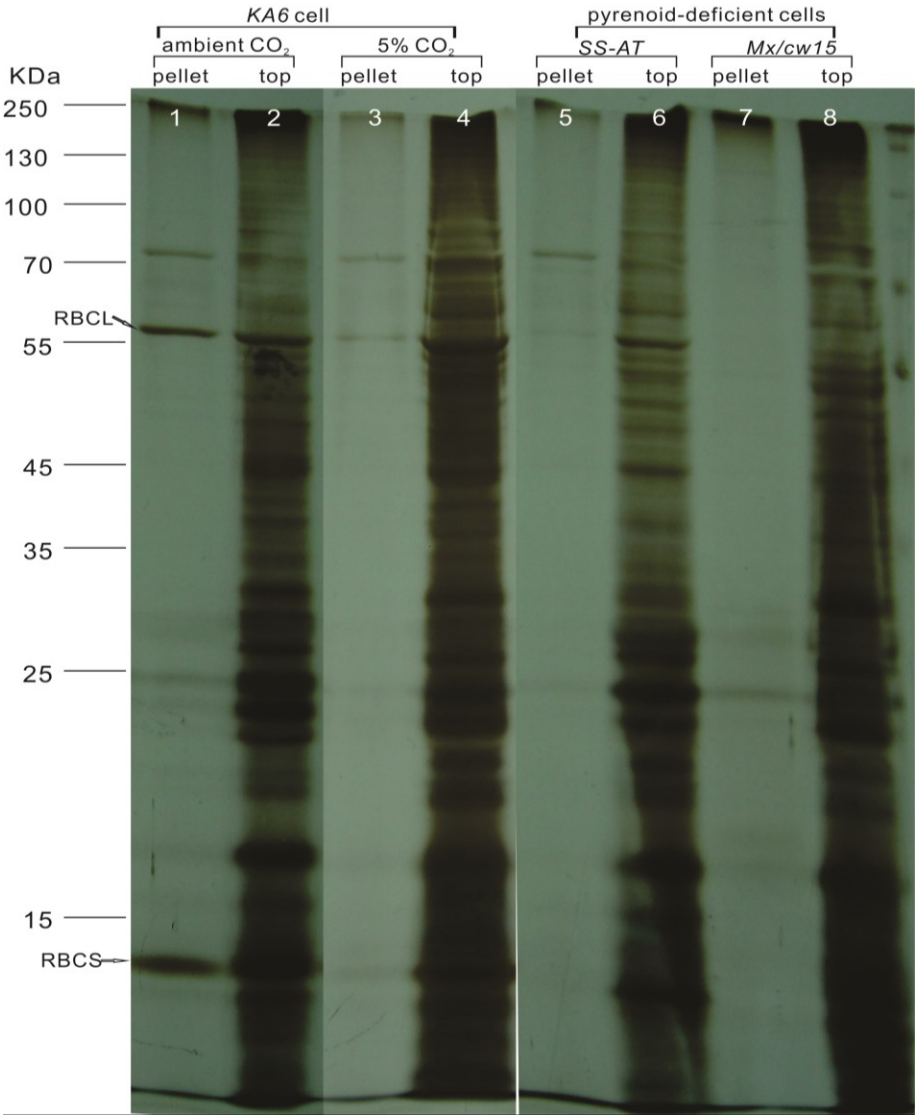

Figure 3.2 Proteins in the top and pellet fractions from pyrenoid-containing strain *KA6* and two pyrenoid deficient strains; *SS-AT* and *MX3312/cw15* were characterized by silver staining.

The pyrenoid fraction (Lane 1) from *KA6* grown in ambient CO_2 was enriched with RBCL and RBCS but not other proteins when compared to top fraction (Lane 2). The pyrenoid-containing strain *KA6* had less RBCL and RBCS in pellet fraction cultured under high CO_2 (Lane 3) than normal CO_2 (Lane 3). Two pyrenoid deficient mutants had almost no RBCL or RBCS in the pellet fraction (Lane 5 and 7).

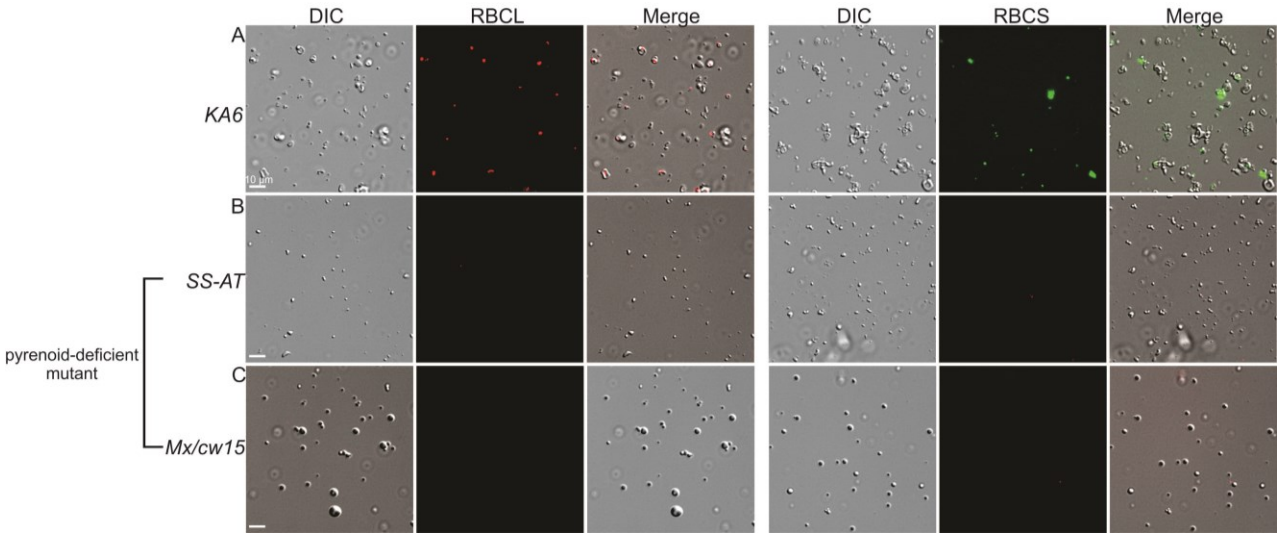

Figure 3.3 IF staining of pellet fractions from *KA6, SS-AT* and *MX3312/cw15* revealed the presence of pyrenoid in *KA6*.

The pellets were IF-stained with RBCL (red) or RBCS (green) separately. A) *KA6* showed circular structures (DIC) with staining of both RBCL and RBCS in pellet fraction. B) Small undefined particles were found in SS-AT. They lacked the staining of RBCL or RBCS. C) Round and solid particles were detected in MX3312/cw15. Since they were not IF-stained with either RBCL or RBCS, they could be large stroma starch granules, which were found in this strain before.

The pellet fractions from wild-type strain and two mutants were also examined by light microscopy. The pellet fraction from wild-type cells contained spherical bodies with a similar size as pyrenoids. These were indeed pyrenoids because they IF-stained with antibodies against RBCL and RBCS (Fig. 3.3 A). The circular structure surrounding them could be the starch sheath of pyrenoid, which was induced under low CO_2 condition and co-pelleted with pyrenoid. In addition, these fractions contained some unidentified small particulate material (Fig 3.3 A). Not all the spherical bodies from wild-type cells showed IF staining of RBCL and RBCS. That is a suggestion of a leakage of the components of pyrenoid during the isolation and/or IF staining process, or there is another type of structure, possibly stromal starch granules in the pyrenoid fraction we isolated. These spherical pyrenoids that IF-stained for RBCL and RBCS were absent in the pellets from pyrenoid-deficient strain *SS-AT* (Fig 3.3 B). However, I saw a lot of round, spherical bodies in the other pyrenoid-deficient strain *MX3312/cw15*. These spherical bodies were not IF-stained with RBCL or RBCS (Fig 3.3 C). Cells of *MX3312/cw15* normally have more than one round starch granules as seen by DIC microscopy. Thus I strongly suspect that these spherical objects were stromal starch granules. The absence of pyrenoids; spherical bodies that IF-stained for RBCL and RBCS, in two pyrenoid-deficient mutants revealed that the pellet fractions from the two mutants (*MX3312/cw15* and *SS-AT*) could be useful for the identification of contaminants by their subtraction during the proteome.

Unfortunately, the initial MS analyses of the pyrenoid pellet fractions obtained from cells showed that many proteins found in the pyrenoid pellets were known to be in other subcellular compartments of *C. reinhardtii* (Sup Fig. 3.2 S1 and S2). A major challenge for our proteomics was to further purify the pyrenoid fraction from mitochondrial, cytoplasmic and chloroplastic

contaminants.

3.3.2 Chloroplasts isolation increases the purity of the pyrenoids isolation.

The levels of the marker proteins for mitochondria, cytoplasm, ER and chloroplast showed that the chloroplast isolation efficiently removed most proteins from these compartments, but maintained most chloroplast components (Fig 3.4 A). The ER marker BIP signal decreased to 13.7% of the whole cell level while the signal of mitochondria marker AOX1 and cytoplasmic marker Cyl4 descended even lower in chloroplast: 6.6% and 0.2% of the cell level respectively. On the other hand, two chloroplast markers: a ribosomal protein of the 50S subunit of the chloroplast ribosome and RBCL showed less than 20% loss in the chloroplast samples compared with whole cell samples. Chloroplast breakage may be the reason of the partial loss of the soluble contents. Pyrenoids were isolated from the chloroplasts and the proteins in this pellet fraction were examined by silver staining. It seemed that the RBCL and RBCS signals were more intense in the pyrenoids isolated from chloroplasts then those isolated from cells (compare lanes 1 and 3 in Fig 3.4 B). In deed, some bands, which are absent in the pyrenoid isolated from cells showed up in that from chloroplasts. This suggests that the chloroplast isolation was beneficial for both purity and yield of pyrenoids. The protein pattern in the pyrenoids isolated from chloroplasts was slightly different from that in whole cells on the silver staining gel (Fig 3.4 B), which indicated that chloroplast isolation indeed removed some contaminant proteins in pyrenoid pellet.

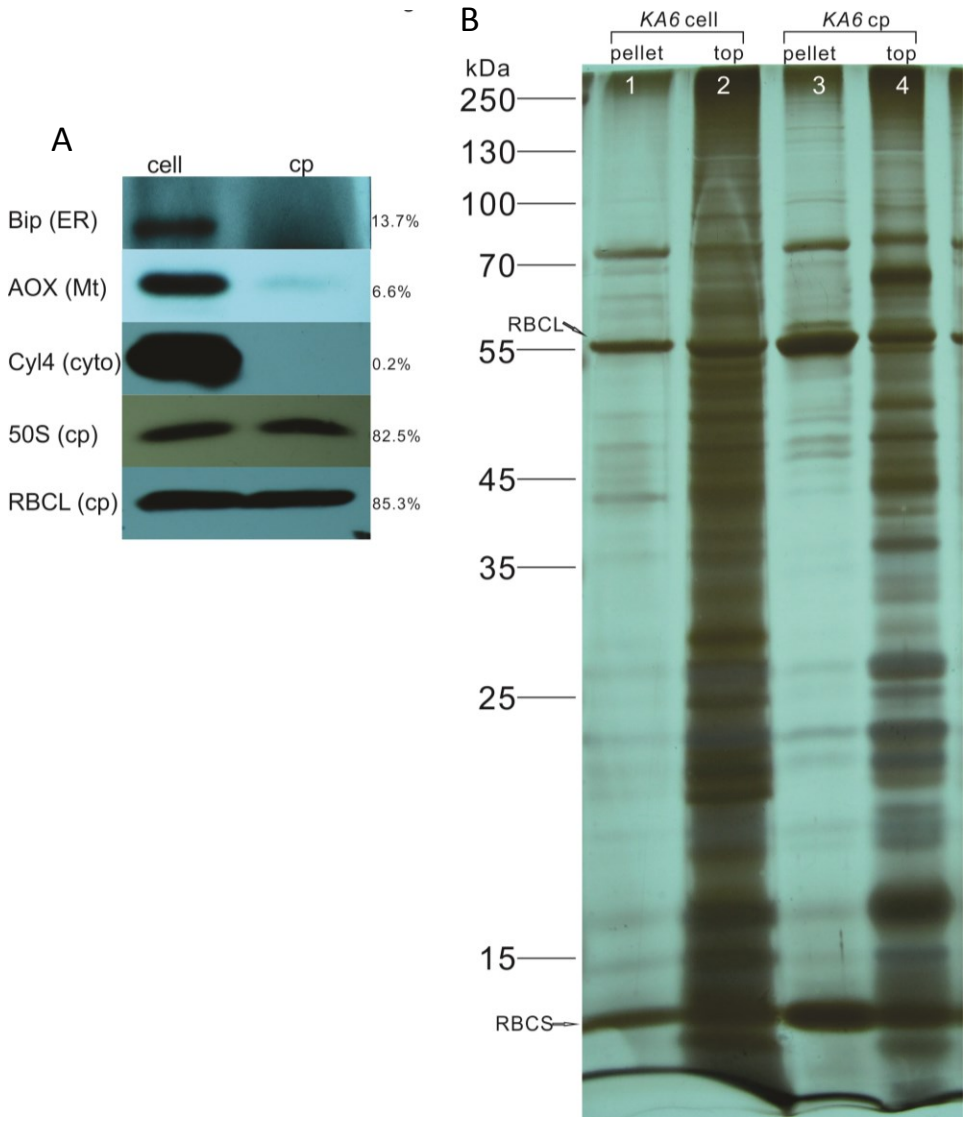

Figure 3.4 Chloroplast isolation prior to pyrenoid purification increased the purity of pyrenoid fraction.

A) Immunoblot experiments showed that chloroplast isolation rid most contamination from ER (BIP), mitochondria (AOX) and cytoplasm (cyl4) while kept most of chloroplast content (RBCL and large ribosomal protein 50S). B) Pyrenoid fraction isolated from chloroplast showed more enrichment of RBCL and RBCL (Lane 3) than that from whole cells (Lane 1). The protein pattern from chloroplast is also different from cells (Lane 3).

3.3.3 Analysis of the functional annotation of the pyrenoid proteome revealed possible functions of this compartment.

1) Chloroplast isolation and subtraction with two pyrenoid-deficient mutants improved the quality of the pyrenoid proteome.

Pellet fractions from wild-type cells and chloroplasts, and cells of *MX3312/cw15* and *SS-AT* were analyzed by mass spectrometry in two biological replicates (S1 and S2). Two technical replicate analyses were performed on each biological replicate sample and these results were pooled (Fig 3.5). Then, the resulting pellet proteomes from the two mutants were subtracted from the proteome of the pellet fraction from the *KA6* (pyrenoid-containing) strain. Finally, 179 proteins were considered as our pyrenoid proteome (Fig. 3.5).

Results of mass spectrometry confirmed that the isolation of chloroplasts before pyrenoid purification get rid of many contaminating proteins. Of the 172 proteins identified in pellet fractions from wild-type cells, only 32.6% were predicted to be chloroplast targeted by PredAlgo analysis. This proportion increased to 58.1% in the proteins identified in the pellet fraction from isolated chloroplasts (Sup Fig. 3.3). The actual proportion of chloroplast-targeted protein is even higher because PredAlgo is known to classify many known chloroplast proteins as O (other) or M (Mitochondria).

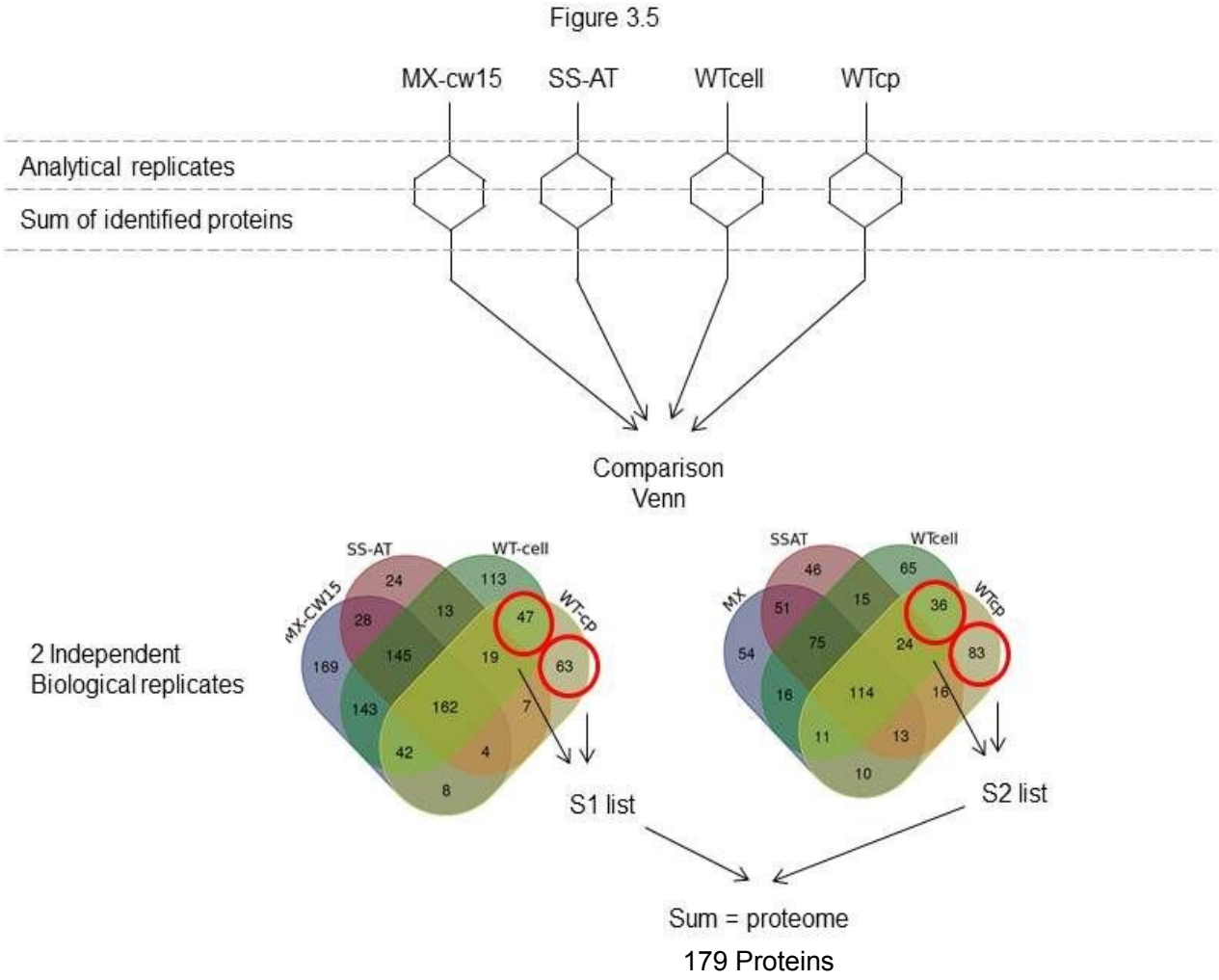

Figure 3.5 Flow chart to show how the final list of pyrenoid proteins were acquired.

Proteins in two technical replicates from same sample were identified and the results were put together to generate a protein pool for this sample. The proteins showed also in the pellet of *KA* cells, *SS-AT* and *MX3312/cw15* were subtracted out from *KA6* chloroplast sample. Two biological replicate samples S1 and S1 were classified in this way and two pools with the proteins only identified in pellet fraction of *KA6* chloroplast were combined together as a final pyrenoid proteome.

Analyses of the pellet fractions obtained from the two pyrenoid-deficient mutants indeed identify many contaminating proteins for subtraction from pellet fraction from wild-type strain to give our pyrenoid proteome. However, several known pyrenoid proteins were also removed from the list by this subtraction, e.g. RBCL and Rubisco activase [26]. This was due to a trace amount of RBCL was detected in *SS-AT* strain on silver staining gel. RBCL is one of the most abundant proteins in plants (Fig 3.2). Moreover, RBCL is known to aggregate with other proteins and a fraction of the total pool is known to become insoluble in Triton X-100 treatment (Fig. 4, Appendix II) [238]. Rubisco activase was also found in the aggregation under stress and it is also abundant [239]. Thus, detection of RBCL and Rubisco activase in the pyrenoid-deficient mutants due to their abundance or ability to aggregate could not eliminate their appearance in the pyrenoid. This also indicated that our subtraction method was very stringent and our pyrenoid proteome, while partial, have proteins that are identified with high confidence.

2) Functional annotation of the pyrenoid proteome.

Among the 179 proteins that we identified in the pyrenoid proteome, there were 115 proteins of known functions, and 64 have unknown functions (Sup Fig 3.4). KEGG analyses classified the 115 proteins into the following level one categories; “Metabolism” (72 proteins), “Genetic information processing” (38 proteins), “Stress response/Redox homeostasis” (1 protein), “Cellular process” (1 protein), “Environmental Information Processing” (3 proteins) (Fig. 3.6, Sup Fig. 3.4). The KEGG pathways were characterized by the interactions between molecules and network reactions. In KEGG level one groups, proteins were separated to more defined sub-groups based on functions (Fig. 3.6, Sup Fig 3.4). All 15 sub-groups with their components were listed in colored circles in Fig. 3.7. The color difference in the same sub-group

indicated more detailed level of functional annotation in the sub-group. Some intriguing proteins were identified and what they confirm and may reveal about pyrenoid functions is discussed below.

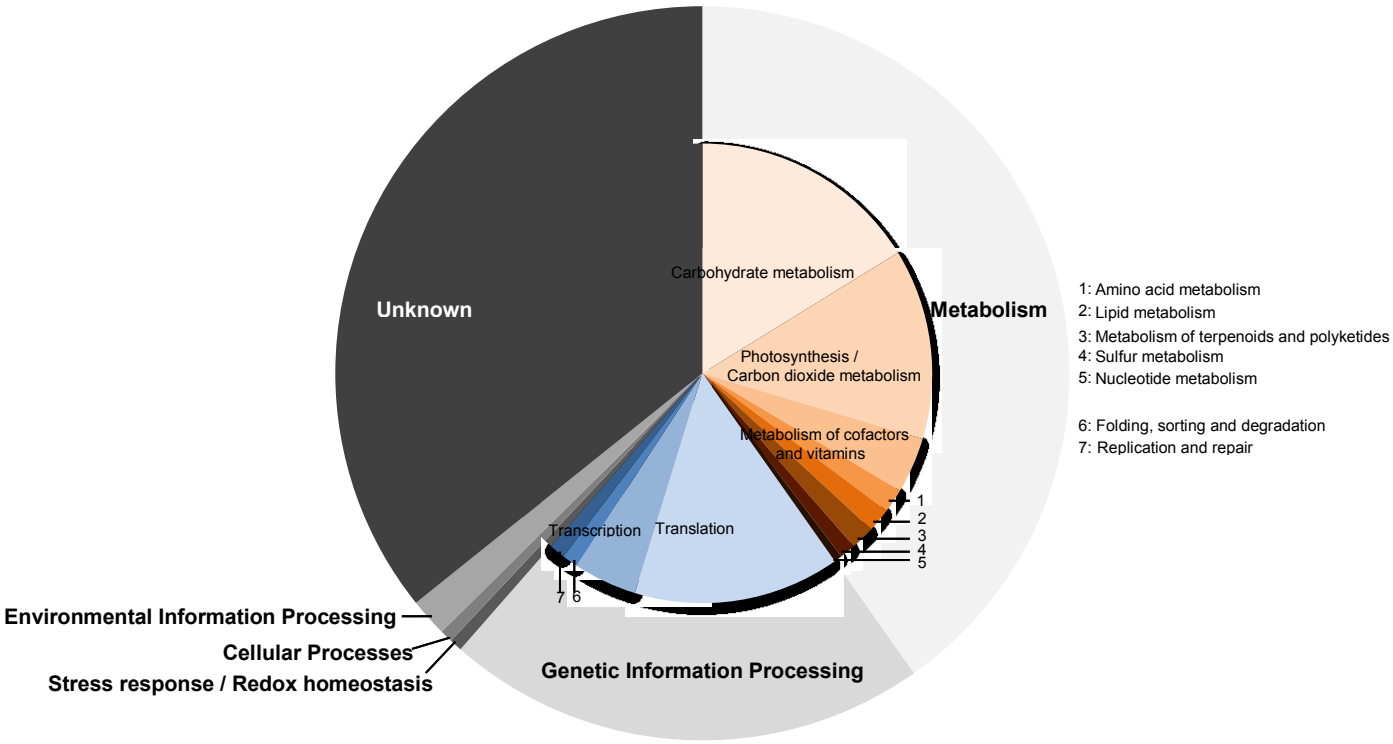

Figure 3.6 The pie chart showed the protein categories identified in pyrenoid proteome.

179 proteins were separated in six Kegg level one groups in functional annotation analysis; Metabolism (72), Genetic information processing (38), Stress response/Redox homeostasis (1), Cellular process (1), Environmental Information Processing (3) and Unknown (64).

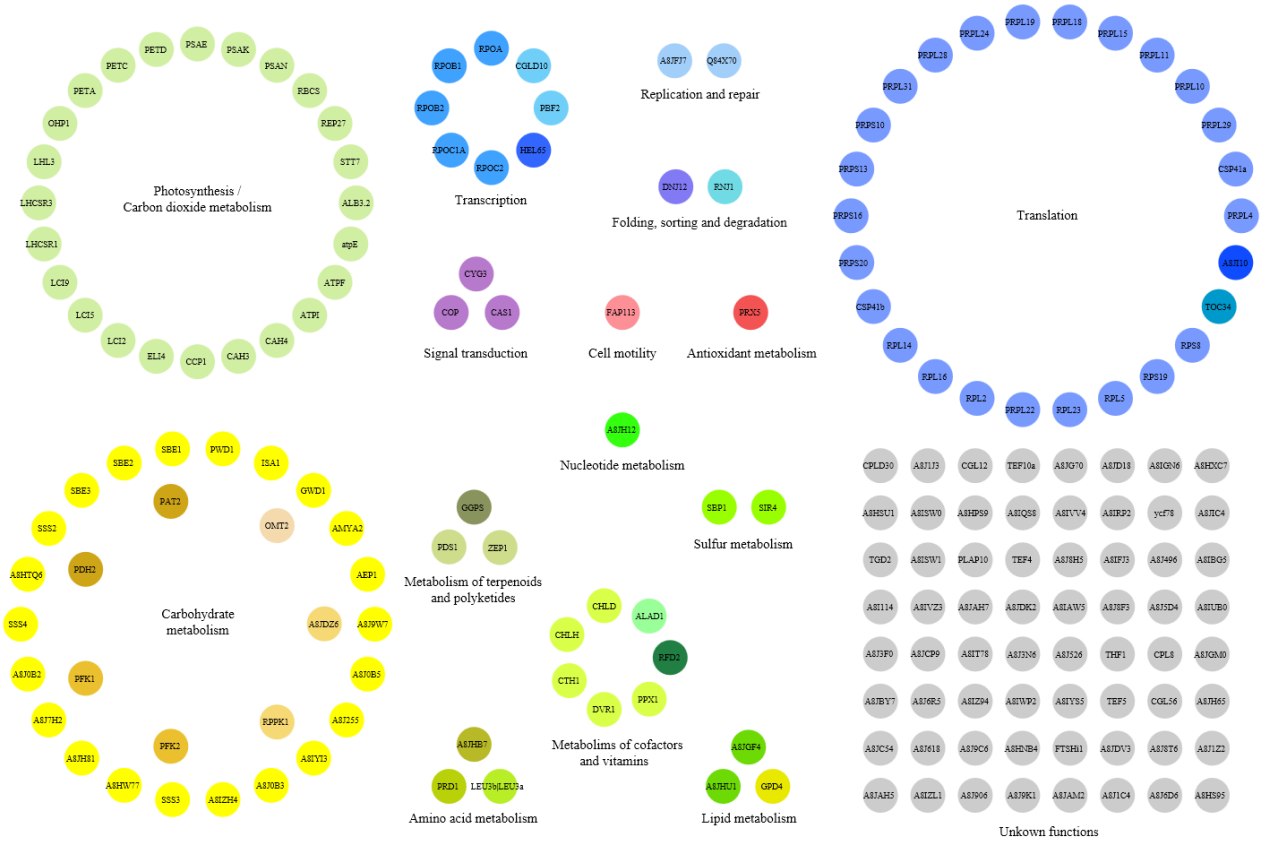

Genetic information processing

- Transcription factors
- RNA degradation
- Chaperones and folding catalysts
- DNA repair and recombination proteins
- Miscellaneous
- Polymerase activity
- Ribosome
- Translation factors
- Chloroplast biogenesis

Environmental information processing

- Miscellaneous

Cellular process

- Flagellar / cytoskeleton protein

Stress response / redox homeostasis

- Miscellaneous

Metabolism

- Photosynthesis / carbon dioxide metabolism
- Sulfur metabolism
- Fatty acid biosynthesis
- Glycerophospholipid metabolism
- Starch and sucrose metabolism
- Miscellaneous
- Glycolysis / gluconeogenesis
- Pyruvate metabolism
- Membrane transport
- Purine / pyrimidine metabolism
- Porphyrin and chlorophyll metabolism
- Porphobilinogen
- Riboflavin metabolism
- Terpenoid backbone synthesis
- Carotenoid biosynthesis
- Phenylalanine, tyrosine and tryptophan biosynthesis
- Valine, leucine and isoleucine biosynthesis
- Glycine, serine and threonine metabolism

Figure 3.7 The graph showed fifteen level two KEGG groups with their protein components. Different colors of balls in the same circle showed more detailed level three KEGG groups. The protein identifiers used were Gene Name and UniProt ID.

CCM:

The CCM is one of two processes that are known to occur in the pyrenoid. All cultures were grown under CCM inducing conditions, and, therefore, CCM proteins are expected to be found in the pyrenoid proteome. Indeed 12 proteins whose expression are known to be regulated by the low CO_2 were identified (Sup Fig. 3.5) [240]. Eleven of these were identified in the KEGG 2 category "Carbon dioxide metabolism". Moreover, 5 proteins among them were directly participated in CCM: Low-CO2-inducible protein (LCI5, 15011441), Low-CO_2-inducible chloroplast envelope protein (CCP1, 158278383), Carbonic anhydrase 3 (CAH3, 2301259), Mitochondrial carbonic anhydrase beta type (CAH4, 1323549) and Rubisco small subunit (RBCS, 20150214). These validate the results, as many known pyrenoid proteins are found. It also suggests that some of the proteins of unknown function, might function in the CCM.

Starch metabolism:

When CCM is induced, the starch sheath forms around pyrenoid [241]. Moreover, the product of CO_2 fixation in pyrenoid, 3-PGA, activates the enzyme for this starch sheath synthesis [242]. This raised the possibility that synthesis of starch sheath occurs in, or close to the pyrenoid. In our proteomic results, 22 proteins, including 4 starch synthases and 3 starch branching enzymes, were grouped in the starch and sucrose metabolism category (Sup Fig 3.4). On the silver stained polyacrylamide gel of pyrenoid pellet from chloroplasts (Fig 3.2), there was an intensive band around 70 kDa that could represent the soluble starch synthase (SSS4, 71 kDa, 8901183). In addition, seven predicted proteins might have starch-related functions, based on the presence of predicted domains for the alpha amylase catalytic domain (1 protein) or starch-binding domains (6 proteins). Four proteins function in starch degradation; alpha-amylase

(AMYA2, 158275185), alpha-glucan water dikinase (GWD1, 158281332), phosphoglucan water dikinase (PWD1, 158274573) and isoamylase (ISA1, 158274418). This implies that starch metabolism, including both synthesis and degradation, happens in or close to the pyrenoid.

A recent finding that a pyrenoid deficient mutant was not impaired in starch synthesis led to the abandonment of this hypothesis [241]. However, stromal starch granules could be synthesized at the different location with different enzymes from the pyrenoid starch sheath [241]. It still remains possible that the pyrenoid is the location where the pyrenoid starch sheath is made and broken down.

Photosynthesis:

The pyrenoid sequesters Rubisco from the O_2 produced by PSII in thylakoid membranes throughout the chloroplast. In addition, it has been proposed that the thylakoid membranes of the tubules in the pyrenoid lack PSII, and this is supported by results of histochemical staining and electron microscopy [232]. The absence of PSII subunits in our pyrenoid proteome substantiates this finding (Sup Fig 3. 4). Consistent with a previous report of PSI in pyrenoid tubule membranes histochemical staining, we found that three PS I reaction center subunits in the pyrenoid proteome. (PSI does not produce O_2 and, therefore, would not affect the O_2/CO_2 ratio in the pyrenoid). In addition, we identified three ATP synthase subunits and three cytochrome b_6f complex subunits. Like PSI and PSII, these complexes are known to be embedded in thylakoid membranes. Therefore, our results suggest that all of the major photosynthesis complexes, except PSII, are present in the thylakoid membranes of the tubules within the pyrenoid. Moreover, the absence of PSII reaction center subunits in the pyreniod proteome makes the presence of other photosystems unlikely to be a contamination by non-

pyrenoidial thylakoid membranes. In the absence of PSII, the other complexes can synthesize ATP using cyclic electron flow and photophosphorylation [243]. Our results provide further support of the previous hypothesis that ATP synthesis occurs in pyrenoid. To reiterate a major finding here; the absence of PSII subunits in our pyrenoid proteome, and the presence of subunits of each of the other major photosynthesis complexes (see below) provides the first biochemical support of this hypothesis that PSII is excluded from the pyrenoid to suppress the O_2/CO_2 ratio (Sup Fig 3. 4).

The major, abundant light-harvesting proteins that are associated with PSI and PSII were not in the proteome. However, the PSII proteins can be seen in the pellet fractions of all strains; the pyrenoid-positive WT strain and the pyrenoid-deficient mutants (Fig 3.2, Sup Fig 3.2 S1 and S2). They were just subtracted from the final proteome list. Therefore, our results did not determine whether LHC I and II proteins are in the pyrenoid or not. However, we did identify four LHC-like proteins with known or predicted roles in light-stress responses: stress-related chlorophyll a/b binding protein 1 and 3 (LHCSR1 and 3, 1865773 and 158275235), early light-inducible protein (ELI4, 158276363) and low molecular mass early light-induced protein (LHL3, 54649970) (Sup Fig 3.4). LHCSR proteins played a crucial role in dissipating excess light energy for photo-acclimation [244]. These proteins may be involved in regulating photosynthesis in the thylakoid membranes of the pyrenoid tubules. Whether there is a special requirement for the light stress responses carried out by these proteins in the pyrenoid remains to be determined.

Chlorophyll synthesis:

Historically, the location of chlorophyll synthesis in chloroplasts of plants and algae has been controversial and very little is known in *C. reinhardtii* [245]. Therefore, it was intriguing to find 6

proteins in the tetrapyrrole and chlorophyll synthesis pathway in the pyrenoid proteome (Sup Fig 3.4). It is widely assumed, but not tested, that chlorophyll synthesis is localized at or near the locations of the assembly of the photosystems and their LHCs [22]. This assumption is based on the fact that ROS and oxidative damage can be caused by free chlorophyll intermediates; i.e. in the absence of the photochemical and non-photochemical chlorophyll quenching mechanisms carried out by these complexes [246]. Thus newly synthesized chlorophyll is predicted to be integrated to the photosynthetic complex quickly [94]. Previous work in the lab identified the location of PSII subunit synthesis and assembly immediately adjacent to the pyrenoid, in the T-zone and chloroplast translation membranes (which have the marker proteins found in the T-zone) [212]. If chlorophyll is synthesized in or close to pyrenoid, it could be rapidly loaded into assembling PSII complexes in the neighboring T-zone. This could minimize the accumulation and toxicity of unassembled, non-quenched chlorophyll.

Lipid synthesis:

Biogenesis of thylakoid membrane needs the biosynthesis of galactolipids of the bilayer and the assembly of the photosystem complex. Since pyrenoid is adjacent to the PSII assembly location, I wondered if there would be any evidence of lipid synthesis in our proteome.

We did identify three proteins with roles in, or related to, lipid biosynthesis. One of these is the E1 subunit of pyruvate dehydrogenase (PDH2, 158277372), which catalyzes the conversion of pyruvate into acetyl-CoA as the beginning of lipid synthesis. The E2 subunit, DLA2, was not identified in the final list, because it was detected in the primary lists of proteins identified by MS in the wild-type and two mutant strains. This protein has a dual function as a translational activator of *psbA* translation, for the synthesis of the D1 subunit of PSII, and it is localized in the

T-zone [201]. Also identified in the pyrenoid proteome were two subunits of acetyl-CoA carboxylase (158271224, 158270727), which carboxylates acetyl-CoA to form malonyl-CoA [247]. The identification of these enzymes in fatty-acid synthesis in the pyrenoid raises the possibility of lipid metabolism in, or close to, the pyrenoid. Three elements related to thylakoid biogenesis; PSII assembly, chlorophyll synthesis and lipid synthesis all localized in or close to pyrenoid. Taken together, our results suggested that the location at the perimeter of pyrenoid could be the site of thylakoid membrane biogenesis.

Transcription:

The chloroplast DNA-directed RNA polymerase is composed of four core subunits and additional proteins as sigma factor and polymerase associated proteins [248]. Five of the identified proteins were subunits of chloroplast RNA polymerase. These proteins represented all four core polymerase subunits α (RPOA, 23307781), β (RPOB1, 24209933; RPOB2, 24209934), β' (RPOC1A, 213517451), β" (RPOC2, 213517428) respectively [248]. Although the sigma factor was not found in the pyrenoid proteome, the finding of entire core subunits of RNA polymerase and the fact that chloroplast nucleoids localized close to pyrenoid suggests it has a role in transcription of the chloroplast genome [19].

Translation:

Proteins of the chloroplast translation system were identified in the pyrenoid proteome. These include 22 ribosomal proteins; 15 of the large subunits and 6 of the smalls subunits. In addition, there is one mitochondria ribosomal protein (MRPL29, 158282820). Two chloroplast stem-loop binding proteins (CSP41a, 158280041 and CSP41b, 34398360) were also in this category and they are known to have endoribonuclease activity and function (directly or

indirectly) in transcription and translation [249].

CSP41a could initiate and regulate specific RNA turn-over in tobacco chloroplasts. CSP41b was found associated with 70S ribosome in *C. reinhardtii* and involved in mRNA processing, endonuclease activity, cleavage and translation [250, 251]. Except these two RNA-binding proteins, one ATP-dependent RNA helicase (HEL65, 158274646) and one RNase J-like protein (RNJ1, 187766731) were also found in pyrenoid proteome list. These four proteins might have a function related to RNA degradation. This proteomic result, together with the finding of 8-oxoG RNA in pyrenoid (Chapter 2), indicated that pyrenoid could be a location for oxidized RNA metabolism, for example, degradation. Degradation process of oxidized RNA would prevent their translation and limit the synthesis of aberrant proteins.

Stress response:

According to annotation information, peroxiredoxin, type II (PRX5, 158283443) was the only protein which had been categorized to "stress response" in the functional annotation. Peroxiredoxin scavenges ROS and it also plays a role in ROS signalling [252]. There are three types of peroxiredoxins II in *C. reinhardtii*, however, only one of them contains a putative chloroplast transit peptide, which was exactly the one we identified in pyrenoid proteome [252].

Other than this, proteins that have been characterized to the other functional groups could also have stress related functions. For example, Zeaxanthin epoxidase (ZEP1, 28629442) that was categorized to "Carotenoid Biosynthesis", which is required for the resistance of osmatic, drought and light stress [253, 254]. Although the function of lipid-associated proteins (PLAP10, 158278755) was "unknown" in *C. reinhardtii*, it is thought to response to oxidative, aging and

biotic stress in Solanaceae [255]. This might indicate a stress related function of this protein. Those stress-related proteins identified in the pyrenoid proteome could imply a role of pyrenoid in stress response or regulation.

3.4 Discussion

3.4.1. How might future work enhance the purity of the isolated pyrenoids?

Although the chloroplast isolation rid lots of contaminants from mitochondria and cytoplasm, we still need to further enrich the pyrenoids in the pellet. I tried to use immunoprecipitation with magnetic beads to purify pyrenoids from the crude pyrenoids fractions isolated by Triton X-100 as described above. Both RBCL and RBCS antibodies were used for purification. In the elution using affinity purified RBCL antibody and polyclonal RBCL antibody, there was a band which corresponds to the molecular weight of RBCS on the silver-staining polyacrylamide gel (Sup Fig. 3.6). This band was absent in the control experiment with pre-immune serum of RBCL (Sup Fig. 3.6). This result indicated that there might be some Rubisco or even pyrenoids isolated by RBCL antibodies. Other than RBCL and RBCS, there were other protein bands identified on the gel. However, I was unable to see pyrenoids by light microscopy in the elution. The purification with affinity purified RBCS antibody also showed a band at the molecular mass of RBCL (56 kDa), however, that is also the size of heavy chain of the antibody. It was not determined if RBCL was immunoprecipitated with RBCS yet. A specific secondary antibody, which does not detect heavy chain, could solve this problem. Although more detailed analysis would be needed to characterize the components of the eluted material from the immunoprecipitation, it offered a new possible method for further purification of the isolated pyrenoids.

3.4.2. The majority of stroma proteins were not found in pyrenoid proteome.

The results of previous work suggests that thylakoid membranes form the thylakoid tubules that extended into the pyrenoid [233]. High resolution 3D electron tomography analysis of *C. reinhardtii* chloroplast revealed that the junctions are incredibly complex, where mini-tubules containing stroma extend into thylakoid membranes which make up the thylakoid tubules [35]. These mini-tubules are in contact with the pyrenoid matrix allowing direct continuity of the chloroplast stroma. This might explain why 19 proteins in our list were found in the stroma proteome (Sup Fig. 3.7). The finding of mini-tubules indicated a direct exchange between stroma and pyrenoid and also suggested that stroma proteins in our pyrenoid proteome might not be just contaminants but actually might function in the pyrenoid.

3.4.3. Function of pyrenoid in oxidized RNA metabolism.

One important reason for us to characterize the proteome of the pyrenoid is that my results reveal that 8-oxoG oxidized RNA is localized in the pyrenoid and the major pyrenoid protein RBCL controls the level of RNA oxidation (Chapter 2). mRNA was never detected in the pyrenoid matrix by FISH [38, 212, 214]. However, when I stained wild-type cells of *C. reinhardtii* with the RNA-specific dye (SYTO® RNASelect™ Green Fluorescent cell Stain, life technologies), I did detect weak staining of pyrenoid (Sup. Fig. 3. 8). This further supports the presence of RNA in the pyrenoid. The finding of 5 RNA polymerase subunits and 22 ribosomal subunits indicated the possible function related to transcription and translation. In addition, the enzymes related to RNA degradation as RNase J, ATP-dependent RNA helicase, and CSP41 a/b were also found in pyrenoid. These results build upon the evidence that that pyrenoid has a role in RNA metabolism and a possible oxidized RNA quality control (Chapter 2). This moonlighting function

of RBCL could be the protection of intact RNA from oxidation, or repair/ degradation of oxidized RNA. The identification of enzymes related to RNA turn-over and processing supports this proposed function of the pyrenoid in RNA metabolism and quality control. The protein that could be involved in protection and repair mechanisms were not found, however, 36% of the proteins in the pyrenoid proteome are still uncharacterized.

In summary, my results describe a partial proteome of the pyrenoid with valuable new information about this micro-compartment and establish methods for a more convincing characterization of this proteome.

Chapter 4: Newly synthesized chlorophyll is localized at the perimeter of the pyrenoid and at the ends of lobes.

4.1 Introduction

The tetrapyrroles, chlorophyll and heme, are synthesized in the chloroplast in a pathway with common steps at the beginning and then branches after the synthesis of the porphyrin ring into separate pathways for each [256]. The location(s) of the steps in these pathways has been a subject of a controversial debate; with localization to the chloroplast stroma, the inner envelope membrane and thylakoid membranes proposed for various steps. However, these conclusions are based almost exclusively on subcellular fractionation studies that compared equivalent mass amounts of protein from these compartments [85]. Many of the studies compared enzyme activity levels, which are affected by other components of fractions and often labile. This drastically overrepresented the amount of envelope membrane and, hence, the proportion of proteins in the envelope, relative to others (i.e. thylakoid membranes and stroma).

Six proteins in the pyrenoid proteome are known enzymes in tetrapyrrole synthesis, including four that are specific to the chlorophyll biosynthesis branch of the pathway (Chapter 3). This suggests that the pyrenoid could be the location of chlorophyll synthesis. Indeed, two previous papers provided preliminary evidence of this hypothesis [257, 258].

A previous study in our lab revealed that there are special punctate foci, called translation zone (T-zone) localized with a chloroplast translation membrane (CTM) at the perimeter of pyrenoid. This T-zone appears to be a privileged location for PSII subunit synthesis and assembly [214]. Chlorophyll is an important component of photosynthesis complexes; it is the major pigment that harvests light energy. It transfers this energy by resonance energy

transfer to the photosystems, and chlorophyll positioned in the reaction centers of PSI and PSII act as cofactor in the charge separation and electron transport reactions [259]. While it has been supposed that chlorophyll synthesis is localized to the site of synthesis and assembly of chlorophyll-binding proteins, this has not been demonstrated to my knowledge. Surprisingly, the same question regarding heme synthesis is also unresolved; i.e. whether or not it is co-localized with cytochrome synthesis. One reason for such a co-localization is the toxicity of free chlorophyll and heme, which can produce ROS if not controlled with a variety of protective mechanisms or sequestered within protein. Therefore, it is supposed that newly synthesized chlorophyll should be rapidly bound with other components to form photosynthesis complexes. Our abovementioned results of the proteomic characterization pyrenoid suggest that the pyrenoid and adjacent region could be a location of chlorophyll synthesis.

Protoporphyrin IX is the intermediate in the biosynthesis of both chlorophyll and heme which has the porphyrin ring but lacks the central metal atom; Mg or Fe, respectively. Insertion Mg^{2+} into protoporphyrin IX by Mg-chelatase (CHLI, CHLH and CHLD) is the initial step for the specific biosynthesis of chlorophyll [90, 91]. Mg-protoporphyrin IX is then methylated and converted to divinyl-protochlorophyllide (DV-Pchlide) in two sequential steps catalyzed by Mg-protoporphyrin IX methyltransferase (PPMT) and a Mg-protoporphyrin IX monomethyl ester (oxidative) cyclase (CRD1 and CTH1) [92, 97]. CRD1 (Copper response defect 1) is the cyclase that accumulates under conditions of either copper-deficiency and oxygen-deficiency while CTH1 is expressed under copper-sufficient and oxygenated conditions [260]. Protochlorophylide (Pchlide) is a reduced product from DV-Pchlide by a DV-Pchlide-8-vinyl reductase (DVR) [99] [100]. Chlorophyllide *a* is generated by the reduction of pyrrole ring of Pchlide by one of two

distinct isoforms of protochlorophylilde oxidoreductase (POR), one light-dependent the other light-independent [102, 107]. The last step for chlorophyll *a* formation from chlorophyllide a was catalyzed by chlorophyll synthase (CHS) [117]. Chlorophyll *b* is synthesized from chlorophyllide *b* which is synthesized from chlorophyllide *a* by chlorophyllide *a* oxidase (CAO). This step was also catalyzed by chlorophyll synthase (CHS) [120, 121].

In the work described in this chapter, I asked whether chlorophyll synthesis is localized to the pyrenoid. I detected the localization of newly synthesized chlorophyll and a chlorophyll biosynthetic enzyme with fluorescence microscopy. The chlorophyll mutant *y-1* was used to detect the newly synthesized chlorophyll. This mutant has a mutation in the nuclear *y-1* gene, which is needed for ChlL translation [112]. ChlL is one important subunit for light independent POR (LID-POR). Therefore *y-1* cannot reduce protochlorophyllide to chlorophyllide in the dark. There is no chlorophyll synthesized and the color of this strain is yellow in the dark. However, this strain can synthesize light-dependent POR (LD-POR), which can reduce protochlorophyllide with light incubation. It will produce the chlorophyll when shifted to light and the color of the culture will turn from yellow to green. This process is called “greening”. Thus, localization of newly synthesized chlorophyll was detected in greening *y-1*.

The newly synthesized chlorophyll was found in two locations; in the posterior lobe of the chloroplast (which contains the pyrenoid [Chapter 1]), and tips of lobes, near the flagella. The auto-fluorescence of chlorophyll was not enriched in the pyrenoid. LD-POR only localized at the periphery of pyrenoid in *y-1* mutant when it was grown in dark. By contrast, LD-POR in a wild-type strain (CC503) showed a ring-like pattern of LD-POR IF signal in a region called the lobe junction. My colleagues and I showed that the chloroplast protein import complexes TIC and

TOC are localized in this pattern, suggesting that chloroplast protein import is localized in regions adjacent to the T-zone [214]. The results revealed much more complex patterns of chlorophyll fluorescence in the early greening *y-1* cells than simple appearance within the pyrenoid (described below), but are nevertheless consistent with the pyrenoid or its surface being a primary location of chlorophyll synthesis.

The appearance of the first chlorophyll fluorescence at the ends of the lobes in early greening *y-1* cells suggests that these regions are also locations of synthesis of chlorophyll and, by extension, chlorophyll-binding proteins. Previous work in the lab, reviewed above, found evidence only for the localized synthesis of PSII subunits and RBCL in the T-zone [212]. T-zone localization was not observed for the *psaA* chloroplast mRNA, encoding a major core subunit of PSI (PsaA), or a biochemical factor that is specifically involved in PSI assembly [212]. Similarly, the CTM showed markers of PSII assembly, but not PSI assembly [214]. Although the *psaA* mRNA and the PSI assembly factors were not seen to localize *in situ* to the lobe ends, this pattern was observed for chloroplast ribosomal proteins (markers of the chloroplast ribosome and, potentially, translational activity). Therefore, it will be important to explore the possibility that the ends of the lobes are biogenic regions for PSI, or the light-harvesting complex.

4.2 Materials and Methods

Cell culturing and treatment

Cell stains used in this chapter were listed below.

Table 4.1 strains used in the chlorophyll detection

Name	Mutation place	Chl intermediate accumulation	Color and growth condition
CC-503 (wild type)	-	-	Green/ light or dark
CC-339	*CHLH*	Protoporphyrin IX	Brown/ dark
CC-4261	*CHLM*	Mg-protoporphyrin IX	Yellow/ dark
y-1	*y* gene	Protochlorophyllide	Yellow in dark; green in light

Cells were cultured to the density of 2-4 X10^6 cells/ ml. CC-339, CC-4261 and *y-1* were grown in the dark condition while CC503 was grown under moderate light (50 µE m^{-2} s^{-1}). The dark-grown *y-1* culture was transferred to the moderate light condition for 1, 2, 3, 20 and 92 hours incubation and then detected for chlorophyll auto-fluorescence.

Chlorophyll auto-fluorescence imaging in living cells

Cells were added to equal amount of 100% (v/v) glycerol, in order to immobilize them during imaging by microscopy. The mixture was spread in the center of the microscope slide and covered with a cover slip then sealed with nail polish. This step was not done under completely dark condition, thus *y-1* cells examined in "0 h" light exposure condition were actually exposed to dim light for a couple minutes. The slides were examined by a laser scanning confocal microscope Leica TCS SP2 (Leica). The excitation wavelength was 488 nm and the emission filter was adjusted to 600 nm to 700 nm.

IF staining

All procedures were described previously [202]. The primary antibodies used were chicken AtpB (1:2000), chicken D1 (1:1000) (Agrisera), rabbit POR (1:2000). Goat anti-chicken FITC secondary antibody and Alexa Fluor 488 or 568 goat anti rabbit IgG (H+L) secondary antibody (Invitrogen) were used to introduce fluorescent signal to detection. The specimens were examined by a Leica DMI 6000 epi-fluorescent microscope with a 63X/1.4 objective, a Hamamatsu OrcaR2 camera, and Volocity acquisition software (Perkin-Elmer) in the DIC, GFP and Texas Red channels.

4.3 Results

4.3.1 Chlorophyll fluorescence in the *y-1* mutant was detected around the periphery of the pyrenoid and in the end regions of the lobes.

In the preliminary results of pyrenoid proteome, six enzymes related to the chlorophyll biosynthesis were identified (Chapter 3). The proteome of the pyrenoid opens a new avenue to the localization of this process. I used fluorescence microscopy to detect newly synthesized chlorophyll in living cells.

The chlorophyll fluorescence was imaged in *y-1* cells that were dark-grown and then maintained in near darkness (Materials and Methods) (0 h) or exposed to light to initiate greening for 1 h, 2 h, 3 h, 20 h or 96 h. The chlorophyll fluorescence was seen around the pyrenoid and at the ends of the lobes in the cells from the 0 h, 1 h and 3 h time points (Fig. 4.1 A). There was weak chlorophyll fluorescence showing in cells from the 0 h time point, which was particularly localized to the perimeter of pyrenoid, with less fluorescence from within the pyrenoid (Fig. 4.1 A). The chlorophyll fluorescence in *y-1* cells was elevated in the cells adapted to light for 1h to 3h compared to the signal in “0h” light incubated cells (Fig. 4.1 A).

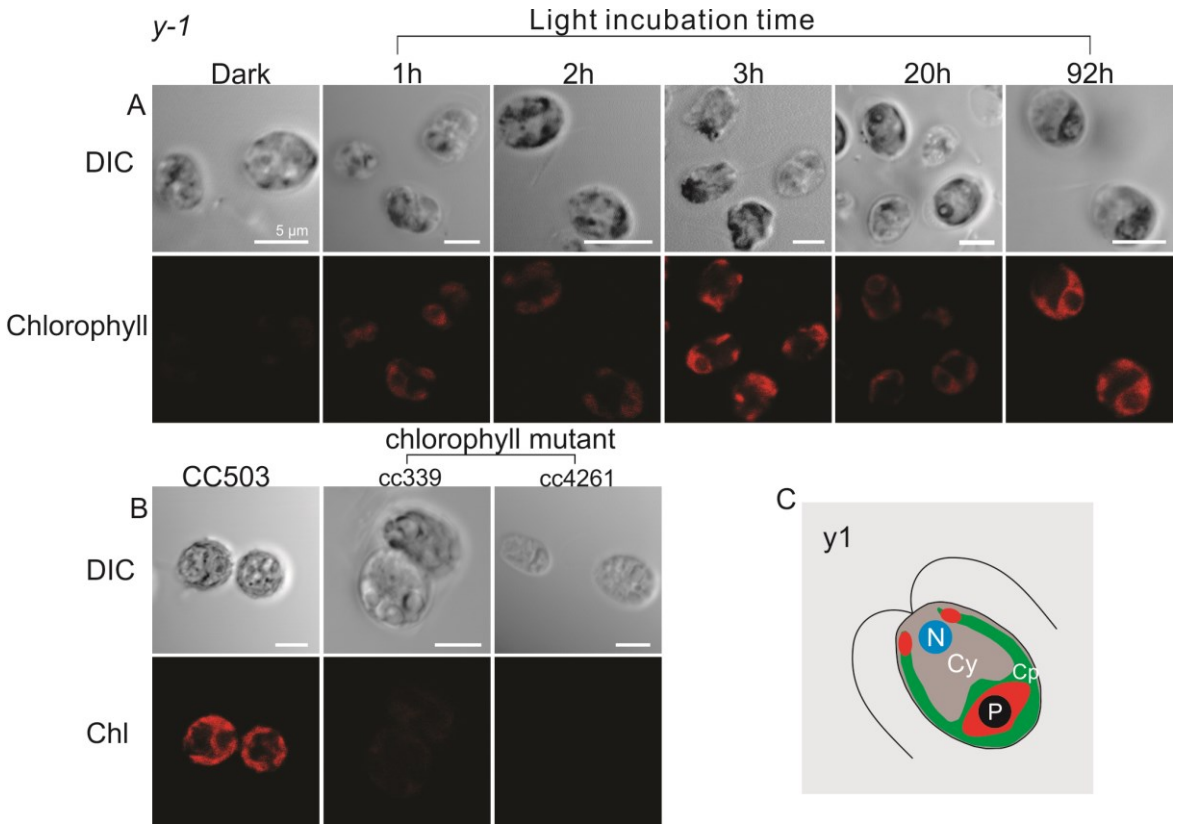

Figure 4.1 Auto-fluorescence of chlorophyll was examined in *y-1*, CC503 and two other chlorophyll mutants.

A) Auto-fluorescence of newly synthesized chlorophyll (red) in *y-1* was detected in dark grown culture and in the culture transferred to light incubation for 1h, 2h, 3h, 20h and 92 h by laser scanner confocal microscopy. Cell shape was observed in DIC channel B) The chlorophyll in CC503 grown under constant light was examined (left). The two chlorophyll mutants; CC339 and CC4261 showed weak signal of chlorophyll in them (right). C) A cartoon illustration showed newly synthesized chlorophyll distribution in *y-1* strain (red) (N; nucleous, Cy; cytoplasm, cp; chloroplast). Size bar indicated 5 µm.

In addition to the localization around the pyrenoid, I also observed that some of the cells had signal specifically enriched in T-zone [214], for example the cells in Fig. 4.1 A (the 2 h light incubation). The t-zone and CTM are identified as locations for PSII biosynthesis and assembly [38]. This might indicate that the biosynthesis of chlorophyll is related to the assembly of PSII.

In *y-1* cells after 20 h of greening, the patterns of chlorophyll fluorescence around the pyrenoid and the ends of lobes was not as obvious as at the earlier time points and the fluorescence was dispersed throughout the chloroplast (Fig. 4.1 A, Sup Fig 4.1). Over 3 days exposure to the light, the chlorophyll fluorescence was similar shape of the chloroplast that was seen in the wild-type (*CC503*) cells. The color of the *y-1* cultures at this time point also had become green from their original yellow (Fig. 4.1 A and B). Although newly synthesized chlorophyll did not localize in the pyrenoid, the close location to pyrenoid also suggest that pyrenoid could relate to the biosynthesis of chlorophyll.

In order to confirm that the auto-fluorescence described above is indeed from chlorophyll, I also analysed two chlorophyll deficient mutants as negative controls. *CC339* lacks the CHLH subunit of Mg-chelatase and accumulates protoporphyrin IX [261]. *CC4261* lacks Mg-protoporphyrin IX methyltransferase and accumulates Mg-protoporphyrin IX [261]. They both lack chlorophyll. When examined under the same microscopy settings as the *y-1* cells, neither mutant showed auto-fluorescence signal (Fig. 4.1 B). These results control for the possibility that one or more other molecules generated the auto-fluorescence attributed to chlorophyll in the greening *y-1* cells.

4.3.2 The localization of chlorophyll signal at the perimeter of pyrenoid and tip of lobes was not due to the abnormal shape of chloroplast in *y-1*.

When cultured in the dark, yellow *y-1* cells were shown to not have mutual thylakoid membranes and photosynthesis [262]. When it was transferred to light, the thylakoid biogenesis and chlorophyll synthesis initiated. An alternative explanation for the chlorophyll auto-fluorescence patterns in early greening stages of *y-1* cells could be that the shape of chloroplast is abnormal, being constricted between the basal region (posterior part with the pyrenoid) and the ends of the lobes. In this case, all the chloroplast proteins would show a similar pattern.

A chloroplast marker protein, ATP synthase B (AtpB) was detected by IF staining to show the chloroplast shape in cells from the same cultures and time points that were analyzed for chlorophyll auto-fluorescence (described above). At the 0 h time point, the AtpB IF straining showed a complete chloroplast in all optical sections and I did not see the patterns that were seen for the chlorophyll auto-fluorescence; in perimeter of pyrenoids or at the ends of the lobes (Fig. 4.2). In contrast, the chlorophyll signal of living cells showed the special pattern as seen before (Fig. 4.1). The IF signal were more obvious after incubated in the light. After 3 h of greening, the chlorophyll signal was still concentrated around the pyrenoid and at the ends of the lobes, while the signal of AtpB was dispersed throughout the chloroplast. Therefore, the auto-fluorescence patterns attributed to localized newly synthesized chloroplast were distinct from the in situ distribution of a soluble protein in the chloroplast.

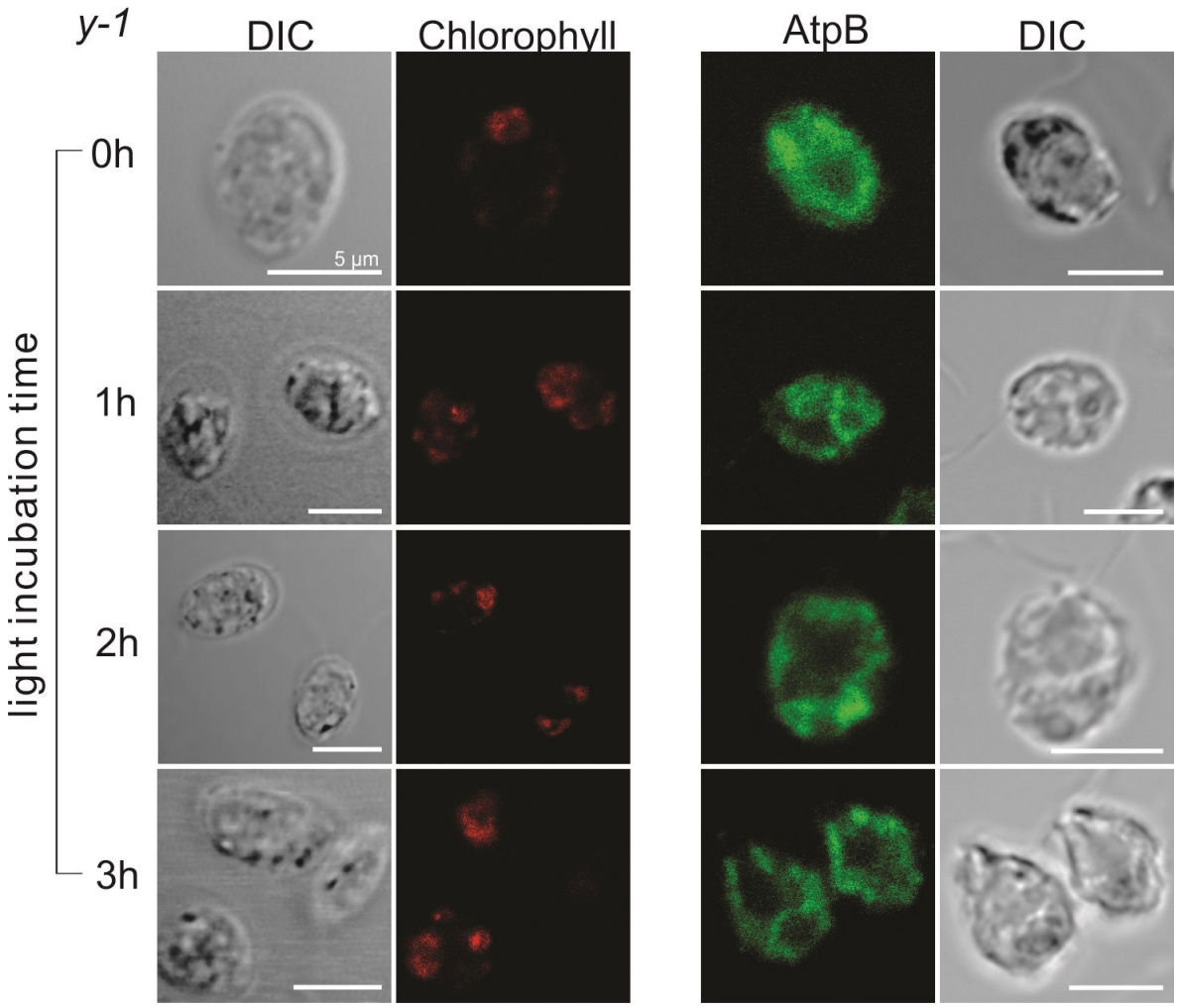

Figure 4.2 The newly synthesized chlorophyll distribution in *y-1* was different from the chloroplast marker ATP synthase B.

The auto-fluorescence signal of chlorophyll was observed in *y-1* grown in dark and with 1h, 2h and 3h light incubation (red) as described in Fig 4.1. The distribution of ATP synthase B from the same culture was detected by IF (greed). Size bar indicated 5 µm.

4.3.3 Immunoflourescence microscopy reveals LD-POR *in situ* at lobe junctions and in a ring-like pattern in wild-type cells

After figuring out the localization of newly synthesized chlorophyll, I would like to know the location of enzymes in this pathway. As a crucial enzyme, LD-POR was found previously to associate with envelope membrane and thylakoid membranes, based on subcellular fractionation experiments [263]. There is no *in situ* evidence to verify these results. Thus, I used IF staining to detect whether LD-POR is localized in the wild-type strain *CC503* and, if so, where is it localized? *CC503* was grown under constant light, transferred to the dark for 2 hours, and then exposed to moderate light (20 μE m^{-2} s^{-1}) for 5 min. The short time light exposure could initiate chlorophyll and photosystem complex re-generation. The LD-POR signal was mainly seen in the chloroplast lobes instead of pyrenoid periphery, where the newly chlorophyll was found (Fig 4.3). The LD-POR IF signal at lobe junctions appeared to surround a finger-like lobe where it connects to the chloroplast basal region (Fig. 4.3). This was seen as a perforation of the IF-signal; a non-staining spot attributed to the presence of the lobe. A similar pattern was seen with antibodies against proteins of the chloroplast protein import machinery (I am one of the coauthors, Appendix III) [214]. It was proposed that this pattern represents specialized domains of the chloroplast envelope at these lobe junctions, which are responsible for the localized import of newly synthesized proteins from the cytoplasm.

These perforations were seen in the cells from constant light, dark 2h and 5 min light conditions. This ring-like pattern existed in about 59% cells gown in constant light and this number increased to 73% in dark and 85% in cells that were dark adapted and then transferred to light (Sup Fig 4.2). The perforation was not seen with thylakoid marker protein D1. This

indicated that this pattern is not associated to the shape of thylakoid membrane, one of the currently proposed locations of LD-POR [263].

The intriguing perforation-structure at the lobe junction in *CC503* is different from the pattern of newly synthesized chlorophyll in *y-1*. This suggests that the localization of POR could show an import pattern instead of the location of chlorophyll synthesis.

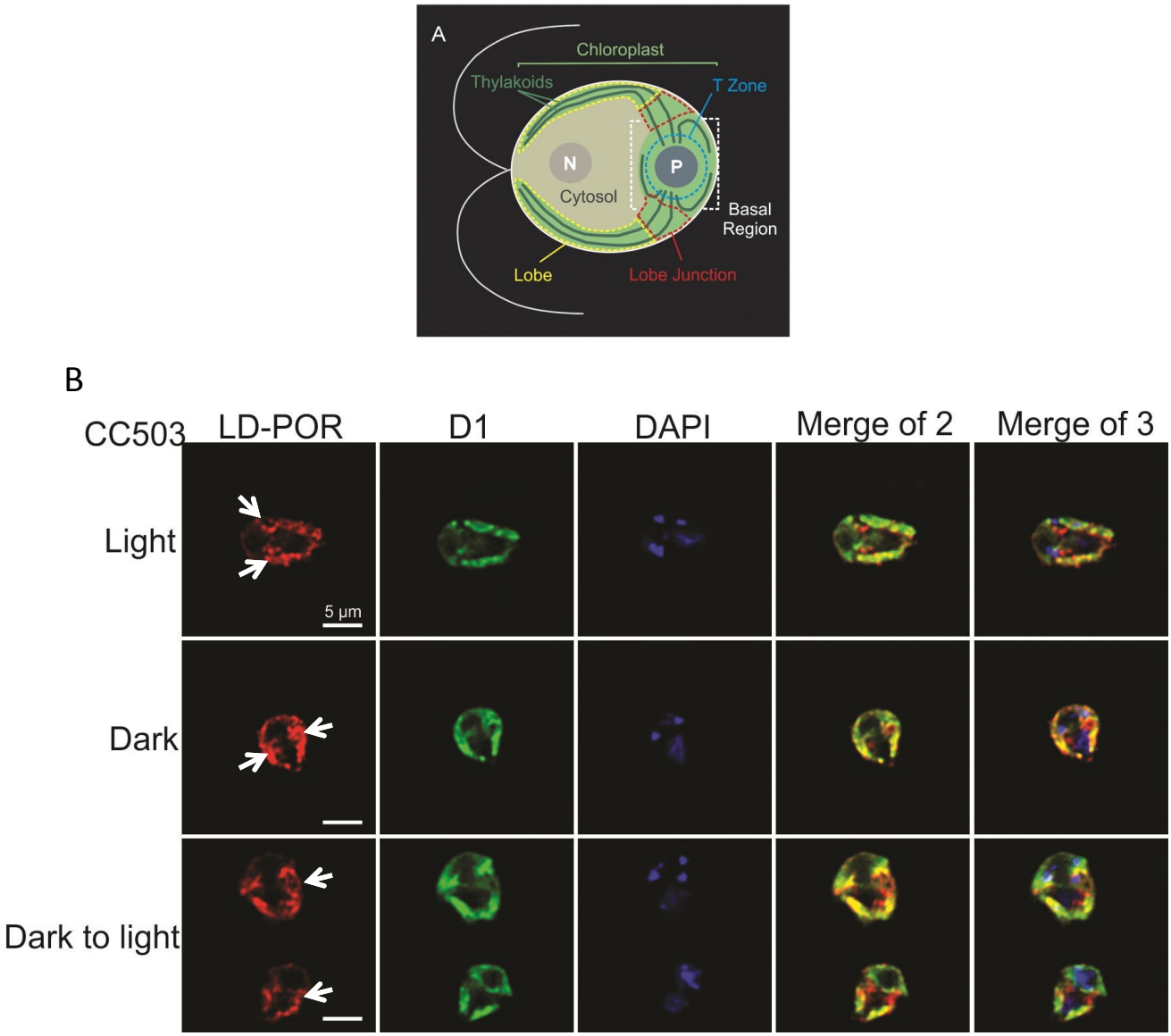

Figure 4.3 LD-POR formed a perforation at the chloroplast lobe junction in CC503.

A) An illustration to show where is the lobe junction (red region) [214]. B) The LD-POR distribution in CC503 was examined in the cells in constant light, dark (2h) adaption and dark to light (5 min) conditions. The LD-POR (red) localized mainly on the chloroplast lobes. It also formed perforation structure (white arrow) at the lobe junction where is thought to be import site for nuclear encoded chloroplast targeted proteins. A photosystem complex D1 (green) was IF-stained to show the location of thylakoid membrane. DAPI (blue) were used to localize nucleus and nucleoids. The merge of IF signal of LD-POR and D1 and all three staining were also showed. Size bar indicated 5 µm.

4.4 Discussion

4.4.1. Newly synthesized chlorophyll signal at the periphery of pyrenoid and at the ends of lobes could be confirmed by chlorophyll synthesis inhibitor.

Because the *y-1* mutant cannot reduce protochlorophyllide to chlorophyllide in the dark, there is no chlorophyll synthesis in dark. Therefore, the chlorophyll signal detected after exposing to light should come from newly synthesized chlorophyll. Moreover, this fluorescent signal is not detected in the chlorophyll deficient mutants, which accumulate only chlorophyll intermediates instead of chlorophyll (Fig. 4.1 B). That means the signal I detected was unlikely from the chlorophyll intermediates. Also, because *y-1* is known to initiate chlorophyll synthesis upon illumination [233] and that chlorophyll is a highly fluorescent molecule, it is likely that the fluorescence signal is from newly synthesized chlorophyll. However, more evidence is needed to show that this auto-fluorescence is newly synthesized chlorophyll. To test this, chlorophyll inhibitors can be used to block the chlorophyll biosynthesis in the *y-1* strain in light. If the signal observed disappears when treated with chlorophyll inhibitors, it indicates the signal I detected around the pyrenoid and at the tips of lobs should come from newly synthesized chlorophyll.

4.4.2. Chlorophyll synthesis vs thylakoid membrane biogenesis

Newly synthesized chlorophyll was used as a marker for thylakoid membrane biogenesis in *y-1* strain when it was transferred from dark to light [262]. This paper revealed that newly synthesized chlorophyll synthesis was assembled in functional PSI and PSII complexes within a few seconds after dark adapted cells were exposed to light. Since chlorophyll synthesis occurred prior to thylakoid membrane biogenesis and it was an important component in photosynthesis complex on thylakoids, its localization might give some information for the localization of

thylakoid membrane biogenesis.

T-zone and CTM had been identified as a PSII synthesis and an assembly place by a previous student in our lab [212]. They may also relate to the biogenesis of thylakoid membrane. Part of newly synthesized chlorophyll signal was found around the pyrenoids and some of it was concentrated at T-zone area (Fig 4.1 A). This interesting finding made a bridge of PSII assembly and chlorophyll synthesis. Chlorophyll is very important component of PSII complex. It is reasonable that these two share the same or very close localization for synthesis or assembly.

Besides the newly synthesized chlorophyll, I was wondering where were the enzymes related to the chlorophyll synthesis. If they also localized in T-zone or CTM, I would have more confidence of the connection of PSII synthesis and assembly with chlorophyll biosynthesis. LD-POR localized around pyrenoids but did not localize at the tips of lobes in the dark in *y-1*. When I consider the fact that CTM was localized at the perimeter of pyrenoid, the IF signal of POR could be also in CTM. The finding implied that the localization of chlorophyll biosynthesis enzymes might relate to the localization of PSII synthesis and assembly.

A PratA-defined membrane (PDM) was identified as a place for PSII assembly as CTM in cyanobacteria [247]. Interestingly, POR found in PDM revealed a tight connection between chlorophyll synthesis and PSII assembly [247]. It also raised a possibility that PDM is for both PSII biogenesis and chlorophyll synthesis in cyanobacteria. The IF signal of POR in *y-1* was found at the perimeter of pyrenoid, where was identified as CTM region. In addition, lipid metabolism proteins were found in pyrenoid proteome. Taking all these elements together, CTM or generally speaking the perimeter of pyrenoid might be a strong candidate for the localization of

thylakoid membrane biogenesis.

Unlike PSII, the localization of PSI synthesis and assembly was still not very clear. PSI is also an important component of thylakoid membrane and its assembly could relate to thylakoid membrane biogenesis. The localization of newly synthesized chlorophyll could also offer a possible hypothesis for PSI localization. The newly synthesized chlorophyll localized to the perimeter of pyrenoids and the tips of lobe. The perimeter of pyrenoids was also identified as a localization of CTM for PSII synthesis and assembly. Then I wanted to know what else could happen at the tips of lobes. One hypothesis is that the tips of lobes are the major localization for PSI synthesis and assembly.

Besides the newly synthesized chlorophyll, some other proteins like ribosomal protein were also found located at the tips of lobes (Data not shown). The chloroplast nucleoids located at the perimeter of pyrenoid as well as tips of lobes at the 2h and 6h in the light cycle of the synchronised cultures [19]. The finding of DNA and ribosomal protein implied that tips of lobes could be localization of protein synthesis. If mRNA signal could also be detected at the same place, tips of lobes could be another T-zone specifically for PSI.

We have already known that 1) nucleoids were localized around pyrenoid and at the tips of lobes at certain time in synchronized cells; 2) newly synthesized chlorophyll was localized at the perimeter of pyrenoids and tips of lobes and it may be related to the thylakoid membrane biogenesis; 3) T-zone and related membrane CTM are the major location for PSII synthesis and assembly; 4) tips of lobes could be another location for some protein synthesis and complex assembly, such as PSI. All the information composed an intriguing hypothesis that the localization of thylakoid membrane biogenesis might be around the pyrenoids or at the tips of

lobes together with chlorophyll synthesis.

4.4.3 LD-POR localized at the chloroplast protein import machinery could be beneficial for the photosystem assembly.

The ring-like pattern of LD-POR localization at lobe junctions is intriguing because it resembles a pattern seen for the TIC and TOC proteins, which are involved in the import of proteins into the chloroplast [214]. We proposed in that paper that import of the nuclear genome-encoded proteins of PSII (and possibly other complexes) is localized to lobe junctions to build upon newly assembled PSII reaction centers in the neighboring T-zone. The TIC and TOC complexes import the major chlorophyll-binding proteins of the chloroplast, the light harvesting complex (LHC) proteins associated with PSI and PSII [214]. One intriguing possibility is that the LD-POR is localized to the envelope at lobe junctions to provide the chlorophyll to the LHC proteins when or soon after they enter the chloroplast. As the expression of LHC proteins is strongly light-induced [264], it would be beneficial to use a light-dependent POR to synthesis the chlorophyll for them.

This ring-like pattern of LD-POR localization at the lobe junctions and in the lobes contrasts the appearance of the initial chlorophyll fluorescence in greening *y-1* cells (compare Figs 4.3 and 4.4). I can only speculate that the former is to provide chlorophyll for the incoming LHC proteins and the latter is the newly synthesized chlorophyll for the assembling PSI and PSII reaction centers in these regions.

4.4.4. Could newly synthesized chlorophyll localize differently from the enzymes in chlorophyll synthesis?

IF staining of POR did not show exact pattern as I identified of newly synthesized chlorophyll

localization. There are two possibilities for this, the first one is that perimeter of pyrenoids and tips of lobes are the localization of chlorophyll synthesis. Some enzyme might localize with the newly synthesized chlorophyll while the others not. To explore more about this possibility, the localization of other chlorophyll synthesis enzymes, especially the ones that I found in the pyrenoid proteomics, should be determined. I would like to localize these proteins by IF staining if there are commercial antibodies against them or I would add HA tag to those proteins and examine their localization pattern under microscope. Second hypothesis is that the newly synthesized chlorophyll is transported to the perimeter of pyrenoid and tips of lobes after being synthesized. Chlorophyll could be generated in seconds when the cells were exposed to light. Before I checked the chlorophyll localization, I exposed the culture in dim light for a couple minutes to prepare the slides. It is long enough for the initiation of chlorophyll synthesis and these newly synthesized chlorophyll could be transferred to the other place for function. The appearance of chlorophyll at the perimeter of pyrenoid and tips of lobes may relate to the thylakoid membrane biogenesis.

Reference

1. Harris, E.H., *The Chlamydomonas sourcebook : a comprehensive guide to biology and laboratory use*. 1989, San Diego: Academic Press. xiv, 780 p.

2. Boynton, J.E., et al., *Chloroplast transformation in Chlamydomonas with high velocity microprojectiles.* Science, 1988. **240**(4858): p. 1534-8.

3. Goldschmidt-Clermont, M., *Coordination of nuclear and chloroplast gene expression in plant cells.* Int Rev Cytol, 1998. **177**: p. 115-80.

4. Ettl, H., *[About the progress of chloroplast division in chlamydomonas (author's transl)].* Protoplasma, 1976. **88**(1): p. 75-84.

5. luykx, P., *Contractile vacuoles*, in *Vacuolar Compartments*, D.G.R.a.J.C. Rogers, Editor. 2000, Sheffield Academic Press: Sheffield. p. 43-70.
6. Nickelsen, J. and U. Kuck, *The unicellular green alga Chlamydomonas reinhardtii as an experimental system to study chloroplast RNA metabolism.* Naturwissenschaften, 2000. **87**(3): p. 97-107.

7. Grief, C., M.A. O'Neill, and P.J. Shaw, *The zygote cell wall of Chlamydomonas reinhardii: a structural, chemical and immunological approach.* Planta, 1987. **170**(4): p. 433-45.

8. Terashima, M., M. Specht, and M. Hippler, *The chloroplast proteome: a survey from the Chlamydomonas reinhardtii perspective with a focus on distinctive features.* Curr Genet, 2011. **57**(3): p. 151-68.

9. Lacoste-Royal, G. and S.P. Gibbs, *Immunocytochemical Localization of Ribulose-1,5-Bisphosphate Carboxylase in the Pyrenoid and Thylakoid Region of the Chloroplast of Chlamydomonas reinhardtii.* Plant Physiol, 1987. **83**(3): p. 602-606.

10. de Vitry, C. and O. Vallon, *Mutants of Chlamydomonas: tools to study thylakoid membrane structure, function and biogenesis.* Biochimie, 1999. **81**(6): p. 631-43.

11. Merchant, S.S., et al., *The Chlamydomonas genome reveals the evolution of key animal and plant functions.* Science, 2007. **318**(5848): p. 245-50.

12. Blaby, I.K., et al., *The Chlamydomonas genome project: a decade on.* Trends Plant Sci, 2014. **19**(10): p. 672-80.

13. Goksoyr, J., *Evolution of eucaryotic cells.* Nature, 1967. **214**(5093): p. 1161.

14. Gray, M.W., *The endosymbiont hypothesis revisited.* Int Rev Cytol, 1992. **141**: p. 233-357.

15. Gray, M.W., G. Burger, and B.F. Lang, *Mitochondrial evolution.* Science, 1999. **283**(5407): p. 1476-81.

16. Bogorad, L., *Evolution of early eukaryotic cells: genomes, proteomes, and compartments.* Photosynth Res, 2008. **95**(1): p. 11-21.

17. Maul, J.E., et al., *The Chlamydomonas reinhardtii plastid chromosome: islands of genes in a sea of repeats.* Plant Cell, 2002. **14**(11): p. 2659-79.

18. Ris, H. and W. Plaut, *Ultrastructure of DNA-containing areas in the chloroplast of Chlamydomonas.* J Cell Biol, 1962. **13**: p. 383-91.

19. T Ehara, Y.O., T Osafune, E Hase, *Behavior of Chloroplast Nucleoids During the Cell Cycle of Chlamydomonas reinhardtii in Synchronized Culture.* Current Research in Photosynthesis, 1990. **26**(2): p. 7.

20. Shi, L.X. and S.M. Theg, *The chloroplast protein import system: from algae to trees.* Biochim Biophys Acta, 2013. **1833**(2): p. 314-31.

21. Zerges, W. and C. Hauser, eds. *Chapter 28 - Protein Synthesis in the Chloroplast*. The Chlamydomonas Sourcebook (Second Edition), ed. E. Harris, Stern DB, Witman, GB. Vol. 2. 2009, Elsevier. 967-1025.

22. Zerges, W., *Translation in chloroplasts.* Biochimie, 2000. **82**(6-7): p. 583-601.

23. Morita, E., et al., *Presence of the CO2-concentrating mechanism in some species of the pyrenoid-less free-living algal genus Chloromonas (Volvocales, Chlorophyta).* Planta, 1998. **204**(3): p. 269-76.

24. Nozaki, H., K. Onishi, and E. Morita, *Differences in pyrenoid morphology are correlated with differences in the rbcL genes of members of the Chloromonas lineage (volvocales, chlorophyceae).* J Mol Evol, 2002. **55**(4): p. 414-30.

25. Chan, K., *The pyrenoids of the green algae (Chlorophyceae).* Academic Annual, 1972. **2**: p. 16.

26. Mckay, R.M.L. and S.P. Gibbs, *Composition and Function of Pyrenoids - Cytochemical and Immunocytochemical Approaches.* Canadian Journal of Botany-Revue Canadienne De Botanique, 1991. **69**(5): p. 1040-1052.

27. Badger, M.R., et al., *The diversity and coevolution of Rubisco, plastids, pyrenoids, and chloroplast-based CO2-concentrating mechanisms in algae.* Canadian Journal of Botany-Revue Canadienne De Botanique, 1998. **76**(6): p. 1052-1071.

28. McKay, R.M. and S.P. Gibbs, *Phycoerythrin is absent from the pyrenoid of Porphyridium cruentum: photosynthetic implications.* Planta, 1990. **180**(2): p. 249-56.

29. Suss, K.H., I. Prokhorenko, and K. Adler, *In Situ Association of Calvin Cycle Enzymes, Ribulose-1,5-Bisphosphate Carboxylase/Oxygenase Activase, Ferredoxin-NADP+ Reductase, and Nitrite Reductase with Thylakoid and Pyrenoid Membranes of Chlamydomonas reinhardtii Chloroplasts as Revealed by Immunoelectron Microscopy.* Plant Physiol, 1995. **107**(4): p. 1387-1397.

30. Gowik, U. and P. Westhoff, *The path from C3 to C4 photosynthesis.* Plant Physiol, 2011. **155**(1): p. 56-63.

31. Mariscal, V., et al., *Differential regulation of the Chlamydomonas Nar1 gene family by carbon and nitrogen.* Protist, 2006. **157**(4): p. 421-33.

32. Fukuzawa, H., et al., *Ccm1, a regulatory gene controlling the induction of a carbon-concentrating mechanism in Chlamydomonas reinhardtii by sensing CO2 availability.* Proc Natl Acad Sci U S A, 2001. **98**(9): p. 5347-52.

33. Meyer, M.T., et al., *Rubisco small-subunit alpha-helices control pyrenoid formation in Chlamydomonas.* Proc Natl Acad Sci U S A, 2012. **109**(47): p. 19474-9.

34. Sager, R. and G.E. Palade, *Structure and development of the chloroplast in Chlamydomonas. I. The normal green cell.* J Biophys Biochem Cytol, 1957. **3**(3): p. 463-88.

35. Engel, B.D., et al., *Native architecture of the Chlamydomonas chloroplast revealed by in situ cryo-electron tomography.* Elife, 2015. **4**.

36. T, M.S.a.H., *Further confirmation of the presence of DNA in the pyrenoid core of the siphonous green algal genus Caulerpa (Caulerpales, Ulvophyceae, Chlorophyta).* Phycological Research, 1995. **43**: p. 4.

37. Shukla, M., et al., *UVI31+Is a DNA Endonuclease That Dynamically Localizes to Chloroplast Pyrenoids in C. reinhardtii.* Plos One, 2012. **7**(12).

38. Uniacke, J. and W. Zerges, *Stress induces the assembly of RNA granules in the chloroplast of Chlamydomonas reinhardtii.* J Cell Biol, 2008. **182**(4): p. 641-6.

39. Goldberg, I. and I. Ohad, *Biogenesis of chloroplast membranes. V. A radioautographic study of membrane growth in a mutant of Chlamydomonas reinhardi y-1.* J Cell Biol, 1970. **44**(3): p. 572-91.

40. Michaels, A.S., C.L. Jelsema, and R.J. Barrnett, *Membrane lipid metabolism in Chlamydomonas reinhardtii 137+ and y-1: II. Cytochemical localization of acyltransferase activities.* J Ultrastruct Res, 1983. **82**(1): p. 35-51.

41. Bauwe, H., M. Hagemann, and A.R. Fernie, *Photorespiration: players, partners and origin.* Trends Plant Sci, 2010. **15**(6): p. 330-6.

42. Andersson, I. and A. Backlund, *Structure and function of Rubisco.* Plant Physiol Biochem, 2008. **46**(3): p. 275-91.

43. Spreitzer, R.J. and M.E. Salvucci, *Rubisco: structure, regulatory interactions, and possibilities for a better enzyme.* Annu Rev Plant Biol, 2002. **53**: p. 449-75.

44. Goldschmidt-Clermont, M., M. Rahire, and J.D. Rochaix, *Redundant cis-acting determinants of 3' processing and RNA stability in the chloroplast rbcL mRNA of Chlamydomonas.* Plant J, 2008. **53**(3): p. 566-77.

45. Kuchitsu, K., M. Tsuzuki, and S. Miyachi, *Characterization of the Pyrenoid Isolated from Unicellular Green-Alga Chlamydomonas-Reinhardtii - Particulate Form of Rubisco Protein.* Protoplasma, 1988. **144**(1): p. 17-24.

46. Morita, E., et al., *High localization of ribulose-1,5-bisphosphate carboxylase/oxygenase in the pyrenoids of Chlamydomonas reinhardtii (Chlorophyta), as revealed by cryofixation and immunogold electron microscopy.* Journal of Phycology, 1997. **33**(1): p. 68-72.

47. He, P., *Gold immunolocalization of Rubisco and Rubisco activase in pyrenoid of Chlamydomonas reinhardtii.* Algae, 2003. **18**: p. 7.

48. Markelova, A.G., *Ultrastuctural localization of ribulose bisphosphate carboxylase in algal cells.* Fiziol. Rast, 1990. **37**: p. 5.

49. Vladimirova, M.G., *Use of the cytoimmunofluorescent method to clarify localization of ribulose bisphosphate carboxylase in pyrenoids of unicellular algae.* Sov.Plant Phsiol., 1982. **29**(10): p. 725.

50. Klein, U., J.D. De Camp, and L. Bogorad, *Two types of chloroplast gene promoters in Chlamydomonas reinhardtii.* Proc Natl Acad Sci U S A, 1992. **89**(8): p. 3453-7.

51. Barnes, D., et al., *Contribution of 5'- and 3'-untranslated regions of plastid mRNAs to the expression of Chlamydomonas reinhardtii chloroplast genes.* Mol Genet Genomics, 2005. **274**(6): p. 625-36.

52. Blowers, A.D., et al., *Functional in vivo analyses of the 3' flanking sequences of the Chlamydomonas*

chloroplast rbcL and psaB genes. Mol Gen Genet, 1993. **238**(3): p. 339-49.

53. Johnson, X., *Manipulating RuBisCO accumulation in the green alga, Chlamydomonas reinhardtii.* Plant Mol Biol, 2011. **76**(3-5): p. 397-405.

54. Yosef, I., et al., *RNA binding activity of the ribulose-1,5-bisphosphate carboxylase/oxygenase large subunit from Chlamydomonas reinhardtii.* J Biol Chem, 2004. **279**(11): p. 10148-56.

55. Recuenco-Munoz, L., et al., *Targeted quantitative analysis of a diurnal RuBisCO subunit expression and translation profile in Chlamydomonas reinhardtii introducing a novel Mass Western approach.* J Proteomics, 2015. **113**: p. 143-53.

56. Vance, P.a.S., M. H., *Growth, Photosynthesis and Gene Expression in Chlamydomonas Over a Range of CO2 Concentrations and CO2/O2 Ratios: CO2 Regulates Multiple Acclimation States*. 2005: Iowa State University. 198.

57. Moroney, J.V., et al., *Photorespiration and carbon concentrating mechanisms: two adaptations to high O2, low CO2 conditions.* Photosynth Res, 2013. **117**(1-3): p. 121-31.

58. Burow, M.D., et al., *Isolation of cDNA clones of genes induced upon transfer of Chlamydomonas reinhardtii cells to low CO2.* Plant Mol Biol, 1996. **31**(2): p. 443-8.

59. Duanmu, D., et al., *Knockdown of limiting-CO2-induced gene HLA3 decreases HCO3- transport and photosynthetic Ci affinity in Chlamydomonas reinhardtii.* Proc Natl Acad Sci U S A, 2009. **106**(14): p. 5990-5.

60. Van, K. and M.H. Spalding, *Periplasmic carbonic anhydrase structural gene (Cah1) mutant in chlamydomonas reinhardtii.* Plant Physiol, 1999. **120**(3): p. 757-64.

61. Badger, M.R. and G.D. Price, *Carbonic Anhydrase Activity Associated with the Cyanobacterium Synechococcus PCC7942.* Plant Physiol, 1989. **89**(1): p. 51-60.

62. Tirumani, S., et al., *Regulation of CCM genes in Chlamydomonas reinhardtii during conditions of light-dark cycles in synchronous cultures.* Plant Mol Biol, 2014. **85**(3): p. 277-86.

63. Miura, K., et al., *Expression profiling-based identification of CO2-responsive genes regulated by CCM1 controlling a carbon-concentrating mechanism in Chlamydomonas reinhardtii.* Plant Physiol, 2004. **135**(3): p. 1595-607.

64. Pollock, S.V., et al., *The Chlamydomonas reinhardtii proteins Ccp1 and Ccp2 are required for long-term growth, but are not necessary for efficient photosynthesis, in a low-CO2 environment.* Plant Mol Biol, 2004. **56**(1): p. 125-32.

65. Rolland, N., et al., *Disruption of the plastid ycf10 open reading frame affects uptake of inorganic carbon in the chloroplast of Chlamydomonas.* EMBO J, 1997. **16**(22): p. 6713-26.

66. Wang, Y., D. Duanmu, and M.H. Spalding, *Carbon dioxide concentrating mechanism in Chlamydomonas reinhardtii: inorganic carbon transport and CO2 recapture.* Photosynth Res, 2011. **109**(1-3): p. 115-22.

67. Wang, Y. and M.H. Spalding, *LCIB in the Chlamydomonas CO2-concentrating mechanism.* Photosynth Res, 2014. **121**(2-3): p. 185-92.

68. Yamano, T., et al., *Isolation and characterization of mutants defective in the localization of LCIB, an*

essential factor for the carbon-concentrating mechanism in Chlamydomonas reinhardtii. Photosynth Res, 2014. **121**(2-3): p. 193-200.

69. Moroney, J.V. and R.A. Ynalvez, *Proposed carbon dioxide concentrating mechanism in Chlamydomonas reinhardtii.* Eukaryot Cell, 2007. **6**(8): p. 1251-9.

70. Borkhsenious, O.N., C.B. Mason, and J.V. Moroney, *The intracellular localization of ribulose-1,5-bisphosphate Carboxylase/Oxygenase in chlamydomonas reinhardtii.* Plant Physiol, 1998. **116**(4): p. 1585-91.

71. Wang, Y., D.J. Stessman, and M.H. Spalding, *The CO2 concentrating mechanism and photosynthetic carbon assimilation in limiting CO2 : how Chlamydomonas works against the gradient.* Plant J, 2015. **82**(3): p. 429-48.

72. Karlsson, J., et al., *A novel alpha-type carbonic anhydrase associated with the thylakoid membrane in Chlamydomonas reinhardtii is required for growth at ambient CO2.* EMBO J, 1998. **17**(5): p. 1208-16.

73. Sinetova, M.A., et al., *Identification and functional role of the carbonic anhydrase Cah3 in thylakoid membranes of pyrenoid of Chlamydomonas reinhardtii.* Biochim Biophys Acta, 2012. **1817**(8): p. 1248-55.

74. Meyer, M. and H. Griffiths, *The internal plumbing of algal chloroplasts.* Elife, 2015. **4**.

75. Wang, Y., D.J. Stessman, and M.H. Spalding, *The CO Concentrating Mechanism and Photosynthetic Carbon Assimilation in Limiting CO : how Chlamydomonas works against the gradient.* Plant J, 2015.

76. Xiang, Y., J. Zhang, and D.P. Weeks, *The Cia5 gene controls formation of the carbon concentrating mechanism in Chlamydomonas reinhardtii.* Proc Natl Acad Sci U S A, 2001. **98**(9): p. 5341-6.

77. Fang, W., et al., *Transcriptome-wide changes in Chlamydomonas reinhardtii gene expression regulated by carbon dioxide and the CO2-concentrating mechanism regulator CIA5/CCM1.* Plant Cell, 2012. **24**(5): p. 1876-93.

78. Nelson, E.B. and N.E. Tolbert, *The regulation of glycolate metabolism in Chlamydomonas reinhardtii.* Biochim Biophys Acta, 1969. **184**(2): p. 263-70.

79. Marek, L.F. and M.H. Spalding, *Changes in Photorespiratory Enzyme Activity in Response to Limiting CO(2) in Chlamydomonas reinhardtii.* Plant Physiol, 1991. **97**(1): p. 420-5.

80. Ramazanov Z, R.M., Margaret C. Henk, Catherine B. Mason, Sharon W. Matthews, James V. Moroney, *The induction of the CO2-concentrating mechanism is correlated with the formation of the starch sheath around the pyrenoid of Chlamydomonas reinhardtii.* planta, 1994. **195**(2): p. 7.

81. Badger, M.R.a.P., G.D., *The Role of Carbonic Anhydrase in Photosynthesis.* Annual Review of Plant Physiology and Plant Molecular Biology, 1994. **45**: p. 23.

82. Geraghty, A.M. and M.H. Spalding, *Molecular and Structural Changes in Chlamydomonas under Limiting CO2 (A Possible Mitochondrial Role in Adaptation).* Plant Physiol, 1996. **111**(4): p. 1339-1347.

83. Huertas, I.E., B. Colman, and G.S. Espie, *Mitochondrial-driven bicarbonate transport supports photosynthesis in a marine microalga.* Plant Physiol, 2002. **130**(1): p. 284-91.

84. Dall'Osto, L., M. Bressan, and R. Bassi, *Biogenesis of light harvesting proteins.* Biochim Biophys Acta, 2015.

85. Paul A. Castelfranco, S.I.B., *CHLOROPHYLL BIOSYNTHESIS: Recent Advances and Areas of Current Interest.* Ann. Rev. Plant Physiol., 1983. **34**: p. 36.
86. Beale, S.I., *Chloroplast signaling: retrograde regulation revelations.* Curr Biol, 2011. **21**(10): p. R391-3.
87. Moulin, M. and A.G. Smith, *Regulation of tetrapyrrole biosynthesis in higher plants.* Biochem Soc Trans, 2005. **33**(Pt 4): p. 737-42.
88. Beale, S.I., *Biosnythesis of Chlorophylls and Hemes*, in *The Chlamydomonas sourcebooke*, D.B. Stern, Editor. 2009, Elsevier.
89. Dailey, T.A. and H.A. Dailey, *Identification of [2Fe-2S] clusters in microbial ferrochelatases.* J Bacteriol, 2002. **184**(9): p. 2460-4.
90. Fuesler, T.P., Y.S. Wong, and P.A. Castelfranco, *Localization of Mg-Chelatase and Mg-Protoporphyrin IX Monomethyl Ester (Oxidative) Cyclase Activities within Isolated, Developing Cucumber Chloroplasts.* Plant Physiol, 1984. **75**(3): p. 662-4.
91. Castelfranco, P.A., et al., *The Mg insertion step in chlorophyll biosynthesis.* Arch Biochem Biophys, 1979. **192**(2): p. 592-8.
92. Walker, C.J. and R.D. Willows, *Mechanism and regulation of Mg-chelatase.* Biochem J, 1997. **327 (Pt 2)**: p. 321-33.
93. Walker, C.J. and J.D. Weinstein, *The magnesium-insertion step of chlorophyll biosynthesis is a two-stage reaction.* Biochem J, 1994. **299 (Pt 1)**: p. 277-84.
94. Grossman, A.R., M. Lohr, and C.S. Im, *Chlamydomonas reinhardtii in the landscape of pigments.* Annu Rev Genet, 2004. **38**: p. 119-73.
95. Larkin, R.M., et al., *GUN4, a regulator of chlorophyll synthesis and intracellular signaling.* Science, 2003. **299**(5608): p. 902-6.
96. Alawady, A., et al., *Cloning and expression of the tobacco CHLM sequence encoding Mg protoporphyrin IX methyltransferase and its interaction with Mg chelatase.* Plant Mol Biol, 2005. **57**(5): p. 679-91.
97. Bollivar, D.W. and S.I. Beale, *The Chlorophyll Biosynthetic Enzyme Mg-Protoporphyrin IX Monomethyl Ester (Oxidative) Cyclase (Characterization and Partial Purification from Chlamydomonas reinhardtii and Synechocystis sp. PCC 6803).* Plant Physiol, 1996. **112**(1): p. 105-114.
98. Moseley, J., et al., *The Crd1 gene encodes a putative di-iron enzyme required for photosystem I accumulation in copper deficiency and hypoxia in Chlamydomonas reinhardtii.* EMBO J, 2000. **19**(10): p. 2139-51.
99. Parham, R. and C.A. Rebeiz, *Chloroplast biogenesis: [4-vinyl] chlorophyllide a reductase is a divinyl chlorophyllide a-specific, NADPH-dependent enzyme.* Biochemistry, 1992. **31**(36): p. 8460-4.
100. Parham, R. and C.A. Rebeiz, *Chloroplast biogenesis 72: a [4-vinyl]chlorophyllide a reductase assay using divinyl chlorophyllide a as an exogenous substrate.* Anal Biochem, 1995. **231**(1): p. 164-9.
101. Beale, S.I., *Biosnythesis of Chlorophylls and Hemes*, in *The Chlamydomonas sourcebooke*, D.B. Stern, Editor. 2009, Elsevier. p. 755.
102. Dehesh, K. and M. Ryberg, *The NADPH-protochlorophyllide oxidoreductase is the major protein constituent*

of prolamellar bodies in wheat (Triticum aestivum L.). Planta, 1985. **164**(3): p. 396-9.

103. Sun, Y. and W. Zerges, *Translational regulation in chloroplasts for development and homeostasis.* Biochim Biophys Acta, 2015. **1847**(9): p. 809-20.

104. Barthelemy, X., et al., *Localization of NADPH-protochlorophyllide reductase in plastids of barley at different greening stages.* Photosynth Res, 2000. **64**(1): p. 63-76.

105. Joyard, J., et al., *Envelope membranes from mature spinach chloroplasts contain a NADPH:protochlorophyllide reductase on the cytosolic side of the outer membrane.* J Biol Chem, 1990. **265**(35): p. 21820-7.

106. Apel, K., et al., *The protochlorophyllide holochrome of barley (Hordeum vulgare L.). Isolation and characterization of the NADPH:protochlorophyllide oxidoreductase.* Eur J Biochem, 1980. **111**(1): p. 251-8.

107. Choquet, Y., et al., *A chloroplast gene is required for the light-independent accumulation of chlorophyll in Chlamydomonas reinhardtii.* EMBO J, 1992. **11**(5): p. 1697-704.

108. Gao, Y., et al., *Action spectra of chlorophyll a biosynthesis in cyanobacteria: dark-operative protochlorophyllide oxidoreductase-deficient mutants.* Z Naturforsch C, 2009. **64**(1-2): p. 117-24.

109. Cahoon, A.B. and M.P. Timko, *yellow-in-the-dark mutants of Chlamydomonas lack the CHLL subunit of light-independent protochlorophyllide reductase.* Plant Cell, 2000. **12**(4): p. 559-68.

110. Yamazaki, S., J. Nomata, and Y. Fujita, *Differential operation of dual protochlorophyllide reductases for chlorophyll biosynthesis in response to environmental oxygen levels in the cyanobacterium Leptolyngbya boryana.* Plant Physiol, 2006. **142**(3): p. 911-22.

111. Clark Ford, S.M., Wei-yeh Wang, *Characterization of NADPH: Protochlorophyllide oxidoreductase in the y-7 and pc-1 y-7 mutants of Chlamydomonas reinhardtii.* Molecular and General Genetics 1983. **192**(1-2): p. 3.

112. Clark Ford, W.-y.W., *Temperature-sensitive yellow mutants of Chlamydomonas reinhardtii.* Molecular and General Genetics 1980. **180**(1): p. 6.

113. Nomata, J., et al., *Nitrogenase Fe protein-like Fe-S cluster is conserved in L-protein (BchL) of dark-operative protochlorophyllide reductase from Rhodobacter capsulatus.* FEBS Lett, 2006. **580**(26): p. 6151-4.

114. Beale, S.I., *Biosnythesis of Chlorophylls and Hemes*, in *The Chlamydomonas sourcebooke*, D.B. Stern, Editor. 2009, Elsevier. p. 758.

115. Schäfer, S.S.a.W., *Tetrahydrogeranylgeraniol, a Precursor of Phytol in the Biosynthesis of Chlorophyll a — Localization of the Double Bonds.* Z. Naturforsch, 1978: p. 5.

116. Rudiger, W., J. Benz, and C. Guthoff, *Detection and partial characterization of activity of chlorophyll synthetase in etioplast membranes.* Eur J Biochem, 1980. **109**(1): p. 193-200.

117. Rüdiger, W., *Chlorophyll Synthetase and its Implication for Regulation of Chlorophyll Biosynthesis.* Progress in Photosynthesis Research, 1987: p. 7.

118. Schneegurt, M.A. and S.I. Beale, *Origin of the chlorophyll b formyl oxygen in Chlorella vulgaris.* Biochemistry, 1992. **31**(47): p. 11677-83.

119. Porra, R.J., et al., *Derivation of the formyl-group oxygen of chlorophyll b from molecular oxygen in*

greening leaves of a higher plant (Zea mays). FEBS Lett, 1993. **323**(1-2): p. 31-4.

120. Tanaka, A., et al., *Chlorophyll a oxygenase (CAO) is involved in chlorophyll b formation from chlorophyll a.* Proc Natl Acad Sci U S A, 1998. **95**(21): p. 12719-23.

121. Espineda, C.E., et al., *The AtCAO gene, encoding chlorophyll a oxygenase, is required for chlorophyll b synthesis in Arabidopsis thaliana.* Proc Natl Acad Sci U S A, 1999. **96**(18): p. 10507-11.

122. Rochaix, J.D., M. Goldschmidt-Clermont, and S. Merchant, *The molecular biology of chloroplasts and mitochondria in Chlamydomonas*. Advances in photosynthesis. 1998, Dordrecht ; Boston: Kluwer Academic Publishers. xviii, 733, 7 p. of col. plates.

123. Hippler, M., K. Redding, and J.D. Rochaix, *Chlamydomonas genetics, a tool for the study of bioenergetic pathways.* Biochim Biophys Acta, 1998. **1367**(1-3): p. 1-62.

124. Nishimura, Y., *Uniparental inheritance of cpDNA and the genetic control of sexual differentiation in Chlamydomonas reinhardtii.* J Plant Res, 2010. **123**(2): p. 149-62.

125. Nichols, G.L.a.S., P.J., *Nitrate reductase deficient mutants of Chlamydomonas reinhardii. .* J.Gen.Microbiol, 1978. **108**(Isolation and genetics): p. 7.

126. Rochaix, J.D., et al., *Nuclear and chloroplast mutations affect the synthesis or stability of the chloroplast psbC gene product in Chlamydomonas reinhardtii.* Embo J, 1989. **8**(4): p. 1013-21.

127. Kim, E.J. and H. Cerutti, *Targeted gene silencing by RNA interference in Chlamydomonas.* Methods Cell Biol, 2009. **93**: p. 99-110.

128. Gonzalez-Ballester, D., et al., *RNA-Seq Analysis of Sulfur-Deprived Chlamydomonas Cells Reveals Aspects of Acclimation Critical for Cell Survival.* Plant Cell, 2010. **22**(6): p. 2058-84.

129. Hu, S.X., K.W.K. Lau, and M. Wu, *Cadmium sequestration in Chlamydomonas reinhardtii.* Plant Science, 2001. **161**(5): p. 987-996.

130. Rubinelli, P., et al., *Cadmium- and iron-stress-inducible gene expression in the green alga Chlamydomonas reinhardtii: evidence for H43 protein function in iron assimilation.* Planta, 2002. **215**(1): p. 1-13.

131. Hanikenne, M., et al., *A comparative inventory of metal transporters in the green alga Chlamydomonas reinhardtii and the red alga Cyanidioschizon merolae.* Plant Physiol, 2005. **137**(2): p. 428-46.

132. Gillet, S., et al., *Cadmium response and redoxin targets in Chlamydomonas reinhardtii: a proteomic approach.* Photosynth Res, 2006. **89**(2-3): p. 201-11.

133. Francois, L., C. Fortin, and P.G. Campbell, *pH modulates transport rates of manganese and cadmium in the green alga Chlamydomonas reinhardtii through non-competitive interactions: implications for an algal BLM.* Aquat Toxicol, 2007. **84**(2): p. 123-32.

134. Mittler, R., *Oxidative stress, antioxidants and stress tolerance.* Trends Plant Sci, 2002. **7**(9): p. 405-10.

135. Takahashi S, M.N., *How do environmental stresses accelerate photoinhibition?* Trends Plant Sci., 2008. **13**(4): p. 5.

136. Li, Z., J. Wu, and C.J. Deleo, *RNA damage and surveillance under oxidative stress.* IUBMB Life, 2006. **58**(10): p. 581-8.

137. Foyer, C.H. and G. Noctor, *Redox regulation in photosynthetic organisms: signaling, acclimation, and practical implications.* Antioxid Redox Signal, 2009. **11**(4): p. 861-905.

138. Neri, S., et al., *Effects of antioxidants on postprandial oxidative stress and endothelial dysfunction in subjects with impaired glucose tolerance and type 2 diabetes.* Eur J Nutr, 2010. **49**(7): p. 409-16.

139. Murik, O. and A. Kaplan, *Paradoxically, prior acquisition of antioxidant activity enhances oxidative stress-induced cell death.* Environ Microbiol, 2009. **11**(9): p. 2301-9.

140. Shan, X., H. Tashiro, and C.L. Lin, *The identification and characterization of oxidized RNAs in Alzheimer's disease.* J Neurosci, 2003. **23**(12): p. 4913-21.

141. Shen, Z., W. Wu, and S.L. Hazen, *Activated leukocytes oxidatively damage DNA, RNA, and the nucleotide pool through halide-dependent formation of hydroxyl radical.* Biochemistry, 2000. **39**(18): p. 5474-82.

142. Ames, B.N. and L.S. Gold, *Endogenous mutagens and the causes of aging and cancer.* Mutat Res, 1991. **250**(1-2): p. 3-16.

143. Li, Z., et al., *Battle against RNA oxidation: molecular mechanisms for reducing oxidized RNA to protect cells.* Wiley Interdiscip Rev RNA, 2014. **5**(3): p. 335-46.

144. Hofer, T., et al., *A method to determine RNA and DNA oxidation simultaneously by HPLC-ECD: greater RNA than DNA oxidation in rat liver after doxorubicin administration.* Biol Chem, 2006. **387**(1): p. 103-11.

145. Shan, X. and C.L. Lin, *Quantification of oxidized RNAs in Alzheimer's disease.* Neurobiol Aging, 2006. **27**(5): p. 657-62.

146. Bazin, J., et al., *Targeted mRNA oxidation regulates sunflower seed dormancy alleviation during dry after-ripening.* Plant Cell, 2011. **23**(6): p. 2196-208.

147. Liu, M., et al., *Characterization of RNA damage under oxidative stress in Escherichia coli.* Biol Chem, 2012. **393**(3): p. 123-32.

148. Wu, J., et al., *Polynucleotide phosphorylase protects Escherichia coli against oxidative stress.* Biochemistry, 2009. **48**(9): p. 2012-20.

149. Chen, X., et al., *An ortholog of the Ro autoantigen functions in 23S rRNA maturation in D. radiodurans.* Genes Dev, 2007. **21**(11): p. 1328-39.

150. Piwowarski, J., et al., *Human polynucleotide phosphorylase, hPNPase, is localized in mitochondria.* J Mol Biol, 2003. **329**(5): p. 853-7.

151. Wu, J. and Z. Li, *Human polynucleotide phosphorylase reduces oxidative RNA damage and protects HeLa cell against oxidative stress.* Biochem Biophys Res Commun, 2008. **372**(2): p. 288-92.

152. Hayakawa, H., et al., *Binding capacity of human YB-1 protein for RNA containing 8-oxoguanine.* Biochemistry, 2002. **41**(42): p. 12739-44.

153. Hayakawa, H., et al., *Human proteins that specifically bind to 8-oxoguanine-containing RNA and their responses to oxidative stress.* Biochemical and Biophysical Research Communications, 2010. **403**(2): p. 220-224.

154. Chen, X.G., A.M. Quinn, and S.L. Wolin, *Ro ribonucleoproteins contribute to the resistance of Deinococcus*

radiodurans to ultraviolet irradiation. Genes & Development, 2000. **14**(7): p. 777-782.

155. Wurtmann, E.J. and S.L. Wolin, *RNA under attack: cellular handling of RNA damage.* Crit Rev Biochem Mol Biol, 2009. **44**(1): p. 34-49.

156. Fortini, P., et al., *8-Oxoguanine DNA damage: at the crossroad of alternative repair pathways.* Mutat Res, 2003. **531**(1-2): p. 127-39.

157. Vascotto, C., et al., *APE1/Ref-1 interacts with NPM1 within nucleoli and plays a role in the rRNA quality control process.* Mol Cell Biol, 2009. **29**(7): p. 1834-54.

158. Ito, R., et al., *Multiple enzyme activities of Escherichia coli MutT protein for sanitization of DNA and RNA precursor pools.* Biochemistry, 2005. **44**(17): p. 6670-4.

159. Taddei, F., et al., *Counteraction by MutT protein of transcriptional errors caused by oxidative damage.* Science, 1997. **278**(5335): p. 128-30.

160. Anderson, P. and N. Kedersha, *Stress granules: the Tao of RNA triage.* Trends Biochem Sci, 2008.

161. Ishii, T., et al., *Role of Auf1 in elimination of oxidatively damaged messenger RNA in human cells.* Free Radic Biol Med, 2015. **79**: p. 109-16.

162. Parker, R. and U. Sheth, *P bodies and the control of mRNA translation and degradation.* Mol Cell, 2007. **25**(5): p. 635-46.

163. Mitchell, S.F. and R. Parker, *Principles and properties of eukaryotic mRNPs.* Mol Cell, 2014. **54**(4): p. 547-58.

164. Brengues, M., D. Teixeira, and R. Parker, *Movement of eukaryotic mRNAs between polysomes and cytoplasmic processing bodies.* Science, 2005. **310**(5747): p. 486-489.

165. Bhattacharyya, S.N., et al., *Stress-induced reversal of microRNA repression and mRNA P-body localization in human cells.* Cold Spring Harbor Symposia on Quantitative Biology, 2006. **71**: p. 513-521.

166. Buchan, J.R. and R. Parker, *Eukaryotic Stress Granules: The Ins and Outs of Translation.* Molecular Cell, 2009. **36**(6): p. 932-941.

167. Kedersha, N., et al., *Stress granules and processing bodies are dynamically linked sites of mRNP remodeling.* J Cell Biol, 2005. **169**(6): p. 871-84.

168. Buchan, J.R., *mRNP granules. Assembly, function, and connections with disease.* RNA Biol, 2014. **11**(8): p. 1019-30.

169. Kedersha, N., et al., *Dynamic shuttling of TIA-1 accompanies the recruitment of mRNA to mammalian stress granules.* J Cell Biol, 2000. **151**(6): p. 1257-68.

170. Mazroui, R., et al., *Inhibition of the ubiquitin-proteasome system induces stress granule formation.* Mol Biol Cell, 2007. **18**(7): p. 2603-18.

171. Updike, D.L. and S. Strome, *A genomewide RNAi screen for genes that affect the stability, distribution and function of P granules in Caenorhabditis elegans.* Genetics, 2009. **183**(4): p. 1397-419.

172. Buchan, J.R., et al., *Eukaryotic stress granules are cleared by autophagy and Cdc48/VCP function.* Cell, 2013. **153**(7): p. 1461-74.

173. Zhao, Y., E. Tian, and H. Zhang, *Selective autophagic degradation of maternally-loaded germline P granule components in somatic cells during C. elegans embryogenesis.* Autophagy, 2009. **5**(5): p. 717-9.

174. Kedersha, N.L., et al., *RNA-binding proteins TIA-1 and TIAR link the phosphorylation of eIF-2 alpha to the assembly of mammalian stress granules.* J Cell Biol, 1999. **147**(7): p. 1431-42.

175. Arimoto, K., et al., *Formation of stress granules inhibits apoptosis by suppressing stress-responsive MAPK pathways.* Nat Cell Biol, 2008. **10**(11): p. 1324-32.

176. Kim, W.J., et al., *Sequestration of TRAF2 into stress granules interrupts tumor necrosis factor signaling under stress conditions.* Mol Cell Biol, 2005. **25**(6): p. 2450-62.

177. Gowrishankar, G., et al., *Inhibition of mRNA deadenylation and degradation by different types of cell stress.* Biol Chem, 2006. **387**(3): p. 323-7.

178. Snee, M.J. and P.M. Macdonald, *Live imaging of nuage and polar granules: evidence against a precursor-product relationship and a novel role for Oskar in stabilization of polar granule components.* J Cell Sci, 2004. **117**(Pt 10): p. 2109-20.

179. van Dijk, E., et al., *Human Dcp2: a catalytically active mRNA decapping enzyme located in specific cytoplasmic structures.* EMBO J, 2002. **21**(24): p. 6915-24.

180. Ingelfinger, D., et al., *The human LSm1-7 proteins colocalize with the mRNA-degrading enzymes Dcp1/2 and Xrnl in distinct cytoplasmic foci.* RNA, 2002. **8**(12): p. 1489-501.

181. Lykke-Andersen, J., *Identification of a human decapping complex associated with hUpf proteins in nonsense-mediated decay.* Mol Cell Biol, 2002. **22**(23): p. 8114-21.

182. Kshirsagar, M. and R. Parker, *Identification of Edc3p as an enhancer of mRNA decapping in Saccharomyces cerevisiae.* Genetics, 2004. **166**(2): p. 729-39.

183. Wilczynska, A., et al., *The translational regulator CPEB1 provides a link between dcp1 bodies and stress granules.* J Cell Sci, 2005. **118**(Pt 5): p. 981-92.

184. Mehta, R.A., et al., *Oxidative stress causes rapid membrane translocation and in vivo degradation of ribulose-1,5-bisphosphate carboxylase/oxygenase.* J Biol Chem, 1992. **267**(4): p. 2810-6.

185. Cohen, I., Y. Sapir, and M. Shapira, *A conserved mechanism controls translation of Rubisco large subunit in different photosynthetic organisms.* Plant Physiol, 2006. **141**(3): p. 1089-97.

186. Knopf, J.A. and M. Shapira, *Degradation of Rubisco SSU during oxidative stress triggers aggregation of Rubisco particles in Chlamydomonas reinhardtii.* Planta, 2005. **222**(5): p. 787-93.

187. Cohen, I., et al., *A proposed mechanism for the inhibitory effects of oxidative stress on Rubisco assembly and its subunit expression.* Plant Physiol, 2005. **137**(2): p. 738-46.

188. Moreira, P.I., et al., *Nucleic acid oxidation in Alzheimer disease.* Free Radic Biol Med, 2008. **44**(8): p. 1493-505.

189. Holmstrom, K.M. and T. Finkel, *Cellular mechanisms and physiological consequences of redox-dependent signalling.* Nat Rev Mol Cell Biol, 2014. **15**(6): p. 411-421.

190. Cadet, J., T. Douki, and J.L. Ravanat, *Oxidatively generated base damage to cellular DNA.* Free Radic Biol

Med, 2010. **49**(1): p. 9-21.

191. Wurtmann, E.J. and Sandra L. Wolin, *RNA under attack: Cellular handling of RNA damage.* Critical Reviews in Biochemistry and Molecular Biology, 2009. **44**(1): p. 34-49.

192. Thomas, M.G., et al., *RNA granules: The good, the bad and the ugly.* Cellular Signalling, 2011. **23**(2): p. 324-334.

193. Apel, K. and H. Hirt, *Reactive oxygen species: metabolism, oxidative stress, and signal transduction.* Annu Rev Plant Biol, 2004. **55**: p. 373-99.

194. Sies, H., *Oxidative stress: oxidants and antioxidants.* Exp Physiol, 1997. **82**(2): p. 291-5.

195. Michael, R., L. McKay, and S.P. Gibbs, *Composition and function of pyrenoids: cytochemical and immunocytochemical approaches.* Canadian Journal of Botany, 1991. **69**(5): p. 1040-1052.

196. Dent, R.M., et al., *Functional genomics of eukaryotic photosynthesis using insertional mutagenesis of Chlamydomonas reinhardtii.* Plant Physiol, 2005. **137**(2): p. 545-56.

197. Johnson, X., *Manipulating RuBisCO accumulation in the green alga, Chlamydomonas reinhardtii.* Plant Molecular Biology, 2011. **76**(3-5): p. 397-405.

198. Gorman, D.S. and R.P. Levine, *Cytochrome f and plastocyanin: their sequence in the photosynthetic electron transport chain of Chlamydomonas reinhardii.* Proc Natl Acad Sci U S A, 1965. **54**(6): p. 1665-9.

199. Murray, M.G. and W.F. Thompson, *Rapid isolation of high molecular weight plant DNA.* Nucleic Acids Research, 1980. **8**(19): p. 4321-4326.

200. Sambrook, J. and D.W. Russell, *Molecular cloning : a laboratory manual*. 3rd ed. 2001, Cold Spring Harbor, N.Y.: Cold Spring Harbor Laboratory Press. 3 v.

201. Bohne, A.V., et al., *Reciprocal regulation of protein synthesis and carbon metabolism for thylakoid membrane biogenesis.* PLoS Biol, 2013. **11**(2): p. e1001482.

202. Uniacke, J., D. Colon-Ramos, and W. Zerges, *FISH and immunofluorescence staining in Chlamydomonas.* Methods Mol Biol, 2011. **714**: p. 15-29.

203. Randolph-Anderson, B.L., N.W. Gillham, and J.E. Boynton, *Electrophoretic and immunological comparisons of chloroplast and prokaryotic ribosomal proteins reveal that certain families of large subunit proteins are evolutionarily conserved.* J Mol Evol, 1989. **29**(1): p. 68-88.

204. Abramoff, M.D., P.J. Magelhaes, and S.J. Ram, *Image Processing with ImageJ.* Biophotonics International, 2004. **11**(7): p. 36-42.

205. Barraclough, R. and R.J. Ellis, *Protein synthesis in chloroplasts. IX. Assembly of newly-synthesized large subunits into ribulose bisphosphate carboxylase in isolated intact pea chloroplasts.* Biochim Biophys Acta, 1980. **608**(1): p. 19-31.

206. Sambrook, J.R., D, *Molecular Cloning: A Laboratory Manual*. Vol. 2. 2000: Cold Spring Harbor Lab Press.

207. Fischer, B.B., et al., *Function and regulation of the glutathione peroxidase homologous gene GPXH/GPX5 in Chlamydomonas reinhardtii.* Plant Mol Biol, 2009. **71**(6): p. 569-83.

208. Rawat, M., et al., *Chlamydomonas reinhardtii mutants without ribulose-l,5-bisphosphate carboxylase-oxygenase lack a detectable pyrenoid.* Planta, 1996. **198**: p. 263-270.

209. Genkov, T., et al., *Functional Hybrid Rubisco Enzymes with Plant Small Subunits and Algal Large Subunits: engineered rbcS cDNA for expression in Chlamydomonas.* Journal of Biological Chemistry, 2010. **285**(26): p. 19833-19841.

210. Chang, H.L., et al., *Reactive oxygen species modulate the differential expression of methionine sulfoxide reductase genes in Chlamydomonas reinhardtii under high light illumination.* Physiol Plant, 2014. **150**(4): p. 550-64.

211. Rasala, B.A., et al., *Enhanced genetic tools for engineering multigene traits into green algae.* PLoS One, 2014. **9**(4): p. e94028.

212. Uniacke, J. and W. Zerges, *Photosystem II assembly and repair are differentially localized in Chlamydomonas.* Plant Cell, 2007. **19**(11): p. 3640-54.

213. Uniacke, J. and W. Zerges, *Chloroplast protein targeting involves localized translation in Chlamydomonas.* Proc Natl Acad Sci U S A, 2009. **106**(5): p. 1439-44.

214. Schottkowski, M., et al., *Biogenic membranes of the chloroplast in Chlamydomonas reinhardtii.* Proc Natl Acad Sci U S A, 2012. **109**(47): p. 19286-91.

215. Schroda, M., et al., *A chloroplast-targeted heat shock protein 70 (HSP70) contributes to the photoprotection and repair of photosystem II during and after photoinhibition.* Plant Cell, 1999. **11**(6): p. 1165-78.

216. Tabita, F.R., et al., *Function, structure, and evolution of the RubisCO-like proteins and their RubisCO homologs.* Microbiology and Molecular Biology Reviews, 2007. **71**(4): p. 576-+.

217. Oberlerchner, J.T., T. Rosenau, and A. Potthast, *Overview of Methods for the Direct Molar Mass Determination of Cellulose.* Molecules, 2015. **20**(6): p. 10313-10341.

218. Krause, K., *From chloroplasts to "cryptic" plastids: evolution of plastid genomes in parasitic plants.* Current Genetics, 2008. **54**(3): p. 111-121.

219. Hentze, M.W. and T. Preiss, *The REM phase of gene regulation.* Trends in biochemical sciences, 2010. **35**(8): p. 423-6.

220. Nunomura, A., et al., *RNA oxidation is a prominent feature of vulnerable neurons in Alzheimer's disease.* Journal of Neuroscience, 1999. **19**(6): p. 1959-1964.

221. Tanaka, M., P.B. Chock, and E.R. Stadtman, *Oxidized messenger RNA induces translation errors.* Proceedings of the National Academy of Sciences, 2007. **104**(1): p. 66-71.

222. Gaillard, H. and A. Aguilera, *A Novel Class of mRNA-containing Cytoplasmic Granules Are Produced in Response to UV-Irradiation.* Molecular Biology of the Cell, 2008. **19**(11): p. 4980-4992.

223. Adjibade, P. and R. Mazroui, *Control of mRNA turnover: Implication of cytoplasmic RNA granules.* Semin Cell Dev Biol, 2014.

224. Walters, R. and R. Parker, *Is there quality control of localized mRNAs?* The Journal of Cell Biology, 2014. **204**(6): p. 863-868.

225. Stoecklin, G. and B. Bukau, *Telling right from wrong in life - cellular quality control.* Nature Reviews Molecular Cell Biology, 2013. **14**(10): p. 613-615.

226. Decker, C.J. and R. Parker, *P-bodies and stress granules: possible roles in the control of translation and mRNA degradation.* Cold Spring Harb Perspect Biol, 2012. **4**(9): p. a012286.

227. Kolesinski, P., et al., *Rubisco Accumulation Factor 1 from Thermosynechococcus elongatus participates in the final stages of ribulose-1,5-bisphosphate carboxylase/oxygenase assembly in Escherichia coli cells and in vitro.* FEBS J, 2014. **281**(17): p. 3920-32.

228. Giordano, M., J. Beardall, and J.A. Raven, *CO2 concentrating mechanisms in algae: mechanisms, environmental modulation, and evolution.* Annu Rev Plant Biol, 2005. **56**: p. 99-131.

229. Villarreal, J.C. and S.S. Renner, *Hornwort pyrenoids, carbon-concentrating structures, evolved and were lost at least five times during the last 100 million years.* Proc Natl Acad Sci U S A, 2012. **109**(46): p. 18873-8.

230. Chochois, V., et al., *Hydrogen production in Chlamydomonas: photosystem II-dependent and -independent pathways differ in their requirement for starch metabolism.* Plant Physiol, 2009. **151**(2): p. 631-40.

231. Moroney, J.V. and A. Somanchi, *How Do algae concentrate CO2 to increase the efficiency of photosynthetic carbon fixation?* Plant Physiol, 1999. **119**(1): p. 9-16.

232. Mckay, R.M.L. and S.P. Gibbs, *Phycoerythrin Is Absent from the Pyrenoid of Porphyridium-Cruentum - Photosynthetic Implications.* Planta, 1990. **180**(2): p. 249-256.

233. Ohad, I., P. Siekevitz, and G.E. Palade, *Biogenesis of chloroplast membranes. I. Plastid dedifferentiation in a dark-grown algal mutant (Chlamydomonas reinhardi).* J Cell Biol, 1967. **35**(3): p. 521-52.

234. Anderson, N.L. and N.G. Anderson, *Proteome and proteomics: new technologies, new concepts, and new words.* Electrophoresis, 1998. **19**(11): p. 1853-61.

235. Porra, R.J., *The chequered history of the development and use of simultaneous equations for the accurate determination of chlorophylls a and b.* Photosynthesis Research, 2002. **73**(1-3): p. 149-156.

236. Wessel, D. and U.I. Flugge, *A Method for the Quantitative Recovery of Protein in Dilute-Solution in the Presence of Detergents and Lipids.* Analytical Biochemistry, 1984. **138**(1): p. 141-143.

237. Holdsworth, R.H., *The isolation and partial characterization of the pyrenoid protein of Eremosphaera viridis.* J Cell Biol, 1971. **51**(21): p. 499-513.

238. Bracher, A., et al., *Crystal structure of a chaperone-bound assembly intermediate of form I Rubisco.* Nat Struct Mol Biol, 2011. **18**(8): p. 875-80.

239. Zhou, J., et al., *E3 ubiquitin ligase CHIP and NBR1-mediated selective autophagy protect additively against proteotoxicity in plant stress responses.* PLoS Genet, 2014. **10**(1): p. e1004116.

240. Brueggeman, A.J., et al., *Activation of the carbon concentrating mechanism by CO2 deprivation coincides with massive transcriptional restructuring in Chlamydomonas reinhardtii.* Plant Cell, 2012. **24**(5): p. 1860-75.

241. Izumo, A., et al., *Effects of granule-bound starch synthase I-defective mutation on the morphology and structure of pyrenoidal starch in Chlamydomonas.* Plant Sci, 2011. **180**(2): p. 238-45.

242. Ball, S., et al., *A Chlamydomonas-Reinhardtii Low-Starch Mutant Is Defective for 3-Phosphoglycerate Activation and Orthophosphate Inhibition of Adp-Glucose Pyrophosphorylase.* Planta, 1991. **185**(1): p. 17-26.

243. Allen, J., *Photosynthesis of ATP-electrons, proton pumps, rotors, and poise.* Cell, 2002. **110**(3): p. 273-6.

244. Maruyama, S., R. Tokutsu, and J. Minagawa, *Transcriptional regulation of the stress-responsive light harvesting complex genes in Chlamydomonas reinhardtii.* Plant Cell Physiol, 2014. **55**(7): p. 1304-10.

245. Joyard, J., et al., *Chloroplast proteomics and the compartmentation of plastidial isoprenoid biosynthetic pathways.* Mol Plant, 2009. **2**(6): p. 1154-80.

246. Erickson, E., S. Wakao, and K.K. Niyogi, *Light stress and photoprotection in Chlamydomonas reinhardtii.* Plant J, 2015. **82**(3): p. 449-65.

247. Rast, A., S. Heinz, and J. Nickelsen, *Biogenesis of thylakoid membranes.* Biochim Biophys Acta, 2015.

248. Borner, T., et al., *Chloroplast RNA polymerases: Role in chloroplast biogenesis.* Biochim Biophys Acta, 2015. **1847**(9): p. 761-9.

249. Yang, J., G. Schuster, and D.B. Stern, *CSP41, a sequence-specific chloroplast mRNA binding protein, is an endoribonuclease.* Plant Cell, 1996. **8**(8): p. 1409-20.

250. Bollenbach, T.J., D.A. Tatman, and D.B. Stern, *CSP41a, a multifunctional RNA-binding protein, initiates mRNA turnover in tobacco chloroplasts.* Plant J, 2003. **36**(6): p. 842-52.

251. Yamaguchi, K., et al., *Proteomic characterization of the Chlamydomonas reinhardtii chloroplast ribosome. Identification of proteins unique to th e70 S ribosome.* J Biol Chem, 2003. **278**(36): p. 33774-85.

252. Dayer, R., et al., *The peroxiredoxin and glutathione peroxidase families in Chlamydomonas reinhardtii.* Genetics, 2008. **179**(1): p. 41-57.

253. Niyogi, K.K., A.R. Grossman, and O. Bjorkman, *Arabidopsis mutants define a central role for the xanthophyll cycle in the regulation of photosynthetic energy conversion.* Plant Cell, 1998. **10**(7): p. 1121-34.

254. Xiong, L., et al., *Regulation of osmotic stress-responsive gene expression by the LOS6/ABA1 locus in Arabidopsis.* J Biol Chem, 2002. **277**(10): p. 8588-96.

255. Langenkamper, G., et al., *Accumulation of plastid lipid-associated proteins (fibrillin/CDSP34) upon oxidative stress, ageing and biotic stress in Solanaceae and in response to drought in other species.* J Exp Bot, 2001. **52**(360): p. 1545-54.

256. Brzezowski, P., A.S. Richter, and B. Grimm, *Regulation and function of tetrapyrrole biosynthesis in plants and algae.* Biochim Biophys Acta, 2015. **1847**(9): p. 968-85.

257. Allen, M.D., J. Kropat, and S.S. Merchant, *Regulation and localization of isoforms of the aerobic oxidative cyclase in Chlamydomonas reinhardtii.* Photochem Photobiol, 2008. **84**(6): p. 1336-42.

258. A, W., *The pyrenoid as a place of chlorophyll formation in algae chloroplasts. I.* Arch Mikrobiol, 1965. **6**(52): p. 8.

259. Ben-Shem, A., F. Frolow, and N. Nelson, *Light-harvesting features revealed by the structure of plant photosystem I.* Photosynth Res, 2004. **81**(3): p. 239-50.

260. Moseley, J.L., et al., *Reciprocal expression of two candidate di-iron enzymes affecting photosystem I and light-harvesting complex accumulation.* Plant Cell, 2002. **14**(3): p. 673-88.

261. von Gromoff, E.D., et al., *Heme, a plastid-derived regulator of nuclear gene expression in Chlamydomonas.* Plant Cell, 2008. **20**(3): p. 552-67.

262. White, R.A. and J.K. Hoober, *Biogenesis of Thylakoid Membranes in Chlamydomonas reinhardtii y1 (A Kinetic Study of Initial Greening).* Plant Physiol, 1994. **106**(2): p. 583-590.

263. Barthelemy, X., et al., *Localization of NADPH-protochlorophyllide reductase in plastids of barley at different greening stages.* Photosynthesis Research, 2000. **64**(1): p. 63-76.

264. Malnoe, P., S.P. Mayfield, and J.D. Rochaix, *Comparative analysis of the biogenesis of photosystem II in the wild-type and Y-1 mutant of Chlamydomonas reinhardtii.* J Cell Biol, 1988. **106**(3): p. 609-16.

Appendix I: Supplementary Figures (Fourteen in total)

<u>Eight Excel Figures (In a separate folder)</u>

Supplemental Figure 3.2 All S1 samples information.

Supplemental Figure 3.2 All S2 samples information.

Supplemental Figure 3.3 PredAglo results of pyrenoid proteome.

Supplemental Figure 3.4 Annotations of 179 proteins in pyrenoid proteome.

Supplemental Figure 3.5 Proteins in pyrenoid proteome were encoded by LCI genes.

Supplemental Figure 3.7 Proteins in pyrenoid proteome found in storma proteome.

Supplemental Figure 4.1 Analysis of chlorophyll distribution in y1.

Supplemental Figure 4.2 Analysis of POR distribution in CC503.

Six Picture Figures:

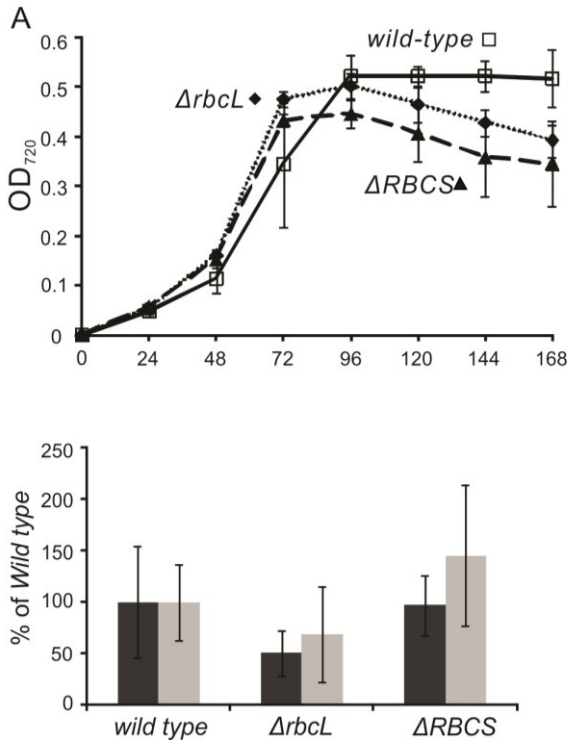

Supplementary Fig 2.1 Growth rates, levels of marker transcripts for oxidative stress, and H_2O_2 amounts in wild-type, *ΔrbcL* and *ΔRBCS* cultures.

A) Growth rates of the wild-type strain, *ΔrbcL*, and *ΔRBCS* were monitored using OD_{720} values, measured at 24 h time points. B) Transcript levels of oxidative stress marker genes were measured with the Quantigene2 assay (Panomics Inc.). The marker genes for oxidative stress are *GPX5* (XM_001698523) and *GSTS2* (XM_001699214) [207]. Transcript levels were normalized to the level of the *RPS26* (XP_001691901) transcript. Bar heights indicate the mean level of each transcript graphed as the percent of the level in the wild-type strain. C) H_2O_2 concentrations in cultures of the wild-type strain, *ΔrbcL*, and *ΔRBCS* were measured at hourly time points over 8 h and graphed as the percent of the initial concentration (4.0 mM). Error bars indicate the standard error of the mean.

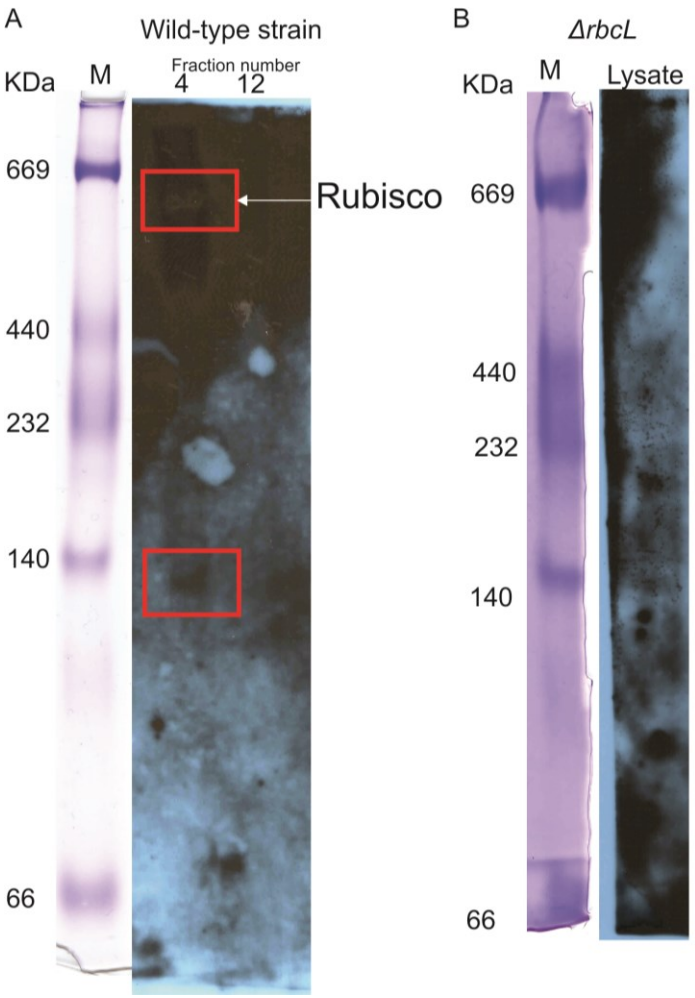

Supplemental Figure 2.2 RBCL complex was detected in the *wild-type* cells but not in *ΔrbcL.*

A) Fraction 4 and 12 from the polysome isolation of *wild-type* cells were examined by a non-denatured gel and immunoblot by the antibody against RBCL. The very intensive band in the red square on the top of the film indicated the Rubisco holoenzyme (560 KDa). The faint band in the red square on the bottom indicated a complex with RBCL. B) The crude lysate of *ΔrbcL* was also run on the non-denatrued gel and examined by immunoblot for RBCL. High molecular weight marker was used to indicate the size of complexes.

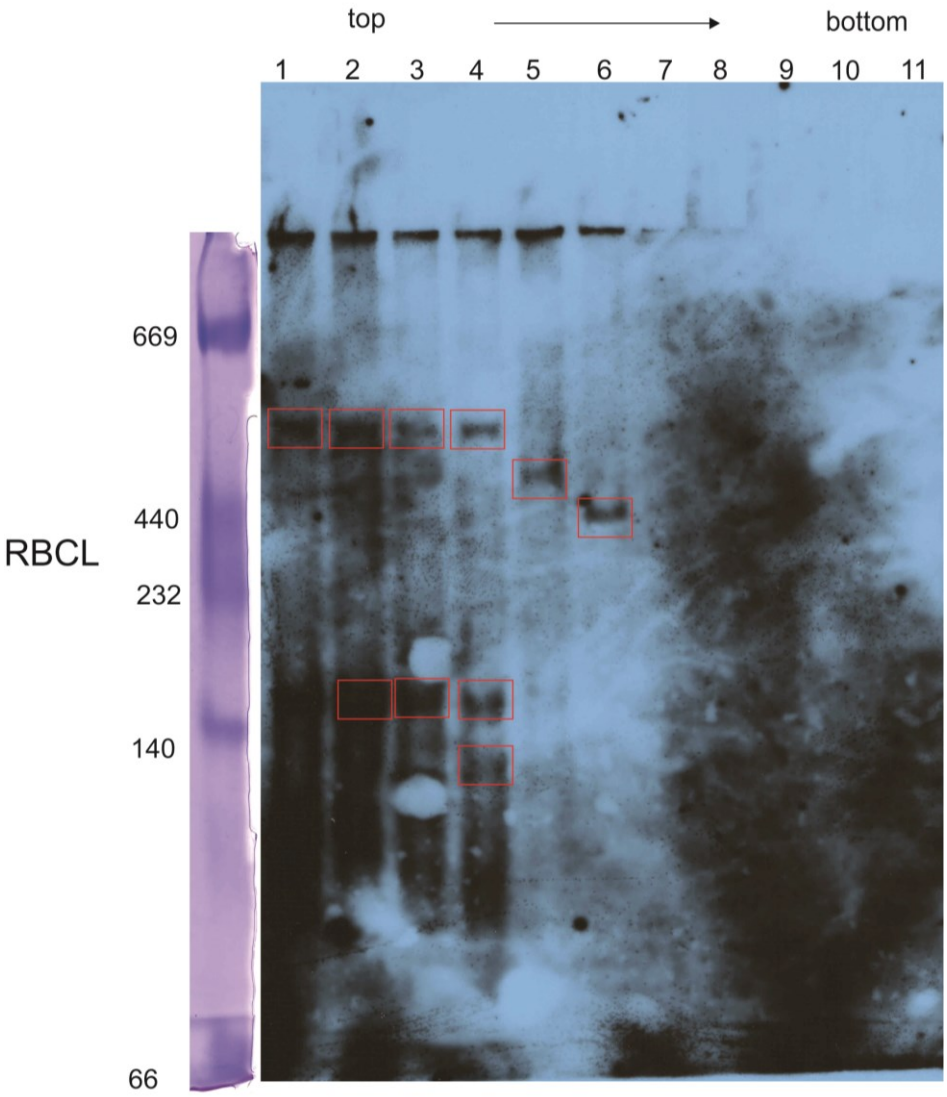

Supplemental Figure 2.3 Other RBCL complexes were detected in *ΔRBCS.*

Polysome profiles isolated in *ΔRBCS* were examined by non-denatured gel. Immunoblot analysis with the antibody against RBCL showed there were other RBCL complexes at different sizes other than around 100 KDa in the top 1-6 (red square). High molecular weight marker was used to calculate approximate size of the complex.

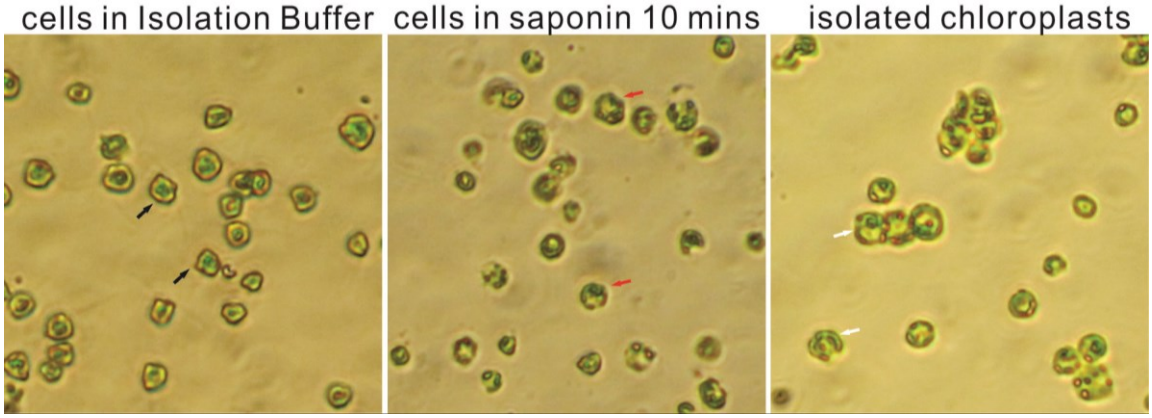

Supplemental Figure 3.1 Saponin solubilized the plasma membrane prior to chloroplast isolation.

Light microscopy was used to observe the shape of cells or chloroplasts in different solution. Cells in isolation buffer showed irregular shape because isolation buffer is hypertonic to the cytoplasma. Saponin treated cells swelled to the normal shape because the plasma membrane was solubilized. The cup-like chloroplasts were detected in the third picture to show successful isolation of chloroplast.

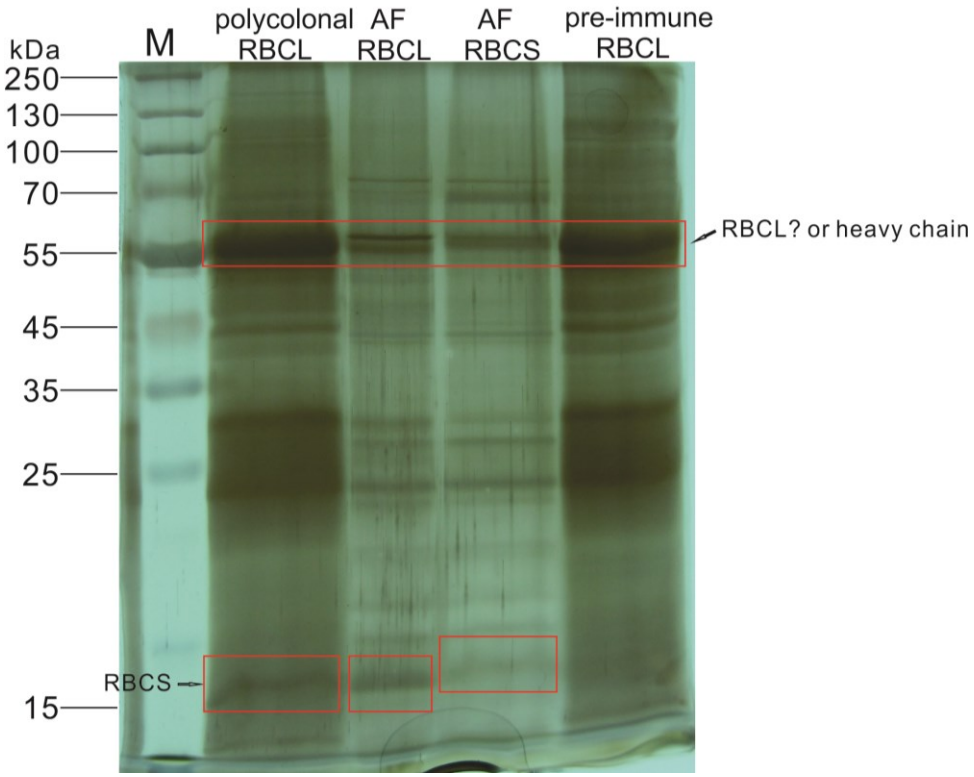

Supplemental Figure 3.6 Immunoprecipitation of pyrenoid from crude pyrenoid pellet with antibodies.

Three antibodies were used to further immunoprecipitated pyrenoid; a polycolonal antibody against RBCL, an affinity purified antibody against RBCL (AF RBCL) and an affinity purified antibody against RBCS (AF RBCS). Pre-immune RBCL was used as a negative control of the experiment. A band around 15 KDa which indicated the size of RBCS was found on the silver staining gel with the samples pulled out by two different RBCL antibodies (Lane 1 and 2). This band was absent in negative control (Lane 4). In the RBCS antibody pull out result, a band at the size of RBCL was also found (Lane 3). Molecular weight marker was used to indicate the size.

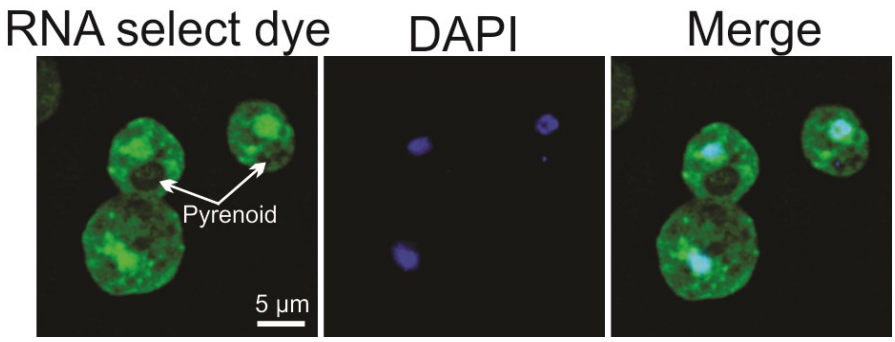

Supplemental Figure 3.8 Faint RNA staining was found in the pyrenoid.

SYTO® RNASelect™ Green Fluorescent Cell Stain (Life technology) was used to stain the cells (green). Nucleus and some nucleoids were staining by DAPI (blue). Most signal of RNA was showed in nucleus and punctated foci in cytoplasm or chloroplast. Pyrenoid was faintly stained with the RNA select dye.

Appendix II:

Localized control of oxidized RNA

Yu Zhan[1,4], James Dhaliwal[1,4], Pauline Adjibade[2], James Uniacke[3],

Rachid Mazroui[2], and William Zerges[1,5]

1) Biology Department & Centre for Structural and Functional Genomics, Concordia University, 7141 Sherbrooke W, Montreal, Quebec, Canada, H4B 1R6

2) Department of Molecular Biology, Medical Biochemistry, and Pathology, Laval University, Centre de Recherche le CHU de Quebec, Quebec, Canada

3) Current address: Department of Molecular and Cellular Biology, Science Complex University of Guelph, Guelph, Ontario, Canada, N1G 2W1

4) These authors contributed equally to this work.

5) Corresponding author: william.zerges@concordia.ca Tel: (514) 848-2424 extension 3416

Key words: ROS, Rubisco, stress granule, RNA, chloroplast.

ABSTRACT

The oxidation of biological molecules by reactive oxygen species can render them inactive or toxic. This includes the oxidation of RNA, which appears to underlie detrimental effects of oxidative stress, aging, and certain neurodegenerative diseases. Here we investigate the management of oxidized RNA in the chloroplast of the green alga *Chlamydomonas reinhardtii*. Results of immunofluorescence microscopy reveal oxidized RNA (with 8-hydroxyguanine) in the pyrenoid, a chloroplast microcompartment where CO_2 is assimilated by the Calvin cycle enzyme Rubisco. Results of genetic analyses and biochemical fractionation reveal that RBCL, the Rubisco large subunit, controls the level of oxidized RNA. This represents a dual "moonlighting" function of RBCL, possibly related to its known RNA-binding activity. Results of preliminary experiments in human (HeLa) cells reveal oxidized RNA is localized to cytoplasmic foci which are distinct from stress granules, processing bodies, and mitochondria. Our results support a role of RBCL and the pyrenoid in the control of oxidized RNA in algal chloroplasts and suggest that the compartmentalization of oxidized RNA quality control is a general phenomenon.

INTRODUCTION

The oxidation of biological molecules by reactive oxygen species (ROS) can render them inactive or toxic (Holmstrom and Finkel, 2014). While DNA, lipids and proteins have long been considered as critical intracellular targets of oxidation, recent evidence suggests roles of RNA oxidation in oxidative stress, aging, and certain neurodegenerative diseases (Wurtmann and Wolin, 2009). For example, the translation of oxidized mRNAs generates aberrant proteins (Tanaka et al., 2007; Nunomura et al., 2009) and elevated RNA oxidation in neurons is associated with Alzheimer disease, Parkinson disease, dementia with Lewy bodies and amyotrophic lateral sclerosis (Nunomura et al., 2009).

Molecular quality control systems specifically recognize oxidized molecules and subject them to repair, sequestration, or degradation (Stoecklin and Bukau, 2013). Quality control systems have been characterized for oxidized DNA, proteins, and lipids, but not for oxidized RNA (Wurtmann and Wolin, 2009). However, oxidized RNA quality control may involve YB-1, Auf1 and PNPase because these proteins bind oxidized RNA and control its accumulation (Li et al., 2014). Moreover, the intracellular location(s) of oxidized RNA quality control in eukaryotic cells have been hypothesized to include stress granules (SGs) and processing bodies (PBs) (Wurtmann and Wolin, 2009; Thomas et al., 2011; Walters and Parker, 2014). For SGs, this is supported by their recruitment of YB-1 and Auf1, and their formation under oxidative stress conditions when excess ROS causes oxidative damage (Onishi et al., 2008; Bravard et al., 2010; Tanaka et al., 2014). Similarly, PBs increase in size and number during oxidative stress and they contain mRNA degradation machinery, a component of RNA quality control (Thomas et al., 2011; Walters and Parker, 2014). While our understanding of the quality control of oxidized RNA is advancing, the precise intracellular locations are still unknown.

In the chloroplasts of plants and green algae, antioxidant systems and molecular quality control are particularly important because photosynthesis produces ROS as hydrogen

peroxide (H_2O_2), singlet oxygen, superoxide and the hydroxyl radical (Foyer and Shigeoka, 2011). Moreover, chloroplasts have a genome and a gene expression system which are targets of oxidation and mutagenesis by ROS (Wurtmann and Wolin, 2009; Zheng et al., 2014). While chloroplasts are known to have quality control systems for oxidized DNA, proteins, and lipids (Apel and Hirt, 2004), nothing is known about how they manage oxidized RNAs.

An avenue to study RNA quality control and its localization in chloroplasts arose with our discovery of SG-like bodies that form during oxidative stress in the chloroplast of the unicellular green alga *Chlamydomonas reinhardtii* (hereafter "Chlamydomonas") (Uniacke and Zerges, 2008). These "chloroplast stress granules" (cpSGs) were seen by confocal fluorescence microscopy as stress-induced foci containing mRNAs encoded by the chloroplast genome and SG marker proteins. cpSGs form at the inner perimeter of the pyrenoid, a micro-compartment in the chloroplasts of most algae where CO_2 fixation is catalyzed by the Calvin cycle enzyme ribulose bisphosphate carboxylase/oxygenase (Rubisco) (McKay and Gibbs, 1991). cpSGs are enriched in the large subunit of Rubisco, RBCL, but not the Rubisco holoenzyme; they are not similarly enriched in the small subunit of this complex, RBCS (Uniacke and Zerges, 2008). The RBCL in cpSGs might function in RNA metabolism because, under oxidizing conditions, the protein has been shown to acquire an RNA-binding activity and form aggregates which might represent a biochemical form of cpSGs (Yosef et al., 2004; Knopf and Shapira, 2005). Together, these results suggest that cpSGs, RBCL, and the pyrenoid have some undefined role(s) in chloroplast RNA metabolism during stress. This hypothesis and the previously reported role of RBCL in autoregulatory feedback translational repression are mutually compatible (Cohen et al., 2006).

Here we show that oxidized RNA localizes to the pyrenoid with results of immunofluorescence (IF) microscopy using an antibody against a major oxidized base in RNA and DNA, 8-hydryoxyguanine (8-oxoG) (Nunomura et al., 1999; Wurtmann and Wolin, 2009). We also show that RBCL controls the level of oxidized RNA in the chloroplast and

does so independently of its function as a subunit of the Rubisco holoenzyme. We extend our discovery of the localization of oxidized RNA to human cells by showing that HeLa cells under arsenite-induced oxidative stress localize oxidized RNA to cytoplasmic foci which are neither SGs nor PBs. Our results reveal a factor involved in the control of oxidized RNA in an algal chloroplast and suggest that the compartmentalization of oxidized RNA quality control is a general phenomenon.

RESULTS

Oxidized RNA localizes within the pyrenoid.

We characterized the distribution of oxidized RNA in Chlamydomonas cells by IF microscopy using an antibody against 8-oxoG. The IF signal was specific because it was eliminated when the antibody was incubated with 8-oxoG prior to staining (Fig. 1 A and B).

Inspection of cell images revealed higher 8-oxoG IF signal in the chloroplast than in the central region with the nucleus and most cytosolic compartments (Fig. 1 A). The 8-oxoG IF signal was seen in two distinct patterns; throughout the pyrenoid and in punctate foci located in or near the chloroplast. In order to determine whether these patterns represent 8-oxoG in DNA or RNA, we used two approaches. First, we co-stained cells with DAPI, to visualize the nucleus and the chloroplast nucleoids (the latter contain the multicopy chloroplast genome). These DNA-containing structures only weakly IF-stained for 8-oxoG (Fig. 1 A) and were clearly distinct from the 8-oxoG IF-staining of the pyrenoid and foci. Therefore, most of the 8-oxoG detected with this method is not in the genomic DNA of either the nucleus or chloroplast. Second, we asked whether RNase or DNase treatment altered the 8-oxoG IF-staining of the pyrenoid, the foci, or both. Cells (fixed and permeabilized) were exposed to either RNase or DNase prior to staining with the 8-oxoG antibody and DAPI. The 8-oxoG IF signal in the pyrenoid was eliminated by treatment with RNase, but not DNase, revealing that it represents oxidized RNA (Fig. 1 C). By contrast the 8-oxoG IF signal in most punctate foci was eliminated by treatment with DNase, but not with RNase, revealing that it represents

oxidized DNA (Fig. 1 D). These foci could be the DNA of mitochondria, which are localized adjacent to the chloroplast (Rasala et al., 2014). These foci were not explored further here. DNase treatment often generated a diffuse 8-oxoG IF signal throughout the chloroplast for unknown reasons (Fig. 1 D).

We focused on the 8-oxoG IF-staining of the pyrenoid because it represents oxidized RNA and was atypical; we did not see this pattern for any of four chloroplast mRNAs or nine chloroplast proteins that we analyzed previously (not including RBCL and RBCS, which were seen in the pyrenoid) (Uniacke and Zerges, 2007; Uniacke and Zerges, 2008; Uniacke and Zerges, 2009; Schottkowski et al., 2012; Bohne et al., 2013). Therefore, 8-oxoG IF-staining of the pyrenoid represents the specific localization of oxidized RNA and is not due, for example, to nonspecific entry into the pyrenoid of RNA from the surrounding stroma, the "cytoplasm" of the chloroplast.

When cells were exposed to H_2O_2, a ROS used to induce oxidative stress, the percentage in which the pyrenoid IF-stained for 8-oxoG increased from 44% (n=215) to 64% (n=189). This result suggests that oxidized RNA localizes to the pyrenoid for quality control.

Oxidized RNA did not localize to cpSGs, which were IF-stained for two marker proteins; RBCL or a protein of the 30S subunit of the chloroplast ribosome (Fig. 1 E and F) (Uniacke and Zerges, 2008). During the stress induced by H_2O_2 cpSGs formed, but the 8-oxoG IF signal remained throughout the pyrenoid (Fig. 1 E and F). This result suggests that cpSGs do not accumulate oxidized RNA.

Oxidized RNA localizes to foci in cultured mammalian cells.

To determine whether the compartmentalization of oxidized RNA is a general phenomenon, we asked whether it occurs in human cells. HeLa cells were treated with the oxidative stressor arsenite and then IF-stained for 8-oxoG. The 8-oxoG IF signal was detected in multiple cytoplasmic foci in more than 40% of these cells, as compared to 5% of untreated cells (Fig. 2 A). These foci were distinct from SGs and PBs, which were IF-stained for marker

proteins specific to each of these RNA granule types (Fig. 2 A and B). They were also not within mitochondria and therefore could not be oxidized RNA or DNA of the mitochondrial genetic system (Fig. 2 C). Nuclei also had 8-oxoG-containing bodies, which appear to be nucleoli (Lee et al., 2014). RNA with 8-oxoG, and not DNA, was detected in these bodies, both cytoplasmic and nuclear, because they did not stain for DNA with DAPI and they were not detected in RNase-treated cells (Fig. 2 A). These results reveal that mammalian cells compartmentalize oxidized RNA to cytoplasmic structures, which we name here "oxidized RNA bodies" (ORBs). They also substantiate the localization of oxidized RNA to nucleoli reported previously (Nunomura et al., 1999).

RBCL controls the level of oxidized RNA in the chloroplast.

Returning to the chloroplast; we hypothesized that RBCL functions in the quality control of oxidized RNA based on the localization of 8-oxoG RNA to the pyrenoid, the fact that RBCL is a major protein of the pyrenoid, and the evidence that RBCL has a dual function involving RNA during stress (Yosef et al., 2004). For example, RNA bound by RBCL might be protected from oxidation, repaired of oxidative damage, or be directed to the RNA degradation machinery of the chloroplast. To test this hypothesis, we asked if an RBCL knockout mutant, MX3312 (hereafter "*ΔrbcL*"), has an elevated level of 8-oxoG in RNA. The results of immuno-slot-blot analyses revealed a significantly higher mean level of 8-oxoG in RNA from *ΔrbcL* than in RNA from the wild-type strain (Fig. 3 A). Therefore, RBCL is required to control oxidized RNA. This oxidized RNA is probably from the chloroplast because RBCL is a chloroplast protein and most 8-oxoG RNA was detected in this organelle (Fig. 1).

The elevated level of oxidized RNA in *ΔrbcL* is not due to Rubisco-deficiency because it was not detected in another Rubisco-deficient mutant, one that lacks RBCS, but has RBCL (*ΔRBCS-CAL005.01.13*, hereafter *"ΔRBCS"*) (Fig. 3 A) (Dent et al., 2005). On the contrary, RNA from *ΔRBCS* showed an even lower mean level of 8-oxoG than that of the wild-type

strain (Fig. 3 A). This surprising phenotype is not due to genetic background because transformation of *ΔRBCS* with a wild-type copy of *RBCS2* restored the mean level of 8-oxoG RNA to nearly that of the wild-type strain (Fig. 3 A). This low level of 8-oxoG in RNA from *ΔRBCS* is also not due to a deficiency for some unknown RBCS function because a mutant lacking both RBCL and RBCS was found to have a high mean level of 8-oxoG in RNA, similar to that of *ΔrbcL* (Fig. 3 A). Based on these results, we conclude that RBCL controls the level of oxidized RNA independently of Rubisco.

Exposure of the cells to H_2O_2 did not significantly change the mean level of 8-oxoG RNA from wild type, *ΔrbcL*, or *ΔRBCS* (Fig. 3 A). This RBCL-dependent control of oxidized RNA under both non-stress and stress conditions supports a constitutive role of RBCL in controlling oxidized RNA.

RBCL probably does not control the level of oxidized DNA, because similar mean levels of 8-oxoG were detected in total DNA from *ΔrbcL* and the wild-type strain (Fig. 3 B). While the level of 8-oxoG was higher in DNA from *ΔrbcL* than in DNA from *ΔRBCS*, this difference was 1.4-fold versus 10-fold for the same comparison of 8-oxoG in RNA (described above) (Fig. 3 A). Moreover, as stated above, chloroplast nucleoids did not IF-stain for 8-oxoG (Fig. 1 A and C).Treatment of cultures with H_2O_2 increased the variability in the level of 8-oxoG in DNA between biological replicate experiments but did not increase the mean levels relative to DNA from the non-treated cultures (Fig. 3 B). No differences in mean levels of oxidized protein were found between the wild-type strain, *ΔrbcL*, or *ΔRBCS* mutant strains, measured as carbonylated amino acid residues in total protein (Fig. 3 C). Therefore, our results do not support a role of RBCL in controlling the levels of oxidized DNA or protein.

Biochemical evidence of an RBCL pool that controls the level of oxidized RNA.

Our finding that RBCL has a Rubisco-independent function in the control of oxidized RNA suggests the existence of a pool of the protein that carries out this function which is distinct from the RBCL in the Rubisco holoenzyme. Therefore, we carried out biochemical

fractionation experiments to identify such an RBCL pool. In addition to the major RBCL pool of the Rubisco holoenzyme, three forms of RBCL are known. Two forms of RBCL were detected in cells undergoing oxidative stress or senescence: one was in insoluble aggregates (Knopf and Shapira, 2005) and the other was membrane-associated (Knopf and Shapira, 2005; Marin-Navarro and Moreno, 2006). In addition, RBCL that is newly synthesized and unassembled was proposed to autoregulate *rbcL* translation during oxidative stress (Cohen et al., 2005). To determine whether the RBCL that controls the level of these pools, we developed a differential centrifugation scheme to separate soluble and insoluble proteins into three fractions (Fig. 4 B): S16 has soluble proteins; P16-TS has insoluble proteins that can be solubilized by Triton X-100, e.g. membrane proteins; and P16-TI has insoluble proteins that cannot be solubilized by Triton X-100.

Analyses of fractions from the wild-type strain revealed that S16 had both RBCL and RBCS, representing Rubisco holoenzyme (Fig. 4 C). Detection of other RBCL forms in fractions of wild -type strains was hampered by contamination of most subcellular fractions by of the Rubisco holoenzyme due to its extremely high abundance (Spreitzer, 2003). For example, fraction P16-TI from the wild-type strain contained both RBCL and RBCS, presumably in the Rubisco holoenzyme (Fig. 4 C). This contamination was not a problem with *ΔRBCS* because it lacks the Rubisco holoenzyme, it accumulates RBCL to only 1-10% of the wild-type level (Fig. 4 A), and it has enhanced RBCL function in the control of oxidized RNA (Fig. 3 A). Therefore, we presumed that most RBCL in *ΔRBCS* represents a pool dedicated to the control of oxidized RNA in the chloroplast. Analysis of fractions obtained from *ΔRBCS* cells revealed RBCL primarily in P16-TI and, as expected (because this mutant lacks Rubisco), only in trace amounts in S16 (Fig. 4 D). The RBCL in P16-TI from *ΔRBCS* is not newly synthesized because this form is soluble, as revealed by ^{35}S-pulse-labelling (Fig. 4 E). Furthermore, this RBCL is probably not insoluble due to membrane-association, because it was not with detergent-solubilized membrane proteins in P16-TS (Fig.

4 C and D). These results suggest that the major form of RBCL in *ΔRBCS* differs in physiochemical properties from the soluble RBCL pools of the Rubisco holoenzyme and the newly synthesized protein. Therefore, this RBCL could represent a pool of the protein that is dedicated to the control of oxidized RNA in the chloroplast.

To address the possibility that the RBCL in the P16-TI fraction from *ΔRBCS* represents the form in cpSGs, we asked whether P16-TI has another feature of cpSGs; enrichment in the 30S subunit of the chloroplast ribosome over the 50S subunit (Uniacke and Zerges, 2008). Indeed, results of immunoblot analyses revealed a greater proportion of the 30S subunit pool in P16-TI fractions, whereas the 50S subunit pool was not similarly enriched. This difference was observed in analyses of both *ΔRBCS* and the wild-type strain (Fig. 4 C, D). However, while stress induces the recruitment of RBCL and 30S subunits to cpSGs, neither shifted from the soluble pool (S16) to P16-TI when cells were exposed to H_2O_2 (Fig. 4 C and D). This result provides further support of a constitutive role of RBCL in the control of oxidized RNA is constitutive and raises the possibility that cpSGs are a manifestation of an RBCL-containing ribonucleoprotein particle that exists at the submicroscopic level under non-stress conditions (see Discussion).

Survival under oxidative stress inversely correlates with the level of oxidized RNA

To obtain evidence that the differential levels of oxidized RNA in the wild-type and mutant strains (Fig. 3 A) have relevance *in vivo*, we tested *ΔrbcL* for impaired tolerance to stress induced by exogenous H_2O_2. *ΔRBCS* was again used to control for the effects of Rubisco-deficiency. Cultures of the wild-type strain, *ΔrbcL*, and *ΔRBCS* were exposed to a toxic concentration of H_2O_2 (4.0 mM) and the percentage of live cells was monitored over 8 h (Fig. 5 A). The results revealed that *ΔrbcL* cells died significantly faster than did the wild-type cells. Therefore, the elevated level of oxidized RNA in *ΔrbcL* correlates with impaired H_2O_2 tolerance. *ΔRBCS* exhibited H_2O_2 hypertolerance, measured both as cell survival (Fig. 5 A) and in a more stringent assay of viability, as the percent initial colony forming unit

concentration (Fig. 5 B). Therefore, in *ΔRBCS*, the low mean level of oxidized RNA and H_2O_2 hypertolerance are both opposite to loss-of-function phenotypes for these traits in *ΔrbcL*. Similarly, the rescued *ΔRBCS* mutant (by transformation with *RBCS2*) showed wild-type H_2O_2 tolerance (Fig. 5 C) and a wild-type mean level of oxidized RNA (Fig. 3A). Finally, like *ΔrbcL*, the mutant for both RBCL and RBCS showed impaired H_2O_2 tolerance and a high oxidized RNA level (Fig. 5 D). These differences in H_2O_2 tolerance did not reflect inherent differences in growth rate, transcript levels of oxidative stress marker genes, or the rate of H_2O_2 degradation in the medium (Fig. S1). Thus, biological relevance of the differential levels of oxidized RNA detected *in vitro* is supported the role of RBCL in H_2O_2 tolerance *in vivo*.

DISCUSSION

Our results reveal oxidized RNA in the pyrenoid of an algal chloroplast and in cytoplasmic ORBs in cultured human cells (Fig. 1 and 2). These findings in such phylogenetically distant genetic systems suggest that the compartmentalization of oxidized RNA has fundamental significance. Compartmentalization of DNA and protein quality control is well documented and is believed to have several functions (Stoecklin and Bukau, 2013; Adjibade and Mazroui, 2014; Walters and Parker, 2014). The sequestration of damaged molecules prevents them from interfering with the processes in which they normally function. It prevents the degradation or attempted repair of undamaged substrates. Finally, compartmentalization could enhance local concentrations of substrate molecules and quality control factors to establish favorable thermodynamic parameters that favor forward reactions in, for example, repair or degradation. Our results open avenues to study the role of compartmentalization in RNA quality control.

Our results show that RBCL controls the level of oxidized RNA in the chloroplast (Fig. 3) and is a determining factor in H_2O_2 tolerance (Fig. 5). These functions are independent of Rubisco and, therefore, could explain the evolutionary retention of RBCL in plant and algal lineages that have lost photosynthesis (Krause, 2008). We also identify an insoluble RBCL pool that is not part of the Rubisco holoenzyme and could carry out this dual "moonlighting" function (Fig. 4). This explains non-colocalization of the IF signal from 8-oxoG RNA in the pyrenoid with the strongest patches of RBCL IF signal, which was probably Rubisco holoenzyme. Recently, evidence of an extra-Rubisco RBCL pool was reported; results of quantitative mass spectrometry analysis in Chlamydomonas revealed that RBCL accumulates several fold above the equal stoichiometric amount with RBCS required in the Rubisco holoenzyme complex (Recuenco-Muñoz et al., 2015). RBCL appears to be a particularly critical and determining factor in the control of oxidized RNA in the chloroplast; if any other factor would function more so, then the RBCL in *ΔRBCS* would not be able to lower the level of oxidized RNA (Fig. 3 A) or enhance the H_2O_2 tolerance (Fig. 5 A and B), relative to wild- type. In *ΔRBCS*, the enhanced level of RBCL activities in controlling oxidized RNA and H_2O_2 tolerance could, for example, be due to greater availability of the protein for these functions when it cannot be assembled in the Rubisco holoenzyme.

Our results also support the inclusion of RBCL in a class of metabolic proteins that have dual functions as RNA-binding proteins (Yosef et al., 2004). This class of proteins has been proposed to coordinate metabolism and gene expression and to enhance the functional diversity of proteomes (Hentze and Preiss, 2010). For only a few such proteins has evidence of the dual function been demonstrated *in vivo*, as we have done here for RBCL.

How RBCL controls oxidized RNA remains to be determined. This could involve the protection of undamaged RNA from ROS or selection of oxidized RNA for sequestration from translated pool, repair, or degradation. Our finding that the IF signal from 8-oxoG RNA was not enriched in cpSGs (Fig. 1 E and F) is inconsistent with sequestration of oxidized

RNA, but compatible with the other mechanisms. For example, cpSGs would not accumulate oxidized RNA if they protect non-oxidized RNA from ROS and might not if they rapidly degrade or repair oxidized RNA. Nevertheless, it remains to be determined whether or cpSGs function in the quality control of oxidized RNA.

Our findings have potential relevance to the biology of SGs and PBs. These RNA granules have been implicated in fundamental cell biological processes, but their functions and physiochemical properties are only partially understood. Our results reveal an extra-Rubisco biochemical pool of RBCL which is insoluble, a feature that might be expected of cpSG proteins because cpSGs are aggregates of RNA and protein and insolubility in Triton X-100 is a property of PB proteins (Teixeira et al., 2005). Furthermore, the P16-TI fraction with this RBCL pool, like cpSGs, has an excess of the 30S subunit of the chloroplast ribosome over the 50S subunit (Fig. 4). But even under non-stress conditions, when most cells do not have cpSGs, RBCL was detected in the insoluble form and shown to control oxidized RNA under non-stress conditions, when most cells do not have cpSGs (Fig. 3). Together, these results suggest that RBCL controls oxidized RNA at the submicroscopic level, independently of cpSGs, and constitutively. Whether or not SGs and PBs also have these features remains to be determined.

Oxidized RNA arises under optimal growth conditions and the mean level did not to increase during stress (Fig. 3). RNA oxidation might result from ROS produced as a byproduct of photosynthesis, which occurs under both non-stress and stress conditions {Foyer, 2009 #3516}. Moreover, a presumed detrimental nature of oxidized RNA in the chloroplast seems at odds with the wild-type growth rate *ΔrbcL* despite its having an elevated level of oxidized RNA (relative to wild-type) (Fig. 3 A and Fig. S1 A). Our results are consistent with a certain level of oxidized RNA being benign under optimal conditions (Fig.S1 A) and becoming detrimental in the presence of H_2O_2 (Fig. 5). For example, oxidized bases in chloroplast mRNAs could result in the synthesis of aberrant iron-binding proteins

with Fenton activity (conversion of H_2O_2 to the highly toxic hydroxyl radical) and thereby potentiate the toxicity of H_2O_2 (Foyer and Noctor, 2009).

MATERIALS AND METHODS

Culturing of *C. reinhardtii*. The wild-type strain was *4A+* (CC-4051); *ΔrbcL* was CC-4696 (*MX3312*) (Dr. Genhai Zhu, Pioneer Hi-Brid) (Satagopan and Spreitzer, 2004); *ΔRBCS* was CAL005.01.13 (*dim1*) (Dent et al., 2005). *ΔrbcL* and *ΔRBCS* are non-photosynthetic, but fully viable under heterotrophic conditions (Satagopan and Spreitzer, 2004). Because Rubisco mutants are highly light-sensitive (Johnson, 2011), all cultures were grown and tested under heterotrophic conditions; in the dark on Tris-acetate phosphate (TAP) medium, at 24^0C, with orbital shaking (Gorman and Levine, 1965). To generate the complemented *ΔRBCS* strain, the wild-type *RBCS2* gene (on plasmid pSS2) (Khrebtukova and Spreitzer, 1996) was introduced into *ΔRBCS* by glass bead-mediated transformation as described previously (Purton, 2007). The double mutants for *rbcL* and the *RBCS* locus (*RBCS1* and *RBCS2*) were obtained from a cross between *ΔrbcL* (*mt+*) and *ΔRBCS (mt-*). It was critical to use cultures in exponential growth phase and in the density range of 2-4 x 10^6 cells/ml.

***C. reinhardtii* microscopy and IF-staining**. The IF protocol for *C. reinhardtii* was reported previously (Uniacke et al., 2011). To induce cpSG formation, live cells were treated with 2.0 mM H_2O_2 for 15 min prior to fixation. Where indicated, fixed and permeabilized cells were treated for 1h at 37^0C with 10 μg/ml RNase A (Fermentas) or 50 μg/ml DNase I (Invitrogen). 8-oxoG was immunodetected with a monoclonal mouse antibody (QED Bioscience Inc., clone 15A3). The specificity of this antibody *in situ* was confirmed by incubating with its antigen 8-hydroxy-2′-deoxyguanosine (1.0 mg/mL) for 2 h before IF-staining. Rabbit antibodies were used to immunodetect RBCL (Agrisera AS03037) and the 30S subunit chloroplast ribosomal-protein (S-20) (Randolph-Anderson et al., 1989). Secondary antibodies were: Alexa Fluor 488 goat anti-mouse IgG and Alexa Fluor 568 goat anti-rabbit IgG

(Invitrogen Inc.). Images were acquired by epifluorescence microscopy using a Leica DMI 6000 microscope (Leica Microsystems) with a 63X/1.4 objective, a Hamamatsu OrcaR2 camera, and Volocity acquisition software (Perkin-Elmer). Z-stacks were taken by series capture at a thickness of 0.2 μm per section. Stacks were deconvoluted with AutoQuant X3 (Media Cybernetics Inc.) (Abramoff et al., 2004).

Mammalian tissue culture. HeLa cervical cancer cells were obtained from the American Type Culture Collection (Manassas, VA; ATCC). Cells were cultured at 37^0C in DMEM (Sigma-Aldrich, St. Louis, MO) supplemented with 10% fetal bovine serum, penicillin and streptomycin (all from Sigma-Aldrich). Fixed and permeabilized cells were treated with 10 μg/ml RNase for 1h, where indicated. 1.0 mM sodium arsenite treatments of live cells were for 1.0 hr under the conditions described above.

Mammalian cell IF-staining.

The protocol was described previously (Fournier et al., 2013). Primary antibodies were; αG3BP1 from Dr. Imed Gallouzi (McGill University), αRCK and αTOM20 (FL-145) from Santa Cruz Biotechnology, and α8-oxoG from QED Bioscience Inc. (clone 15A3). The secondary antibodies were Alexa Fluor 488 goat anti-mouse IgG, Alexa Fluor 598 goat anti-mouse IgG, and Alexa Fluor 568 goat anti-rabbit IgG (Invitrogen Inc.). IF signals were visualized by an LSM 700 confocal laser scanning microscope (Zeiss), controlled with 2009 ZEN software for image acquisition and analysis. Images were acquired using the following settings: 63X oil objective (zoom 1.0), 0.06 μm for pixel size, and 1.00 airy units as pinhole.

Analyses of oxidized RNA, DNA and Protein. In each biological replicate experiment, RNA, DNA, and protein were isolated from the same culture. Where indicated, live cells were exposed to 2.0 mM H_2O_2 for 15 min. Total RNA was extracted using TRI-reagent (Sigma-Aldrich) according to the manufacturer's protocol. Qualification and quantification of RNA were confirmed by electrophoretic analysis by bioanalyzer (Agilent). Total DNA was extracted using hexadecyltrimethylammonium bromide, as described previously (Murray and

Thompson, 1980). The DNA preparations were rid of RNA by precipitation with $LiCl_2$, as confirmed by nanochip analysis with a 2100 Bioanalyzer (Agilent) (Sambrook and Russell, 2001). RNA and DNA concentrations were quantified by bioanalyzeranalyses by nanochip and UV spectrophotometry, respectively. Total RNA (5 µg) and DNA (1 µg) samples were transferred to a nitrocellulose membrane with a Minifold-II slot blot system (Schleicher & Schuell). Filters were reacted with the commercial antibody against 8-oxoG (QED Bioscience Inc., clone 15A3) overnight, at 4°C (Sambrook and Russell, 2001). A goat anti-mouse secondary antibody (KPL) was used and ECL detection was performed with a commercial kit (Millipore). To isolate total protein, cells were pelleted (3,000 x g, 3 min) and broken in 50 mM Tris-Cl pH 8.0, 1 mM EDTA, 50 mM NaCl, 1 mM PMSF, 100 mM DTT by bead-beating (Hopkins, 1991). Protein samples (20 µg) were analyzed with the OxyBlot Kit according to the manufacturer's protocol (Millipore). Total protein concentration was determined as described previously (Smith et al., 1985). Quantification was carried out as described previously (Bohne et al., 2013). For statistical analyses, each biological replicate was compared to a corresponding *ΔrbcL* strain prior to the addition of H_2O_2, which was designated as 100% oxidation. Statistical differences were determined in each case using a one-sample t-test.

Differential Centrifugation. Cells from 75 ml cultures were pelleted by centrifugation (5,000 x g, 5 min) at room temperature and resuspended in 5.0 ml ice cold MKT-buffer (25 mM $MgCl_2$, 20 mM KCl, 10 mM Tricine pH 7.5, 1.0% (v/v) protease inhibitor cocktail (Sigma-Aldrich)). Cells were broken by three passages through a chilled French pressure cell at 1,000 psi. The cell lysate was centrifuged at 3,200 x g for 1 min to pellet unbroken cells. The supernatant was collected and centrifuged at 16,000 x g for 20 minutes at 4°C. The resulting supernatant was S16. The pellet (P16) was resuspended in MKT-buffer with 2% (v/v) Triton X-100 and incubated for 15 minutes at room temperature with gentle agitation to solubilize membranes. These samples were then centrifuged at 16,000 x g for 20 minutes at 4°C. The

supernatant was P16-TS. The pellet (P16-TI) was resuspended in MKT-buffer. Protein samples from each fraction were subjected to SDS-PAGE and immunoblot analysis. Protein loading was based on equal proportions of each fraction. The antisera were: αRBCL (Agrisera, AS03037), αRBCS (Dr. Robert Spreitzer, University of Nebraska), αCP43 (Agrisera, 111787) αS-20 (30S r-protein), αL-30 (50S r-protein) (Randolph-Anderson et al., 1989), and αHSP70B (Schroda et al., 1999). Secondary staining used goat anti-rabbit antibody (KPL) incubated for 1 h at room temperature.

***In vivo* ^{35}S-pulse-labeling of proteins.** ^{35}S-pulse-labeling reactions were performed with $^{35}SO_4$ as described previously (Uniacke and Zerges, 2007). Cells (c.a. 1.2 x 10^7 per sample) were then pelleted by centrifugation (5,000 x g, 5 min), washed once with 500 µL 50mM Tris-Cl pH 7.4, resuspended in 80 µL MKT-buffer, and broken by bead-beating (Hopkins, 1991). The cell lysates were centrifuged (16,000 x g, 5 min), and the pellet and supernatant fractions were subjected to SDS-PAGE (7.5-15% acrylamide, 6.0 M urea). ^{35}S-pulse-labelled proteins in dried gels were visualized with a Typhoon phosphoimager (GE Healthcare).

Survival and viability

Cell survival and viability were assayed following addition of H_2O_2 to 4.0 mM. Cell survival was determined by counting the proportion of live cells with the Trypan blue exclusion assay (Sigma-Aldrich). Viability was determined as colony forming units on agar-solidified TAP medium. For statistical analyses of survival and viability, a mixed analysis of variance (ANOVA) was conducted with strain as a between factor and time as a within factor. When appropriate, post hoc analyses were conducted using Tukey's HSD.

ACKNOWLEDGEMENTS

We thank A. Piekny and C. van Oostende for assistance with microscopy, W. Brake for assistance with statistical analyses, M. Schroda for the αHSP70B antiserum; I. Gallouzi for the αG3BP1 antiserum; G. Zhu, and Pioneer Hi-Bred (Redwood City, Ca) for *ΔrbcL-MX3312*, and R. Spreitzer for the pSS2 plasmid and the αRBCS antiserum**.** This work was carried out, in part, in the Centre for Microscopy and in the Centre for Structural & Functional Genomics (Concordia University) and was funded by Natural Sciences and Engineering Council of Canada grants 217566 (WZ) and MOP-702406 (RM) and a Canadian Institutes of Health Research New investigator Scholarship award (RM).

ABBREVIATIONS LIST

8-oxoG, 8-hydroxyguanine; cpSG, chloroplast stress granule; H_2O_2, hydrogen peroxide; IF, immunofluorescence; PB, processing body; SG, stress granule; ROS, reactive oxygen species; RBCL, Rubisco large subunit; RBCS, Rubisco small subunit; Rubisco, ribulose bisphosphate carboxylase/oxygenase.

REFERENCES

Abramoff, M. D., Magelhaes, P. J. and Ram, S. J. (2004). Image Processing with ImageJ. *Biophotonics International* **11**, 36-42.

Adjibade, P. and Mazroui, R. (2014). Control of mRNA turnover: Implication of cytoplasmic RNA granules. *Semin Cell Dev Biol*.

Apel, K. and Hirt, H. (2004). Reactive oxygen species: metabolism, oxidative stress, and signal transduction. *Annu Rev Plant Biol* **55**, 373-399.

Bohne, A. V., Schwarz, C., Schottkowski, M., Lidschreiber, M., Piotrowski, M., Zerges, W. and Nickelsen, J. (2013). Reciprocal regulation of protein synthesis and carbon metabolism for thylakoid membrane biogenesis. *PLoS Biol* **11**, e1001482.

Bravard, A., Campalans, A., Vacher, M., Gouget, B., Levalois, C., Chevillard, S. and Radicella, J. P. (2010). Inactivation by oxidation and recruitment into stress granules of hOGG1 but not APE1 in human cells exposed to sub-lethal concentrations of cadmium. *Mutation Research/Fundamental and Molecular Mechanisms of Mutagenesis* **685**, 61-69.

Cohen, I., Sapir, Y. and Shapira, M. (2006). A conserved mechanism controls translation of Rubisco large subunit in different photosynthetic organisms. *Plant Physiol* **141**, 1089-1097.

Cohen, I., Knopf, J. A., Irihimovitch, V. and Shapira, M. (2005). A proposed mechanism for the inhibitory effects of oxidative stress on Rubisco assembly and its subunit expression. *Plant Physiol* **137**, 738-746.

Dent, R. M., Haglund, C. M., Chin, B. L., Kobayashi, M. C. and Niyogi, K. K. (2005). Functional genomics of eukaryotic photosynthesis using insertional mutagenesis of Chlamydomonas reinhardtii. *Plant Physiol* **137**, 545-556.

Fischer, B. B., Dayer, R., Schwarzenbach, Y., Lemaire, S. D., Behra, R., Liedtke, A. and Eggen, R. I. (2009). Function and regulation of the glutathione peroxidase homologous gene GPXH/GPX5 in Chlamydomonas reinhardtii. *Plant Mol Biol* **71**, 569-583.

Fournier, M. J., Coudert, L., Mellaoui, S., Adjibade, P., Gareau, C., Cote, M. F.,

Sonenberg, N., Gaudreault, R. C. and Mazroui, R. (2013). Inactivation of the mTORC1-eukaryotic translation initiation factor 4E pathway alters stress granule formation. *Mol Cell Biol* **33**, 2285-2301.

Foyer, C. H. and Noctor, G. (2009). Redox regulation in photosynthetic organisms: signaling, acclimation, and practical implications. *Antioxid Redox Signal* **11**, 861-905.

Foyer, C. H. and Shigeoka, S. (2011). Understanding Oxidative Stress and Antioxidant Functions to Enhance Photosynthesis. *Plant Physiology* **155**, 93-100.

Gorman, D. S. and Levine, R. P. (1965). Cytochrome f and plastocyanin: their sequence in the photosynthetic electron transport chain of *Chlamydomonas reinhardii*. *Proc Natl Acad Sci U S A* **54**, 1665-1669.

Hentze, M. W. and Preiss, T. (2010). The REM phase of gene regulation. *Trends in biochemical sciences* **35**, 423-426.

Holmstrom, K. M. and Finkel, T. (2014). Cellular mechanisms and physiological consequences of redox-dependent signalling. *Nat Rev Mol Cell Biol* **15**, 411-421.

Hopkins, T. R. (1991). Physical and chemical cell disruption for the recovery of intracellular proteins. *Bioprocess Technol* **12**, 57-83.

Johnson, X. (2011). Manipulating RuBisCO accumulation in the green alga, Chlamydomonas reinhardtii. *Plant Molecular Biology* **76**, 397-405.

Khrebtukova, I. and Spreitzer, R. J. (1996). Elimination of the Chlamydomonas gene family that encodes the small subunit of ribulose-1,5-bisphosphate carboxylase/oxygenase. *Proc Natl Acad Sci U S A* **93**, 13689-13693.

Knopf, J. A. and Shapira, M. (2005). Degradation of Rubisco SSU during oxidative stress triggers aggregation of Rubisco particles in Chlamydomonas reinhardtii. *Planta* **222**, 787-793.

Krause, K. (2008). From chloroplasts to "cryptic" plastids: evolution of plastid genomes in parasitic plants. *Current Genetics* **54**, 111-121.

Lee, Y. J., Wei, H. M., Chen, L. Y. and Li, C. (2014). Localization of SERBP1 in stress

granules and nucleoli. *FEBS J* **281**, 352-364.

Li, Z., Malla, S., Shin, B. and Li, J. M. (2014). Battle against RNA oxidation: molecular mechanisms for reducing oxidized RNA to protect cells. *Wiley Interdiscip Rev RNA* **5**, 335-346.

Marin-Navarro, J. and Moreno, J. (2006). Cysteines 449 and 459 modulate the reduction-oxidation conformational changes of ribulose 1.5-bisphosphate carboxylase/oxygenase and the translocation of the enzyme to membranes during stress. *Plant, cell & environment* **29**, 898-908.

McKay, M. R. L. and Gibbs, S. P. (1991). Composition and function of pyrenoids: cytochemical and immunocytochemical approaches. *Canadian Journal of Botany* **69**, 1040-1052.

Murray, M. G. and Thompson, W. F. (1980). Rapid isolation of high molecular weight plant DNA. *Nucleic Acids Research* **8**, 4321-4326.

Nunomura, A., Hofer, T., Moreira, P. I., Castellani, R. J., Smith, M. A. and Perry, G. (2009). RNA oxidation in Alzheimer disease and related neurodegenerative disorders. *Acta Neuropathol* **118**, 151-166.

Nunomura, A., Perry, G., Pappolla, M. A., Wade, R., Hirai, K., Chiba, S. and Smith, M. A. (1999). RNA oxidation is a prominent feature of vulnerable neurons in Alzheimer's disease. *Journal of Neuroscience* **19**, 1959-1964.

Onishi, H., Kino, Y., Morita, T., Futai, E., Sasagawa, N. and Ishiura, S. (2008). MBNL1 associates with YB-1 in cytoplasmic stress granules. *J Neurosci Res* **86**, 1994-2002.

Purton, S. (2007). Tools and techniques for chloroplast transformation of Chlamydomonas. *Adv Exp Med Biol* **616**, 34-45.

Randolph-Anderson, B. L., Gillham, N. W. and Boynton, J. E. (1989). Electrophoretic and immunological comparisons of chloroplast and prokaryotic ribosomal proteins reveal that certain families of large subunit proteins are evolutionarily conserved. *J Mol Evol* **29**, 68-88.

Rasala, B. A., Chao, S.-S., Pier, M., Barrera, D. J. and Mayfield, S. P. (2014). Enhanced Genetic Tools for Engineering Multigene Traits into Green Algae. *PLoS One* **9**, e94028.

Recuenco-Muñoz, L., Offre, P., Valledor, L., Lyon, D., Weckwerth, W. and Wienkoop, S. (2015). Targeted quantitative analysis of a diurnal RuBisCO subunit expression and translation profile in Chlamydomonas reinhardtii introducing a novel Mass Western approach. *Journal of Proteomics* **113**, 143-153.

Sambrook, J. and Russell, D. W. (2001). Molecular cloning : a laboratory manual. Cold Spring Harbor, N.Y.: Cold Spring Harbor Laboratory Press.

Satagopan, S. and Spreitzer, R. J. (2004). Substitutions at the Asp-473 latch residue of chlamydomonas ribulosebisphosphate carboxylase/oxygenase cause decreases in carboxylation efficiency and CO(2)/O(2) specificity. *J Biol Chem* **279**, 14240-14244.

Schottkowski, M., Peters, M., Zhan, Y., Rifai, O., Zhang, Y. and Zerges, W. (2012). Biogenic membranes of the chloroplast in Chlamydomonas reinhardtii. *Proc Natl Acad Sci U S A* **109**, 19286-19291.

Schroda, M., Vallon, O., Wollman, F. A. and Beck, C. F. (1999). A chloroplast-targeted heat shock protein 70 (HSP70) contributes to the photoprotection and repair of photosystem II during and after photoinhibition. *Plant Cell* **11**, 1165-1178.

Smith, P. K., Krohn, R. I., Hermanson, G. T., Mallia, A. K., Gartner, F. H., Provenzano, M. D., Fujimoto, E. K., Goeke, N. M., Olson, B. J. and Klenk, D. C. (1985). Measurement of protein using bicinchoninic acid. *Anal Biochem* **150**, 76-85.

Spreitzer, R. J. (2003). Role of the small subunit in ribulose-1,5-bisphosphate carboxylase/oxygenase. *Archives of biochemistry and biophysics* **414**, 141-149.

Stoecklin, G. and Bukau, B. (2013). Telling right from wrong in life - cellular quality control. *Nature Reviews Molecular Cell Biology* **14**, 613-615.

Tanaka, M., Chock, P. B. and Stadtman, E. R. (2007). Oxidized messenger RNA induces translation errors. *Proceedings of the National Academy of Sciences* **104**, 66-71.

Tanaka, T., Ohashi, S. and Kobayashi, S. (2014). Roles of YB-1 under arsenite-induced stress: translational activation of HSP70 mRNA and control of the number of stress granules. *Biochim Biophys Acta* **1840**, 985-992.

Teixeira, D., Sheth, U., Valencia-Sanchez, M. A., Brengues, M. and Parker, R. (2005). Processing bodies require RNA for assembly and contain nontranslating mRNAs. *Rna* **11**, 371-382.

Thomas, M. G., Loschi, M., Desbats, M. A. and Boccaccio, G. L. (2011). RNA granules: The good, the bad and the ugly. *Cellular Signalling* **23**, 324-334.

Uniacke, J. and Zerges, W. (2007). Photosystem II assembly and repair are differentially localized in Chlamydomonas. *Plant Cell* **19**, 3640-3654.

Uniacke, J. and Zerges, W. (2008). Stress induces the assembly of RNA granules in the chloroplast of Chlamydomonas reinhardtii. *J Cell Biol* **182**, 641-646.

Uniacke, J. and Zerges, W. (2009). Chloroplast protein targeting involves localized translation in Chlamydomonas. *Proc Natl Acad Sci U S A* **106**, 1439-1444.

Uniacke, J., Colon-Ramos, D. and Zerges, W. (2011). FISH and immunofluorescence staining in Chlamydomonas. *Methods Mol Biol* **714**, 15-29.

Walters, R. and Parker, R. (2014). Is there quality control of localized mRNAs? *The Journal of Cell Biology* **204**, 863-868.

Wurtmann, E. J. and Wolin, Sandra L. (2009). RNA under attack: Cellular handling of RNA damage. *Critical Reviews in Biochemistry and Molecular Biology* **44**, 34-49.

Yosef, I., Irihimovitch, V., Knopf, J. A., Cohen, I., Orr-Dahan, I., Nahum, E., Keasar, C. and Shapira, M. (2004). RNA binding activity of the ribulose-1,5-bisphosphate carboxylase/oxygenase large subunit from Chlamydomonas reinhardtii. *J Biol Chem* **279**, 10148-10156.

Zheng, G., Fu, Y. and He, C. (2014). Nucleic Acid Oxidation in DNA Damage Repair and Epigenetics. *Chemical Reviews* **114**, 4602-4620.

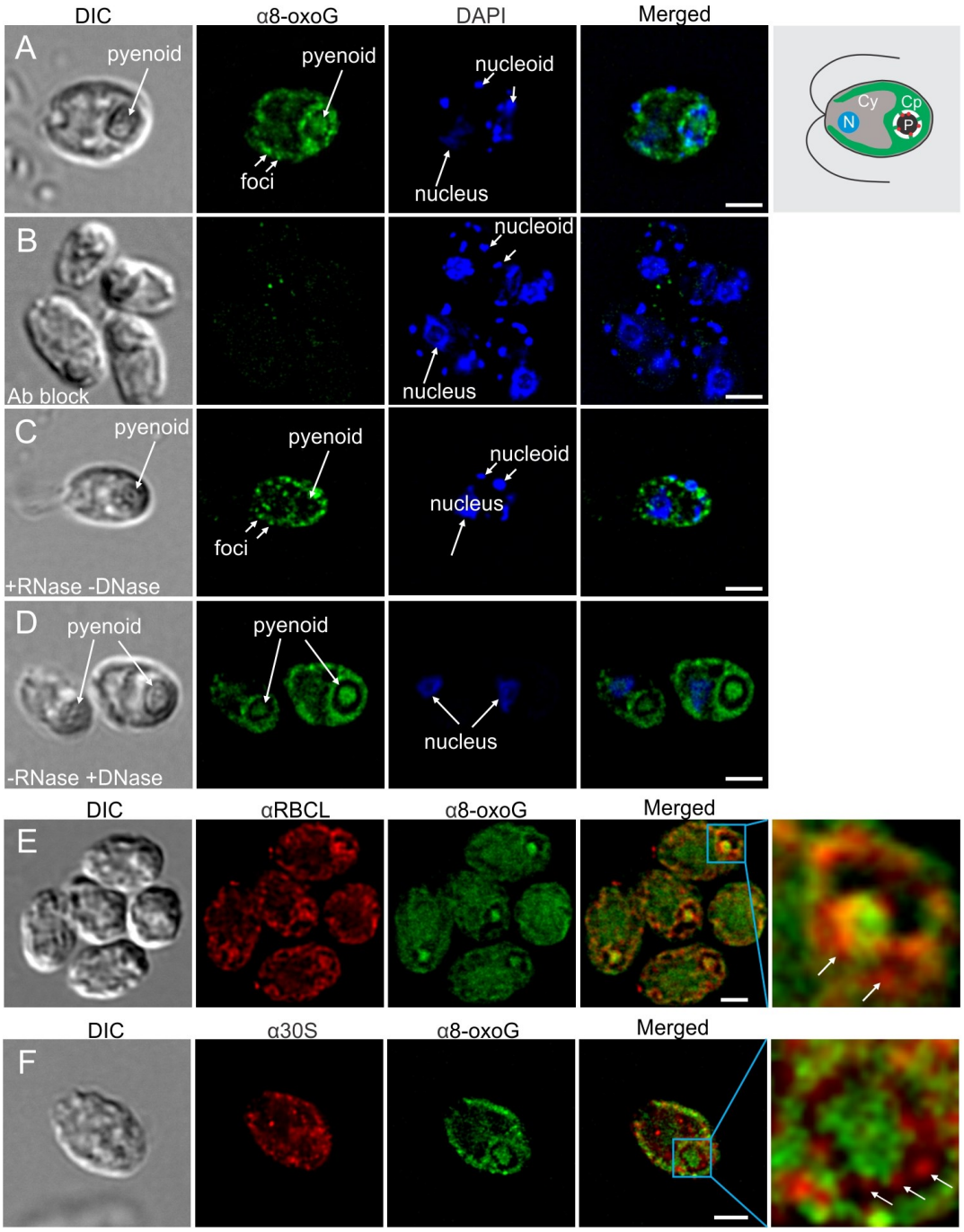
DIC
α8-oxoG
DAPI
Merged
A
pyenoid
pyenoid
foci
nucleoid
nucleus
Cy
Cp
N
P
B
Ab block
nucleoid
nucleus
C
pyenoid
pyenoid
foci
nucleoid
nucleus
+RNase -DNase
D
pyenoid
pyenoid
nucleus
-RNase +DNase
DIC
αRBCL
α8-oxoG
Merged
E
DIC
α30S
α8-oxoG
Merged
F

Fig. 1. The *in situ* distribution of 8-oxoG RNA in Chlamydomonas. A) Wild-type cells were IF-stained for 8-oxoG (green) and co-stained with DAPI to visualize DNA. The pyrenoid is seen in differential interference contrast (DIC) images. A cell illustration (right-hand most image in A) shows the locations of the nucleus (N), cytosol (Cy), and chloroplast (Cp), wherein the pyrenoid (P) is surrounded by a starch sheath (white) and contains cpSGs (red). B) The IF signal from 8-oxoG was eliminated by pre-incubating the primary antibody with 8-oxoG. C) The 8-oxoG IF signal in the pyrenoid is sensitive to RNase (10 μg/ml) treatment. D) DNase (50 μg/ml) treatment did not reduce the 8-oxoG signal in the pyrenoid but did in the punctate foci. E and F) In cells that had been treated with 2.0 mM H_2O_2 to induce cpSG formation, the 8-oxoG IF signal (green) was seen throughout the pyrenoid and not in cpSGs (white arrows), which were IF-stained (red) for either RBCL (E) or the protein of the 30S chloroplast ribosomal subunit (F). Size bars = 5.0 μm.

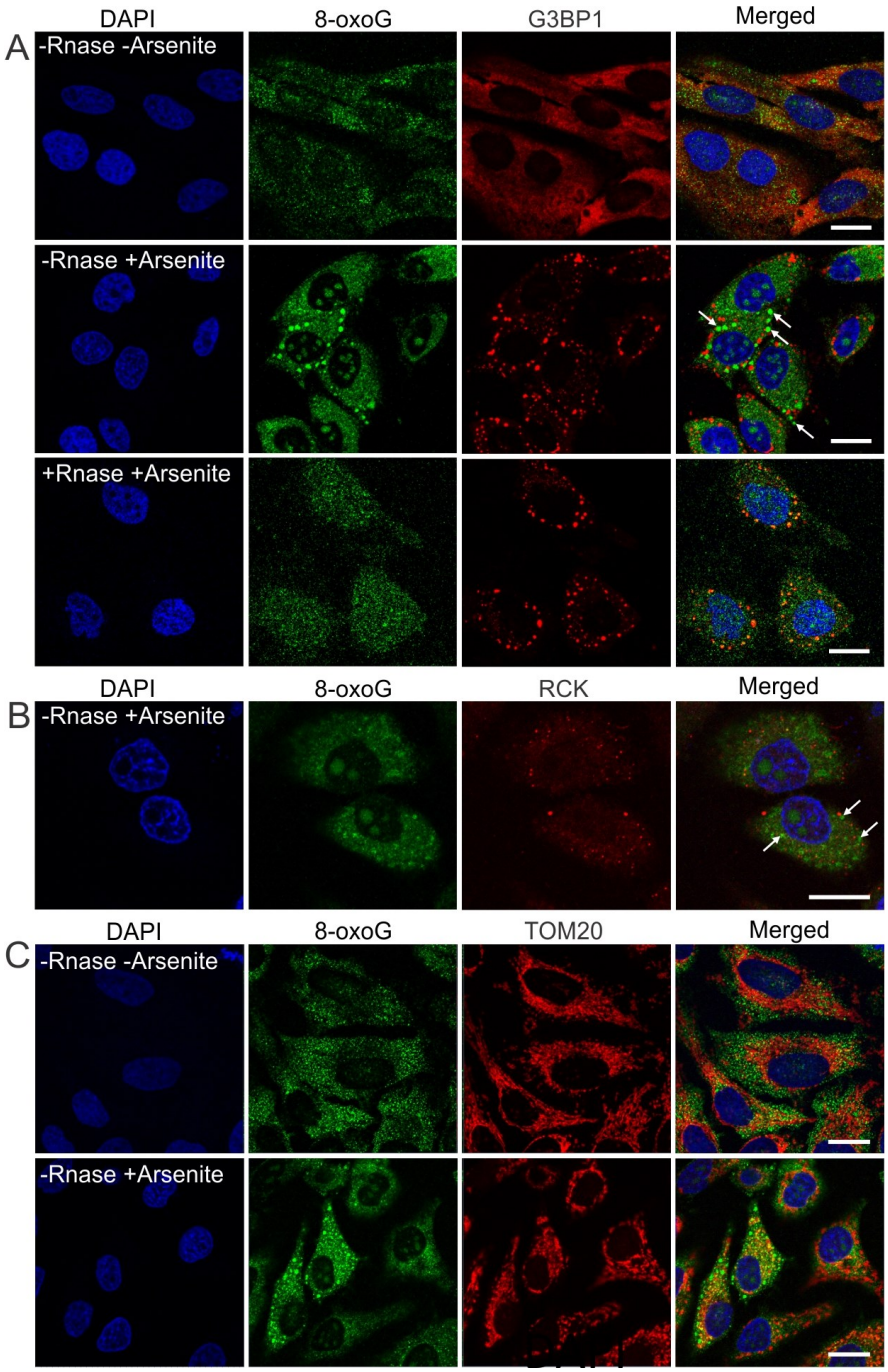

Fig. 2. In cultured human (HeLa) cells, oxidized RNA localizes to cytoplasmic ORBsduring arsenite-induced oxidative stress. Cells were IF-stained for 8-oxoG (green) and DNA was co-stained with DAPI (blue). A) Foci of 8-oxoG were not seen in 95% of cells prior to arsenite treatment. In 40% of arsenite-treated cells, the 8-oxoG IF signal was seen in cytoplasmic foci (white arrows) which are distinct from SGs (seen as foci of the red G3BP1

IF signal). ORBs were not seen in arsenite-treated cells which were treated with RNase after fixation. B) ORBs are also distinct from PBs (seen as foci of the red RAK IF signal). C) Oxidized RNA-containing bodies are not mitochondria. n = 250 cells for each. Size bars = 20 μm.

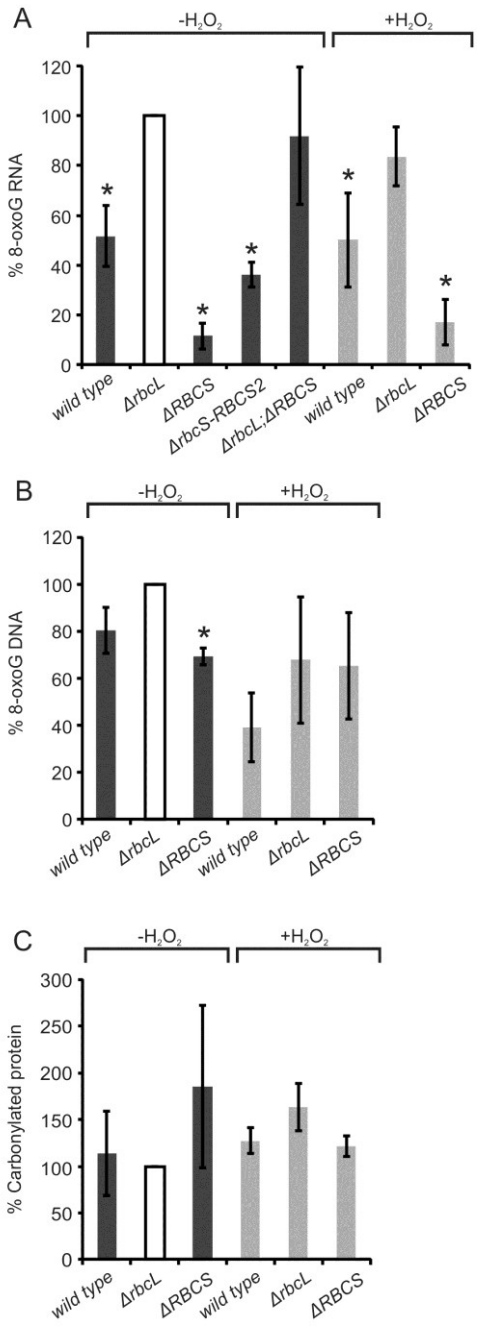

Fig. 3. RBCL controls the level of oxidized RNA, but not the levels or oxidized DNA or protein. A) Levels of 8-oxoG in RNA from the wild-type strain, *ΔrbcL*, *ΔRBCS*, the rescued-*ΔRBCS*, and the double mutant are shown (dark bars). Levels of 8-oxoG in RNA from cells exposed to 2.0 mM H_2O_2 were analysed from the wild-type strain, *ΔrbcL*, *ΔRBCS* (grey bars). Bar height represents the percentage of 8-oxoG enhanced chemo-luminescent signal of *ΔrbcL* strain before stress (white bar; 100%). *B*) The relative levels of 8-oxoG in DNA from the wild-type strain, *ΔrbcL*, and *ΔRBCS* are presented as described for RNA in panel A. *C*) Levels

of carbonylated amino acid residues in protein from the wild-type strain, *ΔrbcL*, and *ΔRBCS* are presented as described for RNA in panel A. Results were analyzed and are presented as described in Materials and Methods. Error bars indicate the standard error of the mean. Asterisks indicate a significant difference from *ΔrbcL*, as determined by one-sample t-tests ($p \leq 0.05$).

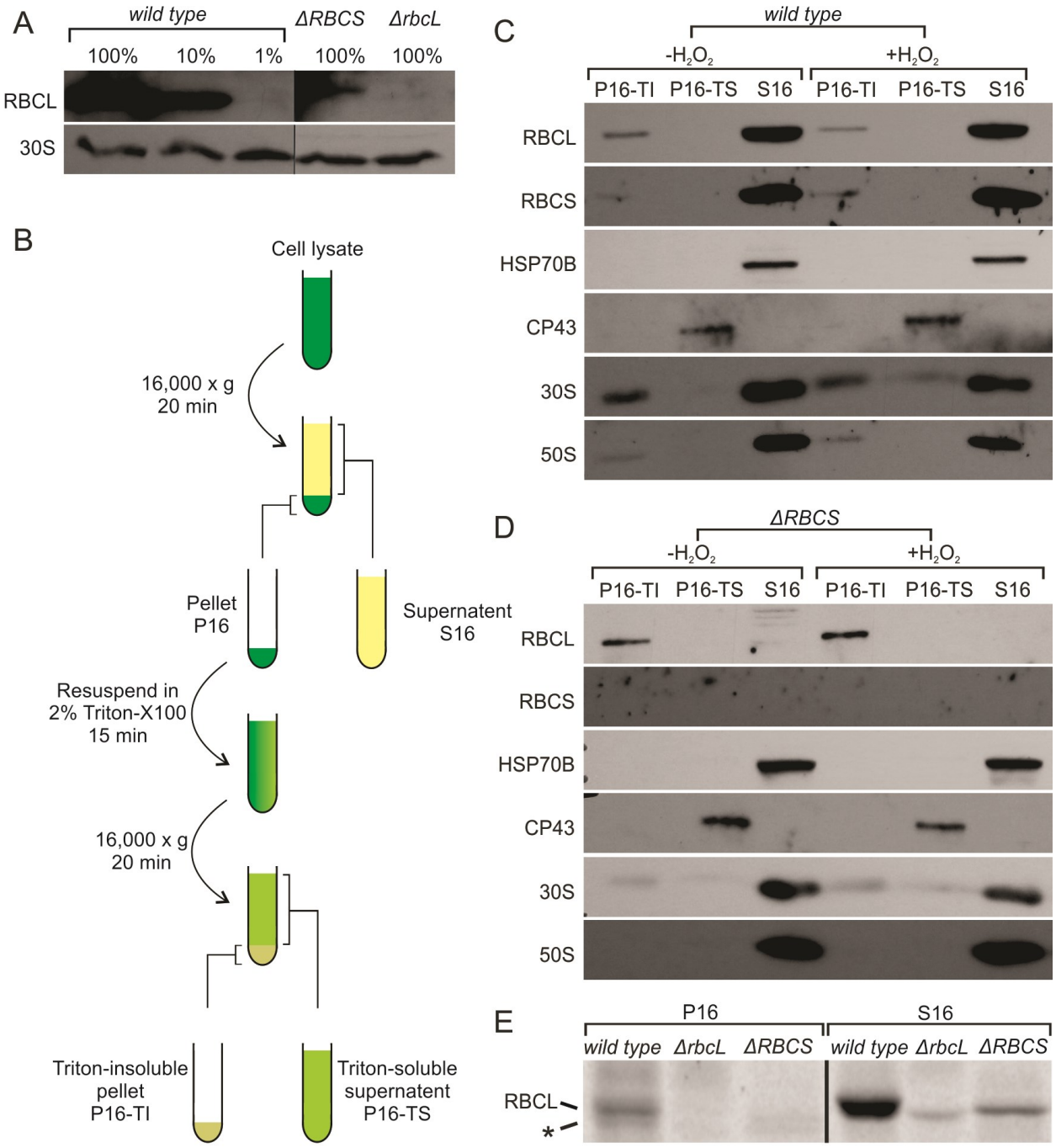

Fig. 4. A minor pool of RBCL correlates with the Rubisco-independent control of oxidized RNA. *A*) The relative levels of RBCL in crude lysates of wild-type, *ΔRBCS* and *ΔrbcL* cells were determined by SDS-PAGE and immunoblot analysis. Dilutions of the wild-type cell lysate were supplemented with lysate from *ΔrbcL* to maintain a constant amount of total protein in each lane. The band attributed to RBCL was not a cross-reacting protein as it was not detected in *ΔrbcL*. The signal from a protein of the 30S subunit of the chloroplast ribosome (30S) was used as a loading control. Black bars indicate adjoined non-adjacent lanes from a single exposure. B) The fractionation scheme is illustrated. *C and D*) RBCL fractionation during differential centrifugation and solubilisation with Triton X-100 was revealed by immunoblot analyses for *C*) the wild-type strain and *D*) *ΔRBCS.* Proteins analyzed were RBCL, RBCS, a soluble protein of the chloroplast stroma (HSP70B), an integral thylakoid membrane protein (CP43), and ribosomal proteins of chloroplast ribosome subunits (30S and 50S). Where indicated, fractions were prepared from cells that had been exposed to 2.0 mM H_2O_2. *E*) ^{35}S-pulse-labelled (newly synthesized) RBCL in the insoluble (P16) and soluble (S16) fractions from the wild-type strain and *ΔRBCS* was revealed by SDS-PAGE and phosphoimaging. As a negative control, fractions from *ΔrbcL* were shown to lack the ^{35}S-pulse-labelled band assigned to RBCL. An unidentified ^{35}S-pulse-labelled protein was detected in both fractions of all three strains (asterisk). Black bars indicate adjoined non-adjacent lanes from the same immunoblot and exposure.

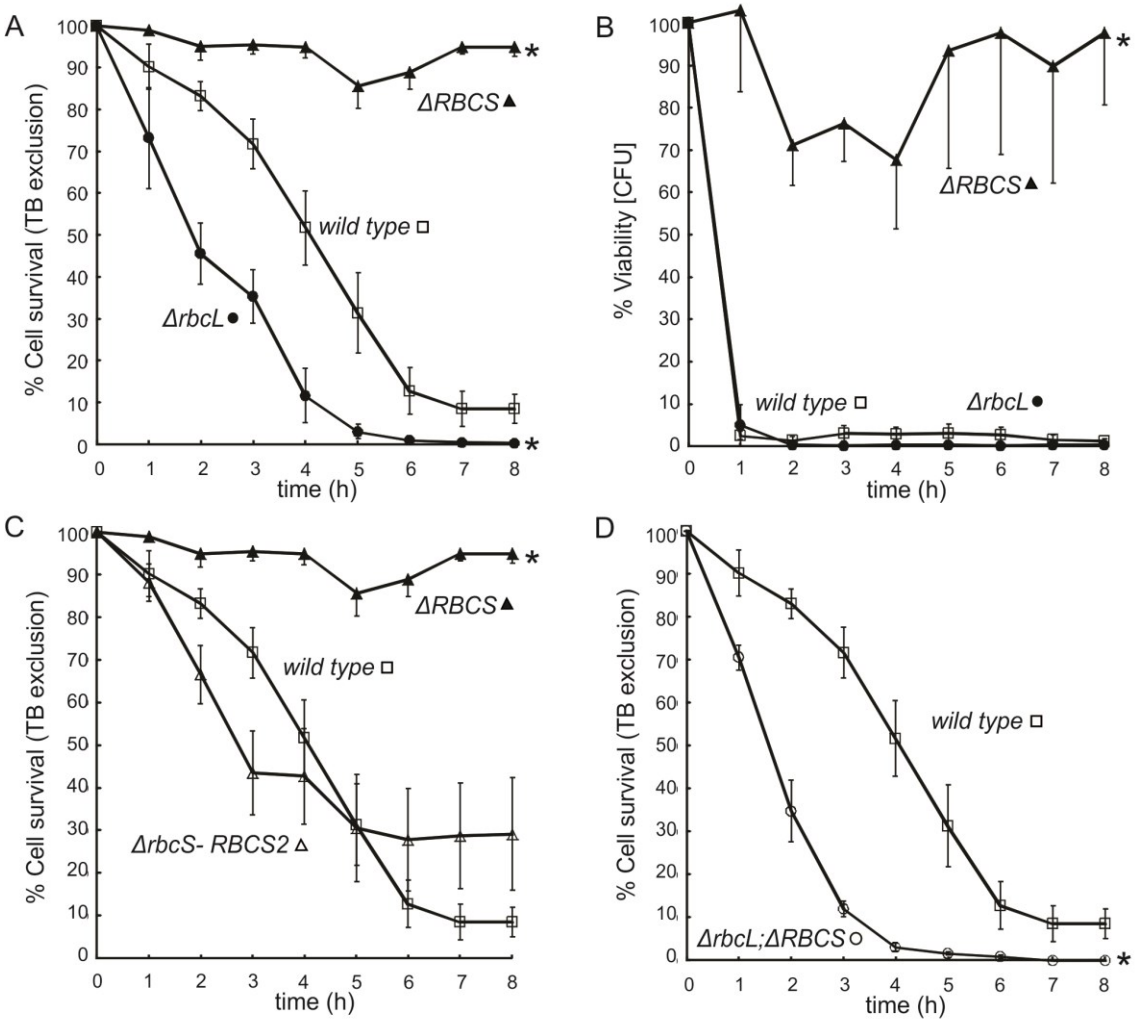

Fig. 5. RBCL functions in H_2O_2 tolerance. A, C, D) The effects of H_2O_2 on cell survival were measured by Trypan blue exclusion and graphed as the mean percentages of the initial values (immediately prior to H_2O_2 exposure). B) The effects of H_2O_2 on viability were measured as colony-forming unit concentration and graphed as the mean percentages of the initial values (immediately prior to H_2O_2 exposure). The strains analysed are indicated in each panel. Asterisks indicate a significant difference from the *wild-type* strain, as determined by mixed analysis of variance (ANOVA) ($p \leq 0.05$).

SUPPLEMENTARY DATA

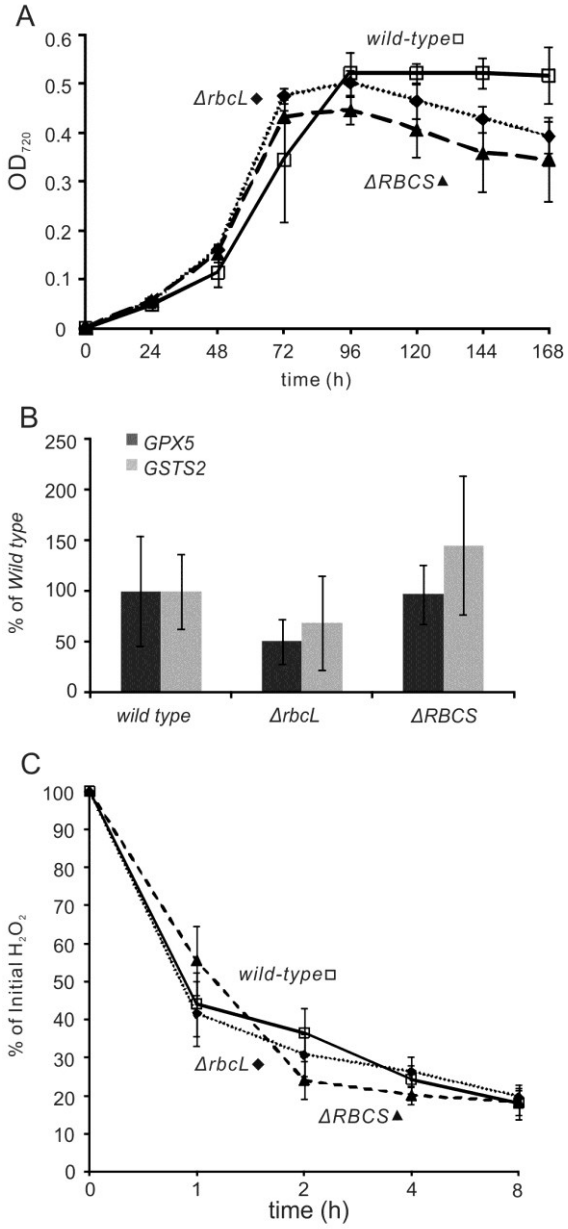

Supplementary Fig. 1. Growth rates, levels of marker transcripts for oxidative stress, and H_2O_2 amounts in wild-type, *ΔrbcL* and *ΔRBCS* cultures. A) Growth rates of the wild-type strain, *ΔrbcL*, and *ΔRBCS* were monitored using OD_{720} values, measured at 24 h time points. B) Transcript levels of oxidative stress marker genes were measured with the Quantigene2 assay (Panomics Inc.). The marker genes for oxidative stress are *GPX5* (XM_001698523) and *GSTS2* (XM_001699214) (Fischer et al., 2009). Transcript levels were normalized to the level of the *RPS26* (XP_001691901) transcript. Bar heights indicate the

mean level of each transcript graphed as the percent of the level in the wild-type strain. C) H_2O_2 concentrations in cultures of the wild-type strain, *ΔrbcL*, and *ΔRBCS* were measured at hourly time points over 8 h and graphed as the percent of the initial concentration (4.0 mM). Error bars indicate the standard error of the mean.

Appendix III:

Biogenic membranes of the chloroplast

in *Chlamydomonas reinhardtii*

Marco Schottkowski[1], Matthew Peters[1], Yu Zhan, Oussama Rifai, Ying Zhang,

and William Zerges

Biology Department and Centre for Structural and Functional Genomics, Concordia University, 7141 Sherbrooke W., Montreal, Quebec, Canada, H4B 1R6.

1) These authors contributed equally to this work.

Running title: Biogenic membranes

Classification: BIOLOGICAL SCIENCES/CELL BIOLOGY

Corresponding author; William Zerges; william.zerges@concordia.ca

ABSTRACT

The polypeptide subunits of the photosynthetic electron transport complexes in plants and algae are encoded by two genomes. Nuclear genome-encoded subunits are synthesized in the cytoplasm by 80S ribosomes, imported across the chloroplast envelope, and assembled with the subunits that are encoded by the plastid genome. Plastid genome-encoded subunits are synthesized by 70S chloroplast ribosomes directly into membranes which are widely believed to belong to the photosynthetic thylakoid vesicles. However, *in situ* evidence suggested that subunits of photosystem II are synthesized in specific regions within the chloroplast and cytoplasm of Chlamydomonas. Our results provide biochemical and *in situ* evidence of novel membranes that are localized to these translation zones. A “chloroplast translation membrane” is bound by the translation machinery and appears to be privileged for the synthesis of polypeptides encoded by the plastid genome. Novel membrane domains of the chloroplast envelope are located adjacent to the cytoplasmic translation zone and enriched in the TOC-TIC protein import complexes, suggesting a coordination of protein synthesis and import. Our findings contribute to a current realization that biogenic processes are compartmentalized within organelles and bacteria.

\body INTRODUCTION

Membrane biogenesis requires the concerted synthesis and localization of component lipids and proteins. The ER organizes these processes for the biogenesis of the nuclear envelope, the endomembrane system, lysosomes, peroxisomes, and the plasma membrane. This coordination involves the localization of ribosomes and mRNAs to the rough ER for translation and the cotranslational membrane translocation of proteins destined for specific subcellular compartments [284]. Other subcellular compartments and structures are also sites of localized translation. For example, localized synthesis of specific proteins occurs in eggs and polarized cells for pattern formation, in neurons for the formation and remodeling of synapses, at the mitotic spindle, mitochondria, chloroplasts, and bacteria for biogenesis [285-287]. Therefore, localized translation is a general mechanism for establishing the correct protein compositions of subcellular compartments.

Here we explore localized translation in the biogenesis of the photosynthetic thylakoid membranes in chloroplasts. Thylakoid membranes form a network of vesicles and contain the complexes of the photosynthetic electron transport system. Their biogenesis involves two distinct translation systems [22]. Subunits encoded by the nuclear genome are synthesized in the cytoplasm by 80S ribosomes, imported across the chloroplast envelope, and targeted to thylakoids. Within the chloroplast, other subunits are encoded by the plastid genome and synthesized by 70S bacterial-like ribosomes. Precisely where thylakoid proteins are synthesized within the cytoplasm and chloroplast is under debate [286].

As chloroplasts enlarge and divide, e.g. in the young green tissue of vascular plants and growing populations of algae, they require protein synthesis to make new photosynthesis complexes. It is widely believed that nascent polypeptides are cotranslationally inserted into stroma-exposed thylakoid membranes because ribosomes are

bound to thylakoid membranes [22]. However, chloroplast ribosomes also translate the *psbA* mRNA to repair photochemically damaged photosystem II (PS II) making it difficult to identify ribosomes involved *de novo* complex biogenesis.

An alternative model proposes that a specific "translation zone" (T-zone) in the chloroplast of the green alga *Chlamydomonas reinhardtii* is a privileged site of protein synthesis for the *de novo* biogenesis of PSII and possibly other complexes [212, 213]. This T-zone was defined by the colocalization of markers of the chloroplast ribosome, chloroplast mRNAs encoding PSII subunits, and the PSII translation factor RBP40*, as seen by confocal microscopy [212]. The T-zone is located in the outer perimeter of the pyrenoid, a spherical body in algal chloroplasts and only relevant here as a cytological landmark. The T-zone was defined only by the results of fluorescence microscopy and, therefore, its ultrastructure and biochemical nature are unknown.

We postulated that the T-zone contains a novel "chloroplast translation membrane" (CTM) as a privileged site for the synthesis of PSII subunits encoded by the chloroplast genome because chloroplasts ribosomes synthesizing PSII subunits are bound to membrane, but the chloroplast envelope and most thylakoid membranes are outside the T-zone [212]. This prediction provided an avenue to test the T-zone model at the biochemical level.

Here a subcellular fractionation scheme was developed to reveal a CTM. This scheme resolves chloroplast membranes with the high density of rough endoplasmic reticulum membrane (9) because we predicted that a CTM would also have a high-density membrane due to its having bound ribosomes. We focused on the location of PSII subunit synthesis because the evidence for the T-zone was established for chloroplast mRNAs encoding PSII subunits (6). We also identified novel domains of chloroplast envelope which are enriched in the TOC-TIC translocons and located adjacent to cytosolic regions where previous *in situ*

*RBP40 is also called RB38 {Schwarz, 2007 #3310;Barnes, 2004 #1477}.

evidence supports the localized translation of the mRNA encoding a subunit of the light harvesting complex II (LHCII), which is peripherally associated with PSII (7). Together, the results reveal two novel biogenic membranes of the chloroplast and suggest a spatiotemporal organization of PSII-LCHII biogenesis.

RESULTS

Subcellular fractionation reveals chloroplast translation membranes.

To study where proteins are synthesized in the chloroplast, we used analytical subcellular fractionation to determine whether the membranes bound by the chloroplast translation machinery have the density of thylakoid membranes, the chloroplast envelope membrane, or an unknown membrane type (10). *C. reinhardtii* cells were broken by French press because other breakage methods leave unbroken cells which contaminate the membranes of interest in subsequent steps. Using isopycnic ultracentrifugation, membranes were floated from a 2.5 M sucrose cushion into a 0.5-2.2 M sucrose concentration gradient where they banded according to density. Non-membrane material either remained in the 2.5 M sucrose cushion or pelleted. Most previous studies of ribosome-bound chloroplast membranes used discontinuous sucrose density gradients to isolate bulk membranes in broad density ranges. Chloroplast envelope membranes are isolated in the density range of 0.4 - 1 M sucrose (11). Thylakoid membranes are considered to be the densest membrane of the chloroplast and, therefore, are collected as bulk dense membranes in the range of 1-2 M sucrose (12, 13). As rough ER membranes are denser than thylakoid membranes (9) it seemed plausible that previous studies inadvertently analysed an analogous ribosome-bound CTM with thylakoids (8). Therefore, to separate membranes in this density range, we used continuous sucrose gradients with a high maximal concentration (2.2 M). Gradient fractions were analysed by immunoblotting to determine the density of membranes

associated with markers of the chloroplast translation machinery and known chloroplast compartments (Fig. 1). Gel lanes had the same proportions of fractions so that the amount of a marker would reflect the proportion of its total cellular pool (10). In other words, samples were not normalized on the basis of mass amounts of protein because this would drastically over-represent markers, on a per cell basis, in fractions with the least amount of protein, and vise versa.

Our major finding was that thylakoid membranes can be resolved from denser membranes that are associated with markers of the chloroplast translation machinery and the T-zone. As seen for the three experimental trials of our subcellular fractionation scheme (Fig. 1), the fractions with thylakoid membranes could be identified by their enrichment in chlorophyll and the subunits of photosystem I (PSI) and PSII, PsaAp and D2, respectively (Panel A, lanes 7-10; B, lanes 7-10; C, lanes 6-9). Envelope membranes are less dense than thylakoids and should be in lanes 4-6 (see below) (Fig. 1A-C) (11). Interestingly, denser membrane fractions had substantial proportions of the total pools of chloroplast ribosomal (r)-proteins and RBP40, and yet they had minor amounts of thylakoid membranes (Fig. 1A, lanes 11-13; B & C, lanes 10-12). As predicted, these dense membranes had similar density to the canonical ribosome-bound membrane of the rough ER revealed by an r-protein of the 60S subunit of the cytoplasmic ribosome (Fig 1C, lanes 6-12). By contrast, CTM were distinct from stroma-exposed thylakoid membranes, the accepted site of PSII subunit synthesis (Fig. 1A and B, PsaAp). These results provided the first evidence of a novel CTM privileged for the synthesis and membrane insertion of PSII subunits and localized in the T-zone.

In PSII assembly, newly synthesized subunits associate to form subcomplexes which then associate to form the monomeric PSII complex RCC1 (14). In an attempt to identify membranes associated with the assembly of chloroplast-encoded subunits, fractions were

immuno-probed with an antiserum against a PSII assembly factor in *Synechocystis* sp. PCC 6803, YCF48, the homologue of HCF136 of *Arabidopsis thaliana* (Fig. 1 A) (15). This antiserum detected a protein of the expected molecular mass (suppl. Fig.1). This putative YCF48\HCF136 was detected in a broad membrane density range (Fig. 1A, lanes 7-13) but not in the non-membrane material (lanes S and 14). Notably, Fraction 7 contained YCF48/HCF136 but had little thylakoid membrane and no detectable CTM (lane 7, Fig. 1A). This result suggests that this fraction contains yet another novel biogenic membrane, one involved in PSII assembly. Although these results are preliminary, they are consistent with the general theme here; that the *C. reinhardtii* chloroplast may have diverse biogenic membranes.

CTM should be physically bound by chloroplast ribosomes. Alternatively, a ribosome-associated membrane could be generated artifactually during cell breakage if free chloroplast ribosome subunits and RBP40 in the chloroplast stroma become trapped within vesicles that form by fragmenting membranes. Detracting from this possibility, however, a marker protein for the chloroplast stroma, HSP70B, was not in CTM fractions, while trace amounts were detected in the thylakoid fractions in lanes 10-12 and 7-9, respectively of Fig. 1C. To more directly address whether chloroplast translation marker proteins are bound to CTM, we asked whether they can be extracted by agents that remove peripheral membrane proteins. Membranes of Fraction 10 in Fig. 1 B were washed with one of the following; 500 mM KCl, 20 mM $NaCO_3$, 1.0 M NaCl, or 2.0 M urea or, as a negative control, without agent. Supernatant and pellet fractions were analysed by immunoblot to determine the degree of extraction of marker proteins for chloroplast ribosome subunits and RBP40. To ensure pelleting of membrane, we followed the low amount of thylakoid membrane in this fraction by immuno-probing for D2. The results revealed that RBP40 and the 50S subunit were extracted by each of the agents, either partially or completely (Fig. 2). Therefore, these

translation components are peripherally bound to CTM. The 30S subunit r-protein was only extracted by high ionic strength (2.0 M NaCl) and only partially. While this result alone is consistent with either of the two possibilities outlined above, the 30S ribosome subunit is probably bound to CTM because it seems improbable that it would be trapped in vesicles while most 50S subunits and RBP40 are not. Therefore, the 30S subunit is probably bound to CTM with particularly high affinity.

Blue-Native (BN) PAGE and immunoblot analyses reveal markers of PSII biogenesis.

Newly synthesized PSII subunits assemble in specific combinations to form precomplexes, which then associate to form the monomeric PSII complex RCC1 (14). We reasoned that unassembled subunits could serve as a marker for a CTM, and precomplexes for specific steps in PSII assembly. Therefore, membrane fractions were compared for the assembly states of the chloroplast-encoded PSII subunits D1 and D2 using BN PAGE and immunoblot analysis (16). Analyses of equal amounts of membrane ensured comparable solubilisation conditions, which can affect quaternary structure artifactually (17). Because this necessitated over-representation of CTM on a per cell basis, the amounts of sample were normalized to the level of the monomeric PSII complex, RCC1. In other words, we asked whether CTM are qualitatively different from thylakoid membranes in ways that support their having a role in PSII subunit synthesis and assembly. The results revealed RCC1 at constant levels across the lanes, confirming proper normalization (Fig. 3A). The higher mobility complex is RC47, the PSII monomer lacking CP43 which is generated primarily during PSII repair (18). Notably, the dimeric PSII, RCC2, was detected in the thylakoid membrane fractions but not in CTM fractions (Fig. 3A, compare lane 1-2 with 4-6). This result suggests that thylakoid membranes are the primary location of RCC1 dimerization to form RCC2, a late step in PSII biogenesis (14).

With 1D BN PAGE we were unable to detect free subunits and subcomplexes for use as CTM markers, possibly due to ill effects of the detergent on detection below 100 kDa (17). Therefore, BN gel lanes with either thylakoid membranes or CTM were subjected to a second dimension of denaturing SDS-PAGE and analysed by immunoblotting. We normalized based on the relative levels of RCC1 in these samples determined by 1D BN PAGE (Fig. 3A). (RCC2 was not detected for unknown reasons on the 2D gel immunoblot analyses.)

The results revealed that D1 in RCC1 and RC47, as well as in an early assembly intermediate subcomplex, the PSII reaction center, and as free unassembled subunit. All were detected in both thylakoid and CTM samples (Fig 3. B & C). Unassembled D1 could not serve as a marker for CTM because it is associated with both the repair and *de novo* biogenesis of PSII. Nevertheless, this result revealed that the assembly step in which the reaction center forms RCC1 does not occur preferentially in CTM over thylakoid membranes. Also, the finding that unassembled D1 can be detected on both immunoblots, serves as a positive control for the subsequent experiments.

These blots were immunoprobed for D2, a PSII subunit whose synthesis is not induced for PSII repair. Therefore unassembled D2 can serve as a marker for PSII biogenesis. D2 was detected in RCC1, RC47, and the RC in both thylakoids and CTM (Fig. 3D and E). Most notably, however, unassembled D2 was detected only in the CTM sample (Fig. 3E). These results suggest that CTM is a privileged location of the synthesis of the plastid genome-encoded subunits for *de novo* assembly of PSII.

Markers of PSI assembly cofractionate with thylakoid membranes

To determine whether CTM has a role in PSI biogenesis, we immuno-probed the 2D

blots for PsaAp (Fig. 3 F and G). Although PsaAp was not detected unassembled, it was detected in the PSI monomeric complex, the PSI monomeric complex lacking PsaK and PsaG, and a larger unidentified complex of c.a. 550 kDa, possibly the PSI dimer (19). Notably, the PSI monomer lacking PsaK/G was more abundant in the thylakoid membrane fraction than in the CTM fraction (Fig. 3 F and G). This result, and previously reported evidence that this complex is a late intermediate in PSI assembly (19), suggest that later steps in PSI assembly occur primarily in thylakoid membranes. Earlier steps in PSI assembly may also occur in thylakoids because we detected an early PSI assembly factor, YCF4, only in thylakoid membrane fractions (Fig. 1C, compare fractions 7-9 and fractions 10-12) (20). Finally, the mRNA encoding PsaAp was not recruited to the T-zone under the same conditions that recruited two PSII subunit mRNAs (6). Together these results suggest that PSI subunit synthesis and assembly occur at thylakoids, and not CTM.

Envelope membranes with the TOC-TIC translocons have higher-than-expected density.

The gradient fractions were also tested for the envelope markers, Toc75 and Tic110; subunits of the TOC and TIC protein import complexes. Instead of finding these proteins in the density range of the envelope membranes (Fig. 1 A-C, fractions 4-6) (11), they were detected with thylakoid fractions and, in certain preparations, also with denser CTM (Fig. 1B and C). Although the basis of this unexpectedly high and variable density of envelope membranes with the TIC and TOC complexes is unknown, their occasional separation from CTM reveals these are distinct membrane types.

The chloroplast protein import machinery localizes to novel envelope domains

To explore the basis of the unexpectedly high density of envelope membranes with Toc75 and Tic110, the *in situ* distribution of these proteins was characterized by immunofluorescence (IF) staining and epifluorescence microscopy. All cells were co-stained

for the chloroplast *psbA* mRNA by fluorescence *in situ* hybridization (FISH) to reveal the T-zone with strong signal localized around the pyrenoid and to stain the chloroplast with weaker diffuse signal. For a description of chloroplast anatomy, see Fig. 4A (6) .

A striking pattern was observed in many cells in which the Toc75 or Tic110 IF signal localized around lobes specifically where they adjoined the basal region (Fig. 4 B and D). We named these sites “lobe junctions” (Fig. 4A). In some cases, the lobe at such a lobe junction could be seen to form a hole in the cloud of IF signal, indicating that the envelope surrounding it was enriched in the TOC-TIC protein import machinery (Fig. 4B). Examples of the cells that did not show this localization pattern are shown in Fig. 4 C & E. Of the cells examined from moderate light growth condition (ML cells), 48% showed the Toc75 IF signal localized around one or two lobe junctions (Fig. 4B, n=188). Similarly, of the ML cells IF-stained for Tic110, 47% showed this pattern (Fig. 4D, n = 199). This pattern is interesting for three reasons. First, it is specific to import machinery because it was not observed for many other chloroplast proteins whose localization we have examined with this method (6, 7, 21). Second, this localization pattern may be physiologically relevant because the percentage of cells showing it dropped during incubation in the dark for 2 h, a condition associated with reduced rates of PSII biogenesis and chloroplast protein import in *C. reinhardtii* (6, 22). When ML cells were dark-adapted (DA) immediately prior to fixation; the percentages showing localization around lobe junctions dropped from 48 to 11% for Toc75 (n= 74) and from 47 to 15% for Tic110 (n= 52). Finally, Toc75 or Tic110 localization at lobe junction was probably present but undetected in many cells. *C. reinhardtii* cells are polarized and must be oriented longitudinally in the microscopy field in order to reveal cytological landmarks necessary to locate lobe junctions, e.g. the cytosol and pyrenoid (Fig. 4A). Moreover, there no protein marker exists for which co-IF-staining can reveal lobe junctions in a particular cell.

These results suggest that lobe junctions have special envelope domains enriched in the TOC-TIC protein import machinery. In light of these results, the unexpectedly high and variable density of envelope membranes with Toc75 and Tic110 could be explained if these import envelope domains have higher density than previously described envelope membranes and had formed to different degrees in the various cultures used for subcellular fractionation.

DISCUSSION

Our results provide biochemical evidence of a CTM as a privileged location of the synthesis of plastid genome-encoded PSII subunits and localized in the T-zone (6, 7). We also report biochemical and *in situ* evidence of a second novel chloroplast membrane compartment; domains of chloroplast envelope which are localized around lobe junctions, possibly to import the nucleus-encoded subunits for the biogenesis of PSII. These include the subunits of the oxygen evolving complex (OEC) and LHCII which are peripherally associated with PSII in the PSII-LHCII supercomplex. The possibility of a third novel chloroplast membrane, one privileged for PSII assembly, is suggested by the enrichment of YCF48/HCF136 in a sucrose gradient fraction with membranes that were neither of thylakoid membranes nor CTM (Fig. 1A). A previously described “low-density” membrane (LDM) of the *C. reinhardtii* chloroplast was suggested to have a role in the translation of chloroplast mRNAs encoding thylakoid proteins because it is physically associated with RNA-binding proteins and thylakoids (23, 24). LDM is distinct from CTM; it is less dense and not associated with chloroplast translation machinery.

Any model unifying these results must explain how the PSII-LHCII supercomplex is assembled from subunits that are localized to distinct chloroplast compartments, i.e., chloroplast-encoded subunits in the T-zone and nucleus-encoded subunits in lobe junctions.

Also it must be explained how the newly assembled PSII-LHCII supercomplex is localized to thylakoid membranes throughout the chloroplast. Finally, such a model should consider that PSII biogenesis begins with the assembly of the chloroplast-encoded subunits to form RCC1, followed by RCC1 dimerization, the incorporation of nucleus-encoded PSII subunits, and the association of the OEC and LHCII (14).

In our model, the T-zone and lobe junctions are early and intermediate compartments in a spatiotemporal pathway of PSII-LHCII supercomplex biogenesis (Figs. 4A and 5). In the T-zone, CTM is a platform for the synthesis of the plastid genome-encoded subunits. Chloroplast ribosome subunits and PSII subunit mRNAs are recruited to membranes in the T-zone by translation independent mechanisms (e.g. tethering by membrane bound RNA-binding proteins) and subsequently translated at CTM (7). The particularly high affinity with which the 30S subunit binds CTM (Fig. 2) may be related to its early role in the assembly of a translation-component ribosome and, consequently, a requirement to maintain its CTM association while it binds the mRNA, large subunit, and initiation factors (5). Newly assembled PSII precomplexes moves by lateral diffusion within CTM to the lobe junctions and assemble to form RCC1 (Fig. 5). The membrane(s) involved could be CTM, thylakoid membranes, or an unknown assembly membrane (above). RCC1 dimerizes and is built upon by nucleus-encoded subunits of PSII, LHCII, and OEC. These are imported locally by TOC-TIC import machinery of the envelope around lobe junctions. Thus, in this model, lobe junctions are convergence points for the pathways that supply polypeptides subunits encoded by the chloroplast and nuclear genomes. Assembled PSII-LHCII supercomplexes move, again by lateral diffusion, to photosynthetic membranes of thylakoid vesicles in the lobes and at the periphery of the chloroplast basal region (Fig. 4A). At each stage, lateral diffusion of subunits and complexes could occur in a contiguous

membrane because EM images have shown that thylakoid vesicles extend from the T-zone to the ends of the lobes or around the periphery of the basal domain (25). In our model, these thylakoid vesicles are laterally heterogeneous such that their extremities in the T-zone are composed of CTM while their opposing extremities in lobes and at the periphery of the basal region are photosynthetic thylakoid membranes. This working model is indirectly supported by similar findings in other organisms (below).

Generality of this model is supported by the identification of a PSII biogenesis compartment in the cyanobacterium *Synechocystis* sp. PCC 6803 and a GFP-tagged Tic20 paralogue which was seen to be localized to specific regions of the chloroplast envelope in *Arabidopsis thaliana* (26, 27). The effect of light on the relocalization of the TIC and TOC import machinery to lobe junctions might be relevant to the light stimulation of chloroplast protein import which has been observed in *C. reinhardtii* and vascular plants (22, 28). Moreover, the Rubisco holoenzyme might be assembled in the pathways described here because its small subunit is imported via the TOC and TIC pathway and the chloroplast mRNA encoding the large subunit localizes *in situ* in the T-zone and is translated in association with membrane (7, 29, 30). Our findings build upon growing evidence of complex cytological organizations of biogenic processes in organelles and bacteria.

METHODS

Culture conditions. *C. reinhardtii* strains CC-4051 or CC-503 were cultured photoautotrophically in high-salt-minimal medium with aeration at 24^{o}C, under a light

intensity of c.a. 100 µE m^{-2} sec^{-1} until mid-log phase (2-4 x 10^6 cells ml^{-1}) (31).

Analytical subcellular fractionation. Cells from a 500 ml culture were pelleted by centrifugation at 4,000 x g for 5 min at 4°C, resuspended in MKT-buffer (25 mM $MgCl_2$, 20 mM KCl, 10 mM Tricine-Cl pH 7.5, Protease Inhibitor (Sigma-Aldrich)). Cells were broken by three passes through an ice-chilled French Pressure Cell at 1,000 psi. Breakage was verified by light microscopy (400X and 1000X magnification). The lysate was ultracentrifuged at 100,000 g for 1 h at 4°C. The supernatant was collected and stored at -80^{o}C. The pellet was resuspended in 2.5 M sucrose, overlaid with a linear sucrose gradient (0.5-2.2 M). All sucrose solutions were prepared in MKT-buffer. The gradient was ultracentrifuged at 100,000 g for 16 h at 4° C. Fractions (0.75 ml) were collected and the pellet was resuspended in KHEG-Buffer (60 mM KCl, 20 mM HEPES, 0.2 mM EDTA, 20% Glycerol). Gradients contained only membrane and associated material based on the buoyant density of bacterial ribosomes in equilibrium CsCl gradient ultracentrifugation (1.67-1.69 g/ml) would be equivalent to 4.9 M sucrose (32).

Quantification of protein and chlorophyll. Protein concentration was determined using the bicinchoninic acid assay (33). Chlorophyll was quantified as described previously (34).

Immunoblot analysis. Equal proportions of the fractions were solubilized in SDS-PAGE loading buffer, denatured at 42^{o}C for 30 min. SDS-PAGE and immunoblot analyses were performed as described previously (35). The antisera were: αD1 (Agrisera), αS-20 (30S r-protein), αL-30 (50S r-protein) and αcyL4 (60S r-protein) (36, 37), αPsaAp (38), αHSP70B (39), and αRBP40 (40).

FISH, IF-staining, and fluorescence microscopy. FISH and IF-staining of cells of strain CC-503 were as described previously (6, 41). The *psbA* FISH probes were labeled with Alexa Fluor 488 and the IF-staining used Alexa Fluor 568-conjugated anti-rabbit secondary antibody

(Invitrogen). Images were captured on a Leica DMI6000B microscope (Leica Microsystems) using a 40X/0.75 objective, a Hamamatsu OrcaR2 camera and Volocity acquisition software (Perkin Elmer).

BN-PAGE. BN PAGE was performed as described previously with the following minor modifications (16, 42).. Aliquots of sucrose gradient fractions containing 6 μg of chlorophyll were concentrated by centrifugation (100,000 g; 1 h; 4 ^{o}C) and resuspended in ACA 750 (750mM aminocaproic acid, 50 mM Bis-Tris, and 0.5 mM EDTA, pH 7.0). Membranes were then solubilized on ice in 0.8% n-Dodecyl-β-D-Maltoside (β-DM) for 5 min. Samples were centrifuged at 17,000 x g for 30 min at 4^{o}C. The supernatant was added to 1/10 Vol of 5% Coomassie Brilliant Blue G-250, 750mM aminocaproic acid whereupon protein complexes were then separated by electrophoresis in a 4.5-12% acrylamide BN gel. To ensure that D2 signal on different 2D gels was normalized to the level of RCC1, comparable amounts of RCC1 were loaded, as determined by results from 1D BN gels, and all steps were carried out in parallel. Results of maximal ECL exposure times are shown for both.

Membrane washing. Aliquots of fraction 10 in Fig. 1 B were diluted 25-fold in washing buffer (20 mM KCl, 10 mM Tricine and 2.0 mM EDTA pH 7.2, protease inhibitor cocktail (Sigma-Aldrich)) and pelleted by centrifugation in a microfuge for 1 h at 17,000 x g at 4^{o}C. Pellets were resuspended in 30 μl of one of the following: washing buffer, 500 mM KCl, 20 mM $NaCO_3$, 1.0 M NaCl, 2.0 M urea, incubated on ice for 30 min, and then subjected to the same centrifugation step. The supernatants were collected and the pellet was washed once and then resuspended in 30 μl SDS-PAGE sample buffer. SDS-PAGE and immunoblot analysis were as described previously (35).

ACKNOWLEDGEMENTS

We thank A. Piekny for assistance with microscopy, D. Bruce, J. Nickelsen, E. Schleiff, Y.

Takahashi, and V. Zazobovitz and members of our lab for stimulating discussions and helpful suggestions, J. Dhaliwal and M. Champagne for critical review of the manuscript, and the following colleagues for generous gifts of antisera; E. Schleiff, αTic110 and αToc75; M. Schroda, αHSP70B; Y. Takahashi, αYCF4; J. Nickelsen, αD2, αYCF48, and αRBP40; K. Redding, αPsaAp; and E. Harris, αS-20, αL-30, αcyL4. This study was funded by a Deutsche Forschungsgemeinschaft postdoctoral fellowship to M.S. and an operating grant from the Natural Sciences and Engineering Council of Canada (217566-03).

REFERENCES

1. Lynes EM & Simmen T (2011) Urban planning of the endoplasmic reticulum (ER): How diverse mechanisms segregate the many functions of the ER. *Biochimica et Biophysica Acta (BBA) - Molecular Cell Research* 1813(10):1893-1905.
2. Vazquez-Pianzola P & Suter B (2012) Conservation of the RNA Transport Machineries and Their Coupling to Translation Control across Eukaryotes. *Comp Funct Genomics* 2012:287852 .
3. Weis BL, Schleiff E, & Zerges W (Protein targeting to subcellular organelles via mRNA localization. *Biochimica et Biophysica Acta (BBA) - Molecular Cell Research* (0).
4. Nevo-Dinur K, Govindarajan S, & Amster-Choder O (2012) Subcellular localization of RNA and proteins in prokaryotes. *Trends Genet* 28(7):314-322 .
5. Zerges W (2000) Translation in chloroplasts. *Biochimie* 82(6-7):583-601.
6. Uniacke J & Zerges W (2007) Photosystem II Assembly and Repair Are Differentially Localized in Chlamydomonas. *Plant Cell* 19(11):3640-3654.
7. Uniacke J & Zerges W (2009) Chloroplast protein targeting involves localized translation in Chlamydomonas. *Proc Natl Acad Sci U S A* 106(5):1439-1444.
8. Muhlbauer SK & Eichacker LA (1998) Light-dependent formation of the photosynthetic proton gradient regulates translation elongation in chloroplasts. *J Biol Chem* 273(33):20935-20940.
9. Lerner RS*, et al.* (2003) Partitioning and translation of mRNAs encoding soluble proteins on membrane-bound ribosomes. *Rna* 9(9):1123-1137 .
10. Quail PH (1979) Plant Cell Fractionation. *Annual Review of Plant Physiology* 30(1):425-484.
11. Salvi D, Rolland N, Joyard J, & Ferro M (2008) Purification and proteomic analysis of chloroplasts and their sub-organellar compartments. *Methods Mol Biol* 432:19-36.
12. Chua NH, Blobel G, Siekevitz P, & Palade GE (1973) Attachment of chloroplast polysomes to thylakoid membranes in Chlamydomonas reinhardtii. *Proc Natl Acad Sci U S A* 70(5):1554-1558.
13. Hoober JK (1970) Sites of synthesis of chloroplast membrane polypeptides in Chlamydomonas reinhardi y-1. *J Biol Chem* 245(17):4327-4334 .

14. Komenda J, Sobotka R, & Nixon PJ (2012) Assembling and maintaining the Photosystem II complex in chloroplasts and cyanobacteria. *Curr Opin Plant Biol*.
15. Komenda J*, et al.* (2008) The cyanobacterial homologue of HCF136/YCF48 is a component of an early photosystem II assembly complex and is important for both the efficient assembly and repair of photosystem II in Synechocystis sp. PCC 6803. *J Biol Chem* 283(33):22390-22399 .
16. Schagger H & von Jagow G (1991) Blue native electrophoresis for isolation of membrane protein complexes in enzymatically active form. *Anal Biochem* 199(2):223-231.
17. Reisinger V & Eichacker LA (2007) How to Analyze Protein Complexes by 2D Blue Native SDS-PAGE. *PROTEOMICS* 7(S1):6-16.
18. Aro EM*, et al.* (2005) Dynamics of photosystem II: a proteomic approach to thylakoid protein complexes. *J Exp Bot* 56(411):347-356.
19. Ozawa S, Onishi T, & Takahashi Y (2010) Identification and characterization of an assembly intermediate subcomplex of photosystem I in the green alga Chlamydomonas reinhardtii. *J Biol Chem* 285(26):20072-20079 .
20. Boudreau E, Takahashi Y, Lemieux C, Turmel M, & Rochaix JD (1997) The chloroplast ycf3 and ycf4 open reading frames of Chlamydomonas reinhardtii are required for the accumulation of the photosystem I complex. *Embo J* 16(20):6095-6104.
21. Uniacke J & Zerges W (2008) Stress induces the assembly of RNA granules in the chloroplast of Chlamydomonas reinhardtii. *J Cell Biol* 182(4):641-646 .
22. Su Q, Schild C, Schumann P, & Boschetti A (2001) Varying competence for protein import into chloroplasts during the cell cycle in Chlamydomonas. *Eur J Biochem* 268(8):2315-2321.
23. Zerges W & Rochaix JD (1998) Low density membranes are associated with RNA-binding proteins and thylakoids in the chloroplast of Chlamydomonas reinhardtii. *J Cell Biol* 140(1):101-110.
24. Zerges W, Wang S, & Rochaix JD (2002) Light activates binding of membrane proteins to chloroplast RNAs in Chlamydomonas reinhardtii. *Plant Mol Biol* 50:573-585.
25. Ohad I, Siekevitz P, & Palade GE (1967) Biogenesis of chloroplast membranes. I. Plastid dedifferentiation in a dark-grown algal mutant (Chlamydomonas reinhardi). *J Cell Biol* 35(3):521-552.
26. Machettira AB*, et al.* (2011) The localization of Tic20 proteins in Arabidopsis thaliana is not restricted to the inner envelope membrane of chloroplasts. *Plant Mol Biol* 77(4-5):381-390.
27. Nickelsen J*, et al.* (2011) Biogenesis of the cyanobacterial thylakoid membrane system--an update. *FEMS Microbiology Letters* 315(1):1-5.
28. Hirohashi T, Hase T, & Nakai M (2001) Maize Non-Photosynthetic Ferredoxin Precursor Is Mis-Sorted to the Intermembrane Space of Chloroplasts in the Presence of Light. *Plant Physiology* 125(4):2154-2163.
29. Breidenbach E, Jenni E, & Boschetti A (1988) Synthesis of two proteins in chloroplasts and mRNA distribution between thylakoids and stroma during the cell cycle of Chlamydomonas reinhardii.

Eur J Biochem 177(1):225-232.

30. Muhlbauer SK & Eichacker LA (1999) The stromal protein large subunit of ribulose-1,5-bisphosphate carboxylase is translated by membrane-bound ribosomes. *Eur J Biochem* 261(3):784-788.
31. Sueoka N (1960) Mitotic Replication of Deoxyribonucleic Acid in Chlamydomonas Reinhardi. *Proc Natl Acad Sci U S A* 46(1):83-91.
32. Fenwick ML (1971) The Density of Ribosomes Bearing Messenger RNA in Phage-Infected and Normal Bacteria. *J Cell Sci* 8(3):649-658.
33. Smith PK*, et al.* (1985) Measurement of protein using bicinchoninic acid. *Anal Biochem* 150(1):76-85.
34. Porra RJ (2002) The chequered history of the development and use of simultaneous equations for the accurate determination of chlorophylls a and b. *Photosynth Res* 73(1-3):149-156.
35. Sambrook J & Russell DW (2001) *Molecular cloning : a laboratory manual* (Cold Spring Harbor Laboratory Press, Cold Spring Harbor, N.Y.) 3rd Ed p 3 v.
36. Randolph-Anderson BL, Gillham NW, & Boynton JE (1989) Electrophoretic and immunological comparisons of chloroplast and prokaryotic ribosomal proteins reveal that certain families of large subunit proteins are evolutionarily conserved. *J Mol Evol* 29(1):68-88.
37. Fleming GH, Boynton JE, & Gillham NW (1987) Cytoplasmic ribosomal proteins from Chlamydomonas reinhardtii: characterization and immunological comparisons. *Mol Gen Genet* 206(2):226-237.
38. Redding K*, et al.* (1999) Photosystem I is indispensable for photoautotrophic growth, CO2 fixation, and H2 photoproduction in Chlamydomonas reinhardtii. *J Biol Chem* 274(15):10466-10473.
39. Schroda M, Vallon O, Whitelegge JP, Beck CF, & Wollman F-A (2001) The Chloroplastic GrpE Homolog of Chlamydomonas: Two Isoforms Generated by Differential Splicing. *Plant Cell* 13(12):2823-2839.
40. Schwarz C, Elles I, Kortmann J, Piotrowski M, & Nickelsen J (2007) Synthesis of the D2 Protein of Photosystem II in Chlamydomonas Is Controlled by a High Molecular Mass Complex Containing the RNA Stabilization Factor Nac2 and the Translational Activator RBP40. *Plant Cell* 19(11):3627-3639.
41. Uniacke J, Colon-Ramos D, & Zerges W (2011) FISH and Immunofluorescence Staining in Chlamydomonas. *Methods Mol Biol* 714:15-29.
42. Schottkowski M*, et al.* (2009) Interaction of the periplasmic PratA factor and the PsbA (D1) protein during biogenesis of photosystem II in *Synechocystis* sp. PCC 6803. *J Biol Chem* 284(3):1813-1819.

Figure legends

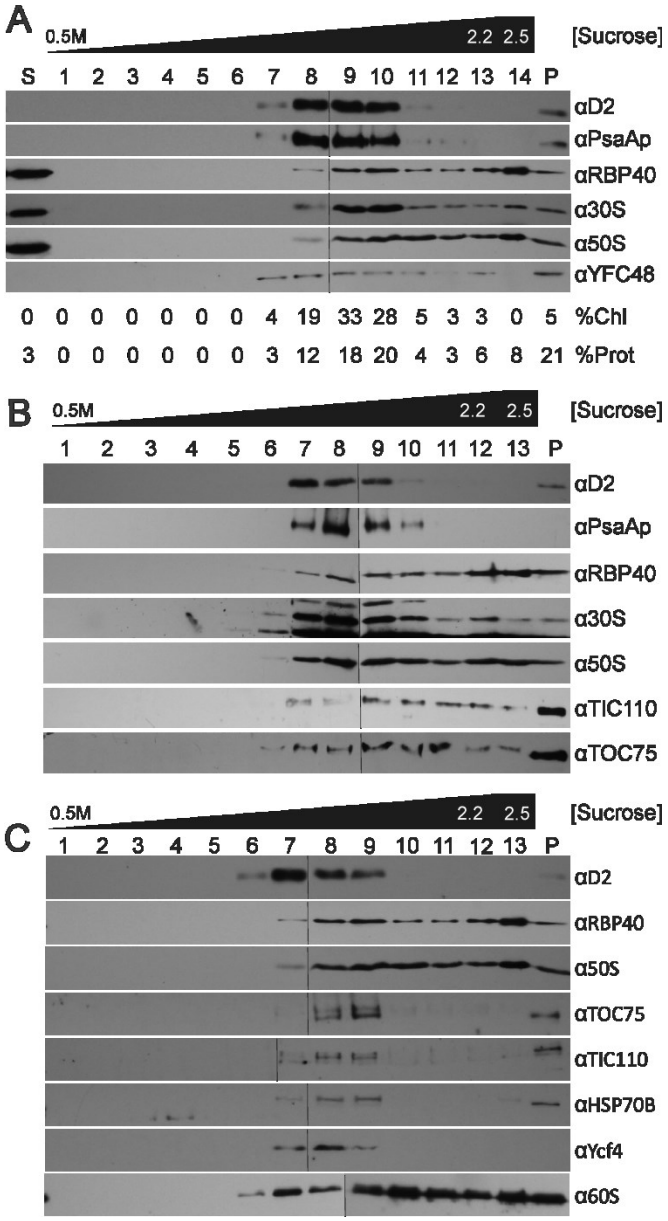

Fig. 1) Chloroplast translation membranes were revealed by subcellular fractionation.

Each panel shows the results from an independent trial. Fractions were assayed by immunoblot analyses for the following marker proteins: appressed (granal) thylakoid membranes (D2), stroma-exposed thylakoid membranes (PsaAp), CTM and the T-zone (RBP40, r-proteins of the 30S and 50S chloroplast ribosomal subunits), the TOC-TIC protein translocons of the outer and inner chloroplast envelope membranes (Toc75 and Tic110, respectively), chloroplast stroma (HSP70B), PSII assembly (YFCF48/HCF136), PSI assembly

(YCF4p), and the cytoplasmic ribosome (60S). (A) Percentages of total chlorophyll (%Chl) and protein (%Prot) in each fraction are indicated. The supernatant of the initial high speed centrifugation is labeled “S”. Membranes of the sucrose gradient were collected as (A) fractions 1-13 or (B and C) fractions 1-12. The 2.5 M sucrose from which membranes were floated is (A) fraction 14 and (B and C) fraction 15. The pellet of the sucrose gradient (P). A thin vertical line in each row distinguishes the images of immunoblots of two gels for which all steps were carried out in the same solutions.

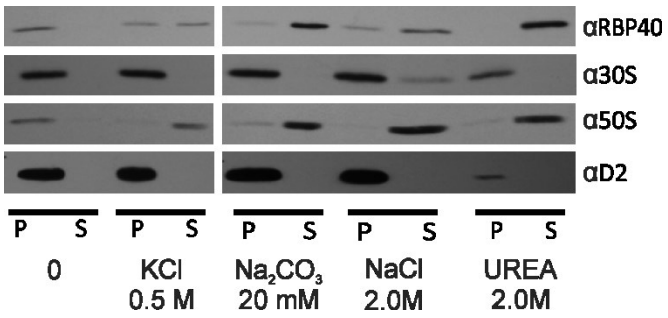

Fig. 2) CTM association of ribosome subunits and RBP40. Samples of CTM (fraction 10 in Fig. 1B) were incubated with the indicated agents to extract peripheral membrane proteins. Membranes were pelleted by centrifugation and then immunoblot analyses compared the non-membrane supernatant (S) and membrane pellet (P) fractions to reveal the degrees of extraction of RBP40 and the 30S and 50S subunits of the chloroplast ribosome. The trace amount of thylakoid membranes in this sample allowed us to ensure pelleting of membranes by immunoprobing for D2.

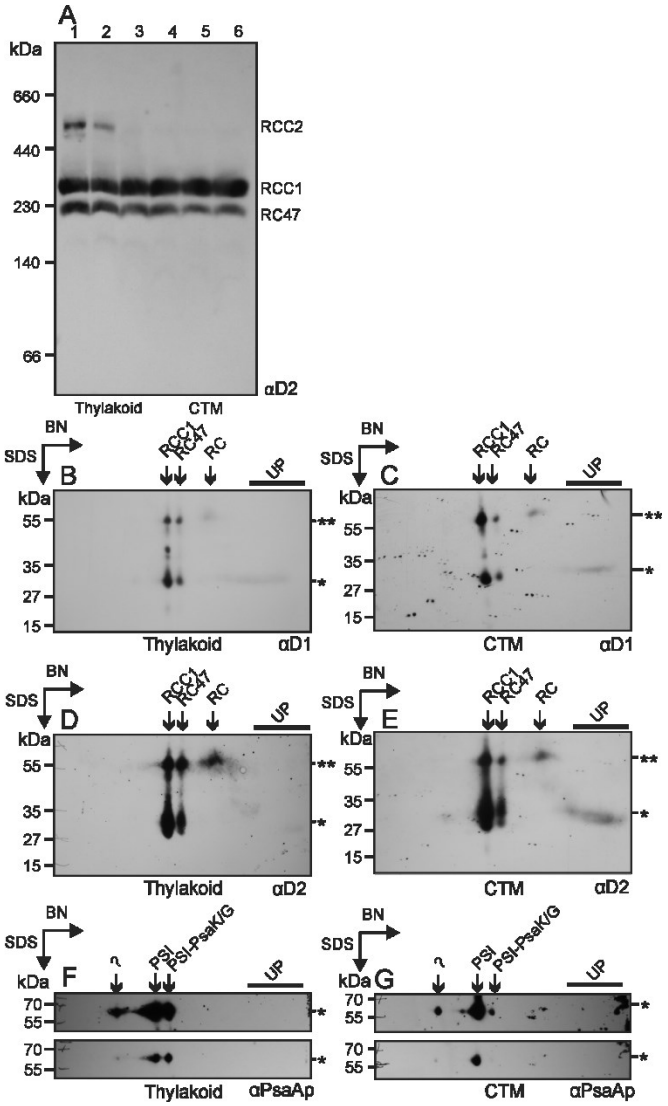

Fig. 3) BN-PAGE revealed markers of protein synthesis for PSII *de novo* assembly and repair.

(A) Analysis by 1D BN PAGE compared the assembly states of D2 in thylakoids (lanes 1-2) and CTM (lanes 3-6); samples of fractions 8-13 in Fig. 1A. D2 was immunodetected in RCC1, RCC2, and RC47. Samples were normalized to the level of RCC1 to ensure comparable solubilisation conditions (see Results). (B-G) In order to reveal subcomplexes and unassembled free subunits, BN-PAGE lanes with thylakoid membranes or CTM, equivalent to lanes 1 and 6 in A, respectively, were subjected to a second dimension of SDS-PAGE prior to immunoblot analyses. RCC1 levels determined in Panel A were used to normalize samples analysed on the 2D gels. The 2D gel-immunoblots of thylakoid membranes (B, D, and F) or CTM (C, E, and G) were first immuno-probed for D1 (B and C); then for D2 (D and E), and finally for the PSI subunit PsaAp (F and G). D1 and D2 were

detected in RCC1, RCC2, and RC47, in smaller assembly intermediate precomplexes (RC47 and PSII reaction center (RC)) and as unassembled subunits (UP). The expected molecular mass of each protein is indicated by an asterisk. Some D1 and D2 was shifted to higher molecular mass positions of the gels (**) due to incomplete denaturation prior to the second dimension of SDS-PAGE. This shift was useful because it resolved the RC (shifted*) from the free subunits (not shifted**). The same results were obtained when this shift did not occur. (F and G) PsaAp was detected in the PSI monomer (PSI), a putative PSI monomer lacking PsaK and PsaG (PSI-PsaK/G), and an unknown complex, possibly the PSI dimer (“?”).

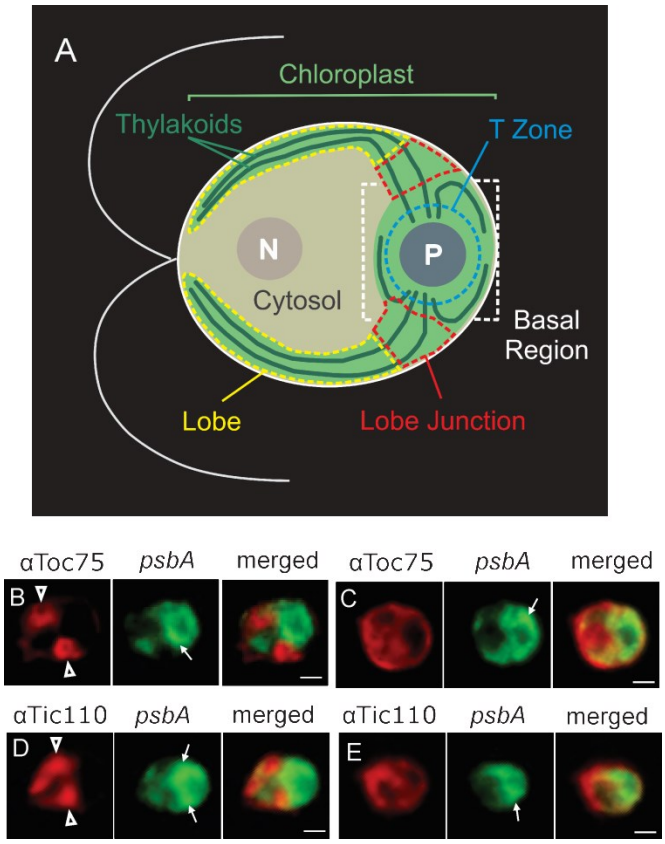

Fig. 4) The TOC and TIC protein import complexes are localized to chloroplast envelope domains.

(A) An illustration of a Chlamydomonas cell shows the nucleus (N), cytosol, and chloroplast with its lobes, lobe junctions, basal region, thylakoid lamellae, T-zone, and pyrenoid (P). The chloroplast lobes extend from the basal region to the anterior cell pole thereby "cupping" the nuclear-cytosolic compartments. (B-E) Representative cells are oriented as in Panel A and show the IF-signal from Toc75 (B and C) or Tic110 (D and E). Co-staining for the *psbA* mRNA by FISH (green) revealed the T-Zone (thin arrows). Cells in B and D (moderate light) show the localization of the Toc75 or Tic110 IF signal at lobe junctions while cells in C and E (dark-adapted) do not show this localization pattern. Bars = 2μm.

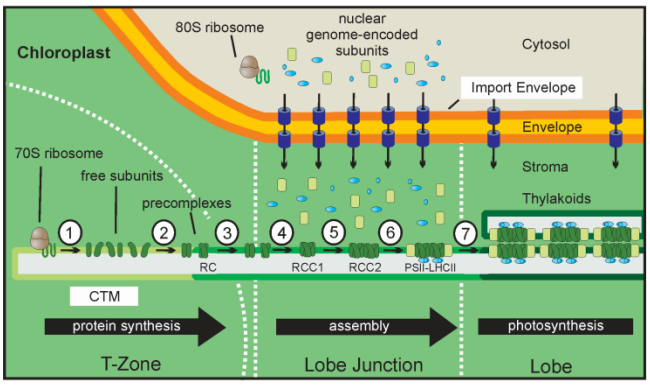

Fig. 5) A working model for the spatiotemporal organization of PSII-LHCII supercomplex biogenesis.

(1) In the T-zone, plastid-encoded subunits are synthesized into CTM. (2) Free subunits assemble to form the PSII reaction center (RC) and the other precomplexes and then (3) move by lateral diffusion to a lobe junction (see also Fig. 4A). (4) There, precomplexes associate to form the PSII monomeric complex, RCC1. (5) RCC1 dimerizes to form RCC2. (6) Nuclear genome-encoded subunits of the OEC (blue) and LHCII (light green) are locally imported by the TOC and TIC complexes (purple) into the lobe junction and assembled upon RCC1 and RCC2. (7) The resulting PSII-LHCII supercomplex diffuses to thylakoid membrane located throughout the chloroplast.

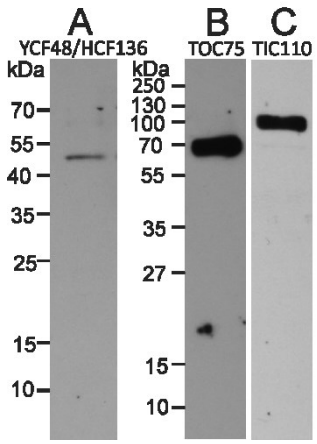

Supplemental data Fig. 1; The antisera against YCF48 of *Synechocystis* sp. PCC 6803 and Toc75 and Tic110 of pea each detect one polypeptide of the expected size in *C. reinhardtii*.

(A) The antiserum against YCF48 detected only one protein of the expected molecular mass; 44 kDa, in a membrane fraction. (B and C) The antisera against Toc75 and Tic110 detect a proteins of the expected molecular masses, 75 and 100 kDa, respectively.